IJHSR International Journal of High School Research

May 2026 | Volume 8 | Issue 10
ijhsr.terrajournals.org
ISSN (Print) 2642-1046
ISSN (Online) 2642-1054

GENIUS OLYMPIAD

Let's build a better future together

International Project Fair focused on Sustainability and Environment for Grades 8-12

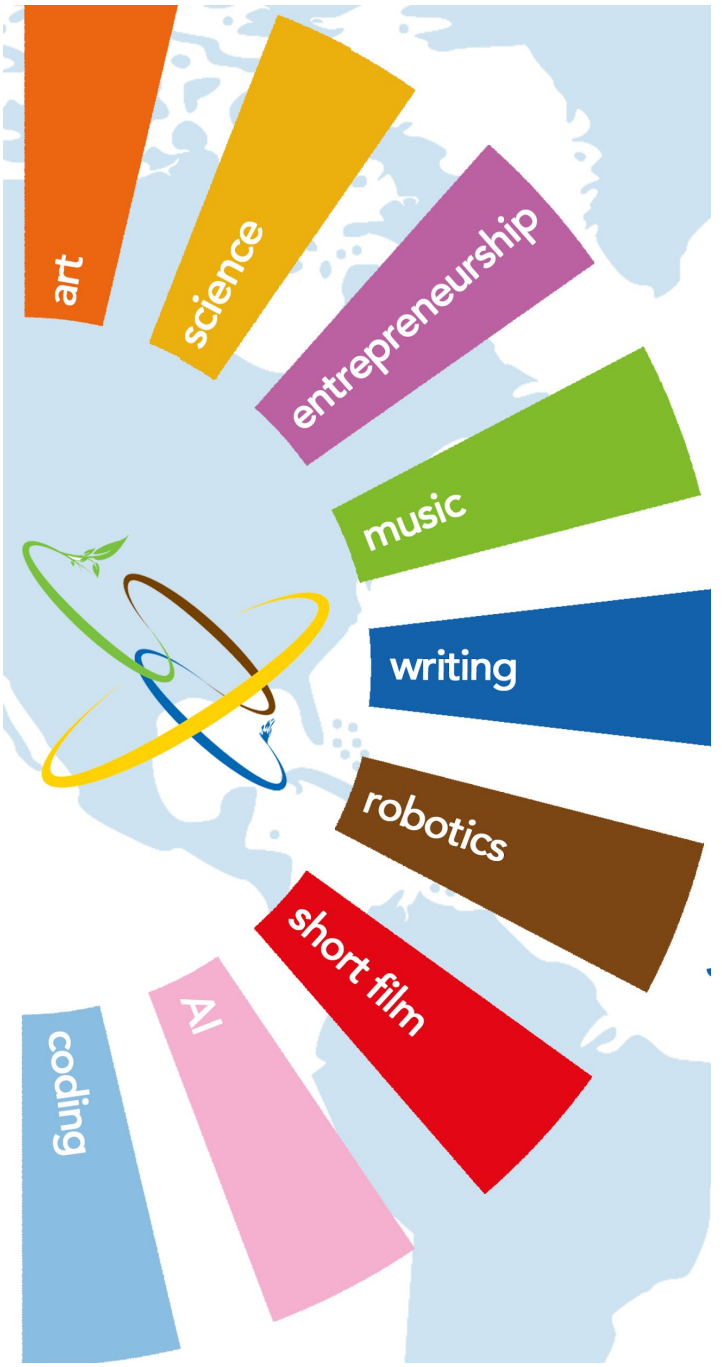

- Since 2011
- Hosted around 1400 participants in 2025 from 35+ states 70+ countries
- **Disciplines:** STEM, Coding, Robotics, AI, Speech, Entrepreneurship, Arts, Short Film, Music
- Applications start on December 1
- Application Deadline is March 1
- Finalists are announced by March 25
- Event is usually scheduled 2nd week of June
- Monday – Friday, includes a trip to Niagara Falls
- Hosted by large universities at Upstate New York
- Application Fee is $60/ project
- Participation Fee is $600/ person, w/ room and board
- Open buffet breakfast, lunch, and dinner
- Trip to Niagara Falls and boat tour is included
- **Instagram and Facebook @Geniusolympiad**
- For more information: **GENIUSOlympiad.org**
- Email: **info@geniusolympiad.org**

GENIUS Olympiad is organized by Terra Science and Education, a N.Y. based 501.c.3 non-profit organization dedicated for project-based learning

Marine Biology Research at Bahamas

Unique and exclusive partnership with the Gerace Research Center (GRC) in San Salvador, Bahamas to offer marine biology research opportunities for high school teachers and students.

- Terra has exclusive rights to offer the program to high school teachers and students around world.
- All trips entail extensive snorkeling in Bahamian reefs as well as other scientific and cultural activities.
- Terra will schedule the program with GRC and book the flights from US to the GRC site.
- Fees include travel within the US to Island, lodging, meals, and hotels for transfers, and courses.
- For more information, please visit terraed.org/bahamas.html

Terra is a N.Y. based 501.c.3 non-profit organization
dedicated for improving K-16 education

Table of Contents

May 2026| Volume 8| Issue 10

1 **Unraveling a CircRNA-MiRNA-mRNA Axis: A Potential Therapeutic Target for Non-small Cell Lung Cancer**
Sahil Patel

10 **Leveraging AI Chatbots for Adolescent Mental Health: Opportunities and Challenges**
Katherine Z. Xu

19 **Applications of CRISPR-Cas9 Genome Editing Technology in the Treatment of Human Diseases**
Elif Baser

31 **From Stars to Stairs: Multichoose, Generating Functions, and a Visual Bijection**
Jaeha Park

37 **Comparative Analysis of Pseudo-Random Binary Sequence Patterns for the High-Speed Digital Systems**
Jaechan Lee

44 **Symptom-Based Predictive Modeling of Retinal Detachment and Patient Response Behavior**
Mahi Kumar

50 **Epidemiological Study on the Evaluation of Adolescent Height Development and Its Multidimensional Influencing Factors**
Qiran Zhou, Jianfeng Long

57 **Finger Injuries among Adolescent Climbers: Causes, Prevention, and Rehabilitation**
Rohan Tare

63 **Adolescent Substance Use and Peer Influence**
Chloe Lee

69 **Investigating the Quality of Biodiesel Synthesized from Used Cooking Oils**
Navaj Nune

77 **Thermoelectric Performance of n-Type Argyrodite Ag_8GeTe_6 with Ultralow Lattice Thermal Conductivity and High Mobility Near Room Temperature**
Juyoung Chang, Runyu Che, Beomjun Kim, Chaemin Lee, Abhijit Debnath, Woo Rin Lee

83 **Migration-Driven Adaptations in Avian Species**
Arshi Aggarwal

94 **The Role of Epigenetics in Gene Regulation: A Study of Histone Modifications**
Vinayak Ramakrishnan

106 **Rebuilding Vision: Evaluating Biomaterials for Next-Generation Artificial Corneas**
Ayaan Cheema

Editorial Board

International Journal of High School Research

IJHSR
ijhighschoolresearch.org
RESEARCH ARTICLE

Unraveling a CircRNA-MiRNA-mRNA Axis: A Potential Therapeutic Target for Non-small Cell Lung Cancer

Sahil Patel

St. Anthony's High School, 275 Wolf Hill Road, Huntington Station, New York, 11747, USA; sahil.p.2008@gmail.com
Mentor: Madhav Subramanian

ABSTRACT: Non-small cell lung cancer (NSCLC) is the leading cause of cancer-related mortality, primarily attributed to NSCLC's early detection rate of approximately 19%. The circRNA-miRNA-mRNA pathway contributes to NSCLC and could be an optimal biomarker/target; its identification can significantly increase survival. From CircNET, CircFNDC3B was found to affect NSCLC development, miR-885-3p had a confidence rating of 3/3, and its target genes showed a significant impact on lung cancer patients' survival (p=0.011) on GEPIA 2 using LUAD and LUSC data sets. The TCGA lung data set was then downloaded into R, and using GSVA, the expression of miR-885-3p and specific genes was calculated. Using GEPIA 2, target gene MCM5 negatively correlated with miRNA expression in lung cancer patients (r = -0.281) and impacted NSCLC survival (p=0.0018). A gene ontology analysis on circFNDC3B and literature was then used to find GSEA gene sets. Enrichment scores were found using GSVA in R Studio with the TCGA lung data set. MCM5 expression was divided into high and low and was correlated with the GSEA gene set enrichment scores to identify differential expression within lung cancer. CircFNDC3B-miR-885-3p-MCM5 axis significantly regulates Ras protein signal transduction and IGF transport and uptake by IGFBP in NSCLC.
KEYWORDS: Biomedical and Health Sciences, Genetics and Molecular Biology of Disease, Non-Small Cell Lung Cancer, Circular RNA, MicroRNA, Messenger RNA.

Introduction

Non-small cell Lung Cancer:

Lung cancer is the second most commonly diagnosed cancer and the leading cause of cancer-related death. Non-small cell lung cancer (NSCLC) is the most common form of lung cancer, being about 85% of all diagnosed types, as stated by Huang *et al.*[1-3] Early diagnosis of NSCLC is vital for survival, drastically changing survival rates from approximately 75% in early diagnosed (stages zero, one, and two) NSCLC to less than 10% (stages three and four). However, early detection rates (detection of NSCLC in stages zero, one, and two) are drastically low at approximately 19%.[4,5] Recently, early detection has been improved by improvements in molecular-driven detection, primarily through regulatory RNAs acting as biomarkers.[6]

Current Biomarkers and Potential NSCLC Biomarkers:

Biomarkers play crucial roles in diagnosis, prognosis, and selection of treatment options. Identifying biomarkers can lead to an increase in early detection by faster diagnosis, and is also necessary for identifying the effectiveness of treatments and specific subtypes of cancers.[7] Circulating biomarkers are easy to measure and primarily consist of non-coding RNA (ncRNA), which are very sensitive and highly stable.[7] There are two main subtypes of ncRNA: long ncRNA and short ncRNA. MicroRNA (miRNA) is a form of short ncRNA and has a significant role in gene regulation through messenger RNA (mRNA) degradation.[8] Numerous research studies have found deregulated miRNAs within the plasma and serum of cancer patients, and over 2500 miRNAs have been identified as being involved in aspects of cancer development within humans.[9] miRNAs often show significant diagnostic value due to their strong specificity, high stability, and availability. This is due to miRNAs' presence in body fluids and regulation of many stages of cancer development.[10] Two miRNA signatures with the potential to be biomarkers for early diagnosis of lung cancer, miR-33a-5p and miR-128-3p, were identified. They found miR-33a-5p (AUC = 0.8644, 95% confidence interval (CI) = 0.8016 to 0.9271, sensitivity = 84.62% and specificity = 76.92%) and miR-128-3p (AUC = 0.9391, 95% CI = 0.9199 to 0.9835, sensitivity = 92.31% and specificity = 83.08%) to have a higher diagnostic value than traditional tumor markers. Traditional tumor markers within lung cancer showed lower diagnostic values such as cytokeratin-19-fragment (CYFR21-1) (AUC = 0.5856, 95% CI = 0.4387 to 0.7324, sensitivity = 63.33% and specificity = 63.33%), neuron-specific enolase (NSE) (AUC = 0.6189, 95% CI = 0.4748 to 0.763, sensitivity = 73.33% and specificity = 56.67%), and cancer antigen 72-4 (CA72-4) (AUC = 0.5206 95% CI = 0.3684 to 0.6727, sensitivity = 86.67% and specificity = 36.67%).[11] This suggests that miRNAs could potentially be used as biomarkers in lung cancer due to their greater ability to identify lung cancer than previously used biomarkers.[8] Further investigation found dysregulated miRNAs within NSCLC. Three miRNAs were specifically deregulated only in Lung Adenocarcinoma (LUAD); miR-6785-3p was upregulated, and miR-101-3p and miR-139-5p were downregulated. Five miRNAs were specifically deregulated in Lung Squamous Cell Carcinoma (LUSC); miRNA-21-3p and miRNA-650 were upregulated, and miRNA-95-5p, miRNA-4639-3p, and miR-744-3p were downregulated. Five miRNAs were commonly deregulated in both LUAD and LUSC; miR-7-5p was up-

DOI: 10.36838/IJHSR810.1

regulated, miR-140-3p, miR-144-3p, and miR-195-5p were downregulated, and miR-375 was seen to be upregulated in LUAD and downregulated in LUSC samples. This shows how different miRNAs can impact and affect specific tissues and cancer types, making them ideal for use as a cancer biomarker.[12] Circular RNA (circRNA) has been associated with interacting with miRNA in NSCLC through miRNA sponging. CircRNA has the potential to be an optimal biomarker/target due to its high stability and tissue specificity, showing potential for further investigation.[13,14]

CircRNAs' effect on NSCLC:

CircRNAs' properties of high resistance to exonuclease degradation lead to much greater stability compared to linear RNAs. CircRNAs are also highly specific in tissues and diseases, which can lead to increased concentrations in specific areas. CircRNA is often distinctly expressed in cancerous and noncancerous cells.[15] These traits lead circRNA to have the potential to be an optimal biomarker/target.

CircRNAs' functions within the cell are microRNA sponging, transcriptional regulation, acting as a protein template, and a few directly translating proteins.[16,17] CircRNAs' primary function is miRNA sponging; circRNA sponges the miRNA by having complementary binding sites. This then forms complexes through hybridization, forming a double-stranded molecule of two complementary single-stranded DNA/RNA molecules. Through circRNA sponging miRNA, the circRNA takes the miRNA away from its primary function of mRNA regulation. This process is often dysregulated due to the deregulation of circRNA, often by altered RNA back-splicing (upstream exon covalently links to the acceptor sequence of a downstream exon) and histone modifications. When this dysregulation occurs, the miRNA is up/downregulated, leading to down/upregulated mRNA; this affects gene expression regulation and causes adverse interactions with RNA-binding proteins (RBP), transcriptional factors, and other proteins, impacting other oncogenic pathways.[18] The dysregulation of the circRNA-miRNA-mRNA has been associated with cancer development through influencing proliferation, tumorigenesis, epithelial-to-mesenchymal transition (EMT), and metastasis.[19-21] Through identifying the circRNA-miRNA-mRNA pathway, knowledge is gained on the effects of particular molecules and the ability to use those molecules for early diagnosis and specific treatments. Due to the limited studies about the circRNA-miRNA-mRNA pathway and its known impacts on oncogenic traits, further investigation is needed.

CircRNA-miRNA-mRNA Pathways in NSCLC:

The dysregulation of the circRNA-miRNA-mRNA pathway leads to various oncogenic traits.[22] Many circRNA-miRNA-mRNA pathways have been found to influence NSCLC. The circ_HIPK3/miR149/Mammalian forkhead box transcription factor (FOXM1) pathway has been found to influence proliferation, migration, invasion, and apoptosis within lung cancer cells. Circ_HIPK3 was found to sponge miR-149, and miR-149 interacts with FOXM1, binding to the 3'UTR site. FOXM1 is a master regulator of tumor metastasis, giving miR-149 a tumor-suppressive role in lung cancer. Circ_HIPK3 has also been associated with regulating miR-124, which impacts target genes SphK1, STAT3, and CDK4 in other cancers.[19,20] Both the circP4HB/miR-113a-5p/vimentin axis and the circPTPRA/miR-96-5p/RASSF8 axis have been shown to lead to an increase in EMT and metastasis within NSCLC. Circ_0067934 regulates the miR-1182/KLF8 axis, influences the Wnt/beta-catenin pathway, and is associated with NSCLC development. Circ_000567/miR-421/TMEM100 axis is involved in the migration and invasion of lung adenocarcinoma.[21] F-circEA1 regulates its parental gene EML4-ALK, which is a fusion protein that impacts downstream signaling pathways such as RAS-RAF-MEK-ERK, P13K-AKT-mTOR, and JAK3-STAT3; the F-circEA1/EML4-ALK axis is involved in proliferation, migration, invasion, and tumor progression.[22] Circ-Foxo3 regulates its parent gene, Foxo3. The Circ-Foxo3/miR-155/Foxo3 axis has been found to influence cell proliferation, migration, and invasion with NSCLC cells.[23]

Circ_0020714/miR-30a-5p/SOX4 has been seen to be involved in immune evasion and resistance to antiPD-1 and showed potential use as an immunotherapeutic target in NSCLC.[24] The dysregulation of the circRNA-miRNA-mRNA pathway often affects multiple oncogenic pathways and traits. Many signaling protein pathways influence NSCLC development, but often, how these pathways are deregulated, such as by circRNA-miRNA-mRNA pathways, and ways to inhibit these pathways are limited. Rat Sarcoma (Ras) pathway and upregulation of the P13k/AKT/mTOR pathway have been involved in proliferation within NSCLC; the inhibition of these pathways has been seen to reduce proliferation.[25,26] Histone deacetylase 1 (HDAC1) has been observed to affect EMT-dependent malignant progression of NSCLC through the influence of MCM5. Abnormal interactions of MCM5 and HDAC1 lead to the downregulation of E-cadherin and upregulation of Vimentin and MMPs; this causes EMT-related tumor metastasis, as seen in Figure 1.[27] Insulin-like growth factor binding protein 3 (IGFBP3) acts as a tumor suppressor by performing its primary function of binding to insulin-like growth factor 1 (IGF1). IGF1 binds to insulin-like growth factor receptor 1 (IGFR1), activating the P13k/AKT/mTOR pathway, stimulating cell growth, and blocking apoptosis. Increases in IGF1 concentrations are associated with increased metastasis and tumorigenesis. This means that downregulated IGFBP3 is associated with an increase in metastasis and tumorigenesis, as illustrated in Figure 1.[28]

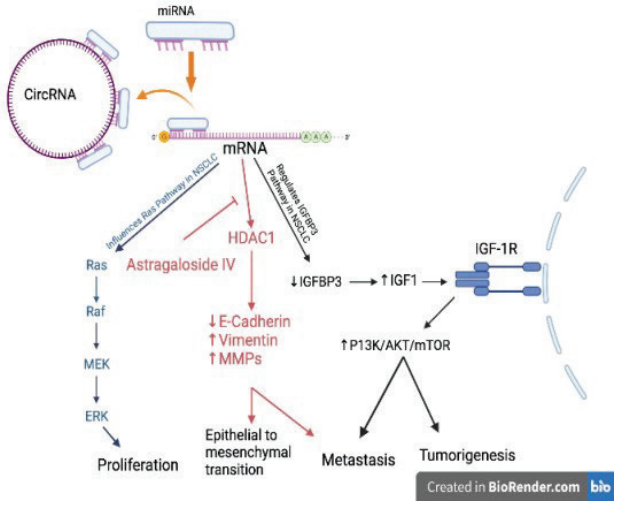

Figure 1: Dysregulated circRNA-miRNA-mRNA pathway. The effects of a dysregulated circRNA-miRNA-mRNA pathway potentially have in NSCLC development through the Ras, HDAC1, and IGFBP3 pathways. The dysregulated circRNA abnormally increases sponging of the miRNA, taking away the miRNAs' ability to suppress the mRNA, leading to a cascade of different gene pathways.

The circRNA-miRNA-mRNA pathways have been associated with regulating signaling pathways that influence oncogenic development. Investigating circRNA-miRNA-mRNA pathways can expand our understanding of cancer development and potentially lead to biomarkers or therapeutic targets in the future.

Objectives:

CircRNA has been recently associated with influencing NSCLC development primarily through the circRNA-miRNA-mRNA pathway. Diagnosis in the late stages of NSCLC has been associated with increased mortality; fully elucidating an influential circRNA-miRNA-mRNA pathway within NSCLC can give rise to biomarkers/therapeutic targets, increasing early detection rates and survival. The first objective is to identify a circRNA with high expression in NSCLC and a high-confidence miRNA target, which impacts the survival of NSCLC patients. This establishes a circRNA-miRNA pathway involved in NSCLC. The second objective is to identify the miRNA-mRNA interactions that are involved in NSCLC survival. The third and last objective is to find the mRNA's biological functions and determine the mRNA's impact on NSCLC. These objectives contribute to the elucidation of a circRNA-miRNA-mRNA pathway involved in NSCLC.

Methods

Identifying the circRNA-miRNA axis with influence on NSCLC survival:

CircNET, a database that analyzes circRNA regulatory networks in cancers, was used to find the most highly expressed circRNA (n=50) in lung cancer.[29] With this, a Gene Ontology (GO) Analysis was run to identify the circRNA's functionality in lung cancer. For each circRNA, the miRNAs it influences were analyzed to find a three-tool (PITA, miRanda, and TargetScan) confidence-level miRNA (n=14). This establishes a circRNA-miRNA regulatory network with confidence in three out of three tool types. Using the three tools, confidence miRNA, and its target genes were loaded into Gene Expression Profiling Interactive Network 2 (GEPIA 2), a database that uses The Cancer Genome Analysis (TCGA) and Genotype-Tissue Expression (GTEx) data to analyze genes in cancers.[30] Using the Lung Adenocarcinoma (LUAD) and Lung Squamous cell carcinoma (LUSC) data sets, which constitute >85% of NSCLC, a Kaplan-Meier graph (log-rank test) was created of the target genes of the miRNA.[3] This was done to determine the miRNAs' effect on NSCLC survival rates. To determine the circRNA-miRNA axis with a significant impact on NSCLC, an evaluation of the Kaplan-Meier graphs was performed to identify p-values less than the alpha value of 0.05. The selection was based on circRNA abundance, miRNA confidence, and miRNA impact/significance on NSCLC.

Identifying the target miRNA-mRNA pathway with significant influence in NSCLC:

First, CircNET was used to identify the mRNA targets of the miRNA. A detailed literature review was then conducted to identify potential mRNAs influenced by the miRNA that have an impact on cancers. GEPIA 2 was then used to identify the mRNA expression in lung cancer compared to normal lung cells; 0.5 was the Log2FC Cutoff, and the p-value was set to 0.05. Then, TCGAs' lung datasets (n = 1129) were loaded into R Studio, and the Gene Set Variation Analysis (GSVA) package was used to calculate the enrichment of gene signatures within the dataset.[31] Using GSVA, the enrichment of miRNA target genes and specific genes in NSCLC was found. After obtaining the enrichment values of the miRNA target genes and specific genes, they were loaded into an Excel sheet. The miRNA target genes enrichment values were then multiplied by -1. This is because GSVA found the enrichment of the targets of the miRNA by multiplying by -1, the proxy for miRNA expression is found; this is due to miRNA regulating its target gene, so as one increases, the other must decrease. A Pearson correlation coefficient was then found using the proxy miRNA enrichment and specific gene enrichment value in Excel. The mRNA with a significant negative correlation was identified using the correlation coefficient. Then, I ran GEPIA 2 and created a Kaplan-Meier graph to identify a specific mRNA influencing NSCLC with a p-value of <0.05. The mRNA with increased expression in lung cancer versus normal lung cells had a significant negative correlation with the given miRNA and was seen to influence NSCLC survival significantly. It was then picked for further analysis.

Identifying the functionality of the circRNA-miRNA-mRNA pathway in NSCLC:

Using the GO analysis of the circRNA function and previous literature, Gene Set Enrichment Analysis (GSEA) gene sets (n=22) were found based on functions within cancerous cells that align with the individual circRNA, miRNA, and mRNA functions previously established in the literature. Using the GSEA gene set, all genes in the sets were composed in an Excel sheet, and a GSVA was run in R Studio to find enrich-

DOI: 10.36838/IJHSR810.1

ment values of the gene sets in NSCLC.[32,33] These enrichment values and mRNA enrichment values were then placed into an Excel sheet, and the top 50% highest mRNA expression in each gene set was found. After finding the values, PRISM was used to place the enriched genes of the gene set that are in the top 50% of mRNA expression under high expression and the bottom 50% under low expression to create scatter dot plots and run t-tests to obtain p-values. These graphs were then used to assess the mRNAs' function in NSCLC. Identifying significant differential expression between low and high expression of mRNA showed that the circRNA-miRNA-mRNA axis influenced the particular function within NSCLC.

Justification of Methods:

Databases and Datasets were used due to their validity, reliability, feasibility, and sample size. The use of databases and datasets allowed for the analysis of data with a far greater sample size than in vitro/vivo experimentation would have allowed. The TCGA lung data set allowed for the use of 1129 patient data; if done in vitro/vivo, it would have taken many years for this study to occur due to permissions needed and costly tests required.

A study by Lin-lin Zhang and colleagues used a methodology similar to my research regarding the analysis of an mRNA, Minichromosome maintenance complex component 5 (MCM5), and its effects on Lung cancer.[27] Lin-Lin Zhang and colleagues aimed to identify MCM5 interaction with HDAC1 and the effects of this interaction on EMT-dependent malignant progression in Lung cancer. Using TCGA data, they compared MCM5 expression in Lung adenocarcinoma and Lung squamous cell carcinoma to normal and found the effects of MCM5 on lung adenocarcinoma survival. My study used a similar methodology, using Kaplan-Meier survival graphs and comparing cancer versus normal cells. My research differed, however, by using TCGA and GTEx data and comparing RNAs to NSCLC, increasing validity by increasing sample size and comparing RNAs to NSCLC, not just lung adenocarcinoma. My study also uses this data in a different context, using it in regard to the circRNA-miRNA-mRNA pathway rather than mRNA-mRNA interactions.

■ Results and Discussion

CircFNDC3B-miR-885-3p is highly expressed in NSCLC and is associated with decreased survival:

According to circNET, CircFNDC3B was found to be the highest expressed circRNA in lung cancer cells, as documented in Table 1. Using circNET, a Gene Ontology analysis was run on CircFNDC3B to identify its functionality in lung cancer. CircFNDC3B was seen to primarily contribute to the regulation of cell morphogenesis, Ras protein signal transduction, gland development, histone modification, and endomembrane system organization, as presented in Figure 2. CircFNDC3B was seen to show 3/3 tool confidence with miRNA-885-3p, meaning that miRNA-885-3p was predicted to be sponged by CircFNDC3B through all three tools (PITA, miRanda, TargetScan). Using GEPIA 2, miR-885-3p's target genes were then used to identify the impact the circFNDC3B-miR-885-3p axis has on NSCLC survival rate. CircFNDC3B-miR-8853p was seen to affect NSCLC survival significantly (p=0.011). Figure 3 shows that dysregulated expression of miR-885-3p led to decreased patient survival.

Table 1: Top 10 highest circRNAs expressed in lung cancer. CircFNDC3B showed the highest amount of expression compared to other circRNAs within lung cancer.

Top	CircRNA (Host Gene)	Expression
1	CircFNDC3B	2208
2	CircCDR1	2105
3	CircFAM13B	989
4	CircCAMSAP1	986
5	CircUBXN7	868
6	CircGSE1	808
7	CircHIPK3	778
8	CircXPO1	771
9	CircSCMH1	747
10	CircCDKAL1	685

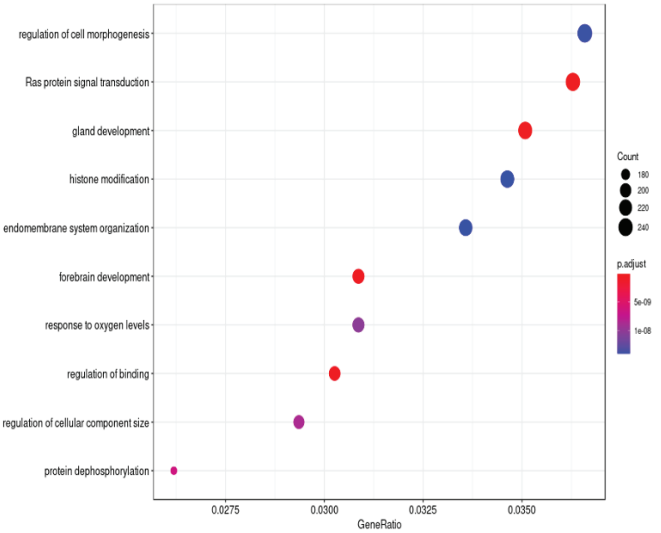

Figure 2: Functions of CircFNDC3B. Gene Ontology Analysis through CircNET to find the functionality of the circRNA-miRNA axis. The gene ratio indicates that circFNDC3B influenced enriched genes over total genes in the given pathway. As the count/size of the point increases, the amount of CircFNDC3B is seen to increase. Regulation of cell morphogenesis and Ras protein signal transduction showed the strongest influence from CircFNDC3B.

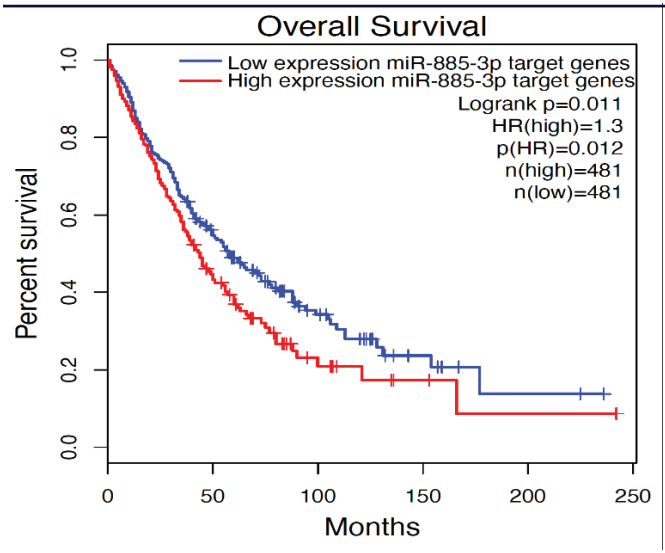

Figure 2: Overall median Kaplan-Meier graph of miR-885-3p target genes in NSCLC. Using TCGA data (LUAD and LUSC), the miR-885-3p effect in NSCLC survival was analyzed. Within LUAD and LUSC, miR-885-3p showed influence with high expression, leading to a significant increase in mortality.

CircRNA-miRNA interactions through circRNA sponging of miRNA have been seen to correlate with cancer development, from the upregulation of circRNA causing downregulation of the miRNA, leading to abnormal expression of mRNA.[34,35] CircFNDC3B has previously been correlated with being involved in cancer and disease progression.[36] CircFNDC3B is seen to exhibit characteristics of more stability, conservatism, and tissue/developmental specificity compared to linear FNDC3B.[37] In this study, CircFNDC3B was the highest expressed circRNA in lung cancer. CircFNDC3B was found to possess many functions within lung cancer, including the regulation of cell morphogenesis, Ras protein signal transduction, gland development, histone modification, and endomembrane system organization, showing the highest involvement of circFNDC3B. CircFNDC3B showed three out of three tool confidence with miR-885-3p; this correlates circFNDC3B activity with miR-885-3p, making the circFNDC3B-miR-885-3p axis. miR-885-3p has been associated with tumorigenesis within LUAD and targets the Wnt10b/βcatenin signaling pathway by regulation from circRNAs.[38] In this study, when miR-885-3p target genes were found to be increased in expression, the NSCLC survival rate decreased. This shows that circFNDC3BmiR-885-3p has a potential influence on NSCLC survival.

mRNA-MCM5 shows high expression in NSCLC and is associated with decreased survival:

MCM5 was found to be an important target of miRNA-885-3p. Previous literature showed MCM5 to have a major impact on EMT and metastasis in NSCLC, as documented in Table 2. Gepia 2, a database that uses TCGA and GTEx data, was used to find MCM5's expression in NSCLC. MCM5 was found to be significantly upregulated in LUAD and LUSC cells compared to normal lung tissue, as indicated in Figure 4. Using GSVA and TCGA lung cancer datasets (n=1129), enrichment scores were calculated for miR-885-3p target genes. To estimate miRNA activity, a proxy for miR-885-3p was generated by multiplying the target gene enrichment score by -1. Importantly, this proxy does not represent physical concentrations of miR-885-3p, but the inferred collective suppressive activity of its target gene set, reflecting functional miRNA activity at the transcriptional level. Figure 5 shows MCM5 to have a significant negative correlation with miRNA-885-3p, with a correlation of -0.281. Although statistically significant, this correlation is modest in strength, reflecting the biological complexity of MCM5 regulation and the fact that miR-885-3p contributes only partially to MCM5 expression variability. To find MCM5's impact on NSCLC, TCGA data were used to find the dysregulation of MCM5 to significantly decrease NSCLC survival, as exemplified in Figure 6 (p=0.0018).

Table 2: miRNA targets genes. The genes listed showed potential for research in NSCLC. Further investigation was conducted with each miRNA target gene; MCM5 showed the best results.

miRNA target mRNAs	NSCLC relationship
Aurora A	Associated with chemoresistance and metastasis [29]-[30]
CDK6	Overexpression is associated with tumorigenesis and EMT [31]-[32]
KRT8	Upregulation in tumors causes cell migration, cell adhesion, and drug resistance [33]
MCM5	Major role in metastasis and EMT through means of epigenetic regulation [27] and [34]
PFN1	Promotes stemness and tumor-initiating ability of cancer cells [35]-[36]

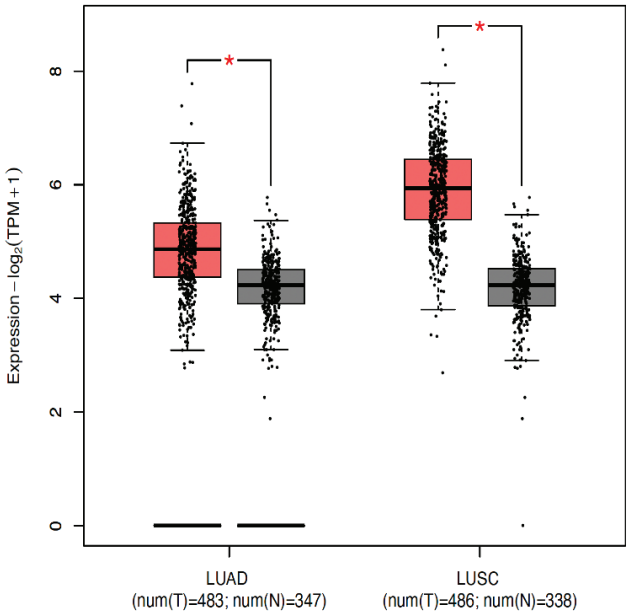

Figure 4: MCM5 expression in TCGA and GTEx NSCLC. MCM5 is significantly expressed in NSCLC compared to normal lung cells (*=<0.05). Red = Tumor lung cell; Grey = Normal lung cell.

DOI: 10.36838/IJHSR810.1

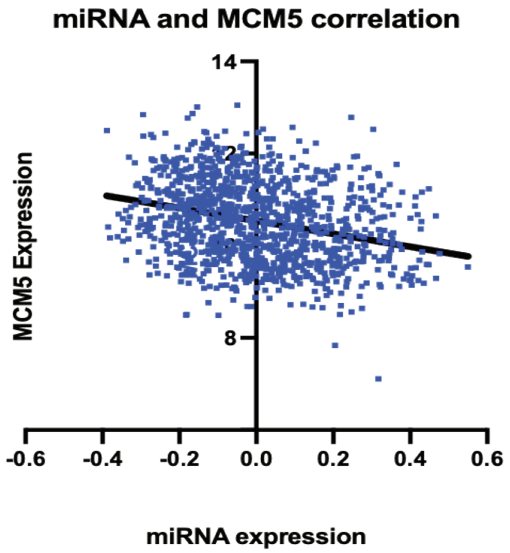

Figure 5: Correlation scatter plot. Correlation of -0.281 between miRNA target genes and MCM5 gene influence in NSCLC using TCGA data (n=1129). As miRNA-885-3p concentration increases, MCM5 concentration decreases and vice versa, indicating an inverse relationship and potentially confirming an influence on each other's expression.

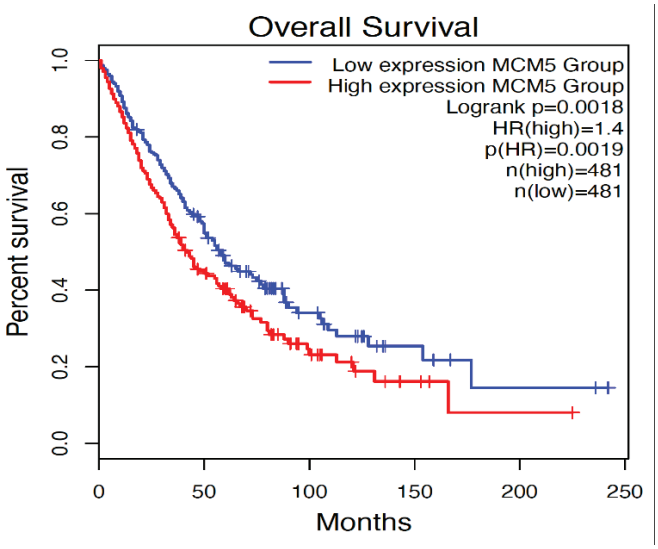

Figure 6: Overall median Kaplan-Meier graph of MCM5 on NSCLC. Using TCGA data (LUAD and LUSC), the effect of mRNA MCM5s on survival was analyzed. High expression of MCM5 was seen to significantly increase mortality rates.

A literature review of miR-885-3p's target genes was performed, and MCM5 was found to show a potential influence on cancer progression. MCM5 was seen to have a significant role in metastasis and EMT by epigenetic regulation.[27, 44] MCM5 expression in LUAD and LUSC using both TCGA and GTEx datasets showed that MCM5 is more highly expressed in LUAD and LUSC compared to normal lung tissue. MCM5 was also previously found to be more highly expressed in both LUAD and LUSC compared to normal lung tissue, although only using TCGA data.[27] MCM5 is seen to be negatively correlated with miR-885-3p; this means that as there is an increase in miR-885-3p, there is a decrease in MCM5 expression. MCM5 was then found to impact lung cancer survival when dysregulated. This means that miR-885-3p's regulation of MCM5 causes an increase in survival, but when circFNDC3B sponges miR-885-3p, it causes a decrease in expression, leading to a decrease in the regulation of MCM5 and increased expression of MCM5, causing oncogenic properties.

MCM5 shows involvement in potential oncogenic pathways:

MCM5 functionality is vital to understanding the circFNDC3B-miR-885-3p-MCM5s' impact on NSCLC. GSEA datasets were obtained using circFNDC3B's GO analysis and literature; the GSEA datasets correlate with circFNDC3B, miR-885-3p, and MCM5s' previously established functions. GSVA scores were produced to show MCM5s' high and low expression in pathways associated with circFNDC3B and NSCLC development. MCM5 showed significant differential expression between high and low expression in Ras protein signal transduction and regulation of Insulin-like growth factor (IGF) transport and uptake by Insulin-like growth factor binding proteins (IGFBP), as seen in Figures 7 and 8, respectively.

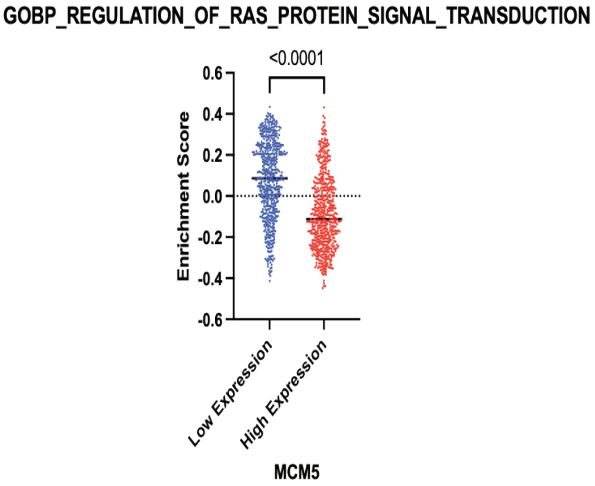

Figure 7: MCM5 expression in Ras protein signal transduction within NSCLC. MCM5 showed significant differential expression when compared to enriched genes involved in Ras protein signal transduction in NSCLC.

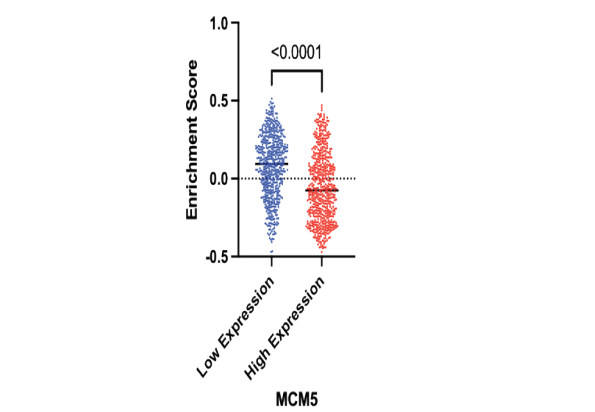

Figure 8: MCM5 expression in the regulation of insulin-like growth factor (IGF) transport and uptake by insulin-like growth factor binding proteins (IGFBP). MCM5 showed significant differential expression when compared to the enriched genes involved in IGF transport and uptake by IGFBPs in NSCLC.

The influence of MCM5 in pathways within NSCLC was then found. MCM5 was seen to significantly influence Ras protein signal transduction and regulation of IGF transport and uptake by IGFBPs. The dysregulation of Ras protein signal transduction has been associated with aggression and cellular proliferation.[47] Dysregulation of IGF transport and uptake by IGFBPs has been associated with EMT and metastasis.[48,49]

Conclusion

Overall, it was found that the CircFNDC3B/miR-885-3p/MCM5 pathway is potentially associated with NSCLC survival through significant regulation of Ras protein signal transduction and IGF transport and uptake by IGFBPs. Through the identification of the circFNDC3B/miR-885-3p/MCM5 pathway within NSCLC, knowledge has been gained of the newly emerged circRNA/miRNA/mRNA regulatory pathways, helping us understand the roles of specific RNA interactions within lung cancer.[50]

Limitations:

A potential limitation of this research is the use of datasets and databases; this is due to only using precomposed data from other scientists, which could lead to flawed results. To attempt to combat this, only highly credible and widely used datasets and databases that had the support of many studies and research from the past were chosen. The use of these datasets and databases was necessary for time, money, resources, and validity purposes. Obtaining patient lung cancer data with a large sample size would have been a complex and tedious process, taking many years to complete.

Further Research

There are many ways in which this research could be continued. Further identifying the positive correlations within the CircFNDC3B-miR-885-3p-MCM5 pathways can lead to potential biomarkers/therapeutic targets in the future to help increase NSCLC early detection rates, therefore increasing survival.

Further investigation should be done on excluded circRNAs, miRNAs, and mRNAs from NSCLC. Identifying the connections between them and the potential for pathways influencing oncogenic factors is vital for the growth of knowledge and understanding of how different pathways and RNAs interact with each other in cancers.

Further investigations should be done with the MCM5-Ras and MCM5-IGFBP interactions to determine further medical applications. This would help further correlate the interactions between the circFNDC3B-miR-885-3p-MCM5 pathway and its functions within NSCLC.

As well as the testing of potential inhibitors of this pathway for use as a biological target in the future. Astragaloside IV is a chemical compound often seen as having a protective effect on the lung; it has been found that Astragaloside IV can block interactions between HDAC1 and MCM5, inhibiting the progression of malignant lung cancer.[27]

Applications:

A potential application for this research would be the early detection of NSCLC through liquid biopsies. CircRNAs are highly abundant due to their resistance to exonuclease degradation, stability, and specificity. Due to this, they are considered novel biomarkers for liquid biopsies.[51] The presence of circRNAs in biofluids has been associated with cancer progression. This can make testing more common, helping people get diagnosed at early stages due to non-invasive and safe testing. Microarray testing is also a promising way to test for cancer development; knowledge of the circRNA axis developed in this study is beneficial, as microarray testing can only investigate known circRNAs.

Another potential application of this research is the development of therapeutic targets for NSCLC. Due to circRNAs' high resistance to exonuclease degradation and high specificity, it is seen as an optimal target.

Another application is the use of this potential axis in future research to develop further pathways and expand our knowledge of how RNAs and RNA pathways interact to cause cancer metastasis, tumorigenesis, proliferation, and more.

Acknowledgments

Thank you to Madhav Subramanian, Dr. Serena McCalla, and Mr. Paul Paino for your guidance during the development of this project.

References

1. Huang, J.; Deng, Y.; Tin, M. S.; Lok, V.; Ngai, C. H.; Zhang, L.; Lucero-Prisno, D. E.; Xu, W.; Zheng, Z.-J.; Elcarte, E.; Withers, M.; Wong, M. C. S. Distribution, Risk Factors, and Temporal Trends for Lung Cancer Incidence and Mortality. *Chest* **2022**, *161* (4), 1101–1111. https://doi.org/10.1016/j.chest.2021.12.655.
2. Sung, H.; Ferlay, J.; Siegel, R. L.; Laversanne, M.; Soerjomataram, I.; Jemal, A.; Bray, F. Global Cancer Statistics 2020: GLOBOCAN Estimates of Incidence and Mortality Worldwide for 36 Cancers in 185 Countries. *CA: a Cancer Journal for Clinicians* **2021**, *71* (3), 209–249.
3. Alduais, Y.; Zhang, H.; Fan, F.; Chen, J.; Chen, B. Non-Small Cell Lung Cancer (NSCLC): A Review of Risk Factors, Diagnosis, and Treatment. *Medicine* **2023**, *102* (8), e32899. https://doi.org/10.1097/md.0000000000032899.
4. Li, C.; Wang, H.; Jiang, Y.; Fu, W.; Liu, X.; Zhong, R.; Cheng, B.; Zhu, F.; Xiang, Y.; He, J.; Liang, W. Advances in Lung Cancer Screening and Early Detection. *Cancer Biology & Medicine* **2022**, *19* (5), 591–608. https://doi.org/10.20892/j.issn.2095-3941.2021.0690.
5. Zhang, C.; Ma, L.; Niu, Y.; Wang, Z.; Xu, X.; Li, Y.; Yu, Y. Circular RNA in Lung Cancer Research: Biogenesis, Functions, and Roles. *International Journal of Biological Sciences* **2020**, *16* (5), 803–814. https://doi.org/10.7150/ijbs.39212.
6. Liu, S.-Y. M.; Zheng, M.-M.; Pan, Y.; Liu, S.-Y.; Li, Y.; Wu, Y.-L. Emerging Evidence and Treatment Paradigm of Non-Small Cell Lung Cancer. *Journal of Hematology & Oncology* **2023**, *16* (1). https://doi.org/10.1186/s13045-023-01436-2.
7. Juan Carlos Restrepo; Dueñas, D.; Corredor, Z.; Liscano, Y. Advances in Genomic Data and Biomarkers: Revolutionizing NSCLC Diagnosis and Treatment. *Cancers* **2023**, *15* (13), 3474–3474. https://doi.org/10.3390/cancers15133474.

DOI: 10.36838/IJHSR810.1

8. Condrat, C. E.; Thompson, D. C.; Barbu, M. G.; Bugnar, O. L.; Boboc, A.; Cretoiu, D.; Suciu, N.; Cretoiu, S. M.; Voinea, S. C. miRNAs as Biomarkers in Disease: Latest Findings Regarding Their Role in Diagnosis and Prognosis. *Cells* **2020**, *9* (2). https://doi.org/10.3390/cells9020276.
9. He, Y.; Lin, J.; Kong, D.; Huang, M.; Xu, C.; Kim, T.-K.; Etheridge, A.; Luo, Y.; Ding, Y.; Wang, K. Current State of Circulating MicroRNAs as Cancer Biomarkers. *Clinical Chemistry* **2015**, *61* (9), 1138–1155. https://doi.org/10.1373/clinchem.2015.241190.
10. Smolarz, B.; Durczyński, A.; Romanowicz, H.; Szyłło, K.; Hogendorf, P. MiRNAs in Cancer (Review of Literature). *International Journal of Molecular Sciences* **2022**, *23* (5), 2805. https://doi.org/10.3390/ijms23052805.
11. Pan, J.; Zhou, C.; Zhao, X.; He, J.; Tian, H.; Shen, W.; Han, Y.; Chen, J.; Fang, S.; Meng, X.; Jin, X.; Gong, Z. A Two-MiRNA Signature (MiR-33a-5p and MiR-128-3p) in Whole Blood as Potential Biomarker for Early Diagnosis of Lung Cancer. *Scientific Reports* **2018**, *8* (1), 16699. https://doi.org/10.1038/s41598-01835139-3.
12. Petkova, V.; Marinova, D.; Kyurkchiyan, S.; Stancheva, G.; Mekov, E.; Kachakova-Yordanova, D.; Slavova, Y.; Kostadinov, D.; Mitev, V.; Kaneva, R. MiRNA Expression Profiling in Adenocarcinoma and Squamous Cell Lung Carcinoma Reveals Both Common and Specific Deregulated MicroRNAs. *Medicine* **2022**, *101* (33), e30027. https://doi.org/10.1097/md.0000000000030027.
13. Sufianov, A.; Begliarzade, S.; Beilerli, A.; Liang, Y.; Ilyasova, T.; Beylerli, O. Circular RNAs as Biomarkers for Lung Cancer. *Non-coding RNA Research* **2023**, *8* (1), 83–88. https://doi.org/10.1016/j.ncrna.2022.11.002.
14. Wang, F.; Yu, C.; Chen, L.; Xu, S. Landscape of Circular RNAs in Different Types of Lung Cancer and an Emerging Role in Therapeutic Resistance (Review). *International Journal of Oncology* **2022**, *62* (2). https://doi.org/10.3892/ijo.2022.5469.
15. Zhang, Z.; Yang, T.; Xiao, J. Circular RNAs: Promising Biomarkers for Human Diseases. *EBioMedicine* **2018**, *34*, 267–274. https://doi.org/10.1016/j.ebiom.2018.07.036.
16. Zhou, W.-Y.; Cai, Z.-R.; Liu, J.; Wang, D.-S.; Ju, H.-Q.; Xu, R.-H. Circular RNA: Metabolism, Functions and Interactions with Proteins. *Molecular Cancer* **2020**, *19* (1). https://doi.org/10.1186/s12943-020-01286-3.
17. Liu, Y.; Wang, L.; Liu, W. Roles of CircRNAs in the Tumorigenesis and Metastasis of HCC: A Mini Review. *Cancer Management and Research* **2022**, *Volume 14*, 1847–1856. https://doi.org/10.2147/cmar.s362594.
18. Li, J.; Zhang, Q.; Jiang, D.; Shao, J.; Li, W.; Wang, C. CircRNAs in Lung Cancer- Role and Clinical Application. *Cancer Letters* **2022**, *544*, 215810. https://doi.org/10.1016/j.canlet.2022.215810.
19. Kim, W. R.; Park, E. G.; Lee, D. H.; Lee, Y. J.; Bae, W. H.; Kim, H.-S. The Tumorigenic Role of Circular RNAMicroRNA Axis in Cancer. *International Journal of Molecular Sciences* **2023**, *24* (3), 3050. https://doi.org/10.3390/ijms24033050.
20. Lu, H.; Han, X.; Ren, J.; Ren, K.; Li, Z.; Sun, Z. Circular RNA HIPK3 Induces Cell Proliferation and Inhibits Apoptosis in Non-Small Cell Lung Cancer through Sponging MiR-149. *Cancer Biology & Therapy* **2019**, *21* (2), 113–121. https://doi.org/10.1080/15384047.2019.1669995.
21. Guo, L.; Jia, L.; Luo, L.-L.; Xu, X.; Xiang, Y.; Ren, Y.; Ren, D.; Shen, L.; Liang, T. Critical Roles of Circular RNA in Tumor Metastasis via Acting as a Sponge of MiRNA/IsomiR. *International Journal of Medical Science* **2022**, *23* (13), 7024–7024. https://doi.org/10.3390/ijms23137024.
22. Huo, Y.; Tangfeng Lv; Ye, M.; Zhu, S.; Liu, J.; Liu, H.; Song, Y. F-CircEA1 Regulates Cell Proliferation and Apoptosis through ALK Downstream Signaling Pathway in Non-Small Cell Lung Cancer. *Human Cell* **2021**, *35* (1), 260–270. https://doi.org/10.1007/s13577-021-00628-7.
23. Wei, J.; Li, M.; Xue, C.; Chen, S.; Zheng, L.; Deng, H.; Tang, F.; Li, G.; Xiong, W.; Zeng, Z.; Zhou, M. Understanding the Roles and Regulation Patterns of CircRNA on Its Host Gene in Tumorigenesis and Tumor Progression. *Experimental and Clinical Cancer Research* **2023**, *42* (1). https://doi.org/10.1186/s13046-023-02657-6.
24. Wu, J.; Zhu, M.-X.; Li, K.-S.; Peng, L.; Zhang, P.-F. Circular RNA Drives Resistance to Anti-PD-1 Immunotherapy by Regulating the MiR-30a-5p/SOX4 Axis in Non-Small Cell Lung Cancer. *Cancer Drug Resistance* **2022**, *5* (2). https://doi.org/10.20517/cdr.2021.100.
25. Fu, N.; Xi, R.; Shi, X.; Li, R.; Zhang, Z.; Li, L.; Zhang, G.; Wang, F. Hexachlorophene, a Selective SHP2 Inhibitor, Suppresses Proliferation and Metastasis of KRAS-Mutant NSCLC Cells by Inhibiting RAS/MEK/ERK and PI3K/AKT Signaling Pathways. *Toxicology and Applied Pharmacology* **2022**, *441*, 115988. https://doi.org/10.1016/j.taap.2022.115988.
26. Tan, A. C. Targeting the PI3K/Akt/mTOR Pathway in Non-Small Cell Lung Cancer (NSCLC). *Thoracic Cancer* **2020**, *11* (3), 511–518. https://doi.org/10.1111/1759-7714.13328.
27. Zhang, L.-L.; Li, Q.; Zhong, D.; Zhang, W.; Sun, X.; Zhu, Y. MCM5 Aggravates the HDAC1-Mediated Malignant Progression of Lung Cancer. *Frontiers in Cell and Developmental Biology* **2021**, *9*. https://doi.org/10.3389/fcell.2021.669132.
28. Kuhn, H.; Frille, A.; Petersen, M. A.; Oberhuber-Kurth, J.; Hofmann, L.; Gläser, A.; Taubenheim, S.; Klagges, S.; Kraemer, S.; Broschewitz, J.; von Laffert, M.; Wirtz, H. IGFBP3 Inhibits Tumor Growth and Invasion of Lung Cancer Cells and Is Associated with Improved Survival in Lung Cancer Patients. *Translational Oncology* **2023**, *27*, 101566. https://doi.org/10.1016/j.tranon.2022.101566.
29. Chen, Y.; Yao, L.; Tang, Y.; Jhong, J.-H.; Wan, J.; Chang, J.; Cui, S.; Luo, Y.; Cai, X.; Li, W.; Chen, Q.; Huang, H.-Y.; Wang, Z.; Chen, W.; Chang, T.-H.; Wei, F.; Lee, T.-Y.; Huang, H.-D. CircNet 2.0: An Updated Database for Exploring Circular RNA Regulatory Networks in Cancers. *Nucleic Acids Research* **2021**, *50* (D1), D93–D101. https://doi.org/10.1093/nar/gkab1036.
30. Tang, Z.; Kang, B.; Li, C.; Chen, T.; Zhang, Z. GEPIA2: An Enhanced Web Server for Large-Scale Expression Profiling and Interactive Analysis. *Nucleic Acids Research* **2019**, *47* (W1), W556–W560. https://doi.org/10.1093/nar/gkz430.
31. Goldman, M. J.; Craft, B.; Hastie, M.; Repečka, K.; McDade, F.; Kamath, A.; Banerjee, A.; Luo, Y.; Rogers, D.; Brooks, A. N.; Zhu, J.; Haussler, D. Visualizing and Interpreting Cancer Genomics Data via the Xena Platform. *Nature Biotechnology* **2020**, *38* (6), 675–678. https://doi.org/10.1038/s41587-020-0546-8.
32. Mootha, V. K.; Lindgren, C. M.; Eriksson, K.-F.; Subramanian, A.; Sihag, S.; Lehar, J.; Puigserver, P.; Carlsson, E.; Ridderstråle, M.; Laurila, E.; Houstis, N.; Daly, M. J.; Patterson, N.; Mesirov, J. P.; Golub, T. R.; Tamayo, P.; Spiegelman, B.; Lander, E. S.; Hirschhorn, J. N.; Altshuler, D. PGC-1α-Responsive Genes Involved in Oxidative Phosphorylation Are Coordinately Downregulated in Human Diabetes. *Nature Genetics* **2003**, *34*(3), 267–273. https://doi.org/10.1038/ng1180.
33. Subramanian, A.; Tamayo, P.; Mootha, V. K.; Mukherjee, S.; Ebert, B. L.; Gillette, M. A.; Paulovich, A.; Pomeroy, S. L.; Golub, T. R.; Lander, E. S.; Mesirov, J. P. Gene Set Enrichment Analysis: A Knowledge-Based Approach for Interpreting Genome-Wide Expression Profiles. *Proceedings of the National Academy of Sciences* **2005**, *102* (43), 15545–15550. https://doi.org/10.1073/pnas.0506580102.

34. Ma, Y.; Zou, H. Identification of the CircRNA-MiRNA-MRNA Prognostic Regulatory Network in Lung Adenocarcinoma. *Genes* **2022**, *13* (5), 885. https://doi.org/10.3390/genes13050885.
35. Huang, J.; Yu, S.; Ding, L.; Ma, L.; Chen, H.; Zhou, H.; Zou, Y.; Yu, M.; Lin, J.; Cui, Q. The Dual Role of Circular RNAs as MiRNA Sponges in Breast Cancer and Colon Cancer. *Biomedicines* **2021**, *9* (11), 1590. https://doi.org/10.3390/biomedicines9111590.
36. Sun, K.; Yao, H.; Zhang, P.; Sun, Y.; Ma, J.; Xia, Q. Emerging Landscape of CircFNDC3B and Its Role in Human Malignancies. *Frontiers in Oncology* **2023**, *13*. https://doi.org/10.3389/fonc.2023.1097956.
37. Kristensen, L. S.; Jakobsen, T.; Hager, H.; Kjems, J. The Emerging Roles of CircRNAs in Cancer and Oncology. Nature Reviews. *Clinical Oncology* **2022**, *19* (3), 188–206. https://doi.org/10.1038/s41571-021-00585-y.
38. Yang, Y.; Fan, X.; Nie, Y.; Liu, D.; Zhu, D.; Wu, K.; Zhang, Y.; Li, W.; Tian, X.; Wang, H.; Fan, Y. CircTUBGCP3 Facilitates the Tumorigenesis of Lung Adenocarcinoma by Sponging MiR-885-3p. *Cancer Cell International* **2021**, *21* (1). https://doi.org/10.1186/s12935-021-02356-2.
39. Cao, J.; Geng, J.; Chu, X.; Wang, R.; Huang, G.; Chen, L. MiRNA-885-3p Inhibits Docetaxel Chemoresistance in Lung Adenocarcinoma by Downregulating AuroraA. *Oncology Reports* **2018**, *41* (2). https://doi.org/10.3892/or.2018.6858.
40. Qian, F.; Lin, Y.; Zhang, M.; Guo, J.; Liu, Y. Circ_0061265 Competitively Binds to MicroRNA-885-3p to Promote the Development of Gastric Cancer by Upregulating AURKA Expression. *Cancer Cell International* **2022**, *22* (1). https://doi.org/10.1186/s12935-022-02646-3.
41. Gong, W.; Wang, L.; Zheng, Z.; Chen, W.; Du, P.; Zhao, H. Cyclin-Dependent Kinase 6 (CDK6) Is a Candidate Diagnostic Biomarker for Early Non-Small Cell Lung Cancer. *Translational Cancer Research* **2020**, *9* (1), 95–103. https://doi.org/10.21037/tcr.2019.11.21.
42. Lin, Z.; Zhou, Z.; Guo, H.; He, Y.; Pang, X.; Zhang, X.; Liu, Y.; Ao, X.; Li, P.; Wang, J. Long Noncoding RNA Gastric Cancer-Related LncRNA1 Mediates Gastric Malignancy through MiRNA-885-3p and Cyclin-Dependent Kinase 4. *Cell Death & Disease* **2018**, *9* (6). https://doi.org/10.1038/s41419-018-0643-5.
43. Xie, L.; Dang, Y.; Guo, J.; Sun, X.; Xie, T.; Zhang, L.; Yan, Z.; Amin, H.; Guo, X. High KRT8 Expression Independently Predicts Poor Prognosis for Lung Adenocarcinoma Patients. *Genes* **2019**, *10* (1), 36. https://doi.org/10.3390/genes10010036.
44. Mao, J.; Shen, J.; Lu, X.; Cai, Y.; Tao, R.; Deng, Y.; Zhang, Y.; Wu, Y.; Chen, W. MCM5 Is an Oncogene of Colon Adenocarcinoma and Promotes Progression through Cell Cycle Control. *Acta Histochemica* **2023**, *125* (6), 152072. https://doi.org/10.1016/j.acthis.2023.152072.
45. Jiang, C.; Ding, Z.; Joy, M.; Chakraborty, S.; Kim, S. H.; Bottcher, R.; Condeelis, J.; Singh, S.; Roy, P. A Balanced Level of Profilin-1 Promotes Stemness and Tumor-Initiating Potential of Breast Cancer Cells. *Cell Cycle* **2017**, *16* (24), 2366–2373. https://doi.org/10.1080/15384101.2017.1346759.
46. Wang, Y.; Wang, Y.; Wan, R.; Hu, C.; Lu, Y. Profilin 1 Protein and Its Implications for Cancers. *ONCOLOGY* **2021**, *35* (3507), 402–409. https://doi.org/10.46883/onc.2021.3507.0402.
47. Alam, M.; Hasan, G. M.; Eldin, S. M.; Adnan, M.; Riaz, M. B.; Islam, A.; Khan, I.; Hassan, Md. I. Investigating Regulated Signaling Pathways in Therapeutic Targeting of Non-Small Cell Lung Carcinoma. *Biomedicine & Pharmacotherapy* **2023**, *161*, 114452. https://doi.org/10.1016/j.biopha.2023.114452.
48. Kerr, A.; Baxter, R. C. Noncoding RNA Actions through IGFs and IGF Binding Proteins in Cancer. *Oncogene* **2022**, *41* (25), 3385–3393. https://doi.org/10.1038/s41388-022-02353-3.
49. Yang, X.; Bai, Q.; Chen, W.; Liang, J.; Wang, F.; Gu, W.; Liu, L.; Li, Q.; Chen, Z.; Zhou, A.; Long, J.; Tian, H.; Wu, J.; Ding, X.; Zhou, N.; Li, M.; Yang, Y.; Cai, J. M6A-Dependent Modulation via IGF2BP3/MCM5/Notch Axis Promotes Partial EMT and LUAD Metastasis. *Advanced Science* **2023**, *10* (25). https://doi.org/10.1002/advs.202206744.
50. Jia, S.; Yu, L.; Wang, L.; Peng, L. The Functional Significance of CircRNA/MiRNA/MRNA Interactions as a Regulatory Network in Lung Cancer Biology. *The International Journal of Biochemistry & Cell Biology* **2024**, *169*, 106548–106548. https://doi.org/10.1016/j.biocel.2024.106548.
51. Zhang, Y.; Wang, Y.; Su, X.; Wang, P.; Lin, W. The Value of Circulating Circular RNA in Cancer Diagnosis, Monitoring, Prognosis, and Guiding Treatment. *Frontiers in Oncology* **2021**, *11*. https://doi.org/10.3389/fonc.2021.736546.

Author

Sahil Patel, a senior at St. Anthony's High School, aspires to work in biomedical computation, specifically computational biology and AI/ML for medicine, as well as global health policy and biotech entrepreneurship. He is an incoming biomedical engineering student and Stamps Scholar at Georgia Institute of Technology. An Eagle Scout, exchange ambulance employee, varsity tennis captain, and president and co-founder of Listen to Lead, a 501(c)(3) nonprofit, he has interned at Cold Spring Harbor Laboratory in the Hammell Lab and at Hofstra University in the Lynch Lab, further advancing his interests in computational biology and biomedical research.

IJHSR
ijhighschoolresearch.org
REVIEW ARTICLE

Leveraging AI Chatbots for Adolescent Mental Health: Opportunities and Challenges

Katherine Z. Xu

Mountain View High School, 3535 Truman Ave, Mountain View, CA 94040; katherinezx27@gmail.com

ABSTRACT: There are increasing concerns about adolescents' mental health worldwide, which is characterized by a high prevalence of mental illnesses like depression and anxiety. The situation is further worsened by the present gap in adequate, affordable mental health care for this vulnerable group. In this context, artificial intelligence (AI), particularly through chatbots, presents a promising avenue to additional support. This paper summarizes the current overview of AI chatbots' role in managing youth mental health, their technology, features, and user experiences, and discusses their advantages and disadvantages. Then the article explores future developments, for example, improving crisis intervention capabilities, and discusses the need for stronger regulatory guidance. The conclusion emphasizes the need for responsible development and human oversight to fully make use of AI chatbots' potential in adolescent mental health.

KEYWORDS: Artificial Intelligence, Psychology, Chatbot, Mental Health, Adolescents/Teenagers.

Introduction

In recent years, mental health has become a significant public health problem, particularly for teenagers, who were especially affected by the COVID-19 pandemic.[1,2] The Substance Abuse and Mental Health Services Administration (SAMHSA) reported in 2021 that approximately 20.1% of 12- to 17-year-olds had experienced some depressive symptoms within the past year, [3] while the anxiety disorders affected 31.9% adolescents.[4] These data demonstrate how common the mental health conditions are among the youth and show that these conditions often first manifest in the teenage years. Given the fact that adolescence is a critical stage for an individual's development both physically and psychologically,[5] there is an urgent need to address this growing mental health crisis.

Teenagers also often face greater challenges than other age groups in accessing mental health support.[6,7] These barriers are the result of several factors, including cultural shame, treatment cost, appointment delays, privacy concerns, and limited access to mental health professionals.[8-10] The fear of privacy violations or being misunderstood is among the primary deterrents to youth who might otherwise seek help, and shortages of funding and mental health staff within schools further reduce the accessibility of care to adolescents.[7,11] Because of all of these, teenagers are hesitant to seek out mental health care.

Artificial Intelligence (AI), as a rapidly advancing technology, can potentially transform various fields. One application is in the Digital Mental Health Interventions (DHMIs), which can provide a scalable, readily accessible, and more affordable form of mental health services.[9,10,12] AI-powered chatbots are an example of a DHMI utilizing AI and are significant due to their potential to reach teenage populations. Younger generations are noted for their high engagement with digital technology and text-based communications.[7,13,14] Coupled with the anonymity that is being offered by chatbots, this digital solution removes several of the barriers faced by youth seeking help.[9,14] An initial interaction with an AI chatbot could serve as a critical first step for teenagers to acknowledge mental health challenges and eventually shift to more formal care.[10,13]

Although promising, chatbots for youth mental health present many challenges, especially to teenagers. For example, they are generally not equipped for crisis detection or intervention, and can delay escalation. They are still in their infancy, with little research focused on their performance and safety in youthful populations.[16,17] To understand the status of chatbots in managing adolescent mental health, selected databases (PubMed, EmBase and Google Scholar) were searched using a combination of keywords, including Artificial Intelligence, chatbot, conversational agents, digital health, mental health, adolescents, and teenagers in July 2025.

This article reviews how AI is being used to support youth mental health, especially for common conditions (e.g., anxiety, depression, and autism-related symptoms). Analyzing insight from psychology, computer science, and ethics, the review provides an overview of mental health chatbots for adolescents, introduces technology and features, considers chatbot pros and cons, and discusses future development opportunities as well as regulatory considerations. It lays the groundwork for future investigation and provides useful advice to youth, professionals, engineers, and policymakers interested in properly incorporating AI chatbots into mental health.

Discussion

Overview of mental health chatbots for adolescents:

Since their conception, chatbots have evolved significantly in terms of technological capabilities. ELISA was one of the most well-known and earliest AI chatbots created by Joseph Weizenbaum in 1966. It used a fairly straightforward rule-based program based on keyword matching and could ask open-ended questions and reflect user input.[18] It had the potential for

DOI: 10.36838/IJHSR810.10

human-computer dialogue and was a significant advancement at the time.

The advent of Natural Language Processing (NLP), Machine Learning (ML), and Large Language Models (LLMs) has since transformed chatbot capabilities. These advancements have made chatbots more capable of understanding, responding, and adapting to user input, making them useful tools in supporting mental health.[19] They became more popular in handling common youth mental health issues like stress, anxiety, depression, or autism-related symptoms.

Wysa is a good example of what contemporary chatbots can do. As a therapeutic equivalent to ChatGPT for mental health support, Wysa provides an anonymous, nonjudgmental space for youth to explore thoughts and emotions, manage stress, and develop mental resilience.[14,20] It currently has more than 6 million users and has already offered over 500 million sessions. The target age group for "Wysa for Children and Young People" is 13+.

The Wysa app uses a free-text conversational interface powered by AI (Figure 1). It deploys evidence-based approaches like cognitive behavioral therapy (CBT), dialectical behavior therapy (DBT), behavioral reinforcement, mindfulness, motivational interviewing, and positive behavior support.[14,20] The primary technology includes both rule-based and more advanced AI-based. In-app activities include journaling, psychoeducational exercises, and methods for managing stress and frustration, and improving sleep (Figure 1). Access to a human coach is a prime function, while the chatbot is free and accessible 24/7. Real-world data have demonstrated Wysa's clinical efficacy. Research showed that people who were more engaged with the software experienced considerably greater changes in depression symptoms, as measured by the Patient Health Questionnaire-9 (PHQ-9), compared to people with lower engagement.[14] Additionally, Wysa has been used in medical settings like the NHS Northeast London Foundation Trust as a complementary mental health service.[21]

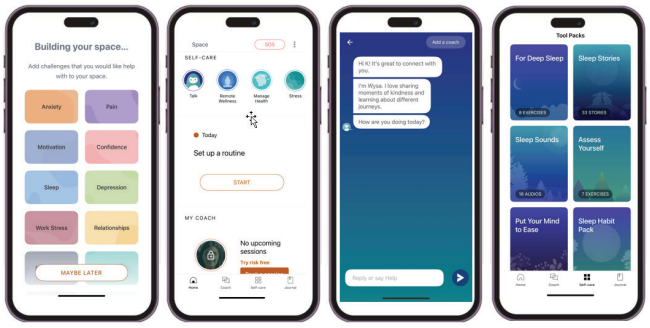

Figure 1: Demo of the Wysa app (screenshots taken by author, used with permission from Wysa). The Wysa app allows users to build their own space, focusing on the challenges they would like help with. Within this space, users can set up routines or receive support from their coaches. They can also have private conversations with the chatbot coach. Additionally, the Wysa app provides users with tool packs, which include exercises, stories, videos, and other resources.

Table 1: Overview of prominent mental health chatbots for teenagers/young adults.

Chatbot Name	Key Mental Health Focus Relevant to Teens	Notable features/ Interaction style	Target Age Group (if specified for teens/youth)	Primary Therapeutic Approach(es)	Primary AI Technology	Developer/ Origin	Platform(s)
TeenChat[13]	Stress	Stress detection, emotional support, guidance	Adolescents	Stress sensing and release, Virtual friend (listening, comforting, encouraging)	Rule-based, NLP for sentence analysis, Linguistic dependency trees	Tsinghua University, China	Browser/ Server
Tess[8,9]	Depression, Anxiety	24/7 emotional support, coping strategies, crisis referral, resilience coaching	College students, teens (via school/institutional partnerships)	Integrative (CBT, Motivational interviewing, Behavioral activation, Emotionally focused therapy, Mindfulness, Self-compassion), Personalized conversations	AI with emotion algorithms, ML, NLP	X2AI Inc./ X2 Foundation, USA	SMS, Facebook Messenger, WhatsApp
Woebot[8,24]	Depression, Anxiety, Substance	Daily check-ins, mood tracking, guided exercises, crisis resources	Young adults and college students [Adolescents (13-17 years) focus]	Primarily CBT, Psychoeducation, Cognitive distortion "word games"	Rule-based, NLP; exploring LLMs (human-written responses as of March 2024)	Woebot Health, USA	Mobile app
Wysa[6,14,20]	Depression, Anxiety, Stress, General well-being	AI coach, 150+ evidence-based exercises, 24/7 support, journaling, anonymous	Users 13+ (or 11+ with provider agreement), specific "Wysa for Children and Young People"	CBT, DBT, Motivational interviewing, Mindfulness, and Positive behavior support	Rule-based, "Emotionally Intelligent" AI, LLMs (OpenAI for Wysa+)	Touchkin, India, UK and USA	Mobile app
MYLO [22]	Problem exploration, Distress reduction, Goal conflict resolution	User-led problem exploration, focusing on goal conflicts	University students, young people (16-24 for PWA co-design)	MOLtherapy, Perceptual control theory, Problem exploration via curious questioning	Rule-based AI	University of Manchester (initial), UK Co-designed with young people	Web application, PWA
Vivibot[23]	Anxiety reduction, Resilience, Coping Skills	Daily emotion ratings, Videos by survivors, Positive psychology exercises; empathetic, warm, humorous	Young adult cancer survivors (18- 29 years)	Positive psychology skills (gratitude, mindfulness, personal strengths, etc.)	Automated, decision-tree structure (stated as non-AI content delivery) and AI (specifics not detailed)	Hopelab, USA	Mobile app Facebook Messenger
Happify/ Anna[12]	Stress reduction, General well-being	Gamified activities, AI coach Anna, teen-specific tracks	"Happify for Teens" (13-17 years)	CBT, Mindfulness, Positive psychology, "Adherence Fidelity" AI algorithm	AI-based chatbot using NLP, ML, "Adherence Fidelity" algorithm	Happify Health (now Twill), USA	Integrated into the Happify platform/app
Replika[6]	Loneliness, Emotional connection, Self-discovery (marketed for depression/ anxiety)	Avatar creation, chat, Coaching programs, Adaptable personality, Relationship statuses; known for fostering strong emotional bonds	General users ("anyone who wants a friend"), including students, lonely individuals	Companionship, Emotional support (not formal therapy)	GPT (LLM)	Luka Inc., USA	Mobile app
LISSA [75]	Autism (Social communication skills)	Simulates face-to-face conversation, Real-time/Post-session feedback on nonverbal behavior, Embodied agent, Written/spoken input, Mixed output	Individuals with autism (including teenagers)	Social skills training	Hidden Markov Model, Rule-based	Rochester Human-Computer Interaction (Univ. of Rochester), USA	Web-based platform

Abbreviations: CBT, Cognitive Behavioral Therapy; DBT, Dialectical Behavior Therapy; LISSA, Live Interactive Social Skills Assistance; LLM, Large Language Model; ML, Machine Learning; MOL, Method of Levels; MYLO, Manage Your Life Online; NLP, Natural Language Processing; PWA, Progressive Web App; SMS, Short Message Service

Wysa is only one of many new chatbots being developed to address the changing needs of younger people and children in terms of mental health. The rapid expansion of digital mental health tools reflects a growing need and awareness of their potential to improve child well-being. However, this expansion also raises important concerns regarding quality, safety, and regulatory oversight, particularly as many of these chatbots are designed for or used by minors.[6,19]

A comparative overview of the most popular mental health chatbots for adolescents and young adults is presented in Table 1 to understand the scenario better. It also includes information on their origins, therapeutic approaches, AI technologies, distribution platforms, and especially appropriate features for teenage users.

Technology, features, user experience:

Mental health AI chatbots for adolescents generally share a common set of features that support their overall objectives of facilitating self-help and creating therapy through a digital channel.

Although Table 1 identifies the AI chatbots' differences, how people use these resources in real life, especially teenagers, is similar. The majority of chatbots enhance user interaction by complementing text with other forms of media, such as videos, emojis, or voice. They have other capacities, such as providing training on coping mechanisms and healing philos-

ophies through educational sessions. Furthermore, interactive tools support patients to manage their mental health by themselves.[19]

Behind these interactions are numerous AI technologies. These comprise rule-based systems, machine learning (ML), and natural language processing (NLP). Predefined codes, decision trees, and keyword matching are the foundation of rule-based systems and are still used in various chatbots, including TeenChat, MYLO, and Vivibot.[13,22,23] These methods are less smart in conversation, despite being simpler to create. On the other hand, as seen in TeenChat, Tess, Anna, Woebot, and Wysa.[9,12-14,24] NLP can be used to assess the user's intent and context information. ML techniques are used to improve personalization further, to strengthen responses over time using previous data.[9,12]

The figure below (Figure 2) illustrates how a chatbot works in general.[78] When a chatbot receives a message, it uses NLP to understand users' intentions and the context of the conversation. Then it uses the Dialog Manager to track the conversation and to request additional information if necessary. It also searches its knowledge database and checks if there are existing appropriate answers. Finally, the chatbot responds by using either a pre-written message or an AI-generated one that sounds natural.

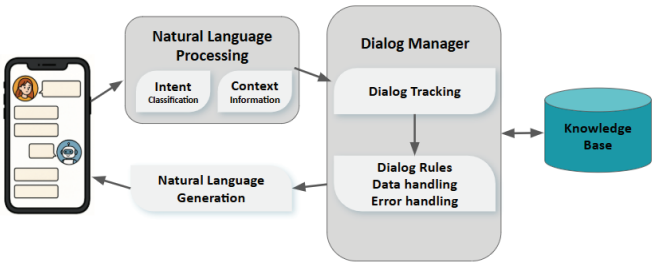

Figure 2: Chatbot's working process (adapted from Dilmegani, 2025,[78] used with permission). A chatbot first uses NLP to detect intent and context, then a dialog manager tracks the dialog flow. It also searches its knowledge base. Finally, the chatbot responds with either a prewritten or AI-generated message.

Large Language Models (LLMs), a type of NLP technology, have been used in chatbots such as Wysa to improve their language capabilities and to make more human-like user interactions.[6] Others like Woebot are working on the integration. However, there are challenges associated with using LLMs, for example, about safety, factual accuracy, and ethical considerations, particularly when minors are targeted users.[6,19] Thus, many chatbots are currently employing a hybrid approach that allows for the predictability of rule-based systems while being able to make use of the advanced understanding and conversational capacity of ML/NLP and LLMs.[6] For instance, Woebot uses human-written content for therapeutic delivery but explores LLMs for greater understanding and personalization.[6]

Not only do mental health AI chatbots use well-established psychological models at the core of their therapeutic approach, including cognitive behavioral therapy (CBT).[25] For example, Woebot uses CBT to guide users to identify and dismantle negative thought patterns.[6,24] Similarly, Wysa, Tess, and Anna also incorporate the CBT rules.[6,9,12,14,20] On the other hand, the Method of Levels (MOL) therapy is used by MYLO to direct users' attention to higher-level targets.[22] Positive Psychology, which emphasizes cultivating love and good emotions, is key to Vivibot and Anna, and is demonstrated by tasks like a gratitude journal.[23] Mindfulness has been incorporated into Wysa, Tess, and Anna to provide immediate coping strategies for anxiety and stress.[6,9,12,14,20] Furthermore, Tess and Wysa draw from multiple therapeutic methods to provide a broader range of support for their diverse user base. These psychological principles are woven into the design of the content, logic for decision-making, and tone of the responses. They guide what the chatbot says, how it guides the conversation, and which tools or exercises it offers based on user input.[6,9,14,20]

Other than technologies and therapeutic models, the next important aspect of a chatbot is how these parts are delivered to users. In other words, the technical advantages of chatbots must be translated into good and safe user experiences. The first step using an AI mental health chatbot is onboarding, which includes setting up, obtaining user and parents' consent, and giving users an introduction to features, functions, and limitations. It is important to clearly state that the chatbot is not intended to replace human therapists at the early stage, to ensure its safe use.[26,27] Chatbots often do regular check-ins, and users can also initiate a conversation whenever they need support. Sessions can be simple conversations or more organized therapy and exercises. For instance, Anna's "Adherence Fidelity" algorithm was developed based on users' feedback and can identify when a user might want to stop engaging in an activity.[12] The output of chatbots is mainly text-based but is often supplemented by emojis and GIFs, as seen in Woebot,[24] videos, as seen in Vivibot, or audio, as seen in Wysa.[14] More output types may increase engagement, specifically for teenagers accustomed to related media interactions.

To make powerful mental health chatbots for teenagers, a simple adaptation of adult versions or general chatbots is not sufficient, and other important changes must be made. These include addressing teenage stressors, such as school pressure, peer relationships, and self-identity issues.[28] Also, age-specific language and teenager-culture should be considered and may include elements like emojis or memes. For example, Happify for Teens ' content targets a fifth-grade reading level. Another consideration is the platform selection for teen users, who strongly prefer apps or progressive web applications (PWAs) that are available on their phones.[12] Engagement strategies usually involve gamification, interactive elements, and additional information that may relate to the youth experiences. The effectiveness of chatbots in treating mental illness depends not solely on AI's capabilities or the therapy's soundness, but also on how well these components are combined, delivered in a user-friendly way that engages teenagers.[19] One way to enable this is to involve teenagers in the design process directly, as seen in MYLO.[22]

Given the large number of chatbots and the diversity in features, therapeutic approaches, and technology (Table 1), it is clear that there is no single, optimal way of delivering AI mental health therapy to the teenage population. A feature critical to this vulnerable population is crisis support, where the chatbot detects severe risk and directs the user to human

DOI: 10.36838/IJHSR810.10

helplines.[29] Finally, AI integration greatly improves the potential to make personalized responses and recommendations.

Analysis of pros and cons:

The incorporation of AI chatbots into youth mental health has great potential, but it also creates key issues and challenges. Therefore, it is important to have a balanced view of the emerging technology.

The most significant benefits of AI chatbots are their increased accessibility and availability, unaffected by geographical locations, and the long waiting list associated with conventional mental health services.[23] For teenagers, this means that support is always accessible regardless of time of the day, the availability of human support, or limitations related to parental schedules and transportation.[6] Regular availability is a significant advantage given the unexpected nature of mental health struggles.

Furthermore, AI chatbots are potentially stigma-free. Teenagers are often reluctant to seek professional help because they are afraid of being judged by peers, families, or the community. Using AI chatbots in a nonjudgmental setting, teens can express their thoughts with more freedom.[6] This is especially important to teenagers who are experiencing challenges like identity development and are at risk of receiving first assistance. Because of their lack of judgment, studies have shown that patients are more likely to give sensitive data to AI than to human therapists.[30,31]

Cost-effectiveness is another advantage of AI chatbots. Mental health chatbots are generally available at a significantly lower cost than standard therapy.[32] For example, Tess claims to be "98% cheaper than face-to-face therapy".[33] The affordability removes the financial barrier for teens who don't have income or whose families cannot afford conventional mental health care.[34]

Another benefit of AI chatbots is their interactive nature and engagement. The texting format is familiar to teens through their use of messaging apps and thus is more attractive than static resources like a self-help book.[28] Gamification can further enhance the motivation of teens. The use of AI may assist in creating a sense of accountability and encourage continued use with features like regular check-ins and personal feedback.[28]

Clinically, AI chatbots can deliver evidence-based interventions such as CBT with fidelity,[15,35] and provide access to a basic level of support based on current therapeutic guidelines for teenagers in areas with few trained mental health professionals.[36] Also, some chatbots were created in collaboration with teenagers, making them more useful and interesting tools.[12]

Despite their potential, AI chatbots pose significant risks and challenges, especially for the adolescent population. First and foremost, chatbots can delay the escalation of severe crises. Access to more intensive treatment may be hampered if using chatbots in place of a human mental health specialist. While anonymity helps reduce stigma, it can be risky. If a teen is in serious distress without anyone being aware or able to intervene, the situation can become dangerous.[41] This threat is increased when a chatbot has insufficient crisis detection or action capabilities for high-risk scenarios, including abuse, self-harm, or suicide. In fact, most chatbots are not designed or equipped to handle serious mental health catastrophes or intervene in suicidal intent effectively.[42] AI typically responds by providing phone information for human-crisis helplines and emergency services, which requires the user to seek immediate assistance. There have been cases reported with tragic outcomes when AI chatbots were used in place of qualified therapists.[43]

Another main concern is the lack of genuine empathy and human connection. While AI can simulate human responses, it still does not provide nuance understanding, shared experience, and personal resonance that constitute the foundation of human interactions.[37,38] Teenagers are in a crucial stage of socio-emotional development. Excessively relying on AI for emotional support may impact how teens form healthy relationships with other people.[39,40] Teens are also prone to engaging in parasocial relationships with chatbots, which have been shown to hinder their development.[39,40]

Chatbots also have limited abilities in problem-solving and in understanding complicated or novel subtleties. It is challenging for the chatbots to understand teen-specific slang, communication style, and social dynamics, which may lead to advice that is not useful.[37] It is especially risky if a chatbot misinterprets or reinforces negative patterns.[77]

Major concerns include the security of data and privacy as well. Providers of mental health chatbots have the responsibility to protect sensitive client information, notably client mental health records.[40] There are strict regulations in place for the collection of such data, as described in the US Children's Online Privacy Protection Act (COPPA). However, there is a requirement for a balance between teens' need for confidentiality and parents' rights to be informed of their children's online activities. It is also important to note that although the Health Insurance Portability and Accountability Act (HIPAA) applies to hospitals, clinics, and doctors, it often does not apply to technology providers and the apps they develop, which leads to privacy protection challenges for the users.[69,79] Chatbot providers may not be liable for privacy breaches because no regulations hold them responsible.[69]

Another issue with chatbots is algorithmic bias. Information used to train AI may already have biases, such as those relating to race, gender, culture, and language, which can lead to dangerous experiences for teenagers from disadvantaged groups. For example, LLMs are often trained on data that represents English-speaking or Western populations.[69,72]

Lastly, AI might unintentionally cause inequities in mental health care. Some teenagers from underserved areas do not have appropriate personal access to smartphones or a reliable internet. They have to rely on devices from the community or schools, which create barriers to using mental health chatbots since these tools are designed to offer immediate support when a crisis happens. As a result of limited access, teenagers may be unable to seek help when they need the support most.[6] Additionally, having to use mental health resources in a shared space reduces privacy and may discourage engagement.[6] However, underserved teenagers with appropriate access to technology

may be more dependent on AI-based tools than those with greater access to conventional mental health services. This could lead to a lower standard of care for those already disadvantaged, considering AI tools are inferior to human therapists. This issue must be considered when developing and deploying these devices for adolescents.[37]

Future developments for teen mental health chatbots:

As AI advances, chatbots must expand their current capabilities, developing a safer and more personalized, engaging, ethical, and effective tool for mental health.

Future chatbots must improve skills to detect and intervene in crises as a top priority, which is critical for the vulnerable population. Alone, they should not manage severe conditions such as self-harm, suicide attempts, or abuse. Strong detection capabilities will enable them to identify crises with more accuracy. Then, the initial intervention by AI chatbots should be followed by connecting users with trusted adults, and then, if necessary, escalating to emergency services. A "panic option" and other features can make immediate support easier. When there isn't immediate assistance from a human, these systems enable fast, life-saving crisis support.[12,61] However, these approaches rely on accurate detection of crisis and may lead to consent complexity.[12,41] In addition, future safety frameworks must strengthen their filters so that disturbing, tempting, or frightening content can be removed more accurately and strictly, especially for teenagers who are more likely to be influenced by the external world.

A key innovation in mental health chatbots could be context-aware and proactive support,[59] where the technology itself starts conversations based on mental health signs rather than waiting for the teenagers to initiate them. It might initiate a conversation if the patient hasn't used the system for some time, is facing stressors from a calendar, or has a daily routine that indicates they are experiencing anxiety. As technology advances, apps may be able to identify individuals at risk and deliver help quickly, thus benefiting those afraid to seek help.[60] This development requires careful design that respects user privacy and autonomy to avoid unnecessary disruption to users' lives.

Hyper-personalization and adaptive learning can be developed in future versions of the chatbots. They can provide users with tailored advice based on a teen's mental health status, previous responses, and upcoming events like a final exam. It could be achieved by detecting keywords that imply that a student is anxious and then adjusting the response accordingly. Personalizing interactions with the teenagers could also be improved by allowing the system to tailor its responses more closely to the flow of each conversation over time, providing the teenagers with information more directly relevant to what they have said, which is important for future engagement.[28,46,47] However, such hyper-personalization would require the collection of sensitive data, which in turn raises issues regarding privacy, security, and ensuring that any data collected is accurately interpreted by clinicians.

Gamification is another appealing method for boosting engagement and motivation, which is a major challenge in digital mental health treatment.[50,51] Chatbots could use unlockable skills or unfold storylines that tie to therapeutic objectives and progress, such as "defeating social anxiety mountain." Chatbots could encourage engagement with evolving characters and unlockable talent trees or provide a story-driven journey that aligns with therapeutic objectives. These factors help lessen therapy fatigue by making therapeutic skill-building more entertaining and rewarding.[52,53] But the key challenge is to avoid trivializing mental health, overusing or making the games excessively competitive, to maintain a balance between fun and clinical value.[52,53]

Integrating wearable physical data into chatbots is another potential future feature. These data may include sleeping patterns, daily exercises, and heart rates. The information may promote personalized support, such as a relaxation session after a night of poor sleep. This connection between physical and mental health could allow for more integrated care.[54,55] Nevertheless, it would risk data rights, privacy, and security, as well as the accurate interpretation of these data.[56]

Recognizing advanced emotions and nuance is also a top focus in future chatbots. AI chatbots must get trained in adolescent language, including slang and irony, and other expressions (e.g., non-verbal cues). Inputs from multiple resources like voice, text, or facial expressions could be analyzed, and a teen's emotional status can be more accurately interpreted. This may increase pertinent responses and foster stronger connections with teens.[46,47] However, even the most sophisticated AI struggles to keep up with teens' rapidly changing culture and communication trends. However, it is important to note that collecting these data from teenagers has significant ethical challenges and computational demands.[57,58]

Creative and expressive tools would give users more ways of expressing themselves non-verbally. These may include a mood-related playlist, a guided journal, or a simple drawing tool. The tools can support self-awareness and boost creativity in teenagers; they are particularly useful for those who are less verbal. Nevertheless, it's still challenging to add these tools into chatbot flows while providing helpful, but not overly interpretive, feedback.[62]

Some chatbots give lessons that teach life skills such as stress management, interpersonal communication, conflict resolution, and digital citizenship, in addition to traditional CBT lessons.[63] These lessons train practical coping skills for teenagers and help them handle real-world challenges.[64] The key issue is that these contents need to be evidence-based, engaging, and relevant to teenagers to achieve goals.[65]

The potential of mental health chatbots amongst youth may be greatest in systems that combine human inputs with AI. AI may provide instant, accessible, and ongoing support, especially where there is a need to address the problem of teenagers who prefer not to communicate with adults. However, there must always be a quick and safe pathway for teens to access human care when they are in need.[66,67]

Regulatory considerations:

As more advanced AI tools become available, the ethical responsibilities of developers increase and require thoughtful

DOI: 10.36838/IJHSR810.10

regulations that can address privacy, security, safety, and legal concerns.[1,6,68]

Regulations for AI, especially in mental health, often lag behind technological advances, raising concerns about how chatbots operate with little or no supervision. Users of these AI mental health tools may not be aware that they are utilizing technology that hasn't been carefully reviewed by any trustworthy authorities, even though some tools, like Woebot, explicitly state that the FDA does not approve them.[10,24,69] To promote public education about the limitations of AI, requirements for crisis responses, and to provide clear guidelines for this rapidly expanding innovation, professional bodies like the American Psychological Association (APA) are actively engaging regulatory agencies like the Federal Trade Commission (FTC).[12,24,69] Additionally, mental health chatbots should comply with data protection laws such as HIPAA, and regulations should mandate that users be informed if an application is not FDA-approved or HIPAA-compliant. Developing regulations indeed requires diverse opinions, from developers, policymakers, mental health professionals, as well as from teens themselves.

Above all, the deployment of AI in mental health requires human involvement and support. Human oversight is critical in every stage of a chatbot, from design and development to deployment and monitoring.[8,9,12,69] Chatbots should be utilized as tools to augment human capabilities and extend the reach of mental health support, not to replace humans.[11,71] Integrated care models, where chatbots strengthen standard therapy by helping users complete homework, offering support between sessions, or performing initial screenings, hold promise for creating a more efficient future for mental health treatment. This solution offers a safety net on which chatbots can rely in challenging situations.[7,12,71] In fact, the state of Utah has proposed legislation requiring licensed mental health professionals to be involved in chatbot development,[70] which is one step towards the goal of strategic human oversight. In addition to getting feedback from mental health professionals, regulatory agencies, and the youth, chatbots must be designed to minimize possible harms, such as an unhealthy reliance on AI and privacy breaches.[12,32]

Strength and limitations:

This article presents a youth perspective on the use of AI to support adolescent mental health and is targeted at other teenagers, which is the strength of the paper. However, it is also important to discuss its limitations. First, current literature did not specify which populations (such as gender or age groups – younger or older teens, or severity of conditions) that can benefit most from the AI mental health chatbots. Although some data suggested that these tools are comparable in their efficacy across both genders, there is a clear bias in chatbots' design, mimicking female stereotypes historically. Additionally, clinical trials on the efficacy of these chatbots had mostly female participants. For instance, the trial for Tess was 70% female,[9] and the Woebot trial was 67% female.[24] Second, technical details regarding specific apps are often unavailable. For example, while "onboarding" is a critical first step, the process was only explicitly described for Wysa and Woebot,[14,24] with other apps missing detailed disclosure about this process. Furthermore, the chatbot's underlying process has not been described specifically for mental health treatment purposes. Also, the literature review in this article was conducted with a narrative, rather than a systematic review approach. However, the paper shares critical insights with peer adolescents, mental health professionals, AI chatbot developers, and regulators about using AI tools in treating mental health conditions in youth.

■ Conclusion

AI-powered chatbots present a new approach to addressing barriers to adolescent mental health services. These technologies have the potential to reduce the stigma associated with limited accessibility of traditional mental health care to the highly vulnerable group and to deliver low-cost and evidence-based therapies to youth in need. This is particularly important in an era when adolescent mental health needs are increasing rapidly. There is a wide range of chatbots, each using distinct features, technology, and approaches, illustrating the diversity of efforts to apply AI to mental health.

The journey to the incorporation of AI chatbots into adolescent mental health still has significant challenges ahead. These chatbots, although advanced, are still not capable of truly replicating the empathy of humans or comprehending the subtleties of human communication, expression, and the social and cultural context that affect adolescents.[6-8,12] Critical issues such as data protection, users' consent, risk of teenagers becoming over-reliant, plus a need for safety protocols, are amplified when AI is targeted at the adolescent group.[10,69,72] Furthermore, the anonymity that makes chatbots so appealing to teenagers could be detrimental in a crisis when human intervention is required.

To progress forward, we need stricter regulations and inputs from a variety of sources, including mental health professionals, educators, governments, regulatory entities like the APA, and youth themselves.[1,12,69,73] Heavy emphasis should be placed on the protection of the privacy and data of minors, and on the level of human intervention required. Additional research should explore methods for improving symptom reduction, user engagement, the therapeutic relationship formed between a chatbot and teen users, and the long-term effects of chatbots on teenagers and their behaviors and development.[7,72-74]

■ Acknowledgments

The author acknowledges with appreciation the contributions of Professor Fang Zhang (Department of Psychology, Assumption University), whose review, editorial guidance, and thoughtful suggestions improved the quality of this manuscript.

■ References

1. Guo, Z., Lai, A., Thygesen, J. H., Farrington, J., Keen, T., & Li, K. (2024). Large Language Models for Mental Health Applications: A Systematic Review. *JMIR Mental Health, 11*: e57400. https://doi.org/10.2196/57400

2. Lawrence, H. R., Schneider, R. A., Rubin, S. B., Matarić, M. J., McDuff, D. J., & Bell, M. J. (2024). The opportunities and risks of large language models in mental health. *JMIR Mental Health, 11*: e59479. https://doi.org/10.2196/59479
3. Substance Abuse and Mental Health Services Administration. (2022). *2021 National Survey on Drug Use and Health: Highlights*. U.S. Department of Health and Human Services. https://www.samhsa.gov/data/sites/default/files/2022-12/2021NSDUHFFRHighlights092722.pdf
4. Merikangas, K. R., He, J., Burstein, M., Swanson, S. A., Avenevoli, S., Cui, L., Benjet, C., Georgiades, K., & Swendsen, J. (2010). Lifetime Prevalence of Mental Disorders in U.S. Adolescents: Results from the National Comorbidity Survey Replication–Adolescent Supplement (NCS-A). *Journal of the American Academy of Child & Adolescent Psychiatry, 49(10)*: 980–989. https://doi.org/10.1016/j.jaac.2010.05.017
5. Crews, F., He, J., & Hodge, C. (2007). Adolescent cortical development: A critical period of vulnerability for addiction. *Pharmacology Biochemistry and Behavior, 86*(2): 189–199. https://doi.org/10.1016/j.pbb.2006.12.001
6. Mansoor, M., Hamide, A., & Tran, T. (2025). Conversational AI in Pediatric Mental Health: A Narrative Review. *Children, 12*(3): 359. https://doi.org/10.3390/children12030359
7. Park, J. K., Singh, V. K., & Wisniewski, P. (2024). Current Landscape and Future Directions for Mental Health Conversational Agents (CAS) for Youth: Scoping Review. *JMIR Medical Informatics, 13*: e62758. https://doi.org/10.2196/62758
8. Bendig, E., Erb, B., Schulze-Thuesing, L., & Baumeister, H. (2019). The next generation: Chatbots in Clinical Psychology and Psychotherapy to Foster Mental Health – A scoping review. *Verhaltenstherapie, 32*(Suppl. 1): 64–76. https://doi.org/10.1159/000501812
9. Fulmer, R., Joerin, A., Gentile, B., Lakerink, L., & Rauws, M. (2018). Using Psychological Artificial Intelligence (TESS) to relieve symptoms of depression and anxiety: randomized controlled trial. *JMIR Mental Health, 5*(4): e64. https://doi.org/10.2196/mental.9782
10. Linardon, J., Cuijpers, P., Carlbring, P., Messer, M., & Fuller-Tyszkiewicz, M. (2019). The efficacy of app-supported smartphone interventions for mental health problems: a meta-analysis of randomized controlled trials. *World Psychiatry, 18*(3): 325–336. https://doi.org/10.1002/wps.20673
11. Wanniarachchi, V. U., Greenhalgh, C., Choi, A., & Warren, J. R. (2025). Personalization variables in digital mental health interventions for depression and anxiety in adolescents and youth: a scoping review. *Frontiers in Digital Health, 7*:1500220 https://doi.org/10.3389/fdgth.2025.1500220
12. Boucher, E. M., Harake, N. R., Ward, H. E., Stoeckl, S. E., Vargas, J., Minkel, J., . . . Zilca, R. (2021). Artificially intelligent chatbots in digital mental health interventions: a review. *Expert Review of Medical Devices, 18*(sup1): 37–49. https://doi.org/10.1080/17434440.2021.2013200
13. Huang, J., Li, Q., Xue, Y., Cheng, T., Xu, S., Jia, J., & Feng, L. (2015). TeenChat: A chatterbot system for sensing and releasing adolescents' stress. In X. Yin, W. Yu, & H. Dong (Eds.), *Health Information Science* (pp. 133–145). Springer. https://doi.org/10.1007/978-3-319-19156-0_14
14. Inkster, B., Sarda, S., & Subramanian, V. (2018). An Empathy-Driven, Conversational Artificial Intelligence Agent (WYSA) for Digital Mental Well-Being: Real-World Data Evaluation Mixed-Methods Study. *JMIR Mhealth and Uhealth, 6*(11): e12106. https://doi.org/10.2196/12106
15. Tong, A. C. Y., Wong, K. T. Y., Chung, W. W. T., & Mak, W. W. S. (2025). Effectiveness of topic-based chatbots on mental health self-care and mental well-being: A Randomized Controlled Trial *Journal of Medical Internet Research*. 27: e70436 https://doi.org/10.2196/70436
16. Ennis, E., O'Neill, S., Mulvenna, M., Bond, R. Chatbots supporting mental health and wellbeing of children and young people; applications, acceptability and usability. In Proceedings of the European Conference on Mental Health, Ljubljana, Slovakia,12–15 September 2023; p. 57.
17. Torous, J., Bucci, S., Bell, I. H., Kessing, L. V., Faurholt-Jepsen, M., Whelan, P., . . . Firth, J. (2021). The growing field of digital psychiatry: Current evidence and the future of apps, social media, chatbots, and virtual reality. *World Psychiatry, 20*(3): 318–335. https://doi.org/10.1002/wps.20883
18. Adamopoulou, E., & Moussiades, L. (2020). Chatbots: History, technology, and applications. *Machine Learning With Applications, 2*: 100006. https://doi.org/10.1016/j.mlwa.2020.100006
19. Mayor, E. (2025). *Chatbots and mental health: A scoping review of reviews. Current Psychology, 44*: 13619–13640. https://doi.org/10.1007/s12144-025-08094-2
20. Gupta, M., Malik, T., & Sinha, C. (2022). Delivery of a mental health intervention for chronic pain through an Artificial Intelligence–Enabled App (WYSA): Protocol for a prospective pilot study. *JMIR Research Protocols, 11*(3): e36910. https://doi.org/10.2196/36910
21. Emma S. Wysa. Wysa Case Studies (2018 Apr 18) NHS Children Services: How the North East London NHS Foundation Trust uses Wysa for children's mental health URL: https://www.wysa.io/blog/nhs-children-services
22. Gaffney, H., Mansell, W., Edwards, R., & Wright, J. (2013). Manage Your Life Online (MYLO): a pilot trial of a conversational Computer-Based intervention for problem solving in a student sample. *Behavioural and Cognitive Psychotherapy, 42*(6): 731–746. https://doi.org/10.1017/s135246581300060x
23. Greer, S., Ramo, D., Chang, Y., Fu, M., Moskowitz, J., & Haritatos, J. (2019). Use of the Chatbot "Vivibot" to Deliver Positive Psychology Skills and Promote Well-Being Among Young People After Cancer Treatment: Randomized Controlled Feasibility Trial. *JMIR Mhealth and Uhealth, 7*(10): e15018. https://doi.org/10.2196/15018
24. Fitzpatrick, K. K., Darcy, A., & Vierhile, M. (2017). Delivering cognitive behavior therapy to young adults with symptoms of depression and anxiety using a fully automated conversational agent (WoeBot): a randomized controlled trial. *JMIR Mental Health, 4*(2): e19. https://doi.org/10.2196/mental.7785
25. Zlomke, K. R., Greathouse, A. D., and Rossetti, K. (2020). Behavioral Therapy and Cognitive-Behavioral Therapy. In: The Encyclopedia of Child and Adolescent Development, John Wiley & Sons, Inc., Hoboken, 128-141. https://doi.org/10.1002/9781119171492.wecad075
26. Lalot, F., & Bertram, A. (2025). When the bot walks the talk: Investigating the foundations of trust in an artificial intelligence (AI) chatbot. *Journal of Experimental Psychology: General. 154*(2): 533–551. https://doi.org/10.1037/xge0001696
27. Park, J.I., Abbasian, M., Azimi, I., Bounds, D.T. *et al.* (2025). *Building Trust in Mental Health Chatbots: Safety Metrics and LLM-Based Evaluation Tools. arXiv (Cornell University)*. https://doi.org/10.48550/arxiv.2408.04650
28. Pratt, N., Madhavan, R., & Weleff, J. (2024b). Digital Dialogue—How youth are interacting with chatbots. *JAMA Pediatrics, 178*(5): 429-430. https://doi.org/10.1001/jamapediatrics.2024.0084

DOI: 10.36838/IJHSR810.10

29. Chow, A. R., & Haupt, A. (2025, June 12). A psychiatrist posed as a teen with therapy chatbots. The conversations were alarming. *TIME*. Retrieved from https://time.com
30. Chaudhry, B. M., & Debi, H. R. (2024). User perceptions and experiences of an AI-driven conversational agent for mental health support. *mHealth*, 10. https://doi.org/10.21037/mhealth-23-55
31. Lucas, G. M., Gratch, J., King, A., & Morency, L. (2014). It's only a computer: Virtual humans increase willingness to disclose. *Computers in Human Behavior, 37*: 94–100. https://doi.org/10.1016/j.chb.2014.04.043
32. Haque, M. D. R., & Rubya, S. (2023). An overview of Chatbot-Based mobile mental health apps: insights from app description and user reviews. *JMIR Mhealth and Uhealth, 11*: e44838. https://doi.org/10.2196/44838
33. iAsk. (2025, June 27). *Top 7 mental health AI chatbots of 2025*. https://iask.ai/articles/7-best-mental-health-ai-chatbots
34. Zhu, S., Wang, Y., and Hu, Y. (2025). Facilitators and Barriers to Digital Mental Health Interventions for Depression, Anxiety, and Stress in Adolescents and Young Adults: A Scoping Review. *Journal of Medical Internet Research 27*: e62870. https://doi.org/10.2196/62870
35. Barreda, M., Cantarero-Prieto, D., Coca, D., Delgado, A., Lanza-León, P., Lera, J., . . . Pérez, F. (2025). Transforming healthcare with chatbots: Uses and applications—A scoping review. *Digital Health*, 11: 1-22. https://doi.org/10.1177/20552076251319174
36. Parks, A., Travers, E., Perera-Delcourt, R., Major, M., Economides, M., & Mullan, P. (2025). Is this chatbot Safe and Evidence-Based? A call for the critical evaluation of Gen AI mental health chatbots. *Journal of Participatory 17:e69534 Medicine*. https://doi.org/10.2196/69534
37. Laymouna, M., Ma, Y., Lessard, D., Schuster, T., Engler, K., & Lebouché, B. (2024). Roles, users, benefits, and Limitations of Chatbots in health care: Rapid review. *Journal of Medical Internet Research*, *26*: e56930. https://doi.org/10.2196/56930
38. Montemayor, C., Halpern, J. & Fairweather, A. (2022). In principle obstacles for empathic AI: why we can't replace human empathy in healthcare. *AI & Soc 37*: 1353–1359 https://doi.org/10.1007/s00146-021-01230-z
39. Maeda, T., & Quan-Haase, A. (2024). When Human-AI interactions become Parasocial: Agency and anthropomorphism in affective design. *2022 ACM Conference on Fairness, Accountability, and Transparency, 24*: 1068–1077. https://doi.org/10.1145/3630106.3658956
40. Kretzschmar, K., Tyroll, H., Pavarini, G., Manzini, A., Singh, I. (2019). Can Your Phone Be Your Therapist? Young People's Ethical Perspectives on the Use of Fully Automated Conversational Agents (Chatbots) in Mental Health Support. *Biomedical Informatics Insights*. 11. https://doi.org/10.1177/1178222619829083
41. Abrams, Z. (2025, March 12). Using generic AI chatbots for mental health support: A dangerous trend. *https://www.apaservices.org*. Retrieved from https://www.apaservices.org
42. Roy, I. (2025, June 14). AI therapy gone Wrong: Psychiatrist reveals how chatbots are failing vulnerable teens. *Health and Me*. Retrieved from https://www.healthandme.com
43. Blease, C., Torous, J. (2023). ChatGPT and mental healthcare: balancing benefits with risks of harms. *BMJ Ment Health. 26*(1):e300884. doi: 10.1136/bmjment-2023-300884
44. Saglam, R. B., Nurse, J. R. C., & Hodges, D. (2021). Privacy concerns in Chatbot interactions: When to trust and when to worry. In *Communications in computer and information science 420*: 391–399. https://doi.org/10.1007/978-3-030-78642-7_53
45. Kim, J., Cai, Z. R., Chen, M. L., Simard, J. F., & Linos, E. (2023). Assessing biases in medical decisions via clinician and AI chatbot responses to patient vignettes. *JAMA Network Open, 6*(10): e2338050. https://doi.org/10.1001/jamanetworkopen.2023.38050
46. Hou, J., Gibson, J., Phi, T., Ritchie, B., Gallagher, L., Strudwick, G., . . . Hawke, L. D. (2025). Designing digital conversational agents for youth with multiple mental health conditions: Insights on key features from a youth-engaged qualitative descriptive study. *Digital Health, 11*. https://doi.org/10.1177/20552076251330550
47. Vanhoffelen, G., Vandenbosch, L., & Schreurs, L. (2025c). Teens, Tech, and Talk: Adolescents' use of and emotional reactions to Snapchat's My AI Chatbot. *Behavioral Sciences, 15*(8): 1037. https://doi.org/10.3390/bs15081037
48. Belavadi, P., Burbach, L., Halbach, P., Nakayama, J., Plettenberg, N., Ziefle, M., & Valdez, A. C. (2020). Filter Bubbles and Content Diversity? An Agent-Based Modeling approach. In *Lecture Notes in Computer Science* (pp. 215 -226).https://doi.org/10.1007/978-3-030-49570-1_15
49. Reid, J. (2025). Digitising "The Big Lie": Algorithmic Curation as an Inhibitor of Media Exposure Diversity online. *Communicatio*, 1–21. https://doi.org/10.1080/02500167.2024.2424841
50. Lipschitz, J. M., Pike, C. K., Hogan, T. P., Murphy, S. A., & Burdick, K. E. (2023). The Engagement Problem: A Review of Engagement with Digital Mental Health Interventions and Recommendations for a Path Forward. *Current Treatment Options in Psychiatry, 10*(3): 119–135. https://doi.org/10.1007/s40501-023-00297-3
51. Liverpool, S., Mota, C. P., Sales, C. M. D., Čuš, A., Carletto, S., Hancheva, C., . . . Edbrooke-Childs, J. (2020). Engaging children and young people in digital mental health interventions: systematic review of modes of delivery, facilitators, and barriers. *Journal of Medical Internet Research, 22*(6): e16317. https://doi.org/10.2196/16317
52. Aschentrup, L., Steimer, P. A., Dadaczynski, K., Call, T. M., Fischer, F., & Wrona, K. J. (2024). Effectiveness of gamified digital interventions in mental health prevention and health promotion among adults: a scoping review. *BMC Public Health, 24*(1) https://doi.org/10.1186/s12889-023-17517-3
53. Litvin, S., Saunders, R., Maier, M. A., & Lüttke, S. (2020). Gamification as an approach to improve resilience and reduce attrition in mobile mental health interventions: A randomized controlled trial. *PLoS ONE, 15*(9): e0237220. https://doi.org/10.1371/journal.pone.0237220
54. Brasier, N., Mahato, K., Princip, M., Gonçalves, V. M., Mutuyimana, C., Bourke, S., . . . Wang, J. (2025). Next-generation wearable sensors for biopsychosocial care in mental health: a narrative review. *BMJ Digital Health and AI, 1*(1): e000018. https://doi.org/10.1136/bmjdhai-2025-000018
55. Kargarandehkordi, A., Li, S., Lin, K., Phillips, K. T., Benzo, R. M., & Washington, P. (2025). Fusing Wearable Biosensors with Artificial Intelligence for Mental Health Monitoring: A Systematic Review. *Biosensors, 15*(4): 202. https://doi.org/10.3390/bios15040202
56. Fúster, J., Solera-Cotanilla, S., Pérez, J., Vega-Barbas, M., Palacios, R., Álvarez-Campana, M., and López, G. (2023). Analysis of security and privacy issues in wearables for minors. *Wireless Networks, 30*(6): 5437–5453. https://doi.org/10.1007/s11276-022-03211-6
57. Facca, D., Smith, M. J., Shelley, J., Lizotte, D., & Donelle, L. (2020). Exploring the ethical issues in research using digital data collection strategies with minors: A scoping review. *PLoS ONE, 15*(8): e0237875. https://doi.org/10.1371/journal.pone.0237875
58. Leschanowsky, A., Rusti, C., Quinlan, C., Pnacek, M., Gorce, L., & Hutiri, W. (2024). A data perspective on Ethical Challenges in voice Biometrics Research. *IEEE Transactions on Biometrics. Behavior and Identity Science*, 1. https://doi.org/10.1109/tbiom.2024.3446846
59. Zhao, Y., Huang, Z., Seligman, M., & Peng, K. (2024). Risk and prosocial behavioural cues elicit human-like response patterns from

AI chatbots. *Scientific Reports, 14*(1): 7095. https://doi.org/10.1038/s41598-024-55949-y
60. Grové, C. (2021). Co-developing a mental health and wellbeing chatbot with and for young people. *Frontiers in Psychiatry, 11*: 606041. https://doi.org/10.3389/fpsyt.2020.606041
61. Maheu, M. M. (2025, June 27). AI Companionship & Teen Suicide Alert: Interventions for Psychotherapists & Healthcare Providers. Retrieved from https://telehealth.org/blog/ai-companionship-teen-suicide-alert-interventions-for-psychotherapist
62. Bednarski, D. (2025, January 6). 7 best AI apps for journaling (Updated 2025). Retrieved from https://www.taskade.com/blog/best-ai-apps-for-journaling/
63. Koyuturk, C., Yavari, M., Theophilou, E., Bursic, S., Donabauer, G., Telari, A., . . . Ognibene, D. (2023). Developing Effective Educational Chatbots with ChatGPT prompts: Insights from Preliminary Tests in a Case Study on Social Media Literacy (with appendix). *arXiv (Cornell University)*. https://doi.org/10.48550/arxiv.2306.10645
64. Aromatario, O., Velardo, F., Martel, E., Couralet, D., Cambon, L., & Martin-Fernandez, J. (2024). Improving personal, social, and life skills in adolescents: a scoping review of key components in interventions. *Journal of Public Health*. https://doi.org/10.1007/s10389-024-02256-5
65. Pergantis, P., Bamicha, V., Skianis, C., & Drigas, A. (2025). AI Chatbots and Cognitive control: Enhancing executive functions through chatbot interactions: A systematic review. *Brain Sciences, 15*(1): 47. https://doi.org/10.3390/brainsci15010047
66. Ghadiri, P., Yaffe, M. J., Adams, A. M., & Abbasgholizadeh-Rahimi, S. (2024). Primary care physicians' perceptions of artificial intelligence systems in the care of adolescents' mental health. *BMC Primary Care, 25*(1):215. https://doi.org/10.1186/s12875-024-02417-1
67. Marshall, N. J., Loades, M. E., Jacobs, C., Biddle, L., & Lambert, J. D. (2025). Integrating Artificial intelligence in youth Mental health care: advances, challenges, and future directions. *Current Treatment Options in Psychiatry, 12*(1):11. https://doi.org/10.1007/s40501-025-00348-x
68. Ma, Z., Mei, Y., & Su, Z. (2023). Understanding the benefits and challenges of using large language model-based conversational agents for mental well-being support. *arXiv (Cornell University)*. https://doi.org/10.48550/arxiv.2307.15810
69. Iqbal, J., Jaimes, D. C. C., Makineni, P., Subramani, S., Hemaida, S., Thugu, T. R., . . . Arain, M. (2023). Reimagining Healthcare: Unleashing the power of artificial intelligence in medicine. *Cureus. 15*(9): e44658. https://doi.org/10.7759/cureus.44658
70. Mithal, M. (2025, April 15). Utah enacts mental health chatbot law | The Data Advisor. Retrieved from https://www.wsgrdataadvisor.com/2025/04/utah-enacts-mental-health-chatbot-law/
71. Sharma, A., Lin, I. W., Miner, A. S., Atkins, D. C., & Althoff, T. (2023). Human–AI collaboration enables more empathic conversations in text-based peer-to-peer mental health support. *Nature Machine Intelligence, 5*(1): 46–57. https://doi.org/10.1038/s42256-022-00593-2
72. Stade, E. C., Stirman, S. W., Ungar, L. H., Boland, C. L., Schwartz, H. A., Yaden, D. B., Sedoc, J., DeRubeis, R. J., Willer, R., & Eichstaedt, J. C. (2024). *Large language models could change the future of behavioral healthcare: A proposal for responsible development and evaluation. npj Mental Health Research, 3*(12). https://doi.org/10.1038/s44184-024-00056-z
73. D'Alfonso, S. (2020). AI in mental health. *Current Opinion in Psychology, 36*: 112–117. https://doi.org/10.1016/j.copsyc.2020.04.005
74. Martinengo, L., Lum, E., & Car, J. (2022). Evaluation of chatbot-delivered interventions for self-management of depression: Content analysis. *Journal of Affective Disorders, 319*: 598–607. https://doi.org/10.1016/j.jad.2022.09.028
75. Razavi, S. Z., Ali, M. R., Smith, T. H., Schubert, L. K., & Hoque, M. (2016). The LISSA Virtual Human and ASD Teens: An overview of initial experiments. In *Lecture Notes in Computer Science* (pp. 460–463). https://doi.org/10.1007/978-3-319-47665-0_55
76. Happify Health. (2020). *Happify for teens* [Press release]. https://static.happify.com/static/pdf/happifyhealth_v2/Happify_for_Teens.pdf?9b17ad138c91388086874bab720954ea953c81c3
77. Coghlan, S., Leins, K., Sheldrick, S., Cheong, M., Gooding, P., & D'Alfonso, S. (2023). To chat or bot to chat: Ethical issues with using chatbots in mental health. *Digital Health, 9*: 1-11. https://doi.org/10.1177/20552076231183542
78. Dilmegani, C. (2025). "How to build a chatbot: Components & architecture in 2026". AIMultiple. https://research.aimultiple.com/chatbot-architecture/
79. Vaidyam, A. N., Wisniewski, H., Halamka, J. D., Kashavan, M. S., & Torous, J. B. (2019). Chatbots and conversational agents in mental health: A review of the psychiatric landscape. *The Canadian Journal of Psychiatry*, 64(7): 456–464. https://doi.org/10.1177/0706743719828977

Author

Katherine Xu, a junior at Mountain View High School (MVHS) in California, is passionate about using technology to support children with special needs, which inspired this paper. She is the co-lead of MVHS's nationally ranked First Robotics Competition Team 971 and has volunteered 200+ hours coaching children with special needs.

DOI: 10.36838/IJHSR810.10

IJHSR
ijhighschoolresearch.org
REVIEW ARTICLE

Applications of CRISPR-Cas9 Genome Editing Technology in the Treatment of Human Diseases

Elif Baser

Nesibe Aydin Yildizlar Science High School, Dumlupinar Bulvari Baglica Kavsagi, No: 1/A, Etimesgut, Ankara, 06890, Turkey; elifbaser2201@gmail.com

ABSTRACT: Genome editing (GED) technologies have advanced substantially and are currently being tested for the treatment of human diseases. Clustered regularly interspaced short palindromic repeats (CRISPR)-CRISPR-associated protein 9 (Cas9) GED technology has advanced biotechnology by providing a relatively simple and cost-effective method for creating precise deoxyribonucleic acid edits compared to other GED technologies. This technology has become a promising method for treating diseases by enabling the targeted disruption, modification, or editing of pathogenic genes. However, several factors, including disease heterogeneity, off-target effects, and technical and ethical challenges in its application, limit the clinical use of CRISPR-Cas9. This article examines the therapeutic efficacy of CRISPR-Cas9 technologies in the treatment of numerous conditions, including cancer, neurodegenerative diseases, viral infections, allergic and immunological diseases, and hematologic diseases.

KEYWORDS: Cellular and Molecular Biology, Genetics, Biotechnology, CRISPR-Cas9, Genome Editing, Human Disease.

Introduction

In recent years, clustered regularly interspaced short palindromic repeats (CRISPR) and CRISPR-associated (Cas) proteins, which originated from bacterial and archaeal adaptive immune systems, have become widely used for genome editing (GED) in biotechnological and biomedical research.[1] GED technologies can enable the precise modification of deoxyribonucleic acid (DNA) sequences in living cells. In addition to CRISPR-Cas9, other advanced GED technologies include zinc finger nucleases (ZFNs) and transcription activator-like effector nucleases (TALENs).[2,3] ZFNs are composed of the zinc finger proteins and the non-specific FokI cleavage domain and are involved in protein-protein interactions and DNA transcription regulation in eukaryotes.[4] Notably, ZFNs can only identify nucleotide triplets in DNA, which limits their site selection.[5] TALENs also consist of FokI endonuclease and a complex of transcription activator-like effectors.[6] Although they are more specific than ZFNs because they can detect a single nucleotide, the larger size of TALENs when compared to ZFNs may cause difficulties in their packaging and delivery.[7]

CRISPR-Cas9 involves a single guide RNA (sgRNA) sequence and the Cas9 endonuclease. The sgRNA is formed by the composition of trans-activating crRNA (tracrRNA) and CRISPR-RNA (crRNA), enabling the Cas9/sgRNA ribonucleoprotein complex to recognize and bind to the target DNA sequence.[8] After DNA targeting occurs, Cas9 creates double-strand breaks (DSBs) in the target region of DNA. The DSBs are then repaired by non-homologous end joining (NHEJ) and homology-directed repair (HDR) mechanisms using template DNA. In the absence of homologous DNA sequences, the cell undergoes NHEJ, which creates small deletions or insertions around the cut site. Since there is no DNA template for repair, this process is somewhat random and thus highly error-prone. If donor DNA with homologous strands matching the genomic DNA is provided, a DNA molecule with high homology to the target region is inserted into the genome following a double-strand break.

The key difference between CRISPR-Cas9, ZFNs, and TALENs is that CRISPR-Cas9 uses an RNA-mediated sequence-specific cutting technique, while the others are protein-based DNA editing techniques. CRISPR-Cas9 provides several advantages over ZFNs and TALENs, such as improved cost-effectiveness, higher target specificity, and the relative ease of designing sgRNAs for diverse target DNAs. Moreover, CRISPR-Cas9 can enable direct genome editing in the embryo and the simultaneous induction of multiple mutations.[9] CRISPR-Cas systems are classified into class 1 and class 2, and the Cas 9 protein belongs to class 2.[10] CRISPR-Cas9 is preferred for GED due to its simplicity when compared to other systems.[11]

CRISPR-Cas9 GED technology is among the most promising and popular methods for treating multiple diseases through GED. This article will discuss various diseases for which CRISPR-Cas9 technology is being tested in treatment.

Discussion

CRISPR-Cas9 GED technology in human diseases:

Cancer:

Cancer is a critical disease resulting from genetic and epigenetic reasons, representing one of the predominant causes of death globally. Because of the complexity of its mechanisms, current cancer treatments (e.g., chemotherapy, surgery, radiotherapy, and targeted therapy) have shown limited effectiveness, highlighting the need for alternative treatment approaches. In recent years, GED has become one of the leading strategies in treating cancer. GED facilitates the manipulation of tumor-associated genes using CRISPR-Cas9 technology, with studies

DOI: 10.36838/IJHSR810.19

indicating that this technology can be effective in cancer treatment. Furthermore, CRISPR-Cas9 technologies continue to hold promise in areas such as tumor immunotherapy and overcoming resistance to chemotherapy drugs.[12] CRISPR-Cas9 GED-based therapy is being investigated in many cancers, such as colorectal cancer, breast cancer, and hepatocellular cancer.[13-15] A primary cause of tumors is the dysregulation of cell proliferation through the activation of proto-oncogenes and the inactivation of tumor suppressor genes.[16] Tumor development or growth can be prevented by knocking out oncogenes or restoring tumor suppressor genes and restoring their function with CRISPR-Cas9 technology.[17]

CRISPR-Cas9 technology can target specific disease-causing genes, as well as different types of genes, such as *epidermal growth factor receptor (EGFR), tumor protein P53 (p53), telomerase reverse transcriptase, v-Raf murine sarcoma viral oncogene homolog B, breast cancer gene (BRCA), human epidermal growth factor receptor 2*, and *Kirsten rat sarcoma viral oncogene homolog (KRAS)*. Liu *et al.* reported that editing genes, such as *E-cadherin, p21,* and *hBax*, via CRISPR-Cas9 decreased cell motility, inhibited cell proliferation, and initiated apoptosis in bladder cancer cells.[18] The *myeloid cell leukemia-1 (MCL-1)* gene plays a role in cell differentiation, proliferation, and tumorigenesis and is becoming a novel target for cancer therapy. It has been shown that the knockout of the MCL-1 gene via the lentiviral (LV) CRISPR-Cas9 system initiates apoptosis of Burkitt lymphoma (BL) cells and, through the repeated induction of sgRNA, impairs tumor development in a xenograft model.[19] CRISPR-Cas9 technology has also been reported to upregulate further sex combs-like 1 protein expression, which significantly reduces leukemia cell growth.[20] Besides, the CRISPR-mediated correction of protein kinase C mutations in a xenograft model has been shown to inhibit colon tumor growth.[21]

Carcinogenic viral infections are a crucial factor in cancer development. For example, hepatitis B virus (HBV) and hepatitis C virus (HCV) are associated with hepatocellular carcinoma (HCC), Epstein-Barr virus (EBV) with nasopharyngeal carcinoma, Hodgkin lymphoma, and Burkitt lymphoma, and human papillomavirus (HPV) with cervical cancer. By using viral genome-specific Cas9-sgRNA and targeting viral oncogenes, cancer cell death can be induced. In cervical cancer, the expression of HPV oncoproteins E6 and E7 causes malignant transformation in normal cells. Studies have shown that interfering with the *E6* and *E7* genes via CRISPR-Cas9 inhibits cervical cancer development and reverses the malignant phenotype.[22,23] Price *et al.* produced *Francisella novicida* Cas9 (FnCas9) to accurately interfere with the HCV RNA genome and observed that FnCas9 suppressed HCV infection by reducing viral protein production.[24] It is also possible to modify the EBV genome via CRISPR-Cas9. In one reported study, seven anti-EBV gRNAs were administered together via transfection into a B cell line obtained from a BL patient with latent EBV infection to disrupt the genome, which gave rise to the initiation of apoptosis, the inhibition of cell proliferation, and a reduction in viral load.[25]

CRISPR-Cas9 technology is increasingly being employed in cancer immunotherapy, which activates the innate or adaptive immune system through various methods rather than directly targeting the tumor. The goal is to mobilize T cells by acting on various control points such as cytotoxic T lymphocyte antigen 4 (CTLA-4), programmed cell death protein 1 (PD-1), and programmed death ligand 1 (PD-L1). Studies are currently underway to strengthen the response of T cells against cancer cells and their capability to successfully destroy cancer cells by knocking out the *PD-1* or *CTLA-4* gene, utilizing CRISPR-Cas9 systems.[26,27]

CRISPR-Cas9 can also be used to reprogram tumor stroma to achieve anticancer effects. A study comparing fibroblasts taken from normal ovarian tissue and ovarian cancer tissue found that cancer-associated fibroblasts expressed more genes involved in glutamine synthesis, and that inactivation of glutamine synthetase—essential for glutamine production—efficiently inhibited cancer cell growth.[28] It has been suggested that inactivation of the glutamine synthetase gene via CRISPR could be implemented to inhibit tumor growth.[29]

Drug resistance is a significant problem in cancer treatment since resistance to a drug can result in resistance to different drugs, resulting in a condition called multidrug resistance (MDR). Many mechanisms serve roles in the emergence of drug resistance, including the increased function of drug efflux pumps like the ATP-binding cassette (ABC), increased DNA repair capacity, increased drug detoxification, disruption of cellular signaling pathways, increased epithelial–mesenchymal transition, and decreased apoptosis.[30,31] Recently, studies have examined CRISPR-Cas9 technology to overcome drug resistance in different cancer treatments. A significant cause of drug resistance in cancer cells is the overexpression of ABC family transporters, which facilitate the excretion of cancer drugs. One study observed that intervention of the *ABCB1* gene via the CRISPR-Cas9 increased doxorubicin (DOX) accumulation in cancer cells, thereby enhancing chemosensitivity.[32] Another study indicated that targeting the *MDR1* gene via the CRISPR-Cas9 quadrupled drug uptake in drug-resistant breast cancer cells.[33] A similar phenomenon has been observed in ovarian cancer and osteosarcoma cells, demonstrating that the CRISPR-Cas9 can substantially reduce *ABCB1* gene expression and increase cancer cell sensitivity to DOX.[34,35]

Cyclin-dependent kinases (CDKs) are enzymes that serve roles in cell proliferation, DNA repair regulation, and the cell cycle. Increased levels of these enzymes in cancer cells suggest that inhibiting these enzymes may have promising results for cancer treatment. For instance, the inactivation of CDK11 in osteosarcoma cells utilizing the CRISPR-Cas9 system has been shown to increase cell death as well as reduce cancer cell invasiveness.[36] CDK6 was also found to be elevated in palbociclib-resistant breast cancer cells, while the CRISPR-Cas9-mediated knockout of CDK6 increased palbociclib sensitivity and induced cancer cell death.[37] Moreover, glutathione S-transferase may contribute to drug resistance by augmenting the detoxification of chemotherapy drugs, upregulating the conjugation of chemotherapy drugs with glutathione, and attenuating apoptosis. For example, disabling

glutathione S-transferase using the CRISPR-Cas9 leads to an increase in the cytotoxic effect of chemotherapeutics in colorectal cancer cells.[38]

Overexpression of *BRCA1* is associated with chemotherapy resistance.[39] Since *BRCA1* mutations can be variable and difficult to target, targeting PARP1, a synthetic lethal partner of *BRCA1*, is a more feasible approach. In breast cancer cells, intervention of *PARP1* with the CRISPR-Cas9 increased sensitivity to chemotherapeutics, resulting in lower drug doses being required to achieve therapeutic efficacy.[40]

Mutations affecting tumor suppressor genes and oncogenes, such as *P53* and *KRAS*, have been shown to serve important roles in drug resistance. In colorectal cancer, targeting *KRAS* via CRISPR-Cas9 technology markedly decreased tumor cell size and improved the efficacy of cetuximab in inducing apoptosis.[41] Moreover, inactivation of mutant *TP53* in osteosarcoma cells with CRISPR-Cas9 systems both increased sensitivity to DOX and reduced the overexpression of anti-apoptotic proteins.[42] CD44 is regarded as a surface marker of cancer stem cells and is also a marker of drug resistance. It has been shown that deactivating CD44 via the CRISPR-Cas9 system can prevent invasion and metastasis in osteosarcoma cells.[43]

Mutations in EGFR are found in various cancers.[44,45] While EGFR inhibitors are useful for treating non-small cell lung cancer (NSCLC) in which EGFR mutations are detected, there are problems with drug resistance.[46] It has been reported that disruption of mutant EGFR in NSCLC cells using the CRISPR-Cas9 leads to a reduction in tumor size, an increase in tumor cell death, and an extension of survival time.[47] RECQL4 helicase is a protein that serves roles in drug resistance and DNA repair, and can increase *MDR1* expression. It has been demonstrated that deactivating RECQL4 via the CRISPR-Cas9 technique in glioma cells can increase the toxic effect of temozolomide on glioma cells.[48]

Neurodegenerative diseases:

Alzheimer's disease (AD), Parkinson's disease (PD), spinocerebellar ataxia (SCA), Huntington's disease (HD), and amyotrophic lateral sclerosis (ALS) are widespread neurodegenerative diseases, all of which involve a gradual deterioration of neuronal structure and function, leading to nerve loss over time.

AD affects memory, speech, behavior, and decision-making ability and can eventually lead to dementia.[49] In this disease, extracellular amyloid plaques composed of amyloid β-protein (Aβ) and neurofibrillary tangles containing hyperphosphorylated tau protein are found. To date, conventional treatments have not been successful in preventing Aβ formation or in clearing toxic proteins from the brain. Although AD is generally sporadic, a small number of cases are familial and result from autosomal dominant mutations in the *amyloid precursor protein (APP), presenilin-1 (PSEN1),* or *presenilin-2 (PSEN2)* genes, with *PSEN1* mutations often being the primary cause; these mutations increase the production of Aβ42, which is more prone to aggregation than Aβ40.[50] A study reported that CRISPR-Cas9 technology could selectively impair the *PSEN1M146L* allele and alter the Aβ42/40 ratio in carriers of this mutation.[51] Similarly, another study reported that CRISPR-Cas9 correction of neurons containing fibroblasts with *PSEN2N141I* mutation could correct the Aβ42/40 ratio.[52] One APP gene, known as the Swedish *KM670/671NL APP*, causes increased levels of Aβ protein.[53] Guyon *et al.* attempted to modify the APP gene using a CRISPR-Cas9-based approach and ultimately reduced Aβ protein accumulation.[54] The *apolipoprotein E (APOE)* gene is a predisposing factor for sporadic AD, with several variants, among which *APOE4* confers an increased risk for the disease. A study using CRISPR-Cas9 technology demonstrated that *APOE4* affects Aβ metabolism.[55] Additionally, Wadhwani *et al.* attempted to correct the *E4* allele to the *E3/E3* genotype in induced pluripotent stem cells (iPSCs) obtained from AD patients using the CRISPR-Cas9 method and observed that *E3* neurons were highly resistant to cytotoxicity and also exhibited decreased tau phosphorylation when compared to *E4* neurons.[56]

PD is characterized by the progressive loss of dopaminergic neurons in the substantia nigra pars compacta, resulting in decreased dopamine levels reaching the striatum. This results in impaired motor function and the emergence of symptoms such as rigidity, tremor, and bradykinesia. Intracytoplasmic Lewy bodies containing α-synuclein and ubiquitin are observed in this disease. Most patients with PD have idiopathic disease, and only a small number have mutations in various genes. In their studies utilizing the CRISPR-Cas9 technology to delete the *A53T-SNCA* gene, Yoon *et al.* observed significant improvement in various conditions associated with PD, such as motor symptoms, reactive microgliosis, α-synuclein overproduction, and dopaminergic neurodegeneration.[57] Furthermore, Chen *et al.* used CRISPR technology to correct neurons generated from iPSCs taken from PD patients with *A53T* and *SNCA* mutations and investigated the role of *SNCA* in the nucleus. Realizing that the absence of *SNCA* caused resistance to Lewy pattern formation, they reported that CRISPR-Cas9 technology could be a promising treatment for PD.[58] Moreover, other studies have been conducted to delete the *PRKN, PARK2, PINK1,* and *ATP13A2* genes using CRISPR-Cas9 technology.[59,60] Loss-of-function mutations in the *DNAJC6* gene have been observed in patients with early-onset PD, and CRISPR-Cas9 techniques were used in human embryonic stem cells to reveal these mutations.[61]

As the most common inherited neurodegenerative disorder, HD is an autosomal dominant disorder and is caused by the formation of a prolonged polyglutamine strand in the N-terminal area of the huntingtin protein due to CAG (cytosine-guanine-adenine) repeat expansions in the *huntingtin* gene (*HTT*). Accumulation of this protein in the brain affects molecular and cellular functions, causing a variety of symptoms, including decreased cognitive function, incoordination, chorea, or dystonia.[62] Since HD occurs due to a single mutation, it is a disease amenable to treatment with GED technology. Shin *et al.* utilized CRISPR-Cas9 technology to inactivate the mutant *HTT* allele selectively.[63] Additionally, Yang *et al.* reported that inactivating *HTT* in HD140Q-KI mice with CRISPR-Cas9 could eliminate the neuronal toxicity caused by polyglutamine accumulation in the brain and improve motor dysfunction.[64]

DOI: 10.36838/IJHSR810.19

Another study in R6/2 mice containing exon 1 of the human *HTT* gene showed that interfering with the mutant *HTT* gene by utilizing CRISPR-Cas9 reduced the formation of neurotoxic inclusions by twofold and improved motor deficits.[65]

ALS is a motor neuron disease characterized by degeneration in the motor neurons of the central nervous system. It can cause muscle weakness, muscle atrophy, paralysis, and in severe cases, respiratory failure and even death.[66] Sporadic cases account for approximately 90% of patients, while familial ALS, which is inherited, accounts for the remaining 10%. The pathogenic genes related to ALS are *C9orf72, SOD1, TARDBP,* and *FUS*.[67] Deng *et al.* demonstrated that CRISPR-Cas9-mediated editing was effective in targeting *hSOD1* in two different *hSOD1-G93A* transgenic mouse models of ALS, resulting in a disease-free state.[68] Yun *et al.* utilized the CRISPR-Cas9 to target gene correction associated with the *SOD1 E100G* mutation in iPSCs from a person with ALS, and these iPSCs were then differentiated into motor neurons.[69] In addition to these studies, Chen *et al.* investigated the CRISPR-Cas9 technique to modify specific point mutations associated with ALS, resulting in either correcting *I114T* mutations in *SOD1* in patient iPSCs or introducing new mutations such as *G94A* in *SOD1* or *H517Q* in *FUS* in iPSCs.[70]

SCA is an autosomal dominantly inherited neurodegenerative disease characterized by speech difficulties and disorders related to balance and coordination. There are more than 40 genetic variants of SCA, with the SCA1, SCA2, SCA3, and SCA6 subtypes constituting the majority of patients. He *et al.* reported that paired sgRNA/Cas9 and homologous recombination techniques could repair the 74 CAG expansion in exon 10 of *ATXN3* in SCA3-iPSCs, thereby reducing mutant ataxin-3 protein expression.[71] Song *et al.* also attempted to correct mutations in SCA3-iPSCs from SCA3 patients using homologous recombination and CRISPR-Cas9 technology.[72] In another study conducted on fibroblasts obtained from SCA1 patients, a reduction in the formation of both healthy and mutated *ATXN1* protein was observed using the G3 and G8 sgRNA/Cas9 complexes.[73]

Viral infections:

Acquired immunodeficiency syndrome (AIDS) is a serious illness caused by both human immunodeficiency virus (HIV)-1 and HIV-2. HIV-1 has higher pathogenicity, and *in vivo* active HIV-1 replication leads to CD4+ T cell depletion. Despite significant success with highly effective antiretroviral therapies, the persistent integration of HIV-1 into the host genome makes this disease difficult to treat. Numerous studies have been designed using CRISPR-Cas9 technology for the treatment of this infection, and in these studies, many genes have been targeted, especially long terminal repeats (LTRs).[74-76] LTRs are repetitive, identical sequences of DNA that aid in the insertion of retroviral DNA into the host chromosome and trigger HIV-1 gene expression. One study reported that CRISPR-Cas9 can cause the degradation of latent HIV-1 provirus by mutating the LTRs.[74]

HBV is a hepatotropic DNA virus and can cause liver cirrhosis and hepatocellular carcinoma. Studies have been conducted using CRISPR-Cas9 to target and cut various functional loci in HBV genomes, such as the surface antigen region and the reverse transcriptase gene.[77,78] The dead Cas9 (dCas9), a variant of Cas9, has also been shown to restrict HBV replication without causing fragmentation of the HBV genome.[79]

Infections with HCV, an RNA virus, can be treated effectively with appropriate pharmacological interventions; however, drug-resistant variants that are untreatable with current therapies may emerge. In this context, manipulation of the HCV genome using CRISPR-Cas9 may offer an alternative therapeutic approach. FnCas9, derived from the bacterium *Francisella novicida*, can target a bacterial mRNA, which can subsequently suppress a viral gene.[80] One study demonstrated that the CRISPR-FnCas9 system exhibits inhibitory activity against the HCV RNA genome in eukaryotic cells. It has been reported that the interaction of FnCas9 with the HCV RNA genome can suppress both the viral environment and genome replication.[24]

HPV infection can cause cervical cancer in women. To date, most studies have generally targeted the *E6* and *E7* regions of the HPV genome. Successful anti-HPV applications have been achieved by directly disrupting the HPV genome with the CRISPR-Cas9 system, and inhibition of tumor growth has been observed in most studies.[81,82]

Herpes simplex virus (HSV)-1, a neurotropic virus, can cause morbidity and even mortality in humans.[83] Studies have investigated the CRISPR-Cas9 targeting of viral proteins: one demonstrated that knockout of ICP0, a protein required for *HSV-1* gene expression, inhibited viral replication, while another reported that the disruption of UL7 using CRISPR-Cas9 reduced genome replication and attenuated neurovirulence.[84,85]

EBV causes infectious mononucleosis and is linked to some types of cancer.[86] Notably, interfering with the EBV nuclear antigen and latent membrane protein domains in the EBV genome with CRISPR-Cas9 has been reported to decrease proliferation and viral load in BL cells with latent EBV infection.[25] One study used two gRNAs to delete the promoter zone of BART, which encodes viral microRNAs, and this was shown to reduce miR-Bart3 expression and viral load in latently infected EBV models.[87] Another study by the same team reported that CRISPR-Cas9 technology reduced viral DNA loads and replication rates in nasopharyngeal carcinoma cells containing latent EBV.[88]

Cytomegalovirus (CMV) can cause serious infections in immunocompetent patients, particularly those undergoing organ transplantation. One study reported that using CRISPR-Cas9 technology to knock out UL122/123, a key CMV gene, disrupted CMV replication.[89] The paper reported that simultaneous targeting of different areas of the viral genome could disrupt multiple viral functions, and that a multiple-targeting strategy was superior to a single-targeting strategy.[89]

Allergic and immunological diseases:

Although CRISPR-Cas9 technologies have emerged relatively recently, they have made significant contributions to the field of allergy and immunology. Janus kinase 3 (JAK3) is a tyrosine kinase involved in signal transduction and leads to cy-

tokine production via T helper 2 cells. Its deficiency leads to a decrease in circulating natural killer (NK) cells and T cells, and disrupted B cell function. JAK3 is involved in the pathogenesis of various diseases, primarily allergic asthma.[90] Correcting the *JAK3* gene deficiency in patients with severe combined immunodeficiency via CRISPR-Cas9 regulated T cell improvement and normalized the number of NK and T cells.[91]

Mucine 18 (MUC18) is a transmembrane glycoprotein that is a marker of tumor progression in melanoma and is also expressed in the airway epithelial cells of patients with some pulmonary diseases, such as chronic obstructive pulmonary disease and asthma.[92] CRISPR-Cas9-mediated blocking of the *MUC18* gene in nasal airway epithelial cells leads to a significant decrease in IL-8, suggesting that *MUC18* serves a proinflammatory role.[93]

There has been growing interest in manipulating causative allergens in allergic diseases via GED to delete allergenic genes or minimize allergens. CYP11A1 is the first enzyme in the steroidogenic pathway that converts cholesterol to pregnenolone.[94] One study showed that children with peanut allergy had approximately 50-fold increased CYP11A1 gene expression in activated peripheral blood CD4+ T cells. Besides, significant increases in interleukin (IL)-4 and IL-13 produced by peanut-specific T cells were also demonstrated, and CYP11A1 mRNA levels were related to increased IL-13 production.[95] As a result of the study, targeting CYP11A1 via CRISPR-Cas9 technology decreased gene expression of CYP11A1 by over 50%, which in turn significantly reduced IL-13 production.[95]

The CRISPR-Cas9-mediated deletion of Fel d 1, the primary cat allergen, has been achieved in individuals with cat allergy.[96] Peanuts are a major cause of food allergy, and CRISPR-Cas9 has been tested in the development of non-allergenic peanuts. Ara h 2 is one of the peanut allergens, and it has been shown that disrupting the Ara h 2 gene in peanut protoplasts using CRISPR-Cas9 technology is possible.[97] Furthermore, CRISPR-Cas9-mediated β-lactoglobulin editing was performed in goat fibroblasts to prevent goat milk allergy.[98] Studies have also tested CRISPR-Cas9 technology to prevent egg allergy.[99]

Hematologic diseases:

CRISPR-Cas9 technology is also being investigated for the treatment of monogenic hematologic diseases, such as β-thalassemia, which result from mutations in the human *hemoglobin beta (HBB)* gene. This disease is characterized by hemolytic anemia and decreased β-hemoglobin production, leading to ineffective erythropoiesis. Using CRISPR-Cas9, it may be possible to repair the *HBB* mutation in β-thalassemia patients.[100] Another strategy for treating this disease is to reactivate the fetal hemoglobin gene by disrupting the *BCL11A* gene, a fetal hemoglobin silencer. It has been shown that the disruption of *BCL11A* by CRISPR-Cas9 may be beneficial in the treatment of β-hemoglobinopathies by facilitating the achievement of threshold levels of functional fetal hemoglobin.[101]

CRISPR-Cas9 technology can also correct the *HBB* gene mutation in sickle cell anemia.[102] Furthermore, Fanconi anemia is a genetic disorder in which most patients have mutations in the *FANCA, FANCC,* or *FANCG* genes, and this disease results in progressive bone marrow failure and a decrease in all blood cell types. CRISPR-Cas9 technology was used to correct a mutation in the *FANCC* gene in patients with Fanconi anemia.[103] X-linked chronic granulomatous disease is one of the primary immunodeficiencies arising from mutations in the *CYBB* gene and can cause fatal infections. Notably, homology-directed repair-based GED technologies have been used to adjust the *CYBB* mutation.[104] Wiskott-Aldrich syndrome (WAS) is a primary immunodeficiency disorder that exhibits X-linked inheritance and is caused by mutations in the WAS gene. Studies aimed to edit the WAS locus in a leukemia cell line using CRISPR-Cas9 technology.[105]

CRISPR-Cas9 GED technology in other diseases:

CRISPR-Cas9 is used for gene editing in cardiovascular disorders, particularly inherited lipid disorders. The *proprotein convertase subtilisin/kexin type 9 (PCSK9)* gene and the *angiopoietin-like 3 (ANGPTL3)* gene serve important roles in lipid hemostasis.[106] For example, the gain-of-function mutation in the *PCSK9* gene is associated with atherosclerosis and hypercholesterolemia.[107] In one study, a gRNA targeting a sequence in the mouse *PCSK9* gene and an adenoviral vector coding SpCas9 were implemented to knock out PCSK9 alleles in hepatocytes, resulting in an approximately 90% reduction in blood *PCSK9* protein levels and an approximately 40% reduction in blood cholesterol levels.[108] In another study, a chimeric liver-humanized mouse model was created, and it was shown that the *PCSK9* gene in hepatocytes was regulated by approximately 50%, and the *PCSK9* protein levels in the blood were decreased by approximately 50%.[109] In another mouse study using an adenoviral vector coding a cytosine base editor and a gRNA targeting the *ANGPTL3* glutamate-135 codon, 35% liver *ANGPTL3* editing was achieved, and approximately 50% decrease in blood *ANGPTL3* protein levels and 20% decrease in blood cholesterol levels were observed.[110]

Transthyretin (TTR) acts as a carrier for thyroxine and vitamin A by forming tetramers. However, unstable TTR monomers can accumulate in the heart, causing cardiomyopathy or polyneuropathy in the nerves. These accumulations are more likely to be caused by the mutant protein. By suppressing TTR expression in hepatocytes, it may be possible to treat diseases caused by the mutant protein. Studies in mice and primates have demonstrated that administering lipid nanoparticles containing a gRNA targeting the *Ttr* and *TTR* genes and SpCas9 messenger RNA resulted in liver remodeling in approximately 70% of all species, resulting in significant reductions in blood TTR protein levels.[111,112]

Duchenne muscular dystrophy (DMD) results from a mutation in the X-linked DMD gene. This gene is responsible for the production of dystrophin, a structural protein that fortifies myofibrils by binding cytoskeletal proteins. Characterized by progressive muscle weakness, this disease can lead to respiratory distress, swallowing problems, and cardiac complications over time. Four different preclinical studies using mouse models with mutations in exon 23 of the *DMD* gene have examined

DOI: 10.36838/IJHSR810.19

the effectiveness of CRISPR-CAS9 editing in the treatment of DMD.[113-116] Two of these studies used the systemic intravenous administration of adeno-associated viruses (AAVs), with one vector containing SaCas9 and the other containing a gRNA targeting the regions surrounding exon 23.[113-114] In another study, an AAV vector containing SaCas9 and two gRNAs was systemically administered to delete exons 21, 22 and 23.[115] In the latter, tandem AAVs were utilized, with one vector containing SpCas9 and the other containing a gRNA targeting the mutant sequence in exon 23.[116] In all of these studies, dystrophin expression was significantly restored in skeletal muscle and the heart, resulting in significant ameliorations in muscle function. In another study, a new rearrangement was induced in a dog model of DMD by the intravenous administration of an AAV vector expressing SpCas9 and a single gRNA targeting a region near the 5' end of exon 51, leading to partial reconstruction of dystrophin expression in heart and skeletal muscle.[117]

Inherited retinal diseases are a significant cause of blindness, yet there is currently no treatment available. However, gene therapy may be a potential treatment for these patients. Due to several distinct characteristics, the human eye could be a priority for gene therapy. Notably, the eye has immune privilege, meaning it has a higher tolerance to antigens.[118] Furthermore, the presence of a blood-retinal barrier reduces the likelihood of viral vectors administered to the eye during gene therapy migrating to other sites.[119] With current ophthalmic techniques, it is easier to reach the target area for gene therapy, resulting in a lower viral load. CRISPR-Cas9 technology has been utilized to target the allele-specific disruption of mutant genes in the treatment of some retinal diseases, such as wet age-related macular degeneration (AMD), Meesman epithelial corneal dystrophy, retinitis pigmentosa (RP), and Leber congenital amaurosis type 10 (LCA10).[120-122] Choroidal neovascularization (CNV) in wet AMD causes the deterioration of central vision. Researchers tested CRISPR-Cas9 to disrupt *Hif1a*, a gene involved in the development of CNV, in mice with laser-induced CNV and reported a significant decrease in CNV area when compared to controls in AAV-Hif1a-treated eyes without impaired cone function.[122] Two studies reported the use of CRISPR-Cas9 to reprogram mutation-susceptible rod cells into cone cells in an established RP model.[123,124] Notably, the transcription factors Nrl and Nr2e3 regulate rod cell differentiation, with the absence of either factor promoting rod-to-cone cell differentiation.[125] Researchers observed the downregulation of rod-specific genes and the upregulation of cone-specific genes following CRISPR-Cas9-mediated targeted gene deactivation of Nrl or Nr2e3 in mice.[123,124]

Cystic fibrosis (CF) is an autosomal recessive disease that affects the lungs and digestive system. CRISPR-Cas9 technology is also being tested to modify mutations in the cystic fibrosis transmembrane conductance regulator (CFTR) gene, which causes CF, and may be a useful approach for treatment in the future. In one of the studies conducted for this purpose, CRISPR-Cas9 was successfully used to correct the CFTR mutation in iPSCs.[126] Another study attempted to correct the CFTR gene using CRISPR-Cas9 in cultured stem cells.[127]

Conclusion

Although CRISPR-Cas9 technology holds great promise for the treatment of diseases, it has certain shortcomings that must be addressed, the most significant of which are off-target effects. The effectiveness of the CRISPR-Cas9 technology depends on various factors, including Cas9 activity and delivery, sgRNA design, target site selection, and off-target effects.[128] Despite sgRNA being designed to target specific DNA sequences with high accuracy, the complexity of the genome, which contains numerous highly homologous sequences, can result in sgRNA binding to off-target sites and inducing unintended gene editing. As such, off-target effects of CRISPR-Cas9 have been demonstrated in some clinical applications, and these effects have been reported to be more common than anticipated.[129] Off-target effects can lead to experimental problems and even false results or phenotypes, which severely limit the application of CRISPR-Cas9 systems.

Accurate delivery of CRISPR-Cas9 cargo to the target tissue also represents a significant challenge. The most commonly used viral vectors for GED are AAVs and LVs.[130] While AAVs are less immunogenic, have serotype specificity, and have a good safety profile, mild toxicity has been demonstrated at high doses in animal models.[131] In addition to their non-immunogenic advantages, LVs also possess pseudotyping capabilities, allowing for changes in cellular tropism. Packaging limitations can also represent an important issue when using these vectors. Moreover, it is also probable that the generated CRISPR-Cas9 complexes can stimulate the host immune system.[132]

In addition to technical difficulties, ethical and legal issues are among the key challenges that could hinder the real-world applicability of the CRISPR-Cas9 systems. Specific deactivation of targeted genes with CRISPR-Cas9 systems may be possible via modifying the genome in the germline. While mutations induced by CRISPR-Cas9 GED in the embryonic period can produce new *in vivo* models and treat different diseases, there is concern that they could lead to ecological imbalances.[133,134] Embryonic genome editing can lead to the inheritance of undesirable changes, leading to irreversible impacts on future generations. Importantly, uncontrolled mutations can create organisms carrying modified genetic traits, potentially disrupting ecological systems.

In conclusion, CRISPR-Cas9 GED technology is a promising method for discovering important disease-associated genes and uncovering potential therapeutic targets. As the technical and ethical challenges encountered with CRISPR-Cas9 technology are overcome, the safety and effectiveness of treatment strategies will increase and continue to hold promise for the treatment of numerous diseases in the future.

Acknowledgments

I would like to thank my supervisor, Elvan Camtepe, for her outstanding support throughout the project. I would also like to thank my family for supporting me in every way.

References

1. Wright, A. V.; Nuñez, J. K.; Doudna, J. A. Biology and Applications of CRISPR Systems: Harnessing Nature's Toolbox for Genome Engineering. *Cell* **2016**, *164* (1-2), 29–44. https://doi.org/10.1016/j.cell.2015.12.035.
2. Ma, D.; Liu, F. Genome Editing and Its Applications in Model Organisms. *Genomics Proteomics Bioinformatic* **2015**, *13* (6), 336–344. https://doi.org/10.1016/j.gpb.2015.12.001.
3. Gaj, T.; Gersbach, C. A.; Barbas, C. F. ZFN, TALEN, and CRISPR/Cas-Based Methods for Genome Engineering. *Trends Biotechnol.* **2013**, *31* (7), 397–405. https://doi.org/10.1016/j.tibtec.2013.04.004.
4. Wolfe, S. A.; Nekludova, L.; Pabo, C. O. DNA Recognition by Cys2His2 Zinc Finger Proteins. *Annu. Rev. Biophys. Biomol. Struct.* **2000**, 29, 183–212. https://doi.org/10.1146/ annurev. Biophys. 29.1.183.
5. Ramirez, C. L.; Foley, J. E.; Wright, D. A.; Müller-Lerch, F.; Rahman, S. H.; Cornu, T. I.; Winfrey, R. J.; Sander, J. D.; Fu, F.; Townsend, J. A.; Cathomen, T.; Voytas, D. F.; Joung, J. K. Unexpected Failure Rates for Modular Assembly of Engineered Zinc Fingers. *Nat. Methods* **2008**, 5, 374–375. https://doi.org/10.1038/nmeth0508-374.
6. Christian, M.; Cermak, T.; Doyle, E. L.; Schmidt, C.; Zhang, F.; Hummel, A.; Bogdanove, A.J.; Voytas, D.F. Targeting DNA Double-Strand Breaks with TAL Effector Nucleases. *Genetics* **2010**, *186* (2), 757–761. https://doi.org/10.1534/genetics.110.120717.
7. Lino, C. A.; Harper, J.C.; Carney, J.P.; Timlin, J.A. Delivering CRISPR: A Review of the Challenges and Approaches. *Drug Deliv.* **2018**, *25* (1), 1234–1257. https://doi.org/10.1080/10717544.2018.1474964.
8. Chylinski, K.; Makarova, K. S.; Charpentier, E.; Koonin, E. V. Classification and Evolution of Type II CRISPR-Cas Systems. *Nucleic Acids Res.* **2014**, *42* (10), 6091–6105. https://doi.org/10.1093/nar/gku241.
9. Bhattacharya, D.; Marfo, C. A.; Li, D.; Lane, M.; Khokha, M. K. CRISPR/ Cas9: An Inexpensive, Efficient Loss of Function Tool to Screen Human Disease Genes in Xenopus. *Dev. Biol.* **2015**, *408* (2), 196–204. https://doi.org/10.1016/j.ydbio.2015.11.003.
10. Makarova, K. S.; Wolf, Y. I.; Iranzo, J.; Shmakov, S. A.; Alkhnbashi, O. S.; Brouns, S. J.; Charpentier, E.; Cheng, D.; Half, D. H.; Horvath, P.; Moineau, S.; Mojica, F. J. M.; Scott, D.; Shah, S. A.; Siksnys, V.; Terns, M. P.; Venclovas, C.; White, M. F.; Yakunin, A. F.; Yan, W.; Zhang, F.; Garrett, R. A.; Backofen, R.; van der Oost, J.; Barrangou, R.; Koonin, E. V. Evolutionary Classification of CRISPR–Cas Systems: A Burst of Class 2 and Derived Variants. *Nat. Rev. Microbiol.* **2020**, *18* (2), 67–83. https://doi.org/10.1038/s41579-019-0299-x.
11. Jinek, M.; Chylinski, K.; Fonfara, I.; Hauer, M.; Doudna, J. A.; Charpentier, E. A Programmable Dual-RNA–Guided DNA Endonuclease in Adaptive Bacterial Immunity. *Science* **2012**, *337*(6096), 816–821. https://doi.org/10.1126/science.1225829.
12. Zheng, N.; Li, L.; Wang, X. Molecular Mechanisms, Off-target Activities, and Clinical Potentials of Genome Editing Systems. *Clin. Transl. Med.* **2020**, *10* (1), 412–426. https://doi.org/10.1002/ctm2.34.
13. Xu, G.; Chhangawala, S.; Cocco, E.; Razavi, P.; Cai, Y.; Otto, J. E.; Ferrando, L.; Selenica, P.; Ladewig, E.; Chan, C.; Paula A. D., Witkin, M.; Cheng, Y.; Park, J.; Serna-Tamayo, C.; Zhao, H. Y.; Wu, F.; Sallaku, M.; Qu, X.; Zhao, A.; Collings, C. K.; D'Avino, A. R.; Jhaveri, K.; Koche, R.; Levine, R. L.; Reis-Filho, J. S.; Kadoch, C.; Scaltriti, M.; Leslie, C.S.; Baselga, J.; Toska, E. ARID1A Determines Luminal Identity and Therapeutic Response in Estrogen-receptor-positive Breast Cancer. *Nat. Genet.* **2020**, *52* (2), 198-207. https://doi.org/10.1038/s41588-019-0554-0.
14. Michels, B. E.; Mosa, M. H.; Streibl, B. I.; Zhan, T.; Menche, C.; Abou-El-Ardat, K.; Darvishi, T.; Czlonka, E.; Wagner, S.; Winter, J.; Medyouf, H.; Boutros, M.; Farin, H. F.; Pooled *In Vitro* and *In Vivo* CRISPR-Cas9 Screening Identifies Tumor Suppressors in Human Colon Organoids. *Cell Stem Cell* **2020**, *26* (5), 782-792.e7. https://doi.org/10.1016/j.stem.2020.04.003.
15. Wu, X.; Ma, W.; Mei, C.; Chen, X.; Yao, Y.; Liu, Y.; Qin, X.; Yuan, Y. Description of CRISPR/Cas9 Development and Its Prospect in Hepatocellular Carcinoma Treatment. *J Exp Clin Canc Res* **2020**, *39* (1), 97. https://doi.org/10.1186/s13046-020-01603-0.
16. Martinez-Jimenez, F.; Muinos, F.; Sentis, I.; Deu-Pons, J.; Reyes-Salazar, I.; Arnedo-Pac, C.; Mularoni, L.; Pich, O.; Bonet, J.; Kranas, H.; Gonzalez-Perez, A.; Lopez-Bigas, N. A Compendium of Mutational Cancer Driver Genes. *Nat. Rev. Cancer* **2020**, *20* (10), 555–572. https://doi.org/10.1038/s41568-020-0290-x.
17. Azangou-Khyavy, M.; Ghasemi, M.; Khanali, J.; Boroomand-Saboor, M.; Jamalkhah, M.; Soleimani, M.; Kiani, J. CRISPR/Cas: From Tumor Gene Editing to T Cell-Based Immunotherapy of Cancer. *Front. Immunol.* **2020**, 11, 2062. https://doi.org/10.3389/fimmu.2020.02062.
18. Liu, Y.; Zeng, Y.; Liu, L.; Zhuang, C.; Fu, X.; Huang, W.; Cai, Z. Synthesizing AND Gate Genetic Circuits Based on CRISPR-Cas9 for Identification of Bladder Cancer Cells. *Nat. Commun.* **2014**, 5, 5393. https://doi.org/10.1038/ncomms6393.
19. Aubrey, B. J.; Kelly, G. L.; Kueh, A. J.; Brennan, M. S.; O'Connor, L.; Milla, L.; Wilcox, S.; Tai, L.; Strasser, A.; Herold, M. J. An Inducible Lentiviral Guide RNA Platform Enables the Identification of Tumor-Essential Genes and Tumor-Promoting Mutations *In Vivo*. *Cell Rep.* **2015**, *10* (8), 1422–1432. https://doi.org/10.1016/j.celrep.2015.02.002.
20. Valletta, S.; Dolatshad, H.; Bartenstein, M.; Yip, B. H.; Bello, E.; Gordon, S.; Yu, Y.; Shaw, J.; Roy, S.; Scifo, L.; Schuh, A.; Pellagatti, A.; Fulga, T. A.; Verma, A.; Boultwood, J. ASXL1 Mutation Correction by CRISPR/ Cas9 Restores Gene Function in Leukemia Cells and Increases Survival in Mouse Xenografts. *Oncotarget* **2015**, *6* (42), 44061–44071. https://doi.org/10.18632/oncotarget. 6392.
21. Antal, C. E.; Hudson, A. M.; Kang, E.; Zanca, C.; Wirth, C.; Stephenson, N L.; Trotter, E.W.; Gallegos, L.L.; Miller, C.J.; Furnari, F.B.; Hunter, T.; Brognard, J.; Newton, A.C. Cancer-Associated Protein Kinase C Mutations Reveal Kinase's Role as Tumor Suppressor. *Cell* **2015**, *160* (3), 489–502. https://doi.org/10.1016/j.cell.2015.01.001.
22. Kennedy, E. M.; Kornepati, A. V.; Goldstein, M.; Bogerd, H. P.; Poling, B. C.; Whisnant, A. W.; Kastan, M. B.; Cullen, B. R. Inactivation of the Human Papillomavirus E6 or E7 Gene in Cervical Carcinoma Cells by Using a Bacterial CRISPR/Cas RNA-Guided Endonuclease. *J. Virol.* **2014**, *88* (20), 11965–11972. https://doi.org/10.1128/JVI.01879-14.
23. Zhen, S.; Lu, J. J.; Wang, L. J.; Sun, X. M.; Zhang, J. Q.; Li, X.; Luo, W. J.; Zhao, L. *In Vitro* and *In Vivo* Synergistic Therapeutic Effect of Cisplatin with Human Papillomavirus16 E6/E7 CRISPR/Cas9 on Cervical Cancer Cell Line. *Transl. Oncol.* **2016**, *9* (6), 498–504. https://doi.org/10.1016/j.tranon.2016.10.002.
24. Price, A. A.; Sampson, T. R.; Ratner, H. K.; Grakoui, A.; Weiss, D. S. Cas9-Mediated Targeting of Viral RNA in Eukaryotic Cells. *Proc. Natl. Acad. Sci. U. S. A* **2015**, *112* (19), 6164–6169. https://doi.org/10.1073/pnas.1422340112.
25. Wang, J.; Quake, S. R. RNA-Guided Endonuclease Provides a Therapeutic Strategy to Cure Latent Herpesviridae Infection. *Proc. Natl. Acad. Sci. U. S. A* **2014**, *111* (36),13157–13162. https://doi.org/10.1073/pnas.1410785111.

DOI: 10.36838/IJHSR810.19

26. Schumann, K.; Lin, S.; Boyer, E.; Simeonov, D.R.; Subramaniam, M.; Gate, R. E.; Haliburton, G. E.; Ye, C. J.; Bluestone, J. A.; Doudna, J. A.; Marson, A. Generation of Knock-In Primary Human T Cells Using Cas9 Ribonucleoproteins. *Proc. Natl. Acad. Sci. U. S. A* **2015**, *112* (33), 10437–10442. https://doi.org/10.1073/pnas.1512503112.
27. Su, S.; Hu, B.; Shao, J.; Shen, B.; Du, J.; Du, Y.; Zhou, J.; Yu, L.; Zhang, L.; Chen, F.; Sha, H.; Cheng, L.; Meng, F.; Zou, Z.; Huang, X.; Liu, B. CRISPR-Cas9 Mediated Efficient PD-1 Disruption on Human Primary T Cells from Cancer Patients. *Sci. Rep*. **2016**, 6, 20070. https://doi.org/10.1038/srep20070.
28. Yang, L.; Achreja, A.; Yeung, T. L.; Mangala, L. S.; Jiang, D.; Han, C.; Baddour, J.; Marini, J. C.; Ni, J.; Nakahara, R.; Wahlig, S.; Chiba, L.; Kim, S. H.; Morse, J.; Pradeep, S.; Nagaraja, A. S.; Haemmerle, M.; Kyunghee, N.; Derichsweiler, M.; Plackemeier, T.; Mercado-Uribe, I.; Lopez-Berestein, G.; Moss, T.; Ram, P. T.; Liu, J.; Lu, X.; Mok, S.C.; Sood, A.K.; Nagrath, D. Targeting Stromal Glutamine Synthetase in Tumors Disrupts Tumor Microenvironment-Regulated Cancer Cell Growth. *Cell Metabol*. **2016**, *24* (5), 685–700. https://doi.org/10.1016/j.cmet.2016.10.011.
29. Chen, M.; Mao, A.; Xu, M.; Weng, Q.; Mao, J.; Ji, J. CRISPR-Cas9 for Cancer Therapy: Opportunities and Challenges. *Cancer Lett*. **2019**, 10, 447:48-55. https://doi.org/10.1016/j.canlet.2019.01.017
30. Gillet, J. P.; Gottesman, M. M. Mechanisms of Multidrug Resistance in Cancer. *Methods Mol. Biol*. **2010**, 596, 47–76. https://doi.org/10.1007/978-1-60761-416-6_4.
31. Zeller, C.; Brown, R. Therapeutic Modulation of Epigenetic Drivers of Drug Resistance in Ovarian Cancer. *Ther. Adv. Med. Oncol*. **2010**, *2*(5), 319–329. https://doi.org/10.1177/1758834010375759.
32. Yang, Y.; Qiu, J.G.; Li, Y.; Di, J. M.; Zhang, W. J.; Jiang, Q.W.; Zheng, D.W.; Chen, Y.; Wei, M. N.; Huang, J. R; wang, K.; shi, Z. Targeting ABCB1- Mediated Tumor Multidrug Resistance by CRISPR/Cas9-Based Genome Editing. *Am. J. Transl. Res*. **2016**, *8* (9), 3986–3994.
33. Ha, J. S.; Byun, J.; Ahn, D.R. Overcoming Doxorubicin Resistance of Cancer Cells by Cas9-Mediated Gene Disruption. *Sci. Rep*. **2016**, 6, 22847. https://doi.org/10.1038/srep22847.
34. Norouzi-Barough, L.; Sarookhani, M.; Salehi, R.; Sharifi, M.; Moghbelinejad, S. CRISPR/Cas9, a New Approach to Successful Knockdown of ABCB1/P-Glycoprotein and Reversal of Chemosensitivity in Human Epithelial Ovarian Cancer Cell Line. *Iran J. Basic Med. Sci*. **2018**, *21* (2), 181–187. https://doi.org/10.22038/IJBMS.2017.25145.6230.
35. Liu, T.; Li, Z.; Zhang, Q.; De Amorim Bernstein, K.; Lozano-Calderon, S.; Choy, E.; Hornicek, F. J.; Duan, Z. Targeting ABCB1 (MDR1) in Multi-Drug Resistant Osteosarcoma Cells Using the CRISPR-Cas9 System to Reverse Drug Resistance. *Oncotarget* **2016**, *7* (50), 83502–83513. https://doi.org/10.18632/oncotarget.13148.
36. Feng, Y.; Sassi, S.; Shen, J. K.; Yang, X.; Gao, Y.; Osaka, E.; Zhang, J.; Yang, S.; Yang, C.; Mankin, H. J.; Hornicek, F.J.; Duan, Z. Targeting CDK11 in Osteosarcoma Cells Using the CRISPR-Cas9 System. *J. Orthop. Res*. **2015**,3 3 (2), 199–207. https://doi.org/10.1002/jor.22745.
37. Cornell, L.; Wander, S. A.; Visal, T.; Wagle, N.; Shapiro, G. I. MicroRNA-Mediated Suppression of the TGF-β Pathway Confers Transmissible and Reversible CDK4/6 Inhibitor Resistance. *Cell Rep*. **2019**, *26* (10), 2667-2680.e7. https://doi.org/10.1016/j.celrep.2019.02.023.
38. Xu, Y.; Zhu, M. Novel Exosomal miR-46146 Transfer Oxaliplatin Chemoresistance in Colorectal Cancer. *Clin. Transl. Oncol*. **2020**, *22*(7), 1105–1116. https://doi.org/10.1007/s12094-019-02237-1.
39. Taron, M.; Rosell, R.; Felip, E.; Mendez, P.; Souglakos, J.; Ronco, M.S.; Queralt, C.; Majo, J.; Sanchez, J.M.; Sanchez, J.J.; Maestre, J. BRCA1 mRNA Expression Levels as an Indicator of Chemoresistance in Lung Cancer. *Hum. Mol.Genet*. **2004**,*13* (20), 2443–2449. https://doi.org/10.1093/hmg/ddh260.
40. Mintz, R. L.; Lao, Y. H.; Chi, C. W.; He, S.; Li, M.; Quek, C. H.; Shao, D.; Chen, B.; Han, J.; Wang, S.; Leong, K. W. CRISPR/Cas9-Mediated Mutagenesis to Validate the Synergy Between PARP1 Inhibition and Chemotherapy in BRCA1-Mutated Breast Cancer Cells. *Bioeng. Transl. Med*. **2020**, *5* (1), e10152. https://doi.org/10.1002/btm2.10152.
41. Ryu, J-Y.; Choi, Y.J.; Won, E-J.; Hui, E.; Kim, H-S.; Cho, Y-S.; Yoon, T-J. Gene Editing Particle System as a Therapeutic Approach for Drug-Resistant Colorectal Cancer. *Nano Res*. **2020**, 13, 1576–1585. https://doi.org/10.1007/s12274-020-2773-1.
42. Tang, F.; Min, L.; Seebacher, N. A; Li, X.; Zhou, Y.; Hornicek, F. J.; Wei, Y.; Tu, C.; Duan, Z. Targeting mutant TP53 as a potential therapeutic strategy for the treatment of osteosarcoma. *J Orthop Res*. **2019**, *37* (3), 789–798. https://doi.org/10.1002/jor.24227.
43. Liu, T.; Yan, Z.; Liu, Y.; Choy, E.; Hornicek, F.J.; Mankin, H.; Duan, Z. CRISPR-Cas9-Mediated Silencing of CD44 in Human Highly Metastatic Osteosarcoma Cells. *Cell Physiol. Biochem*. **2018**, *46* (3), 1218–1230. https://doi.org/10.1159/000489072.
44. Zhen, H. C. The Molecular Mechanisms of Chemoresistance in Cancers. *Oncotarget* **2017**, *8* (35), 59950–59964. https://doi.org/10.18632/oncotarget.19048.
45. Sigismund, S.; Avanzato, D.; Lanzetti, L. Emerging Functions of The EGFR in Cancer. *Mol. Oncol.* **2018**, *12* (1), 3–20. https://doi.org/10.1002/1878-0261.12155.
46. Tomasello, C.; Baldessari, C.; Napolitano, M.; Orsi, G.; Grizzi, G.; Bertolini, F.; Barbieri, F.; Cascinu, S. Resistance to EGFR Inhibitors in Non-Small Cell Lung Cancer: Clinical Management and Future Perspectives. *Crit. Rev. Oncol. Hematol*. **2018**, 123, 149–161. https://doi.org/10.1016/j.critrevonc.2018.01.013.
47. Koo, T.; Yoon, A. R.; Cho, H. Y.; Bae, S.; Yun, C. O.; Kim, J. S. Selective Disruption of an Oncogenic Mutant Allele by CRISPR/Cas9 Induces Efficient Tumor Regression. *Nucleic Acids Res.* **2017**,*45* (13),7897–7908. https://doi.org/10.1093/nar/gkx490.
48. Krol, S.K.; Kaczmarczyk, A.; Wojnicki, K.; Wojtas, B.; Gielniewski, B.; Grajkowska, W.; Kotulska, K.; Szczylik, C.; Czepko, R.; Banach, M.; Kaspera, W.; Szopa, W.; Marchel, A.; Czernicki, T.; Kimanska, B. Aberrantly Expressed RECQL4 Helicase Supports Proliferation and Drug Resistance of Human Glioma Cells and Glioma Stem Cells. *Cancers (Basel)* **2020**, *12* (10), 2919. https://doi.org/10.3390/cancers12102919.
49. Parambi, D. G. T.; Alharbi, K. S.; Kumar, R.; Harilal, S.; Batiha, G. E-S.; Cruz-Martins, N.; Magdy, O.; Musa, A.; Panda, D. S.; Mathew, B. Gene Therapy Approach with an Emphasis on Growth Factors: Theoretical and Clinical Outcomes in Neurodegenerative Diseases. *Mol. Neurobiol.* **2022**, *59* (1),191–233. https://doi.org/10.1007/s12035-021-02555-y.
50. Bertram, L.; Tanzi, R.E. The Genetics of Alzheimer's Disease. *Prog. Mol. Biol. Transl. Sci*. **2012**, 107, 79–100. https://doi.org/10.1016/B978-0-12-385883-2.00008-4.
51. Konstantinidis, E.; Molisak, A.; Perrin, F.; Streubel-Gallasch, L.; Fayad, S.; Kim, D. Y.; Petri, K.; Aryee, M. J.; Aguilar, X.; György, B.; Giedraitis, V.; Joung, K.; Pattanayak, V.; Essand, M.; Erlandsson, A.; Berezovska, O.; Ingelsson, M. CRISPR-Cas9 Treatment Partially Restores Amyloid-β 42/40 in Human Fibroblasts with the Alzheimer's Disease PSEN1 M146L Mutation. *Mol. Ther. Nucleic Acids.* **2022**, 28, 450–461. https://doi.org/10.1016/j.omtn.2022.03.022
52. Ortiz-Virumbrales, M.; Moreno, C.L.; Kruglikov, I.; Marazuela, P.; Sproul, A.; Jacob, S.; Zimmer, M.; Paull, D.; Zhang, B.; Schadt

E. E.; Erlich, M. E.; Tanzi, R.T.; Arancio, O.; Noggşe, S.; Gandy, S. CRISPR/Cas9-Correctable Mutation-Related Molecular and Physiological Phenotypes in iPSC-Derived Alzheimer's PSEN2 N141I Neurons. *Acta Neuropathol. Commun*. **2017**, *5* (1), 77. https://doi.org/10.1186/s40478-017-0475-z.

53. György, B.; Lööv, C.; Zaborowski, M. P.; Takeda, S.; Kleinstiver, B. P.; Commins, C.; Kastanenka, K.; Mu, D.; Volak, A.; Giedraitis, V.; Lannfelt, L.; Maguire, C. A.; Joung, J. K.; Hyman, B. T.; Breakefield, X. O.; Ingelsson, M. CRISPR/Cas9 Mediated Disruption of the Swedish APP Allele as a Therapeutic Approach for Early-Onset Alzheimer's Disease. *Mol. Ther. Nucleic Acids*. **2018**, 11, 429–440. https://doi.org/10.1016/j.omtn.2018.03.007.
54. Guyon, A.; Rousseau, J.; Bégin, F-G.; Bertin, T.; Lamothe, G.; Tremblay, J.P. Base Editing Strategy for Insertion of the A673T Mutation in the APP Gene to Prevent the Development of AD *In Vitro*. *Mol. Ther. Nucleic Acids*. **2021**, 24, 253–263. https://doi.org/10.1016/j.omtn.2021.02.032.
55. Lin, Y-T.; Seo, J.; Gao, F.; Feldman, H.M.; Wen, H-L.; Penney, J.; Cam, H.P.; Gjoneska, E.; Raja, W. K.; Cheng, J.; Rueda, R.; Kritskiy, O.; Abdurrob, F.; Peng, Z.; Milo, B.; Yu, J.C.; Elmsaouri, S.; Dey, D.; Ko, T.; Yankner, B. A.; Tsai, L-H. APOE4 Causes Widespread Molecular and Cellular Alterations Associated with Alzheimer's Disease Phenotypes in Human iPSC-Derived Brain Cell Types. *Neuron*. **2018**, *98* (6), 1141–1154. https://doi.org/10.1016/j.neuron.2018.05.008.
56. Wadhwani, A.R.; Affaneh, A.; Van Gulden, S.; Kessler, J.A. Neuronal Apolipoprotein E4 Increases Cell Death and Phosphorylated Tau Release in Alzheimer's Disease. *Ann Neurol*. **2019**, *85*(5), 726–739. https://doi.org/10.1002/ana.25455.
57. Yoon, H.H.; Ye, S.; Lim, S.; Jo, A.; Lee, H.; Hong, F., Lee, S. E.; Oh, S-J.; Kim, N-R.; Kim, K.; Kim, B-J.; Kim, H.; Lee, C.L. Nam, M-H.; Hur, J. W.; Jeon, S. R. CRISPR-Cas9 Gene Editing Protects from the A53T-SNCA Overexpression-Induced Pathology of Parkinson's Disease *In Vivo*. *CRISPR J*. **2022**, *5*(1), 95–108. https://doi.org/10.1089/crispr.20210025.
58. Chen, V.; Moncalvo, M.; Tringali, D.; Tagliafierro, L.; Shriskanda, A.; Ilich, E.; Dong, W.; Kantor, B.; Chiba-Falek, O. The Mechanistic Role of Alpha-Synuclein in the Nucleus: Impaired Nuclear Function Caused by Familial Parkinson's Disease SNCA Mutations. *Hum. Mol. Genet.* **2020**, *29* (18), 3107–3121. https://doi.org/10.1093/hmg/ddaa183.
59. Zhou, X.; Xin, J.; Fan, N.; Zou, Q.; Huang, J.; Ouyang, Z.; Zhao, Y.; Zhao, B.; Liu, Z.; Lai, S.; Yi, X.; Guo, L.; Esteban, M. A.; Zeng, Y.; Huaqiang, Y.; Lai, L. Generation of CRISPR/Cas9-Mediated Gene-Targeted Pigs Via Somatic Cell Nuclear Transfer. *Cell Mol. Life Sci.* **2015**, *72* (6), 1175–1184.https://doi.org/10.1007/s00018-014-1744-7.
60. Ahfeldt, T.; Ordureau, A.; Bell, C.; Sarrafha, L.; Sun, C.; Piccinotti, S.; Grass, T.; Parfitt, G. M.; Paulo, J. A.; Yanagawa, F.; Uozumi, T.; Kiyota, Y.; Harper, J. W., Rubin, L. L. Pathogenic Pathways in Early-Onset Autosomal Recessive Parkinson's Disease Discovered Using Isogenic Human Dopaminergic Neurons. *Stem Cell Reports*, **2020**, *14* (1), 75–90. https://doi.org/10.1016/ j.stemcr. 2019.12.005
61. Wulansari, N.; Darsono, W. H. W.; Woo, H-J.; Chang, M-Y.; Kim, J.; Bae, E-J.; Sun, W.; Lee, J. H.; Cho, I. J.; Shin, H.; Lee, S. J.; Lee, S. H. Neurodevelopmental Defects and Neurodegenerative Phenotypes in Human Brain Organoids Carrying Parkinson's Disease-Linked DNAJC6 Mutations. *Sci. Adv*. **2021**, *7* (8), eabb1540. https://doi.org/10.1126/sciadv.abb1540.
62. Byun, S.; Lee, M.; Kim, M. Gene Therapy for Huntington's Disease: The Final Strategy for a Cure? *J. Move Disord*. **2022**, *15* (1), 15–20. https://doi.org/10.14802/jmd.21006.
63. Shin, J. W.; Kim, K-H.; Chao, M. J.; Atwal, R. S.; Gillis, T.; MacDonald, M. E.; Gusella, J. F.; Lee, J. M. Permanent Inactivation of Huntington's Disease Mutation by Personalized Allele Specific CRISPR/Cas9. *Hum. Mol. Genet*. **2016**, *25* (20), 4566–4576. https://doi.org/10.1093/hmg/ddw286.
64. Yang, S.; Chang, R.; Yang, H.; Zhao, T., Hong, Y.; Kong, H.E.; sun, X.; Oin, Z.; Jin, P.; Li, S.; Li, X-L. CRISPR/Cas9-Mediated Gene Editing Ameliorates Neurotoxicity in Mouse Model of Huntington's Disease. *J Clin Invest*. **2017**, *127* (7), 2719–2724. https://doi.org/10.1172/JCI92087.
65. Xie, G.; Meng, T.; Luo, Y.; Liu, Z. SKF-LDA: Similarity Kernel Fusion for Predicting lncRNA-Disease Association. *Mol Ther Nucleic Acids*. **2019**, 18, 45–55. https://doi.org/ 10.1016/j.omtn.2019.07.022
66. van den Bos, M.A.; Geevasinga, N.; Higashihara, M.; Menon, P.; Vucic, S. Pathophysiology and Diagnosis of ALS: Insights from Advances in Neurophysiological Techniques. *Int. J. Mol. Sci.* **2019**, *20* (11), 2818. https://doi.org/10.3390/ijms20112818.
67. Bursch, F.; Kalmbach, N.; Naujock, M.; Staege, S.; Eggenschwiler, R.; Abo-Rady, M.; Japtok, J.; Guo, W.; Hensel, N.; Reinhardt, P.; Boeckers, T.M.; Cantz, T.; Sterneckert, J. Van Den Bosh, L.; Hermann, A.; Petri, S.; Wegner, F. Altered Calcium Dynamics and Glutamate Receptor Properties in iPSC-Derived Motor Neurons from ALS Patients with C9orf72, FUS, SOD1 or TDP43 Mutations. *Hum Mol Genet*. **2019**, *28* (17), 2835–2850. https://doi.org/10.1093/hmg/ddz107
68. Deng, H-X.; Zhai, H.; Shi, Y.; Liu, G.; Lowry, J.; Liu, B.; Ryan, E.B.; Yan, J.; Yang, Y.; Zhang, N.; Yang, Z.; Liu, E.; Ma, Y.C.; Siddique, T. Efficacy and Long-Term Safety of CRISPR/Cas9 Genome Editing in the SOD1-Linked Mouse Models of ALS. *Commun Biol*. **2021**, *4* (1), 396. https://doi.org/10.1038/s42003-021-01942-4.
69. Yun, Y.; Ha, Y. CRISPR/Cas9-mediated gene correction to understand ALS. *Int J Mol Sci.* **2020**, *21*(11), 3801. https://doi.org/10.3390/ijms21113801.
70. Chen, CX-Q.; Abdian, N.; Maussion, G.; Thomas, R.A.; Demirova, I.; Cai, E.; Tabatabaei, M.; Beitel, L.K.; Karamchandani, J.; Fon, E. A.; Durcan, T. M. A Multistep Workflow to Evaluate Newly Generated iPSSCs and Their Ability to Generate Different Cell Types. *Methods Protoc*. **2021**, *4*(3), 50. https://doi.org/10.3390/mps4030050
71. He L, Wang S, Peng L, Zhao H, Li S, Han X, de Dieu Habimana, J.; Chen, Z.; Wang, C.; Peng, Y.; Huirong, P.; Xie, Y.; Lei, L.; Deng, Q.; Wan, L., Wan, N., Yuan, H., Gong, Y.; Zou, G.; Li, Z.; Tang, B.; Jiang, H. CRISPR/Cas9 Mediated Gene Correction Ameliorates Abnormal Phenotypes in Spinocerebellar Ataxia Type 3 Patient-Derived Induced Pluripotent Stem Cells. *Transl Psychiatry*. **2021**, *11*(1), 479. https://doi.org/10.1038/s41398-021-01605-2.
72. Song, G.; Ma, Y.; Gao, X.; Zhang, X.; Zhang, F.; Tian, C.; Hou, J.; Liu, Z; Zhao, Z; Tian, Y. CRISPR/Cas9-Mediated Genetic Correction Reverses Spinocerebellar Ataxia 3 Disease-Associated Phenotypes in Differentiated Cerebellar Neurons. *Life Med*. **2022**, *1*(1), 27–44. https://doi.org/10.1093/lifemedi/lnac020.
73. Pappadà, M.; Bonuccelli, O.; Buratto, M.; Fontana, R.; Sicurella, M.; Caproni, A.; Fuselli, S.; Benazzo, A.; Bertorelli, R.; de Sanctis, V.; Cavallerio, P.; Siminio, V.; Tugnoli, V.; Salvatori, F.; Marconi, P. Suppressing Gain-of-Function Proteins via CRISPR/Cas9 System in SCA1 Cells. *Sci. Rep.* **2022**, *12*(1), 20285. https://doi.org/10.1038/s41598-022-24299-y.
74. Ebina, H.; Misawa, N.; Kanemura, Y.; Koyanagi, Y. Harnessing the CRISPR/Cas9 System to Disrupt Latent HIV-1 Provirus. *Sci. Rep*. **2013**, 3, 2510. https://doi.org/10.1038/srep02510

DOI: 10.36838/IJHSR810.19

75. Khalili, K.; Kaminski, R.; Gordon, J.; Cosentino, L.; Hu, W. Genome Editing Strategies: Potential Tools for Eradicating HIV-1/AIDS. *J. Neurovirol*. **2015**, *21* (3), 310–321. https://doi.org/10.1007/s13365-014-0308-9.
76. Liu, Z.; Chen, S.; Jin, X.; Wang, Q.; Yang, K.; Li, C.; Xiao, Q.; Hou, P.; Liu, S.; Wu, S.; Hou, W.; Xiomg, Y., Kong, C.; Zhao, X.; Wu, L.; Li, C.; Sun, G.; Guo, D. Genome Editing of the HIV Co-Receptors CCR5 and CXCR4 by CRISPR-Cas9 Protects CD4(+) T Cells From HIV-1 Infection. *Cell Biosci*. **2017**, 7, 47. https://doi.org/10.1186/s13578-017-0174-2.
77. Seeger, C.; Sohn, J. A. Targeting Hepatitis B Virus With CRISPR/Cas9. *Mol. Ther. Nucleic Acids*. **2014**, *3* (12), e216. https://doi.org/10.1038/mtna.2014.68.
78. Kennedy, E. M.; Bassit, L. C.; Mueller, H.; Kornepati, A. V. R.; Bogerd, H. P.; Nie, T.; Chatterjee, P.; Javanbakht, H.; Schinazi, R. F.; Cullen, B.R. Suppression of Hepatitis B Virus DNA Accumulation in Chronically Infected Cells Using a Bacterial CRISPR/Cas RNA-Guided DNA Endonuclease. *Virology* **2015**, 476, 196–205. https://doi.org/10.1016/j.virol.2014.12.001.
79. Kurihara, T.; Fukuhara, T.; Ono, C.; Yamamoto, S.; Uemura, K.; Okamoto, T.; Sugiyama, M., Motooka, D.; Nakamura, S.; Ikawa, M.; Mizokami, M.; Maehara, Y.; Matsuura, Y. Suppression of HBV Replication by the Expression of Nickase- and Nuclease Dead-Cas9. *Sci. Rep*. **2017**, *7*(1), 6122. https://doi.org/10.1038/s41598-017-05905-w.
80. Sampson, T.R.; Saroj, S.D.; Llewellyn, A.C.; Tzeng, Y.L.; Weiss, D.S. A CRISPR/Cas System Mediates Bacterial Innate Immune Evasion and Virulence. *Nature* **2013**, *497* (7448), 254–257. https://doi.org/10.1038/nature12048.
81. Hu, Z.; Yu, L.; Zhu, D.; Ding, W.; Wang, X.; Zhang, C.; Wang, L.; Jiang, X.; Shen, H.; He, D.; Lİ K, Xi L, Ma D, Wang H. *et al.* Disruption of HPV16-e7 by CRISPR/Cas System Induces Apoptosis and Growth Inhibition in Hpv16 Positive Human Cervical Cancer Cells. *Biomed. Res. Int*. **2014**, 2014, 612823. https://doi.org/10.1155/2014/612823.
82. Yu, L.; Hu, Z.; Gao, C.; Feng, B.; Wang, L.; Tian, X.; Ding, W.; Jin, X.; Ma, D.; Wang, H. Deletion of Hpv18 e6 and e7 Genes Using Dual sgRNA-Directed CRISPRCas9 Inhibits Growth of Cervical Cancer Cells. *Int. J. Clin. Exp. Med*. **2017**, *10* (6), 9206-9213.
83. Westerberg, B.D.; Atashband, S.; Kozak, F.K. A Systematic Review of the Incidence of Sensorineural Hearing Loss in Neonates Exposed to Herpes Simplex Virus (HSV). *Int. J. Pediatr. Otorhinolaryngol*. **2008**, *72* (7), 931–937. https://doi.org/10.1016/j.ijporl.2008.03.001.
84. Roehm, P.C.; Shekarabi, M.; Wollebo, H.S.; Bellizzi, A.; He, L.; Salkind, J.; Khalili, K. Inhibition of HSV-1 Replication by Gene Editing Strategy. *Sci. Rep*. **2016**, 6, 23146. https://doi.org/10.1038/srep23146.
85. Xu, X.; Fan, S.; Zhou, J.; Zhang, Y.; Che, Y.; Cai, H.; Wang, L.; Guo, L.; Liu, L.; Li, Q. The Mutated Tegument Protein ul7 Attenuates the Virulence of Herpes Simplex Virus 1 by Reducing the Modulation of Alpha-4 Gene Transcription. *Virol. J*. **2016**, *13* (1), 152. https://doi.org/10.1186/s12985-016-0600-9.
86. Raab-Traub, N. Novel Mechanisms of EBV-Induced Oncogenesis. *Curr. Opin. Virol*. **2012**, *2* (4), 453–458. https://doi.org/10.1016/j.coviro.2012.07.001.
87. Yuen, K. S.; Chan, C. P.; Wong, N. H.; Ho, C. H.; Ho, T. H.; Lei, T.; Deng, W.; Tsao, S. W.; Chen, H.; Kok, K. H.; Jin, D. Y. CRISPR/Cas9-mediated genome editing of Epstein-Barr virus in human cells. *J. Gen. Virol.* **2015**, 96 (Pt 3), 626–636. https://doi.org/10.1099/jgv.0.000012.
88. Yuen, K. S.; Wang, Z. M.; Wong, N. M.; Zhang, Z. Q.; Cheng, T. F.; Lui, W. Y.; Chan, C. P.; Jin, D. Y. Suppression of Epstein-Barr Virus DNA Load in Latently Infected Nasopharyngeal Carcinoma Cells by CRISPR/Cas9. *Virus Res.* **2018**, 244, 296–303. https://doi.org/10.1016/j.virusres.2017.04.019.
89. Gergen, J.; Coulon, F.; Creneguy, A.; Elain-Duret, N.; Gutierrez, A.; Pinkenburg, O.; Verhoeyen, E.; Anegon, I.; Nguyen, T.H.; Halary, F.A.; Haspot, F. Multiplex CRISPR/Cas9 System Impairs HCV Replication by Excising an Essential Viral Gene. *PLoS ONE* **2018**, *13* (2), e0192602 https://doi.org/10.1371/journal.pone.0192602.
90. Malaviya, R.; Laskin, D.L.; Malaviya, R. Janus Kinase-3 Dependent Inflammatory Responses in Allergic Asthma. *Int Immunopharmacol.* **2010**, *10*(8), 829–836. https://doi.org/10.1016/j.intimp.2010.04.014.
91. Chang C. W.; Lai, Y. S.; Westin, E.; Khodadadi-Jamayran, A.; Pawlik, K. M.; Lamb Jr, L. S.; Goldman, F. D.; Townes, T. M. Modeling Human Severe Combined Immunodeficiency and Correction by CRISPR/Cas9-Enhanced Gene Targeting. *Cell Rep.* **2015**, *12*(10), 1668–1677. https://doi.org/10.1016/j.celrep.2015.08.013.
92. Lehmann, J. M.; Riethmuller, G.; Johnson, J. P. MUC18, a Marker of Tumor Progression in Human Melanoma, Shows Sequence Similarity to the Neural Cell Adhesion Molecules of the Immunoglobulin Superfamily. *Proc Natl Acad Sci U S A*. **1989**, *86* (24), 9891–9895. https://doi.org/10.1073/pnas.86.24.9891.
93. Chu, H.W.; Rios, C.; Huang, C.; Wesolowska-Andersen, A.; Burchard, E. G.; O'Connor BP, Fingerlin, T. E.; Nichols, D.; Reynolds, S. D. Seibold, M. A. CRISPR-Cas9-Mediated Gene Knockout in Primary Human Airway Epithelial Cells Reveals a Proinflammatory Role for MUC18. *Gene Ther.* **2015**, *22* (10), 822–829. https://doi.org/10.1038/gt.2015.53.
94. Pazirandeh, A.; Xue, Y.; Rafter, I.; Sjovall, J.; Jondal, M.; Okret, S. Paracrine Glucocorticoid Activity Produced by Mouse Thymic Epithelial Cells. *FASEB J.* **1999**, *13* (8), 893–901. https://doi.org/10.1096/fasebj.13.8.893.
95. Wang, M.; Strand, M.J.; Lanser, B. J.; Santos, C.; Bendelja, K.; Fish J, Esterl E. A.; Ashino, S.; Abbott, J. K.; Knight, V.; Gelfand, E.W. Expression and Activation of the Steroidogenic Enzyme CYP11A1 is Associated with IL-13 Production in T cells From Peanut Allergic Children. *PLoS One.* **2020**, *15*(6), e0233563. https://doi.org/10.1371/journal.pone.0233563.
96. Brackett, N.F.; Davis, B.W.; Adli, M.; Pomes, A.; Chapman, M.D. Evolutionary Biology and Gene Editing of Cat Allergen, Fel d 1. *CRISPR J.* **2022**, *5*(2), 213–223. https://doi.org/10.1089/crispr.2021.0101.
97. Biswas, S.; Wahl, N.J.; Thomson, M.J.; Cason, J.M.; McCutchen, B.F.; Septiningsih, E.M. Optimization of protoplast isolation and transformation for a pilot study of genome editing in peanut by targeting the allergen gene Ara h 2. *Int. J. Mol. Sci.* **2022**, *23* (2), 837. https://doi.org/ 10.3390/ijms23020837.
98. Zhou, W.; Wan, Y.; Guo, R.; Deng, M.; Deng, K.; Wang, Z.; Zhang, Y.; Wang, F. Generation of Beta-Lactoglobulin Knock-Out Goats Using CRISPR/Cas9. *PLoS One.* **2017**, *12* (10), e0186056. https://doi.org/10.1371/journal.pone.0186056.
99. Mukae, T.; Yoshii, K.; Watanobe, T.; Tagami, T.; Oishi, I. Production and Characterization of Eggs from Hens with Ovomucoid Gene Mutation. *Poult Sci.* **2021**, *100* (2), 452–460. https://doi.org/10.1016/j.psj.2020.10.026.
100. Xie, F.; Ye, L.; Chang, J. C.; Beyer, A. I.; Wang, J.; Muench, M. O.; Kan, Y. W. Seamless Gene Correction of Beta-Thalassemia Mutations in Patient-Specific iPSCs Using CRISPR/Cas9 and PiggyBac. *Genome Res.* **2014**, *24* (9), 1526-1533. https://doi.org/10.1101/gr.173427.114.
101. Canver, M. C.; Smith, E.C.; Sher, F.; Pinello, L.; Sanjana, N.E.; Shalem, O.; Chen, D.D.; Schupp, P.G.; Vinjamur, D.S.; Garcia, S.P.; Luc, S.; Kurita, R.; Nakamura, Y.; Fujiwara, Y.; Maeda, T.; Yuan,

G.C.; Zhang, F.; Orkin, S.H.; Bauer, D. E. BCL11A Enhancer Dissection by Cas9-Mediated Insitu Saturating Mutagenesis. *Nature* **2015**, *527* (7577), 192-197. https://doi.org/10.1038/nature15521.

102. Huang X, Wang Y, Yan W, Smith C, Ye Z, Wang J, Gao Y, Mendelsohn L, Cheng L. Production of Gene-Corrected Adult Beta Globin Protein in Human Erythrocytes Differentiated from Patient iPSCs After Genome Editing of the Sickle Point Mutation. *Stem Cells.* **2015**, *33* (5), 1470-1479. https://doi.org/10.1002/stem.1969.
103. Osborn, M.; Lonetree, C.L.; Webber, B.R.; Patel, D.; Dunmire, S.; McElroy, A.N.; DeFeo, A.P.; MacMillan, M.L.; Wagner, J.; Balzar, B.R.; Tolar, J. CRISPR/Cas9 Targeted Gene Editing and Cellular Engineering in Fanconi Anemia. *Stem Cells Dev.* **2016**, *25* (20), 1591-1603. https://doi.org/10.1089/scd.2016.0149.
104. Sürün, D.; Schwäble, J.; Tomasovic, A.; Ehling, R.; Stein, S.; Kurrle, N.; von Malchner, H.; Schnütgen, F. High Efficiency Gene Correction in Hematopoietic Cells by Donor-Template-Free CRISPR/Cas9 Genome Editing. *Mol Ther Nucleic Acids*. **2018**, 10:1-8. https://doi.org/10.1016/j.omtn.2017.11.001.
105. Gutierrez-Guerrero, A.; Sanchez-Hernandez, S.; Galvani, G.; Pinedo-Gomez, J.; Martin-Guerra, R.; Sanchez- Gilabert, A.; Aguilar-Gonzalez, A.; Cobo, M.; Gregory, P.; Holmes, M.; Benabdellah, K.; Martin, F. Comparison of Zinc Finger Nucleases Versus CRISPR-Specific Nucleases for Genome Editing of the Wiskott-Aldrich Syndrome Locus. *Hum. Gene Ther*. **2018**, *29* (3), 366-380. https://doi.org/10.1089/hum.2017.047.
106. Musunuru, K.; Kathiresan, S. Genetics of Common, Complex Coronary Artery Disease. *Cell*, **2019**, *177* (1), 132–145. https://doi.org/10.1016/j.cell.2019.02.015.
107. Seidah, N.G. Proprotein Convertase Subtilisin Kexin 9 (PCSK9) Inhibitors in the Treatment of Hypercholesterolemia and Other Pathologies. *Curr. Pharm. Des.* **2013**, *19* (17), 3161–3172. https://doi.org/10.2174/13816128113199990313.
108. Ding, Q.; Strong, A.; Patel, K. M.; Ng, S.L.; Gosis, B. S.; Regan, S.N.; Cowan, C.A.; Rader, D. J.; Musunuru, K. Permanent Alteration of PCSK9 with *In Vivo* CRISPR-Cas9 Genome Editing. *Circ Res* **2014**, *115* (5), 488–492. https://doi.org/10.1161/CIRCRESAHA.115.304351.
109. Wang, X.; Raghavan, A.; Chen, T.; Qiao, L.; Zhang, Y.; Ding, Q.; Musunuru, K. CRISPR-Cas9 targeting of PCSK9 in human hepatocytes *in vivo*. *Arterioscler Thromb Vasc EBiol* **2016**, *36* (5), 783–786. https://doi.org/10.1161/ATVBAHA.116.307227.
110. Chadwick A. C.; Evitt, N. H.; Lv, W.; Musunuru, K. Reduced Blood Lipid Levels With *In Vivo* CRISPR-Cas9 Base Editing of ANGPTL3. *Circulation* **2018**, 137, 975–977. https://doi.org/10.1161/CIRCULATIONAHA.117.031335.
111. Finn, J. D.; Smith, A. R.; Patel, M. C.; Shaw, L.; Youniss, M. R.; van Heteren, J.; Dirstine, T.; Ciullo, C.; Lescarbeau, R.; Seitzer, J.; Shah, R. R.; Shah, A.; Ling, D.; Growe, J.; Pink, M.; Rohde, E.; Wood, K. M.; Salomon, W. E.; Harrington, W. F., Dombrowski, C.; Strapps, W. R.; Chang, Y.; Morrissey, D. V. A single administration of CRISPR/Cas9 lipid nanoparticles achieves robust and persistent *in vivo* genome editing. *Cell Rep* **2018**, *22* (9), 2227–2235. https://doi.org/10.1016/j.celrep.2018.02.014.
112. Gillmore, J. D.; Gane, E.; Taubel, J.; Kao, J.; Fontana, M.; Maitland, M. L.; Seitzer, J.; O'Connell, D.; Walsh, K. R.; Wood, K.; Phillips, J.; Xu, Y.; Amaral, A.; Boyd, A.P.; Cehelsky, J.E.; McKee, M.D.; Schiermeier, A.; Harari, O.; Murphy, A.; Kyratsous, C. A.; Zambrowicz, B.; Soltys, R.; Gutstein, D. E.; Leonard, J.; Sepp-Lorenzino, L.; Lebwohl, D. CRISPR-Cas9 *In Vivo* Gene Editing for Transthyretin Amyloidosis. *N Engl J Med* **2021**, *385* (6), 493–502. https://doi.org/10.1056/NEJMoa2107454.
113. Nelson, C. E.; Hakim, C. H.; Ousterout, D. G.; Thakore, P. I.; Moreb, E. A.; Rivera, R. M. C.; Madhavan, S.; Pan, X.; Ran, F. A.; Yan, W. X.; Asokan, A.; Zhang, F.; Duan, D.; Gersbach, C. A. *In Vivo* Genome Editing Improves Muscle Function in a Mouse Model of Duchenne Muscular Dystrophy. *Science* **2016**, *351* (6271), 403–407. https://doi.org/10.1126/science.aad5143.
114. Tabebordbar, M.; Zhu, K.; Cheng, J. K. W.; Chew, W. L.; Widrick, J. J.; Yan, W. X.; Maesner, C.; Wu, E. Y.; Xiao, R.; Ran, F. A.; Cong, L.; Zhang, F.; Vandenberghe, L. H.; Church, G. M.; Wagers, A, J. *In Vivo* Gene Editing in Dystrophic Mouse Muscle and Muscle Stem Cells. *Science* **2016**, *351* (6271), 407–411. https://doi.org/10.1126/science.aad5177.
115. El Refaey, M.; Xu, L.; Gao, Y.; Canan, B. D.; Adesanya, T. M. A.; Warner, S. C.; Akagi, K.; Symer, D. E.; Mohler, P. J.; Ma, J.; Janssen, P. M. L.; Han, R. *In Vivo* Genome Editing Restores Dystrophin Expression and Cardiac Function in Dystrophic Mice. *Circ Res* **2017**, *121*(8), 923–https://doi.org/929.10.1161/CIRCRESAHA.117.310996.
116. Long, C.; Amoasii, L.; Mireault, A. A.; McAnally, J. R.; Li, H.; Sanchez-Ortiz, E.; Bhattacharyya, S.; Shelton, J. M.; Bassel-Duby, R.; Olson, E. N. Postnatal Genome Editing Partially Restores Dystrophin Expression in a Mouse Model of Muscular Dystrophy. *Science* **2016**, *351* (6271), 400–403. https://doi.org/10.1126/science.aad5725.
117. Amoasii, L.; Hildyard, J. C. W.; Li, H.; Sanchez-Ortiz, E.; Mireault, A.; Caballero, D.; Harron, R.; Stathopoulou, T. R.; Massey, C.; Shelton, J. M.; Bassel-Duby, R.; Piercy, R. J.; Olson, E. N. Gene Editing Restores Dystrophin Expression in a Canine Model of Duchenne Muscular Dystrophy. *Science* **2018**, *362*(6410), 86–91. https://doi.org/10.1126/science.aau1549.
118. Benhar, I.; London, A.; Schwartz, M. The Privileged Immunity of Immune Privileged Organs: The Case of the Eye. *Front Immunol.* **2012**, 3, 296. https://doi.org/10.3389/fimmu.2012.00296.
119. Zhou R, Caspi RR. Ocular immune privilege. *F1000 Biol Rep*. **2010**, 2, 3. https://doi.org/10. 3410/B2-3.
120. Bakondi, B.; Lv, W.; Lu, B.; Jones, M. K.; Tsai, Y.; Kim, K. J.; Levy, R.; Akhtar, A. A.; Breunig, J. J.; Svendsen, C. N.; Wang, S. *In Vivo* CRISPR/Cas9 Gene Editing Corrects Retinal Dystrophy in the S334ter-3 Rat Model of Autosomal Dominant Retinitis Pigmentosa. *Mol Ther.* **2016**, *24*(3), 556-563. https://doi.org/10.1038/mt.2015.220.
121. Ruan, G.X.; Barry, E.; Yu, D.; Lukason, M.; Cheng, S. H.; Scaria, A. CRISPR/Cas9-Mediated Genome Editing as a Therapeutic Approach for Leber Congenital Amaurosis 10. *Mol. Ther.* **2017**, *25*(2), 331-341. https://doi.org/10.1016/j.ymthe.2016.12.006
122. Andre, H.; Tunik, S.; Aronsson, M.; Kvanta, A. Hypoxia-Inducible Factor-1alpha Is Associated With Sprouting Angiogenesis in the Murine Laser-Induced Choroidal Neovascularization Model. Invest Ophthalmol Vis Sci. **2015**, *56*(11), 6591-604. https://doi.org/10.1167/iovs.15-16476.
123. Yu, W.; Mookherjee, S.; Chaitankar, V.; Hiriyanna, S.; Kim, J. W.; Brooks, M.; Ataeijannati, Y.; Sun, X.; Dong, L.; Li, T.; Swaroo, A.; Wu, Z. Nrl Knockdown by AAV-Delivered CRISPR/Cas9 Prevents Retinal Degeneration in Mice. *Nat. Commun*. **2017**, 8, 14716. https://doi.org/10.1038/ncomms14716.
124. Zhu, J.; Ming, C.; Fu, X.; Duan, Y.; Hoang, D. A.; Rutgard, J.; Zhang, R.; Wang, W.; Hou, R.; Zhang, D.; Zhang, E.; Zhang, C.; Hao, X.; Xiong, W.; Zhang, K. Gene and Mutation Independent Therapy Via CRISPR-Cas9 Mediated Cellular Reprogramming in Rod Photoreceptors. *Cell Res.* **2017**, *27*(6), 830-833. https://doi.org/10.1038/cr.2017.57.
125. Cheng, H.; Khanna, H.; Oh, E. C.; Hicks, D.; Mitton, K. P.; Swaroop, A. Photoreceptor-Specific Nuclear Receptor NR2E3

DOI: 10.36838/IJHSR810.19

Functions as a Transcriptional Activator in Rod Photoreceptors. *Hum. Mol. Genet.* **2004**, *13* (15), 1563-75. https://doi.org/10.1093/hmg/ddh173.
126. Crane, A.M.; Kramer, P.; Bui, J.H.; Chung, W.J.; Li, X.S.; Gonzalez-Garay, M.L.; Hawkins, F.; Liao, W.; Mora, D.; Choi, S.; Wang, J.; Sun, H.C.; Paschon, D.E.; Guschin, D.Y.; Gregory, P.D.; Kotton, D.N.; Holmes, M.C.; Sorscher, E.J.; Davis, B.R. Targeted Correction and Restored Function of the CFTR Gene in Cystic Fibrosis Induced Pluripotent Stem Cells. *Stem Cell Reports* **2015**, *4*(4), 569–577. https://doi.org/10.1016/j.stemcr.2015.02.005
127.Schwank, G.; Koo, B.-K.; Sasselli, V.; Dekkers, J.F.; Heo, I.; Demircan, T.; Sasaki, N.; Boymans, S.; Cuppen, E.; van der Ent, C.K.; Nieuwenhuis, E.E.S.; Beekman, J.M.; Clevers, H. Functional Repair of CFTR by CRISPR/Cas9 in Intestinal Stem Cell Organoids of Cystic Fibrosis Patients. *Cell Stem Cell* **2013**, *13*(6), 653–658. https://doi.org/10.1016/j.stem.2013.11.002.
128. Peng, R.; Lin, G.; Li, J. Potential Pitfalls of CRISPR/Cas9-mediated Genome Editing. *FEBS J.* **2016**, *283* (7), 1218–1231. https://doi.org/ 10.1111/febs.13586.
129. Zhang, X. H.; Tee, L. Y.; Wang, X. G.; Huang, Q. S.; Yang, S. H. Off-target Effects in CRISPR/Cas9-mediated Genome Engineering. *Mol. Ther. Nucleic Acids* **2015**, *4* (11), e264. https://doi.org/10.1038/mtna.2015.37.
130. Xu, C. L.; Ruan, M. Z. C.; Mahajan, V. B.; Tsang, S.H. Viral Delivery Systems for CRISPR. *Viruses* **2019**, *11* (1), 28. https://doi.org/10.3390/v11010028.
131. Lau, C.H.; Suh, Y. *In Vivo* Genome Editing in Animals Using AAVCRISPR System: Applications to Translational Research of Human Disease. *F1000Res.* **2017**, 6, 2153. https://doi.org/10.12688/ f1000research.11243.1.
132. Kim, S.; Koo, T.; Jee, H.G.; Cho, H.Y.; Lee, G.; Lim, D.G.; Shin, H.S.; Kim, J.S. CRISPR RNAs Trigger Innate Immune Responses in Human Cells. *Genome Res.* **2018**, *28* (3), 367–373. https://doi.org/10.1101/gr.231936.117.
133. Ran, F.A.; Hsu, P.D.; Lin, C.Y.; Gootenberg, J.S.; Konermann, S.; Trevino, A.E.; Scott, D.A.; Inoue, A.; Matoba, S.; Zhang, Y.; Zhang, F. Double Nicking by RNA-Guided CRISPR Cas9 for Enhanced Genome Editing Specificity. *Cell* **2013**, *154*(6), 1380–1389. https://doi.org/10.1016/j. cell. 2013.08.021.
134. Cribbs, A. P.; Perera, S. M. W. Science and Bioethics of CRISPR-Cas9 Gene Editing: An Analysis Towards Separating Facts and Fiction, *Yale J Biol Med* **2017**, *90*(4), 625–634.

■ Author

Elif Baser is a high school student at Nesibe Aydin Yildizlar Science High School, Ankara. She has a special interest in computer science, chemistry, and molecular biology. She was named a mathematics finalist in a national research competition and aspires to be a scientist in the future.

IJHSR
ijhighschoolresearch.org
RESEARCH ARTICLE

From Stars to Stairs: Multichoose, Generating Functions, and a Visual Bijection

Jaeha Park

Seoul International School, Seongnamdae-ro 1518-15, Seongnam-si, Gyeonggi-do 13113, Korea; jaehapark7478@naver.com
Mentor: Hoyoung Woo

ABSTRACT: We present a combinatorial reinterpretation of the concept of combinations with repetition—also known as multicombinations—using non-decreasing *stair sequences* (i.e., sequences of steps with non-decreasing heights). This viewpoint provides an intuitive geometric picture analogous to the classical stars-and-bars approach and naturally leads to a *two-variable generating function* that generalizes the ordinary generating function for combinations. We derive an identity connecting this new generating function for multicombinations to the standard one for ordinary combinations (without repetition) and discuss connections to known results in combinatorics and physics. Historical context and illustrative examples are included to maintain a didactic yet rigorous exposition accessible to students.

KEYWORDS: Mathematics, Combinatorics, Combination with Repetition, Staircase Analogy, Generating Functions.

Introduction

Combinatorics is the art of counting the number of ways discrete objects can be arranged or selected under various rules. Whether we're assigning roles, forming teams, or choosing pizza toppings, understanding when the order matters or when repeated choices are allowed leads to different counting strategies: permutations account for ordered selections; *combinations* ignore order; and *multicombinations*, also known as combinations with repetition, allow repeated choices. These ideas underpin a wide range of problems in mathematics, science, and engineering.

For example, out of $N = 10$ students in a class, choosing a president, vice president, and secretary involves permutations: there are $P(10, 3) = \frac{10!}{(10-3)!} = 720$ possible ordered selections. By contrast, choosing any 3 students to form a committee (with no specific roles) involves combinations, such that the number of possible outcomes is $C(10,3) = \binom{10}{3} = \frac{10!}{3!7!} = 120$. Furthermore, suppose a pizzeria provides $N = 10$ different pizza toppings, and customers can choose $L = 3$ toppings, allowing repetition (e.g., one could take a double or triple portion of a certain topping). This scenario corresponds to multicombination, i.e., selecting items with repetition allowed. The counting formula for this situation, derived via a classic stars-and-bars argument (to be explained below), is $\binom{L+N-1}{L} = \frac{(L+N-1)!}{L!(N-1)!}$. For $N = 10$ and $L = 3$ this yields $\binom{12}{3} = 220$ ways of choosing 3 toppings from 10 types with repetition allowed.

Table 1: All 10 multicombinations of 3 fruits (A = apple, B = banana, C = cherry) are chosen from (A, B, C) , alongside their representation in the stars-and-bars method. A star (here, a letter) represents a chosen item, and a vertical bar "|" represents a separator between different fruit types.

Fruit multiset	Stars-and-bars diagram
AAA	AAAII
AAB	AAIBI
AAC	AAIIC
ABB	AIBBI
ABC	AIBIC
ACC	AIICC
BBB	IBBBI
BBC	IBBIC
BCC	IBICC
CCC	IICCC

In general, the formulas for the number of permutations, combinations, and multicombinations for choosing L items out of N distinct members are, respectively:

$$P(N, L) = \frac{N!}{(N-L)!},$$
$$C(N, L) = \binom{N}{L} = \frac{N!}{L!(N-L)!}, \quad (1)$$
$$\left(\!\binom{N}{L}\!\right) = \binom{N+L-1}{L} = \frac{(N+L-1)!}{L!(N-1)!},$$

where we adopt the notation $\left(\!\binom{N}{L}\!\right)$ (double braces) to denote the multicombination number, i.e., the number of size-L multisets from a set of N types.

While $P(N,L)$ and $C(N,L)$ are conceptually straightforward (they arise directly from the factorial formula and the binomial coefficient, e.g., via Pascal's triangle), the derivation of the multicombination formula is less immediate. One widely used technique to derive $\binom{N+L-1}{L}$ is the *stars-and-bars* method.[1,2] In this method, one represents the L items to be chosen as L "stars" and divides them into N categories (representing the N

DOI: 10.36838/IJHSR810.31

distinct types) using N-1 "bars". The total number of symbols (stars + bars) in such a representation is L+N-1. By choosing which L of these L+N-1 positions are occupied by stars (equivalently, which N-1 positions are occupied by bars), one obtains the formula $\binom{N+L-1}{L}$. In essence, this counts the number of nonnegative integer solutions to

$$a_1 + a_2 + \cdots + a_N = L\,, \tag{2}$$

which is exactly the multicombination scenario where a_s is the number of times the s-th item is chosen (for $1 \le s \le N$)[1,2]

For a concrete illustration, consider N = 3 kinds of fruit: apples (A), bananas (B), and cherries (C). If we multi-choose L = 3 pieces of fruit, there are $\binom{3+3-1}{3} = \binom{5}{3} = 10$ possible selections, corresponding to the number of multisets of size 3. Table 1 lists all 10 outcomes (left column) and shows their corresponding stars-and-bars representation (right column).

In this method, each chosen item is represented by a "star" (e.g., the letters A, B, and C for apples, bananas, and cherries), and vertical bars are inserted to divide the sequence into regions corresponding to each item type. For a selection of three fruit types, two bars are used to partition the stars into three sections. If no stars appear between two bars, that fruit type was not selected. For instance, the multiset {A, A, B}—meaning two apples and one banana—is visually rendered as **AA|B|**, which corresponds equivalently to the star representation ****|*|**. Here, each letter (**A** or **B**) represents an identical star; the use of different letters is purely a visual aid. The interpretation in terms of apples, bananas, or other item types is determined entirely by the positions of the stars relative to the bars. In the present example, the first segment (before the first bar) contains two stars, indicating two apples; the middle segment contains one star, corresponding to a banana; and the final segment is empty, implying that no cherries were chosen. This diagrammatic approach establishes a precise one-to-one correspondence between all possible size-L multisets drawn from N types and all strings consisting of L stars and N-1 bars arranged in a row.

Mastery of these fundamental counting techniques is essential across a wide range of disciplines, including probability,[3] statistics,[4] computer science,[5] and even quantum physics. Historically, the systematic study of combinations and binomial coefficients dates back centuries.[2] The formula for combinations with repetition, and the stars-and-bars argument above, became a standard part of combinatorics by the 19th--20th century.

Another powerful tool in combinatorics is the generating function technique. A generating function is a formal power series in which the coefficient of z^L represents the number of outcomes for a given L. Generating functions allow counting problems to be solved via algebraic methods.[6] The use of generating functions in combinatorics dates back to Leonhard Euler in the 18th century: Euler famously introduced infinite-product generating functions to study *integer partitions*, that is, representations of a positive integer as a sum of smaller positive integers in which the order of the summands does not matter.[7] The associated *partition number* counts how many such decompositions exist. Euler's insight was that one can encode choices of parts in a partition by factors in a product; for example, he considered the infinite product $(1+x)(1+x^2)(1+x^3)\ldots$ and observed how expanding it generates the partition numbers. In the context of combinations, generating functions provide an elegant way to derive counting formulas. We will next review the ordinary generating functions for combinations and multicombinations, before turning to our new interpretation in terms of *stairs*.

The generating function for combinations (without repetition) is obtained from the binomial expansion. Consider $(1+z)^N$: expanding this by the Binomial Theorem gives[6]

$$F_N(z) \equiv (1+z)^N = \sum_{L=0}^{N} \binom{N}{L} z^L\,, \tag{3}$$

since $(1+z)^N = \binom{N}{0} z^0 + \binom{N}{1} z^1 + \cdots + \binom{N}{N} z^N$. This provides exactly the number of ways to choose L items from N without repetition. In this interpretation, in each factor of $(1+z)(z^0+z^1)$, the power z^1 or z^0 represents whether a given item is chosen or not, and the exponent of z in the product $(1+z)^N$ chosen counts the total number of chosen items.

For multicombinations, we allow an unlimited number of each item, implying that we need to use an infinite series. The geometric series[6]

$$\frac{1}{1-z} = 1 + z + z^2 + z^3 + \cdots \tag{4}$$

represents choosing 0, 1, 2, 3, …, of a given item. If we have N types of items available for repetition, the generating function for multicombinations is an infinite series:

$$B_N(z) \equiv \frac{1}{(1-z)^N} = \left(\frac{1}{1-z}\right)^N = \sum_{L=0}^{\infty} \left(\!\binom{N}{L}\!\right) z^L\,. \tag{5}$$

Indeed, multiplying N copies of the geometric series (4) corresponds to choosing some number a_1 of item 1, a_2 of item 2, …,a_N of item N; when we expand $\frac{1}{(1-z)^N}$, the coefficient of z^L in the expansion, it counts all possible ways to pick a total of L items with repetition from N available types, which are $\binom{N+L-1}{L}$. We can also express this formally as:

$$\frac{1}{(1-z)^N} = \sum_{a_1=0}^{\infty} \cdots \sum_{a_N=0}^{\infty} z^{a_1+a_2+\cdots+a_N} = \sum_{L=0}^{\infty} \sum_{\substack{a_1,\ \cdots,\ a_N \ge 0 \\ a_1+\cdots+a_N=L}} z^L\,, \tag{6}$$

where in the double summation, we sum z^L over all N-tuples of nonnegative integers (a_1, a_2, … ,a_n) that sums to L. The coefficient of z^L is therefore the number of solutions to a_1+ …+a_n = L, which matches the multicombination formula. In other words, we have shown combinatorially that

$$\left(\!\binom{N}{L}\!\right) = \sum_{\substack{a_1,\ \cdots,\ a_N \ge 0 \\ a_1+\cdots+a_N=L}} 1\,, \tag{7}$$

reaffirming that $\left(\!\binom{N}{L}\!\right)$ counts the number of nonnegative solutions to (2).

The purpose of the present paper is twofold: (i) to reformulate the multicombination problem in terms of designing *non-decreasing stairs*; and (ii) to show how this point of view naturally leads to a two-variable generalization of the generating functions above, elaborating the connection between combinations with and without repetition. In what follows, we first introduce the stair interpretation and derive the cor-

responding results. Then we discuss how it connects to the classical methods (stars-and-bars) as well as some further implications.

Results and Discussion

Multicombination: A Staircase Analogy:

We recast the multicombination problem as follows: instead of thinking in terms of selecting L items out of N types, consider multi-choosing numbers from 1 up to N. That is, imagine we wish to pick L numbers from the set 1, 2, ..., N, with repetition allowed (equivalently, we wish to pick L not-necessarily-distinct numbers between 1 and N). For each $s \in 1, 2, ..., N$, let as be the number of times s is chosen. If a_s=0, it means s is not chosen at all; if $a_s = 1$, s is chosen once; if $a_s = 2$, s is chosen twice; and so on. Clearly, equation (2) still holds in this scenario, which we recall here for convenience:

$$a_1 + a_2 + \cdots + a_N = L \ . \qquad (8)$$

This is just a rephrasing of the stars-and-bars description in terms of the counts a_s for each number .

Now, let us list the L chosen numbers in non-decreasing order, and call them . By construction, we have

$$\alpha_1 \le \alpha_2 \le \cdots \le \alpha_L \ , \qquad \text{with } 1 \le \alpha_1 \le \alpha_L \le N \ . \qquad (9)$$

In fact, we can write the multiset explicitly in this sorted form as:

$$\underbrace{1,\ 1,\ \cdots,\ 1}_{a_1 \text{ times}},\ \underbrace{2,\ 2,\ \cdots,\ 2}_{a_2 \text{ times}},\ \cdots,\ \underbrace{N,\ N,\ \cdots,\ N}_{a_N \text{ times}} = (\alpha_1, \alpha_2, \cdots, \alpha_L) \ , \qquad (10)$$

which makes it clear that $\alpha_1 \le ... \le \alpha_L$ and that each α_k equals some s (with possible repetition according to a_s). The condition on successive α's is $\alpha_{k+1} - \alpha_k \ge 0$ for $1 \le k \le L$. In this way, we obtain a non-decreasing sequence $\alpha=(\alpha_1, ..., \alpha_L)$ with $1 \le \alpha_k \le N$ for all k.

We now map this -sequence to another sequence $\beta = (\beta_1, \beta_2, ..., \beta_L)$ of the same length L, defined by

$$\beta_k = \alpha_k + (k-1) \qquad \text{for each } k = 1,\ 2,\ \cdots,\ L \ . \qquad (11)$$

In other words, we add 0 to α_1, 1 to α_2, 2 to α_3, and so on (adding k-1 to α_k). This transformation produces a strictly increasing sequence β with $\beta_1 < \beta_2 < ... < \beta_L$. To see this, note that

$$\beta_{k+1} - \beta_k = (\alpha_{k+1} + k) - (\alpha_k + k - 1) = \alpha_{k+1} - \alpha_k + 1 \ .$$

Since $\alpha_{k+1} \ge \alpha_k$, we have $\beta_{k+1} - \beta_k \ge 1$, so indeed $\beta_{k+1} > \beta_k$ for all k. Figure 1 illustrates an example.

What are the possible minimum and maximum values of the β's? From the definition, $\beta_1 = \alpha_1 \ge 1$, so the minimum possible value of β_1 is 1 (achieved when $\alpha_1 = 1$). From

$$\beta_L = \alpha_L + (L-1) \le N + (L-1) \ , \qquad (12)$$

the maximum possible value of β_L is $N+L$-1 (achieved when $\alpha_L = N$). Therefore, the β-sequence is a strictly increasing sequence of length L satisfying

$$1 \le \beta_1 < \beta_2 < \cdots < \beta_L \le N + L - 1 \ . \qquad (13)$$

For example, the two extreme cases are:

$$\boldsymbol{\alpha} = (1,\ 1,\ \cdots,\ 1) \ \Rightarrow \boldsymbol{\beta} = (1,\ 2,\ \cdots,\ L) \ ,$$

and

$$\boldsymbol{\alpha} = (N,\ N,\ \cdots,\ N) \ \Rightarrow \boldsymbol{\beta} = (N,\ N+1,\ \cdots,\ N+L-1) \ .$$

These show that β_1 can be as low as 1 and β_L as high as $N+L$-1.

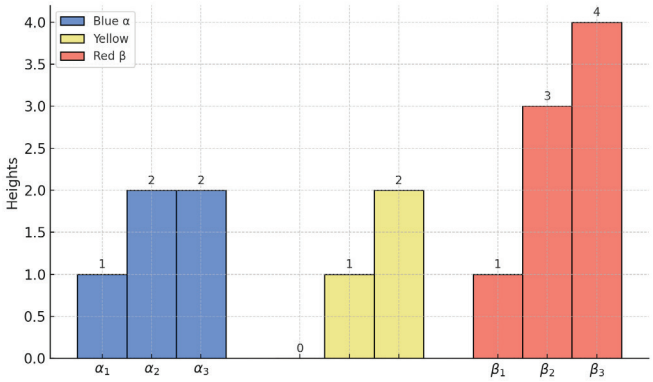

Figure 1: Example of the stair bijection: a non-decreasing α-stair (1,2,2) is mapped one-to-one to a strictly increasing β-stair (1,3,4) via the prescription in equation (11), $\beta_k = \alpha_k + (k\text{-}1)$ for k=1, 2, 3. Blue bars represent the α-sequence, red bars represent the β-sequence, and yellow bars indicate their difference k-1.

It is not hard to see that this $\alpha \mapsto \beta$ mapping is actually a bijection (one-to-one and onto) between the set of non-decreasing α-sequences in $[1, N]$ of length L and the set of strictly increasing β-sequences in $[1, N+L-1]$ of length L. Indeed, given any strictly increasing sequence $1 \le \beta_1 < \beta_2 < ... < \beta_L \le N+L-1$ we can invert the relation (11) as

$$\alpha_k = \beta_k - (k-1) \ ,$$

and check that $\alpha_{k+1} - \alpha_k = (\beta_{k+1} - \beta_k) - 1 \ge 0$, with $1 \le \alpha_1 \le ... \le \alpha_L \le N$. This shows that every valid β-sequence corresponds to a unique non-decreasing α-sequence, and vice versa. Thus, we have established a bijection between multi-choose selections and ordinary combinations in a larger set.

What does this bijection mean combinatorially? It means that choosing L items from N with repetition (multicombinations) is in one-to-one correspondence with choosing L distinct items from a larger set of size $N+L-1$ (ordinary combinations). The β-sequence can be interpreted as the set of L distinct numbers chosen from 1, 2, ... , $N+L-1$, and clearly, there are $\binom{N+L-1}{L}$ such choices. Thus, we have derived the multicombination formula *bijectively*:

$$\left(\!\binom{N}{L}\!\right) = \binom{N+L-1}{L} \ , \qquad (14)$$

recovering the result stated in equation (1). In this interpretation, one can imagine constructing a staircase diagram: the α-sequence $(\alpha_1, ..., \alpha_L)$ can be seen as the heights of L steps (of equal width) in a non-decreasing "staircase," whereas the β-sequence $(\beta_1, ..., \beta_L)$ corresponds to a strictly increasing staircase profile of L steps (each subsequent step strictly higher than the previous one). We will not dwell on the geometric diagram here, but the idea is that each multiset selection corresponds to a unique set of step heights. Below, we will give an explicit example of this correspondence.

Two-variable generating functions for stairs:

The identification of multicombinations with the stair problem leads to a natural generalization of the generating function (5). We now introduce a *two-variable generating function* $B_N(z, x)$ for the stair interpretation:

$$\mathbf{B}_N(z, x) := \prod_{s=1}^{N} \frac{1}{1 - zx^s} \ , \qquad (15)$$

DOI: 10.36838/IJHSR810.31

where z marks the stair length (number of items chosen) and x tracks the total height (sum of the values of the chosen items).

Expanding each factor as a geometric series, we get

$$B_N(z, x) = \prod_{s=1}^{N} \sum_{a_s=0}^{\infty} (zx^s)^{a_s} = \sum_{L=0}^{\infty} B_{N,L}(x)\, z^L \ ,$$

for some coefficient polynomial $B_{N,L}(x)$ (the coefficient of z^L) depending on x. By collecting terms of the same power of z, one acquires

$$B_{N,L}(x) = \sum_{\substack{a_1, \cdots, a_N \geq 0 \\ a_1 + \cdots + a_N = L}} x^{1a_1 + 2a_2 + 3a_3 + \cdots + Na_N} , \qquad (16)$$

since each term of the expansion is of the form $z^{a_1+\ldots+a_n}$, $x^{1a_1+2a_2+\ldots+Na_n}$, and we sum all contributions where the total exponent of z is L. The expression (16) has a clear meaning: we are summing $x^{\sum s \cdot a_s}$ over all multisets of size L, where $\sum s \cdot a_s$ is the sum of the values of the chosen numbers. But $\sum_{s=1}^{N} s \cdot a_s$ can be interpreted in terms of the -sequence of the stair representation. For the expanded list (10), we have

$$\sum_{s=1}^{N} s a_s = \alpha_1 + \alpha_2 + \cdots + \alpha_L \ , \qquad (17)$$

which is exactly the sum of all step heights in the stairs. Thus, we can rewrite (16) as

$$B_{N,L}(x) = \sum_{1 \leq \alpha_1 \leq \cdots \leq \alpha_L \leq N} x^{\alpha_1 + \alpha_2 + \cdots + \alpha_L} , \qquad (18)$$

where the sum runs over all non-decreasing sequences $(\alpha_1, \ldots, \alpha_L)$ of length L with each $1 \leq \alpha_k \leq L$. In other words, $B_{N,L}(x)$ counts all non-decreasing stairs of length L by the total combined height of all steps (with step heights bounded between 1 and N). Setting x=1 in this formula, we recover the ordinary generating function for multicombinations, since $B_{N,L}(1) = \sum_{\alpha} 1 = \binom{N+L-1}{L}$. Indeed, one can see directly that

$$B_N(z, 1) = \prod_{s=1}^{N} \frac{1}{1-z} = \frac{1}{(1-z)^N} = B_N(z) \ , \qquad (19)$$

consistent with our earlier definition of $B_N(z)$ in equation (5). We have used the notation $\boldsymbol{B}$ to emphasize the analogy with bosonic counting (i.e., combinations with repetition). Different arguments indicate standard specializations of the same generating function: $B_N(z)$ denotes the ordinary generating function, $B_N(z, x)$ its two-variable refinement that tracks total height, and $B_{N,L}(z)$ the coefficient of z^L in this expansion. An analogous notation will be introduced below for combinations without repetition, using the letter $\boldsymbol{F}$ (for fermion). In parallel, for ordinary combinations (without repetition), one can define an analogous two-variable generating function:

$$F_N(z, x) := \prod_{t=1}^{N} (1 + zx^t) = \sum_{L=0}^{N} F_{N,L}(x)\, z^L \ , \qquad (20)$$

where

$$F_{N,L}(x) = \sum_{\substack{b_1, \cdots, b_N \in \{0,1\} \\ b_1 + \cdots + b_N = L}} x^{1b_1 + 2b_2 + 3b_3 + \cdots + Nb_N} . \qquad (21)$$

Here $b_t \in \{0,1\}$ indicates whether the item t is chosen (b_t=1) or not (b_t =0). The condition b_1+...+b_N=L means exactly distinct items are chosen. Thus $F_{N,L}(x)$ encodes the total "height" (sum of values) of all choices of L distinct items from 1, ..., N. In fact, if the chosen set of L distinct numbers are written in increasing order (β_1<β_2 <...<β_L), then one can verify

$$\sum_{t=1}^{N} t b_t = \beta_1 + \beta_2 + \cdots + \beta_L \ . \qquad (22)$$

Thus, we can rewrite (21) as

$$F_{N,L}(x) = \sum_{1 \leq \beta_1 < \beta_2 < \cdots < \beta_L \leq N} x^{\beta_1 + \beta_2 + \cdots + \beta_L} \ . \qquad (23)$$

When x=1, $F_{N,L}(1) = \binom{N}{L}$ (the number of ways to choose L distinct items from N), and indeed $F_N(z, 1) = (1 + z)^N = F_N(z)$ as expected.

The generating function $F_N(z, x)$ itself is standard in the theory of generating functions and statistical mechanics;[6,8-10] the novelty here lies in its interpretation in terms of stair sequences and its explicit bijective relation to multicombinations.

Now, an interesting relationship emerges between $B_N(z, x)$ and $F_N(z, x)$. Consider the strictly increasing β-sequence corresponding to a given non-decreasing α-sequence via our stair bijection. For a fixed L, suppose α=(α_1, ..., α_L) maps to β=(β_1, ..., β_L) by the relation $\beta_k = \alpha_k + k - 1$. We can relate the sums of α's and β's (i.e., (17) and (22)) as follows:

$$\sum_{k=1}^{L} \beta_k = \sum_{k=1}^{L} (\alpha_k + k - 1) = \left(\sum_{k=1}^{L} \alpha_k \right) + \frac{1}{2} L(L-1) \ . \qquad (24)$$

Here, the second term $\frac{L(L-1)}{2}$ comes from 0+1+2+...+(L-1). Now, if we consider a combination scenario with N replaced by $N' = N + L - 1$, we note that any strictly increasing sequence (β_1, ..., β_L) with β_1>1 and $\beta_L \leq N + L - 1$ can be viewed as a choice of L distinct numbers from 1, 2, ..., N + L - 1. In fact, as shown earlier, any α-sequence for (N, L) corresponds bijectively to a β-sequence for (N+ L - 1, L). Using the relation (24), we can now connect the two-variable generating functions:

$$F_{N+L-1,L}(x) = x^{\frac{L(L-1)}{2}} B_{N,L}(x) \ . \qquad (25)$$

In words: the sum of $x^{(\text{total height of strictly increasing stair})}$ over all strictly increasing stairs of length L up to height N (which is $F_{N,L}(x)$) is related to the sum of $x^{(\text{total height of non-decreasing stair})}$ over all non-decreasing stairs of length L up to height N (which is $B_{N,L}(x)$), by a factor of $x^{L(L-1)/2}$ ---after adjusting N to N+L-1. Here, the term total height refers to the sum of the heights of all steps in the staircase, rather than the height of the highest step. Equivalently, the total height is the area under the staircase profile. Substituting the relation (25) back into the generating functions (16) and (21) confirms the identity (25). In particular, when x=1, the identity (25) reduces to the multicombination formula, $\binom{N+L-1}{L} = \left(\binom{N}{L}\right)$ as given in equation (14). For example, for N=2 and L=2, we have

$$B_{2,2}(x) = x^2 + x^3 + x^4, \qquad F_{3,2}(x) = x^3 + x^4 + x^5 = xB_{2,2}(x) \ , \qquad (26)$$

which indeed reflects the relation $F_{2+2-1,2}(x) = x^1 B_{2,2}(x)$ in this case (since $L(L-1)/2 = 1$ when L=2).

Correspondence with the stars-and-bars method:

To illustrate the stair interpretation concretely, let us revisit the fruit example in Table 1 and map each multicombination to its corresponding stair sequences.

Table 2 shows the detailed one-to-one correspondences between each fruit multiset, the non-decreasing α-sequence, the strictly increasing β-sequence, and the stars-and-bars representations (both for the β-sequence and for the original fruit

labels). We use the numeric values 1,2,3 for A, B, C, respectively, when writing the α and β sequences.

Table 2: Each row maps a multichoose outcome to its corresponding stair sequences and equivalent stars-and-bars encodings for N=3 and L=3. The α-sequence is the non-decreasing listing of the chosen item values (using 1 for A, 2 for B, 3 for C). The β-sequence is obtained by adding 0, 1, 2 to the α terms, yielding a strictly increasing sequence between 1 and 5. The "β & bars" column shows the positions (1 through 5) of the chosen β's as stars in a stars-and-bars diagram (with two bars for 3 bins), and the last column is the original stars-and-bars diagram for the fruits.

Fruit multiset	α-sequence	β-sequence	β & bars	Fruit & bars
AAA	111	123	123||	AAA||
AAB	112	124	12|4|	AA|B|
AAC	113	125	12||5	AA||C
AAB	122	134	1|34|	A|BB|
ABC	123	135	1|3|5	A|B|C
ACC	133	145	1||45	A||CC
BBB	222	234	|234|	|BBB|
BBC	223	235	|23|5	|BB|C
BCC	233	245	|2|45	|B|CC
CCC	333	345	||345	||CCC

For instance, the selection AAB corresponds to $\alpha = (1, 1, 2)$ (since in sorted order it consists of two 1's and one 2). This yields $\beta = (\alpha_1, \alpha_2 + 1, \alpha_3 + 2) = (1, 2, 4)$. The β-sequence (1, 2, 4) can be interpreted as choosing {1, 2, 4} out of {1, 2, 3, 4, 5} (since N+L-1=5 for this case). The "β & bars" column in Table 2 shows the stars-and-bars diagram corresponding to this β representation: for AAB, choosing {1, 2, 4} out of 5 means positions 1 and 2 are stars, position 3 is a bar, position 4 is a star, and position 5 is a bar, giving the string 12|4|. Finally, replacing the numbers 1, 2, 4 with the corresponding fruit letters in order gives the original fruit diagram AA|B|. This confirms that our stair interpretation is in perfect correspondence with the classical stars-and-bars approach. Table 2 explicitly demonstrates the bijection between the fruit multiset, its α-sequence, β-sequence, and the two equivalent stars-and-bars representations.

Essentially, the β-representation provides another viewpoint on the standard stars-and-bars bijection. The chosen β positions correspond to picking which L of the N+L-1 slots contain stars in the stars-and-bars model.

Discussion:

The two-variable generating functions (15) and (20) offer a refined method for combinatoric enumeration: not only do they distinguish the number of items , but they also track the sum of the values (heights) selected. The identity (25) we derived shows a precise relationship between these refined counts for combinations with and without repetition. By considering an arbitrarily large supply of item types, one finds that the two sequences coincide up to a simple factor. In fact, if is very large compared to , choosing with repetition or without repetition becomes effectively the same for the first positive integers. More formally, in the limit we acquire

$$\lim_{N\to\infty} B_{N,L}(x) = \prod_{s=1}^{L} \frac{x}{1-x^s} = \frac{x^L}{\prod_{s=1}^{L}(1-x^s)},$$

$$\lim_{N\to\infty} F_{N,L}(x) = \prod_{t=1}^{L} \frac{x^t}{1-x^t} = \frac{x^{\frac{1}{2}L(L+1)}}{\prod_{t=1}^{L}(1-x^t)}, \qquad (27)$$

using the formula for geometric series and noting that $F_{N,L}(x)$ for infinite N would include all L distinct positive integers (hence the product from t =1 to L). The higher powers ofin the denominators arise from the contributions of each possible step height in the staircase interpretation: in the infinite-N limit each factor $(1\text{-}x^t)^{-1}$ corresponds to allowing arbitrarily many steps of height t. We see that $\lim_{N\to\infty} F_{N,L}(x)$ equals $\lim_{N\to\infty} B_{N,L}(x)$ times a factor $x^{\frac{L(L-1)}{2}}$. This coincides with our earlier identity (25) in the special case N = ∞.

Interestingly, this type of generating function identity is known in a physics context: in quantum mechanics, *bosons* correspond to combinations with repetition and *fermions* to combinations without repetition. The generating function $\prod_{s=1}^{\infty} \frac{1}{1-zx^s}$ is the grand canonical partition function for bosons, and $\prod_{t=1}^{\infty}(1+zx^t)$ is that for fermions. In the limit of infinitely many states for particles confined to a one-dimensional harmonic potential, the two partition functions coincide up to the overall factor discussed above, reflecting a combinatorial identity recognized by physicists.[8-10]

Finally, beyond the combinatorial insights, the stair interpretation provides a more visual way for students to understand combination problems. By translating an abstract stars-and-bars configuration into a step diagram, one can literally "see" a combination with repetition as building a staircase of a certain length and bounded height. This perspective might be useful in discovering new combinatorial identities or generalizations, as we demonstrated with generating functions.

■ Conclusion

We have introduced a bijective stair interpretation for multicombinations in terms of non-decreasing and strictly increasing sequences (viewed as stairs), and we have derived a generating function identity connecting combinations with and without repetition.

This viewpoint offers an intuitive bijective proof of the formula for combinations with repetition and elucidates the relationship between these and ordinary combinations. We compared the stair method with the traditional stars-and-bars method and found them to be in perfect correspondence, as illustrated in Table 2. Additionally, by incorporating a weight variable x to track the sum of chosen values, we developed two-variable generating functions $B_N(z,x)$ and $F_N(z,x)$ that unify combinations with and without repetition in a single framework. The resulting identity (25) relating $B_{N,L}(x)$ and $F_{N+L-1,L}(x)$ provides a deeper algebraic insight into this connection and links our combinatorial findings to known results in both combinatorics and quantum physics.

We also provided historical context and references to help students appreciate the development of these ideas. In summary, this paper demonstrates how a fresh combinatorial interpretation (the "stairs") can lead to elegant proofs and generalizations of standard counting formulas. The stair viewpoint may, in turn, inspire further generalizations in other combinatorial structures, such as integer partitions[11] or Young tableaux.[12]

DOI: 10.36838/IJHSR810.31

Acknowledgments

We would like to thank Dr. Stephen Angus for his helpful discussion and proofreading.

References

1. O. Levin, *Discrete Mathematics: An Open Introduction*, 3rd Ed., 2019. https://discrete.openmathbooks.org/dmoi3/
2. "Stars and bars (combinatorics)" and "Multiset," *Wikipedia*. https://en.wikipedia.org/wiki/Stars_and_bars_(combinatorics) https://en.wikipedia.org/wiki/Multiset
3. W. Feller, *An Introduction to Probability Theory and Its Applications*, Vol. 1, Wiley, 3rd ed., 1968.
4. G. Casella and R. L. Berger, *Statistical Inference*, 2nd ed., Cengage Learning, 2002.
5. K. Rosen, *Discrete Mathematics and Its Applications*, McGraw-Hill, 7th ed., 2012.
6. H. S. Wilf, *generatingfunctionology* (2nd ed.), Academic Press, 1994. https://www.math.upenn.edu/~wilf/DownldGF.html
7. L. Euler, *Introduction to Analysis of the Infinite*, 1748.
8. F. C. Auluck and D. S. Kothari, "Statistical mechanics and the partitions of numbers," *Proceedings of the Cambridge Philosophical Society*, vol. 42, pp. 272-277, 1946.
9. K. Schonhammer, "Thermodynamics and occupation numbers of a Fermi gas in the canonical ensemble," *American Journal of Physics*, vol. 68, pp. 1032-1037, 2000.
10. W. J. Mullin and J. P. Fernández, "Bose-Einstein condensation, fluctuations, and recurrence relations in statistical mechanics," American Journal of Physics, vol. 71, pp. 661-669, 2003.
11. G. E. Andrews, *The Theory of Partitions*, Cambridge University Press, 1976.
12. W. Fulton, *Young Tableaux: With Applications to Representation Theory and Geometry*, Cambridge University Press, 1997.

Author

Jaeha Park is a senior high school student with a deep interest in classical music and combinatorics. He is inspired by the idea of music as a multicombination of notes, a perspective that motivates both his YouTube channel, *Musical Meanings*, and his research. Jaeha aspires to apply mathematics in fields such as aerospace engineering, music theory, or astrophysics, and enjoys stargazing in his free time.

IJHSR
ijhighschoolresearch.org
RESEARCH ARTICLE

Comparative Analysis of Pseudo-Random Binary Sequence Patterns for the High-Speed Digital Systems

Jaechan Lee

Liberal Arts and Science Academy, 1012 Arthur Stiles Road, Austin, TX, 78721, USA; jaechanlee0924@gmail.com

ABSTRACT: Pseudo-random binary sequences (PRBS) are widely used in high-speed digital systems to evaluate signal integrity and transmission reliability. However, the statistical characteristics of different PRBS degrees have not been as comprehensively analyzed as those of other specialized random sequences. In this study, we investigated the characteristics of PRBS7 through PRBS31, which is commonly used in practice, using a Python-based model. The analysis covered randomness properties, including run-length distribution, frequency balance, entropy, and power spectral density (PSD), as well as how these characteristics vary with noise intensity. The results provide objective criteria for selecting an appropriate PRBS generator, taking into account both statistical quality and implementation cost.

KEYWORDS: Engineering, Digital Electronics, Digital Logic System, Pseudo Random Binary Sequence.

Introduction

With the rapid advancement of technology, the importance of high-speed serial interfaces such as Universal Serial Bus (USB), Peripheral Component Interconnect Express (PCIe), and Ethernet in large-scale data transmission continues to grow. In particular, recent trends in artificial intelligence have explosively accelerated the demand for high-bandwidth input/output (I/O). However, channel insertion loss and noise through cables or printed circuit boards (PCBs) make it difficult to scale the bandwidth of high-speed interfaces and significantly contribute to an increase in bit error rate (BER).[1] Although semiconductor and circuit design technologies have substantially improved the operating speed of integrated circuits, the analysis and verification of such high-speed circuits have become increasingly challenging.

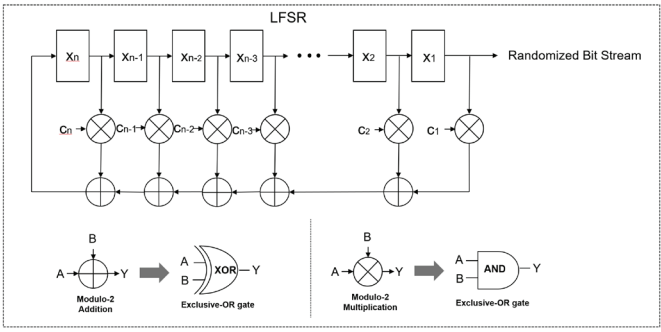

Figure 1: Run length distribution of the PRBS polynomials. The figure illustrates how the feedback shift registers defined by each primitive polynomial generate deterministic pseudo-random bit sequences through modulo-2 addition. Differences in the polynomial coefficients result in distinct sequence characteristics, which are reflected in the observed run-length distributions.

For efficient validation, it is desirable to test circuits at the same speed as their actual operating frequency. PRBS provides a cost- and time-effective solution since it can be integrated directly into digital circuits without the need for expensive test equipment, thereby enabling at-speed testing.[2] Consequently, PRBS-based BER measurement has become a fundamental requirement for verifying the data transmission quality of various high-speed interfaces. Although PRBS appears to be a random sequence, it is in fact a deterministic bit stream generated by a Linear Feedback Shift Register (LFSR), where the previous state of the register determines each output bit.[3] A sequence is defined by a register length N and a corresponding primitive polynomial. For example, when the highest degree of the primitive polynomial is 7, the sequence is denoted as PRBS7, whereas a 15th-degree polynomial defines PRBS15. Figure 1 illustrates an N-degree PRBS generator based on the polynomial $C_n x^n + C_{n-1}x^{n-1} + \cdots + C_2 x^2 + C_1 x^1 + 1$.

LFSR consists of N linearly connected registers X_n and a coefficient set C_n. The feedback function computes the new state based on the initial values of the shift register using modulo-2 addition and multiplication.[4,5] In this operation, addition can be replaced with an exclusive OR (XOR) gate, and the multiplication can be replaced with an AND gate. As an example, the operation of PRBS7 can be explained using the primitive polynomial $x^7 + x^6 + 1$. The corresponding coefficient vector is

$$(C1, C2, C3, C4, C5, C6, C7) = (0, 0, 0, 0, 0, 1, 1)$$

Assume the initial register state is

$$(x1, x2, x3, x4, x5, x6, x7) = (0, 1, 0, 1, 1, 0, 1)$$

The new feedback bit x0 is calculated as a modulo-2 linear combination of the tapped registers

$$x_0 = (C_6 \cdot x_6) \oplus (C_6 \cdot x_7)$$

Substituting the value $x_6 = 0$ and $x_7 = 1$, we obtain

$$x_0 = 0 \oplus 1 = 1$$

This feedback bit is inserted into the first register, while all other register values are shifted to the right. The updated state becomes

$$(x1, x2, x3, x4, x5, x6, x7) = (1, 0, 1, 0, 1, 1, 0)$$

By repeating this process, the PRBS7 generator produces a deterministic bit sequence that appears random but has a max-

DOI: 10.36838/IJHSR810.37

imal length of 2^7–1=127 before repeating. Using this principle, PRBS patterns of different degrees can be generated. Although several studies have investigated pseudo-random number generators,[6–9] most have focused on specialized generators used in applications such as cryptography, and a comprehensive understanding of the statistical and structural properties of PRBS of various degrees used in high-speed systems is still not fully understood in practice. To address this gap, the main objective of this study is to systematically compare and analyze the properties of PRBS sequences of different polynomial degrees employed in high-speed interface designs. Specifically, we implement various PRBS patterns using a Python model and evaluate them against widely used pseudo-random sequence generators. The analysis includes statistical randomness properties, sequence performance, and hardware implementation cost. Through this investigation, we aim to provide useful criteria for selecting the most suitable generator depending on specific design requirements.

Methods

PRBS Polynomials:

In this study, we reviewed several primitive polynomials with PRBS degrees ranging from 7 to 31 in relevant literatures10-12 and selected 9 PRBS polynomials representing short, medium, and long sequences as shown in Table 1. This selection covers a wide range of sequence lengths and reflects the PRBS patterns widely used in digital systems. A Python model was designed for statistical analysis. Each PRBS polynomial was implemented in Python, and the formulas required for the respective statistical analyses were simulated accordingly.

Table 1: Different degrees of PRBS polynomials. This table shows a list of commonly used PRBS patterns, their corresponding primitive polynomials, and degrees N. Using the PRBS patterns defined in the table, various statistical tests are performed to compare their characteristics.

PRBS Pattern	PRBS Polynomial	Degree (N)
PRBS7	$X^7 + X^6 + 1$	7
PRBS9	$X^9 + X^5 + 1$	9
PRBS11	$X^{11} + X^9 + 1$	11
PRBS13	$X^{13} + X^7 + X^3 + X^2 + 1$	13
PRBS15	$X^{15} + X^{14} + 1$	15
PRBS19	$X^{19} + X^5 + X^2 + X + 1$	23
PRBS23	$X^{23} + X^{18} + 1$	23
PRBS27	$X^{27} + X^5 + X^2 + X + 1$	40
PRBS31	$X^{31} + X^{28} + 1$	31

Statical Analysis:

Run Length Distribution:

All selected polynomials have been proven in previous research to be irreducible primitive polynomials.[3-5] This means that the maximum length of the selected polynomial of degree N is 2^n - 1 bits for a given degree N. Run tests were performed to analyze and compare the statistical randomness and maximum run length properties of each generated PRBS sequence.[13] For a PRBS of degree N, the expected run count for run length L is given by:

$$Run\ Count\ = \frac{2^{N+1}}{2^{L+1}}\ (1 \le L \le N-1)$$

Figure 2 shows the run length distributions for each polynomial. The tests were conducted over two full periods of each PRBS sequence. As observed, the run count decreases exponentially with run length, corresponding to a near-linear decline on a logarithmic scale, which indirectly confirms the primitivity of the polynomials.

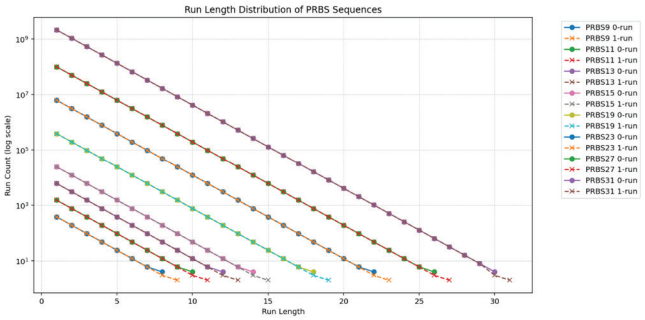

Figure 2: Run length distribution of the PRBS polynomials. This figure compares the run length statistics of different PRBS orders, showing that higher-degree sequences exhibit longer maximum runs and a wider distribution range.

All sequences maintained a near-perfect balance between zeros and ones, and the maximum run lengths matched theoretical predictions. The slight decrease in the number of 1-run near the maximum run length occurs because 1-run reaches the same length as the polynomial's degree when sampling runs, while relatively reducing the number of 1-run of degree N-1. Overall, the simulated results satisfy theoretical expectations, and it can be confirmed that all nine polynomials can generate PRBS sequences of maximum length in practical implementations.

Frequency Test

The frequency test is used to verify whether a PRBS exhibits randomness and whether 0 and 1 occur with equal probability in each bit sequence.[13] S_n, indicating a bias toward bit 1 or 0, can be measured by summing over the entire binary sequence B_k and is expressed as:

$$S_n = \sum_{k=1}^{n} B_k$$

For example, a non-zero positive value for S_n means that 1s are observed more often than 0s in a binary sequence. With S_n, the randomness of a binary sequence can be verified using a probabilistic concept called the *p-value*. This represents the probability that the currently observed result will occur, assuming that the null hypothesis is true.[13] Therefore, the closer the *p-value* is to 1, the more likely it is that the observed data would be observed very commonly under the null hypothesis, indicating a higher probability that the result occurred by chance. P-value is given by:

$$p\_value\ = erfc\left(\frac{|S_n|}{\sqrt{2N}}\right)$$

where N is the maximum degree of the given polynomial, the *erfc* function is a complementary error function, which cal-

culates the probability that a value from a standard normal distribution will exceed a given threshold.[13] The Python math library was used to calculate the complementary error function. Table 2 shows the p-values obtained under two different conditions. First, all PRBSs were simulated with the same number of bits, and second, each PRBS was simulated with a full cycle.

Table 2: Frequency Test P-values for the PRBS Polynomials. This table highlights that insufficient test length can lead to misleadingly low p-values for long PRBS sequences. On the other hand, when performing a Frequency Test using one period, a very distinct pattern appears in which the p-value gradually increases as the PRBS order increases. This indicates that the random characteristics converge to the ideal quickly as the PRBS order increases.

Test Period	PRBS7	PRBS9	PRBS11	PRBS13	PRBS15	PRBS19	PRBS23	PRBS27	PRBS31
10M bits	0.0	0.0	0.0	0.0	6.81e-41	0.909834	0.839661	0.9181876	0.6233868
One period (2^n-1)	0.929291	0.964715	0.982366	0.991184	0.995592	0.998898	0.999724	0.999931	0.999992

As mentioned earlier, a p-value closer to 1 indicates higher randomness. For lower degree PRBSs, the same pattern repeats across 10 million bits, resulting in a deterministic pattern, which increases statistical deviation and results in a p-value of 0. This demonstrates that PRBSs are not completely random but rather closer to deterministic patterns. In contrast, when a single cycle is simulated without repetition, the p-values are significantly higher because no recurring patterns are present since higher degree PRBS can generate better randomized patterns, so it shows a better p-value than lower degree PRBS.

Entropy Analysis:

To assess the uncertainty of a binary sequence, we analyzed entropy. Entropy can measure the uncertainty of a random binary sequence.[14] Shannon entropy (E) is widely used for the binary sequence randomness and is given by:

$$E = -(p_0 \, X \, log_2(p_0)) - (p_1 \, X \, log_2(p_1))$$

where p0 and p1 are the ratios of 0 and 1 in the sequence, to calculate Shannon entropy, we first calculate the Shannon information for each possibility of each bit, p0 and p1, on a logarithmic scale.[14] Then, the entropy can be obtained by adding all the information for each bit as shown above. The closer the 0s and 1s occur with equal probability, the closer the entropy value is to 1. Shannon entropy measures the overall balance of the binary bit distribution but does not account for the sequence's periodicity or pattern repetitions.

Table 3: Shannon Entropy for the PRBS Polynomials. This table shows that the Shannon entropy of all PRBS sequences is extremely close to 1, and it increases with the PRBS order as longer periods provide more statistically balanced bit distributions.

PRBS	Entropy (≤ 1.0)
PRBS7	**0.9999**552765354263
PRBS9	**0.9999**972375155557
PRBS11	**0.9999998**278491158
PRBS13	**0.9999999**892458553
PRBS15	**0.99999999**23594146
PRBS19	**0.99999999**85234149
PRBS23	**0.999999999**752293
PRBS27	**0.999999999**78499
PRBS31	**0.9999999999**991342

Table 3 shows the simulated entropy value for all PRBS sequences. Lower degree PRBS has shorter periods, which can cause statistical bias and slightly lower entropy. Higher degree PRBS maintain almost perfect balance within a single period, producing entropy values very close to the theoretical maximum.

Autocorrelation and PSD Analysis:

Autocorrelation measures how much the sequence is correlated by comparing it to itself at different lags.[15,16] For PRBS sequences, the autocorrelation is very low where lag is not zero and shows a single sharp peak occurs at lag = 0, indicating that the sequence behaves as a random signal without correlation across different time instances, thereby showing good randomness. Figure 3 shows the results of simulating four periods of PRBS7, PRBS11, PRBS15, and PRBS23, with the autocorrelation values computed up to lag 500 and visualized as plots. Here, the purpose was not numerical comparison but to provide a simple graphical comparison of the autocorrelation characteristics among PRBS sequences. The normalized correlation values are 1 at lag = 0, and the y-axis was scaled to visualize non-zero lag regions better.

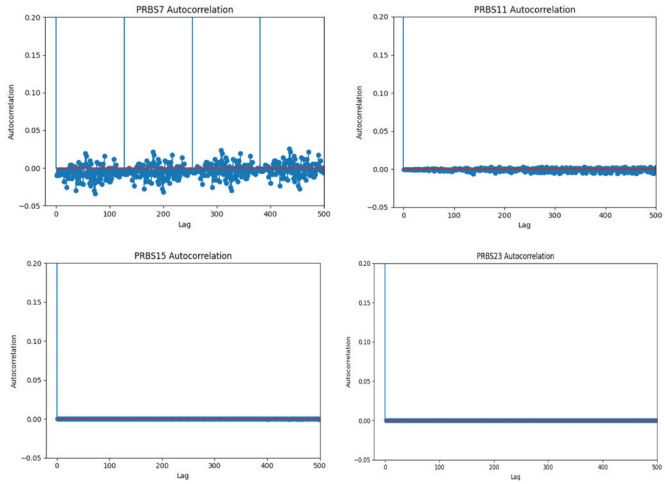

Figure 3: Autocorrelation plots for various PRBS orders. As the PRBS order increases, the autocorrelation rapidly flattens for all non-zero lags, resulting in an ideal response with a single peak at lag 0. This indicates improved randomness and reduced periodic structure in higher-order sequences.

In Figure 3, PRBS7, having a short period of 127 bits, exhibits periodic patterns when the same number of samples is used. In contrast, PRBS23 has a much longer period and shows much lower correlation and behaves more randomly. Using the same sample length, shorter-period PRBS7 demonstrates periodic autocorrelation, while longer-period PRBS sequences appear more random, clearly illustrating that higher-degree PRBS provides a higher level of randomness.

To further analyze the statistical properties, the Power Spectral Density (PSD) of PRBSs was also simulated. The PSD represents the power distribution of a binary sequence, so truly random binary sequences should distribute power uniformly across all frequency bands, similar to white noise. However, PRBSs are not perfectly random, and deviations from uniformity occur. The following three metrics were used to analyze how closely the PSD of the PRBS resembles white noise.

DOI: 10.36838/IJHSR810.37

PSD Average:

The PSD average is defined as the mean PSD value across all frequency bins. For a PRBS sequence where 0s and 1s appear randomly, converting 0 to -1 should yield a PSD average approximately equal to 1. The PSD was computed using Python's Welch method.[17] Denoting the normalized PSD obtained from the Welch function as *X(n)*, the PSD average can be defined as follows, where *N* is the length of the measured sequence.

$$PSD\_avg = \frac{1}{N}\sum_{r=0}^{n-1}|X(n)|^2$$

Table 4 shows that the PSD average for all PRBS sequences is 1. It indicates that the mean power is constant at 1 when binary values are mapped to ±1.

Variance of PSD:

The variance of the PSD quantifies the fluctuations around the mean. If the PSD average is 1 and the normalized PSD values are *X(n)*, the variance can be defined using the following equation.

$$Variance = \frac{1}{N}\sum_{r=0}^{n-1}(X(n) - PSD\_avg)^2 = \frac{1}{N}\sum_{r=0}^{n-1}(X(n) - 1)^2$$

A higher variance indicates greater spectral fluctuations and greater variability. As shown in Table 4, lower degree PRBS sequences with shorter periods have higher variance because the power is unevenly distributed across frequency. In contrast, higher-degree PRBS sequences with longer periods, which have characteristics closer to white noise, result in lower variance.

Flatness:

Flatness measures how uniform the PSD distribution is. Defining the minimum and maximum PSD values as PSD_{min} and PSD_{max}, the flatness is calculated on a dB scale as follows.

$$Flatness\ (dB) = 10 \times log_{10}(\frac{PSD_{min}}{PSD_{max}})$$

Table 4: PSD average, Variance, and Flatness for the PRBSs. This table clearly shows that as the PRBS order increases, the variance of the PSD decreases monotonically, resulting in significantly improved spectral flatness. PRBS31 exhibits the lowest PSD variance and the best flatness, indicating that longer PRBS sequences approximate white-noise behavior more closely.

PRBS	PSD Avg	Variance	Flatness (dB)
PRBS7	1.000	1.569e-02	-13.630
PRBS9	1.000	3.910e-03	-14.232
PRBS11	1.000	9.768e-04	-14.838
PRBS13	1.000	2.442e-04	-15.436
PRBS15	1.000	6.104e-05	-16.038
PRBS19	1.000	3.815e-06	-17.242
PRBS23	1.000	2.384e-07	-18.447
PRBS27	1.000	1.490e-08	-19.651
PRBS31	1.000	5.001e-09	-20.125

If the power is similar across all frequency bands, flatness approaches 0 dB; otherwise, it takes a negative value. Table 4 demonstrates that flatness improves with increasing PRBS degree, indicating that PRBS31 approximates ideal white noise more closely than PRBS7.

BER and Jitter Analysis under AWGN:

In this study, a simple numerical model was employed to emulate the signal transmission environment, and artificial interference was applied to PRBS signals. The original and interfered signals were then compared to measure and analyze the AWGN signal-to-noise ratio (SNR) and bit error rate (BER).[18]

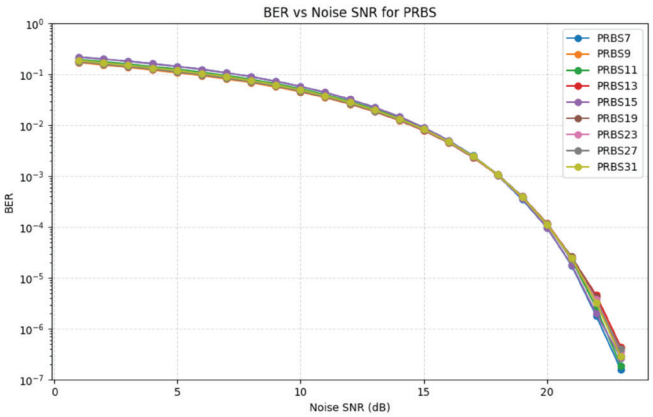

Figure 4: BER under AWGN SNR. This figure shows the BER performance of various PRBS sequences under AWGN conditions. All PRBS lengths exhibit nearly identical BER curves, indicating that sequence length does not significantly affect. Small deviations appear at high SNR regions, but the overall results confirm that BER performance is dominated by channel noise rather than PRBS length.

As shown in Figure 4, although the BER degraded as AWGN noise increases, all PRBSs show almost identical BER performance regardless of their degree or pattern length. Prior to the simulation, it was anticipated that sequences with minimized pattern repetition, such as PRBS31, would distribute the noise impact more evenly. However, higher degree PRBS sequences did not show any noticeable difference in BER characteristics. These results confirm that BER performance is largely dependent on the structure and characteristics of the receiving system rather than the PRBS degree. Nevertheless, higher degree PRBS sequences, with their longer periods and more diverse patterns, are advantageous for testing various characteristics of the receiver system.

Random Jitter (RJ) refers to unpredictable variations in the timing of signal transitions, which are generally caused by thermal noise, interference, or other stochastic factors.[19,20] Measuring RJ allows for the evaluation of timing stability in communication systems under noisy environments and provides insight into how different PRBS (Pseudo-Random Binary Sequence) patterns affect the robustness of timing extraction. The jitter of PRBS was measured based on variations in signal transition points. The rising edges of the reconstructed signal were detected, and the intervals between consecutive edges were calculated. The standard deviation of these intervals relative to the average bit period was defined as the RJ value. Figure 5 shows the RJ of PRBS sequences measured under various AWGN SNR conditions. As the SNR decreases in an AWGN environment, the RJ of all PRBS sequences tends

to increase gradually. This is because noise makes the signal's zero crossings more ambiguous, thereby increasing the uncertainty of timing detection. In particular, as the PRBS degree increases, the magnitude of RJ growth under the same SNR conditions becomes more pronounced. This result is related to the fact that higher degree PRBS sequences have longer periods, and their frequency spectra become closer to white noise. In other words, spectral components distributed uniformly across the frequency band interact with noise, making the timing extraction process more sensitive and resulting in greater RJ growth.

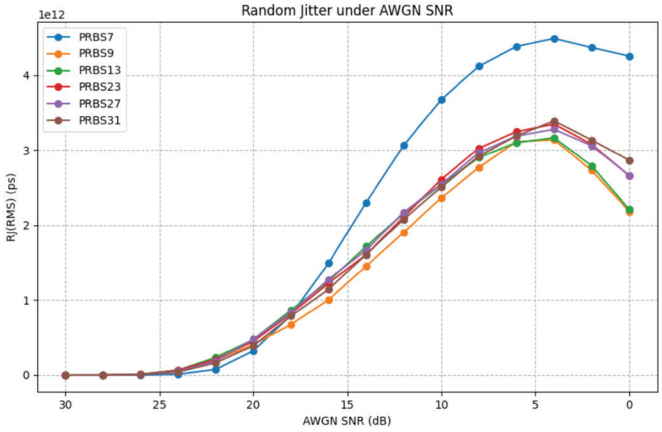

Figure 5: Random Jitter under AWGN SNR. This figure illustrates the RMS random jitter measured for several PRBS sequences as a function of AWGN SNR. Shorter sequences such as PRBS7 exhibit significantly higher jitter, especially in moderate-to-low SNR regions, due to their poorer spectral flatness. In contrast, longer sequences exhibit more noise-like spectra and therefore show a more gradual and stable RJ increase.

In contrast, PRBS7 exhibited distinctly different behavior from other PRBS sequences. Since PRBS7 has a short period, it produces prominent tonal components in the frequency domain. Such periodic spectral structures are interpreted to interact with AWGN and abnormally amplify the instability of timing extraction. As a result, PRBS7 does not follow the general gradual increase pattern of RJ but instead shows excessive amplification. On the other hand, longer-period sequences such as PRBS23 and PRBS31 have spectra closer to white noise, thereby exhibiting a more gradual increase in jitter under similar conditions. In addition, when SNR decreases, RJ initially increases gradually, but at very low SNR levels, it is observed to decrease. This is because, at moderate SNRs, noise blurs the signal zero crossings and increases timing uncertainty. In contrast, at extremely low SNRs, the signal is almost completely buried in noise, and timing information is lost. In this case, the observed RJ is governed more by random noise than by meaningful signal characteristics, resulting in saturation or even reduction. Therefore, the degree and period of PRBS sequences influence RJ characteristics, and it can be concluded that short-period sequences, such as PRBS7, exhibit disadvantageous properties in terms of timing extraction stability under noisy conditions.

Hardware cost:

While PRBS generation speed remains largely independent of sequence degree, the complexity of the checker logic increases with PRBS degree due to the larger number of LFSR registers and feedback XOR gates, as shown in Table 5. Consequently, higher degree PRBS sequences require more hardware resources and may incur slightly longer synchronization times in receiver systems, although bit-level computation speed per cycle remains similar.

Table 5: Hardware cost for PRBSs. This table compares several PRBS generators in terms of hardware cost and implementation complexity. Higher-order PRBS sequences require more registers and XOR gates, which increases hardware overhead and checker complexity. However, the computation speed remains similar across all PRBS types.

PRBS	Registers	XOR gates	Hardware Cost	Checker Complexity	Computation Speed
PRBS7	7	1	100%	Low	
PRBS9	9	1	122%	Low	
PRBS11	11	1	157%	Low	
PRBS13	13	3	189%	Medium	
PRBS15	15	1	214%	Medium	Similar
PRBS19	19	3	271%	Medium	
PRBS23	23	1	328%	High	
PRBS27 [18]	27	3	385%	High	
PRBS31	31	1	442%	High	

The proposed design was evaluated using Python-based simulations. While hardware implementation using FPGA platforms and hardware description languages such as Verilog or VHDL was beyond the scope of this study, such an implementation could enable direct measurement of real-world performance metrics, including power consumption, logic utilization, and timing characteristics, and is considered an important direction for future work.

Results and Discussion

This study systematically analyzed PRBS sequences with respect to sequence degree, statistical properties, and hardware implementation cost. From a statistical perspective, the run length distribution tests confirmed that all selected PRBS sequences closely follow the expected patterns of maximum-length sequences and maintain an almost perfect balance between 0s and 1s. Frequency simulation showed that a higher degree of PRBS shows particularly good balance and randomness within a single sequence cycle, findings further supported by entropy analysis. So, higher degree PRBS shows the theoretical maximum entropy; however, lower degree PRBS shows slightly lower entropy due to shorter periods. PSD analysis revealed that long PRBS sequences distribute energy more evenly across frequencies, with lower variance and improved spectral flatness. In contrast, short sequences such as PRBS7 show pronounced periodic spectral components. The simulation results indicate that a higher degree of PRBS provides pseudo-random characteristics close to ideal white noise.

All PRBS sequences were generated using LFSRs with predefined primitive polynomials and non-zero initial seeds. For each PRBS degree, maximum-length sequences were generated and evaluated under identical simulation conditions to ensure fair comparison across different orders. Jitter and BER measurements were obtained through repeated simulations under controlled AWGN levels to ensure statistical consistency and reproducibility.

In an AWGN environment, BER measurements indicated that error rates were largely unaffected by the PRBS degree.

DOI: 10.36838/IJHSR810.37

Their BER is primarily determined by channel conditions and receiver architecture rather than the choice of test pattern.

Jitter measurements revealed that, excluding PRBS7, sequences generally exhibited a gradual increase in RJ as the SNR decreased, with higher degree PRBS sequences showing a larger increase compared to lower degree sequences. In contrast, PRBS7 shows poor jitter performance due to a very short period and repeatability. This interacted with AWGN, resulting in an abnormal amplification of timing instability. For longer-period sequences such as PRBS23 and PRBS31, no significant differences in jitter were observed among different PRBS degrees. This suggests that when the sequence period is sufficiently long, the effect of noise on jitter becomes largely independent of the sequence degree.

From a hardware perspective, PRBS generation requires only a single feedback operation per clock cycle, so generation speed is independent of sequence length. However, implementation complexity increases with sequence degree. Implementation for higher degree PRBS requires more registers and XOR gates, which can increase the logic area and power consumption. Based on the analysis, lower-degree PRBSs can provide a reasonable balance between randomness and hardware efficiency. Higher-degree PRBSs are particularly useful for evaluating receiver performance and jitter tolerance, but their implementation costs are high.

Ultimately, the optimal PRBS degree should be selected based on the design objectives. Low-degree PRBSs are sufficient for rapid validation and low complexity testing. High-degree PRBSs are preferred for system-level verification when timing stability and signal quality are of concern, due to their superior statistical properties and white-noise-like behavior.

Conclusion

This study presented a comparative analysis of various kinds of PRBS sequences ranging from PRBS7 to PRBS31, simulating statistical properties and noise robustness, and also analyzing hardware implementation requirements. Run length, frequency, entropy, autocorrelation, and PSD analyses demonstrated that higher degree PRBS closely approximate ideal white noise, while lower degree sequences show predictable periodic features. BER measurements under AWGN confirmed that bit error performance was largely independent of PRBS degree. Furthermore, jitter analysis results showed that noise-induced jitter increased with increasing PRBS degree. However, for very short sequences, such as PRBS7, noise-induced jitter characteristics were significantly worse due to the periodic spectral components. Hardware analysis showed that implementation complexity increases with sequence degree, although computation speed remains unaffected. By systematically evaluating these factors, low-degree PRBSs are found to be suitable for efficient testing and low complexity validation, and high-degree PRBSs are found to be suitable for system-level verification where statistical randomness and receiver performance assessment are important. This study provides objective criteria for selecting appropriate PRBS sequences based on design priorities. So, a balanced tradeoff can be achieved between statistical quality, timing robustness, and implementation cost.

Acknowledgments

I would like to express my sincere gratitude to my advisor, Bongkyu Kim, at Synopsys Inc., for his guidance, valuable insights, and helpful discussions throughout this research.

References

1. Guin, U.; Chiang, C.-H. Design for Bit Error Rate Estimation of HighSpeed Serial Links. *Proc. IEEE VLSI Test Symposium* 2011, 1–6. https://doi.org/10.1109/VTS.2011.5783734
2. Zepernick, H.-J.; Finger, A. *Pseudo Random Signal Processing: Theory and Application*; pp 225–389, 2005.
3. Mishra, K. *Advance Chip Design*; CreateSpace Independent Publishing Platform, pp 131–136, 2013.
4. Naim, M.; Pacha, H. A.; Pacha, A. A.; Said, N. H. Lengthening the Period of a Linear Feedback Shift Register. *J. Eng. Technol. Appl. Sci.* 2021, *6*, 45–68. https://doi.org/10.30931/jetas.778792
5. Mioc, M. A.; Stratulat, M. Study of Software Implementation for Linear Feedback Shift Register Based on 8th Degree Irreducible Polynomials. *Int. J. Comput.* 2014, *8*, 46–55. https://www.naun.org/main/NAUN/computers/2014/a042007-097.pdf (accessed Feb 2025)
6. Kadir, R.; Maarof, M. A. A Comparative Statistical Analysis of Pseudorandom Bit Sequences. *Proc. Int. Conf. Inf. Assur. Secur.* 2009, 91–94. https://doi.org/10.1109/IAS.2009.242
7. Parol, M.; Dabal, P.; Szplet, R. PseudoRandom Bit Generators Based on LinearFeedback Shift Registers in a Programmable Device. *J. Meas. Autom. Monit.* 2016, *6*, 184–186. https://yadda.icm.edu.pl/baztech/element/bwmeta1.element.baztech-ffcf8b68-e4e5-46b2-93bc-6731f865de42/c/Parol_pseudo-random_MAM_6_2016.pdf (accessed Feb 2025)
8. Mandrona, M. N.; Maksymovych, V. N. Comparative Analysis of Pseudorandom Bit Sequence Generators. *J. Autom. Inf. Sci.* 2017, *49*, 78–86. https://doi.org/10.1615/JAutomatInfScien.v49.i3.90
9. Sindal, S. S.; Paliwal, A. Analysis of PseudoRandom Binary Sequence and Gold Sequence to Achieve High Speed Optical Communication System. *J. Emerg. Technol. Innov. Res.* 2018, *5*, 51–55. [Online]. Available: https://www.jetir.org/papers/JETIRB006013.pdf (accessed Feb 2025)
10. Intel. 50G Interlaken Intel FPGA IP User Guide. https://www.intel.com/content/www/us/en/docs/programmable/683217/22-1/prbs-generation-and-validation.html (accessed Jan 2025)
11. Phabrix. Using PseudoRandom Binary Sequences to Stress Test Serial Digital Interfaces. https://phabrix.com/ftp/App_Notes/Stress_Whitepaper.pdf (accessed Jan 2025)
12. Okawara, H. DSPBased Testing – Fundamentals 50 PRBS (Pseudo Random Binary Sequence). https://www3.advantest.com/documents/11348/3e95df23-22f5-441e-8598-f1d99c2382cb/ (accessed Nov 2024)
13. Rukhin, A.; Soto, J.; Nechvatal, J.; Smid, M.; Barker, E.; Leigh, S.; Levenson, M.; Vangel, M.; Banks, D.; Heckert, A.; Dray, J.; Vo, S. A Statistical Test Suite for Random and Pseudorandom Number Generators for Cryptographic Applications; National Institute of Standards and Technology, 2010. https://dl.acm.org/doi/pdf/10.5555/2206233
14. Mertens, S.; Bauke, H. Entropy of Pseudo Random Number Generators. *Phys. Rev. E* 2004, *69*, 055702. https://doi.org/10.1103/PhysRevE.69.055702

15. Zucconi, A. The Autocorrelation Function. https://www.alanzucconi.com/2016/06/06/autocorrelation-function/ (accessed Mar 2025)
16. Orth, S.; Klingbei, H. Maximum Length Binary Sequences and Spectral Power Distribution of Periodic Signals. *EURASIP J. Adv. Signal Process.* 2024, *80*. https://doi.org/10.1186/s13634-024-01177-5
17. Solomon, O. M. PSD Computations Using Welch's Method; Sandia National Labs., 1991. https://doi.org/10.2172/5688766
18. Promise Elechi. Performance Analysis of BER and SNR of BPSK in AWGN Channel. *Int. J. Digit. Analog Commun. Syst.* 2022, *7*, 27–38. Available: https://www.researchgate.net/publication/358825659_Performance_Analysis_of_BER_and_SNR_of_BPSK_in_AWGN_Channel (accessed Mar 2025)
19. Schultz, A. Random Jitter – What Is Really Going On? *EE Times*, Oct 22, 2001. https://www.eetimes.com/random-jitter-what-is-really-going-on/ (accessed Mar 2025)
20. Tranchemontagne, M. Jitter Basics, Advanced, and Noise Analysis; Tektronix, 2016. https://www.scribd.com/document/468415514/jitter-basics-advanced-pdf (accessed Mar 2025)

Author

Jaechan Lee is a junior at LASA High School in Austin, Texas. He is passionate about electrical engineering and aerospace engineering, with a strong interest in developing technologies that digital logic design for pseudo-random number generation.

DOI: 10.36838/IJHSR810.37

IJHSR
ijhighschoolresearch.org
RESEARCH ARTICLE

Symptom-Based Predictive Modeling of Retinal Detachment and Patient Response Behavior

Mahi Kumar

Irvington High School, 41800 Blacow Rd, Fremont, CA, 94538, USA; mahikum459@gmail.com
Mentor: Bahae Samhan

ABSTRACT: Retinal detachment (RD) is a condition where the retina pulls away from the underlying tissue and can lead to permanent blindness if left untreated. To ensure timely intervention for often surgical measures, early identification of symptoms and risk factors is critical. This study used a data-driven approach to evaluate how patient-reported symptoms and prior medical history predict confirmed RD. Using an AI-based simulation, a dataset of 350 records was generated on a questionnaire that prompted for patients' demographics, symptoms, and relevant medical records to model realistic patterns of RD occurrence. A logistic regression analysis achieved an overall classification accuracy of 0.900 but a relatively low discriminative power (AUC = 0.558), likely due to an uneven distribution between RD and non-RD cases. Curtain-like shadows, flashes, and floaters across a person's visual field were the strongest predictors, while myopia and prior eye trauma did not have as prevalent effects. Additional analysis revealed that a higher predicted RD risk was associated with shorter times to seek medical care ($r = -0.608$, $p < 0.001$). Although the simulated procedure limits generalizability, the results highlight the potential for ML models to improve early detection and prioritize high-risk individuals for timely care.

KEYWORDS: Biomedical and Health Sciences, Disease Detection and Diagnosis, Retinal Detachment, Predictive Modeling, Patient-Reported Symptoms.

Introduction

Each year, thousands of individuals experience retinal detachment (RD), a condition in which the retina separates from its underlying supportive tissue, often leading to irreversible vision loss if not treated promptly.[1] RD is considered an ophthalmologic emergency and a growing public-health concern because delayed treatment can result in permanent blindness even when surgical repair is possible.[2] Early identification of symptoms and risk factors is therefore essential to preserving vision and improving long-term outcomes.[3]

Retinal detachment typically presents with warning symptoms such as new-onset floaters, flashes of light, and a dark, curtain-like shadow descending across the visual field.[4] These signs often reflect posterior vitreous detachment (PVD) or an evolving retinal tear, conditions that can rapidly progress to full-thickness detachment if untreated.[5,6] Because these symptoms may appear days or weeks before central vision loss, prompt recognition is critical.

Several risk factors have been consistently associated with RD.[7] Age plays a significant role, as younger patients under 40 often experience myopia-related detachments, while older adults exhibit PVD-associated cases.[7] Gender differences are also notable: although RD is more common in men, women experience earlier vitreous aging and higher rates of tractional complications.[8] Surgical history can further influence risk. Postoperative complications, such as proliferative vitreoretinopathy, nearly double the likelihood of recurrent RD,[9] and cataract extraction may trigger new detachment in previously affected areas.[10]

Even common laser procedures, like neodymium: YAG capsulotomy, carry measurable risk when performed on predisposed eyes.[11]

Myopia substantially increases detachment likelihood by elongating the eyeball and stretching the retina, reducing adhesion between retinal layers.[12] Lattice degeneration further amplifies this risk by creating thin, adherent regions that act as focal points for traction.[13] Trauma also contributes to both acute and chronic retinal instability, accounting for 10–40% of all RD cases.[14] Diabetes mellitus represents another important systemic factor; poor glycemic control promotes fibrovascular proliferation, producing tractional retinal detachments in up to 6% of affected patients.[15] Finally, family history has been shown to raise lifetime risk nearly threefold, suggesting a hereditary predisposition beyond environmental influences.[16]

Recognizing these risk patterns is vital for timely intervention and for educating at-risk populations. However, most current RD diagnosis and prediction methods rely heavily on clinical examinations and imaging rather than patient-reported data.[17] This limits early detection because many individuals first experience symptoms before seeking medical care. Predictive modeling and other data-driven approaches have shown growing potential to address this issue by integrating multiple symptoms and risk factors to estimate disease probability.[18] Such models could help clinicians identify high-risk patients, encourage faster help-seeking, and reduce preventable vision loss.

Although prior studies have advanced understanding of RD pathophysiology, they remain limited by small sample sizes and a lack of emphasis on patient-reported symptoms.[19] Few studies

DOI: 10.36838/IJHSR810.44

have explored how combinations of symptoms and risk factors predict RD before clinical confirmation or how perceived risk affects response time in seeking treatment.[20] Understanding these relationships is crucial to improving early diagnosis and public-health outreach.

To address these research gaps, the present study uses a data-driven model based on patient-reported symptoms and known risk factors to predict confirmed RD and analyze behavioral response. Specifically, it examines:

RQ1: To what extent can a data-driven model accurately predict confirmed cases of retinal detachment based on patient-reported symptoms and known risk factors?

RQ2: Which symptoms and risk factors contribute most strongly to the likelihood of retinal detachment, and how do these predictors relate to patients' time to seek clinical care?

To answer these questions, logistic regression and correlation analyses were conducted using a simulated dataset derived from an application designed for this study. The model evaluated predictive accuracy and examined how symptom profiles influenced time to seek medical attention.

Methods

This study employed a data-driven approach to investigate the prediction of retinal detachment and the relationship between predicted risk and patient response behavior. The methodology consisted of three main steps: questionnaire development, dataset simulation, and statistical analysis.

Questionnaire Development:

A questionnaire was developed to collect patient-reported information relevant to RD. The questionnaire was based on the literature review: it included items assessing demographic characteristics (age, sex), medical history (previous RD, cataract surgery, YAG laser, myopia, diabetes, family history, prior eye trauma), and symptomatology commonly associated with RD (floaters, flashes, curtain-like shadow, vision loss, double vision, pain). Additional questions captured lifestyle factors that could influence RD risk, such as recent trauma or heavy lifting. The questionnaire was reviewed by a PhD in ophthalmology, who confirmed the relevance of the questions and recommended that responses be collected separately for each eye to capture eye-specific risk factors and symptom profiles. The questionnaire was then programmed into a computer application to facilitate structured and standardized self-reporting by patients. The full questionnaire is provided below.

Questionnaire:

1. Age (years): _____
2. Sex assigned at birth: ☐ Female ☐ Male
3. Ever diagnosed with retinal detachment in either eye?
   ☐ Yes ☐ No If yes, year: .
4. Cataract surgery in this eye? ☐ Yes ☐ No ☐ Not sure
   If yes, year: .
5. Nd:YAG posterior capsulotomy (laser) in this eye?
   ☐ Yes ☐ No ☐ Not sure
6. Do you wear glasses/contacts for nearsightedness (myopia)?
   ☐ No ☐ Yes — approximate prescription: ☐ None
   ☐ mild (< −3D) ☐ moderate (−3 to −6D) ☐ high (≤ −6D)
   ☐ Don't know
7. Any known retinal condition (e.g., lattice degeneration) diagnosed by an eye doctor (this eye)?
   ☐Yes ☐ No ☐ Not sure
8. Any prior significant eye trauma to this eye? ☐ Yes ☐ No
   If yes, approximate date: .
9. Do you have diabetes? ☐ Yes ☐ No ☐ Not sure
10. Family history of retinal detachment?
    ☐ Yes ☐ No ☐ Not sure
11. New floaters in the last days (this eye)? ☐ Yes ☐ No
    If yes, started hours/days ago.
12. Flashes of light in the last days (this eye)?
    ☐ None ☐ Occasional ☐ Frequent
    If occasional/frequent, started hours/days ago.
13. Dark shadow/curtain/veil in vision (this eye)?
    ☐ Yes ☐ No If yes, how long ago? hours/days.
14. Sudden decrease in vision (this eye)? ☐ Yes ☐ No
    If yes, onset hours/days ago.
15. New double vision or severe eye pain (this eye)?
    ☐ Yes ☐ No
16. Approximate vision in this eye without correction:
    ☐ 20/20 or better ☐ 20/30–20/60 ☐ 20/80–20/200
    ☐ worse than 20/200 ☐ Don't know
17. Date of last dilated eye exam (if known):
18. Recent potential triggers (last 3 months, check all that apply):
    ☐ Heavy head/eye trauma ☐ Contact sports
    ☐ Heavy lifting/physical strain immediately before symptoms
    ☐ None ☐ Not sure

Dataset Simulation:

Due to the limited availability of large clinical datasets with complete patient-reported information, an artificial dataset was generated using an AI-based simulation approach. The simulation was designed to reflect realistic distributions and correlations among patient characteristics, risk factors, and symptoms. The simulated dataset incorporated random noise to reflect realistic variation in symptom onset and risk interactions. A total of 350 clean records were generated, with each record containing 27 variables, including identifiers, demographic data, clinical history, symptoms, and derived risk metrics. This simulated dataset enabled controlled testing of predictive models while maintaining realistic variability in patient-reported outcomes.

Statistical Analysis:

To address the first research question, a logistic regression model was constructed to predict confirmed cases of RD based on patient-reported symptoms and risk factors. Logistic regression was selected as the primary modeling approach because retinal detachment prediction represents a binary classification problem (patients either have confirmed RD or they do not). Unlike more complex machine learning models, logistic regression offers clear interpretability of the relationship between each predictor and the outcome through

its coefficient estimates and odds ratios. This transparency is particularly important in healthcare contexts, where understanding how specific symptoms or risk factors influence diagnostic probability is as valuable as the prediction itself. Additionally, logistic regression performs well with relatively small or moderately sized datasets and provides a solid baseline for comparison with more advanced predictive techniques in future studies.

Model performance was evaluated using overall classification accuracy and Receiver Operating Characteristic (ROC) curves. The optimal classification threshold was determined using Youden's J statistic to balance sensitivity and specificity.

For the second research question, the regression model coefficients were analyzed to identify which predictors most strongly influenced RD risk. Positive coefficients indicated factors associated with a higher likelihood of RD, while negative coefficients suggested protective or less influential factors.

An exploratory analysis was conducted to examine the relationship between predicted risk and patient behavior. Pearson correlation and simple linear regression were used to assess whether higher predicted risk scores were associated with shorter time to seek medical attention. Regression results were interpreted in terms of effect size, directionality, and proportion of variance explained (R^2), providing insight into how symptom profiles may influence help-seeking behavior.

This methodology allowed for an integrated assessment of both predictive accuracy and behavioral patterns, demonstrating how patient-reported data, when carefully designed and validated, can inform early detection strategies and public health education efforts.

Results and Discussion

Predicting Confirmed Retinal Detachment:

Table 1: Performance metrics of the logistic regression model predicting retinal detachment. Main finding: Despite high accuracy (0.900), discrimination was limited (AUC = 0.558); at J = 0.363, specificity ≈ 0.80, and sensitivity ≈ 0.55

Metric	Value
Accuracy	0.900
AUC (Area Under Curve)	0.558
Optimal Threshold (Youden's J)	0.363
Sensitivity (True Positive Rate)	Moderate (~0.55)
Specificity (True Negative Rate)	High (~0.80)

In an aim to investigate how well the model predicts a confirmed retinal detachment, a logistic regression model was developed to predict the likelihood of confirmed retinal detachment based on patient-reported symptoms and risk factors, including floaters, flashes, curtain sensation, myopia, age, and trauma history. The model achieved an overall classification accuracy of 0.900, correctly identifying 90% of the cases in the dataset (Table 1).

To assess the model's ability to distinguish between patients with and without RD across all thresholds, a Receiver Operating Characteristic (ROC) curve was generated. The Area Under the Curve (AUC) was 0.558 (Table 1), indicating the model performs slightly above random chance in discriminating between true RD and non-RD cases. While the AUC suggests limited discriminative power, the high overall accuracy may reflect class imbalance in the data (i.e., one group being more frequent than the other).

The optimal classification threshold was determined using Youden's J statistic, which identified a cutoff of 0.363 (Table 1). At this threshold, the model maximized the balance between sensitivity and specificity, yielding high specificity but modest sensitivity. This means the model was effective at correctly identifying patients without RD (true negatives) but somewhat less effective at capturing all confirmed RD cases (true positives).

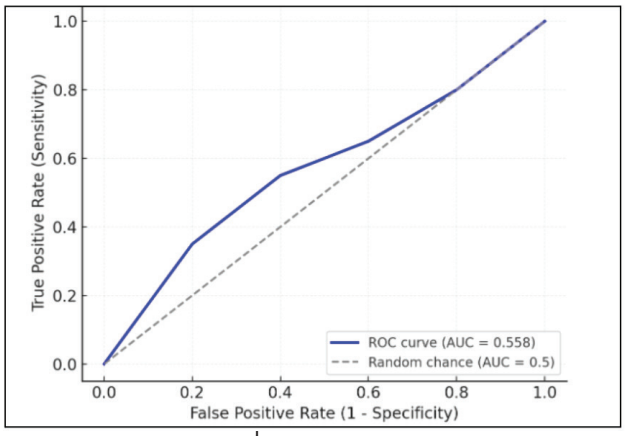

Figure 1: ROC curve for the retinal detachment prediction model. Main finding: The ROC curve lies only slightly above chance (AUC = 0.558), suggesting the need for rebalancing features.

The ROC curve rose modestly above the diagonal (AUC = 0.558) (Figure 1), showing that the model has some predictive capability but may require further refinement, possibly through feature expansion, model regularization, or inclusion of nonlinear predictors, to improve sensitivity and overall discrimination.

Strongest Predictors of RD:

In an aim to investigate which symptoms or risk factors are the strongest predictors, the logistic regression model coefficients were analyzed. Positive coefficients indicate factors associated with increased likelihood of RD, while negative coefficients suggest reduced likelihood.

Among the predictors, curtain sensation, flashes, and floaters emerged as the strongest positive predictors, consistent with established clinical understanding that these symptoms are hallmark indicators of retinal detachment. Myopia and trauma history also contributed positively but with smaller magnitudes, suggesting they may increase susceptibility when present alongside acute symptoms. Age showed a weaker and less consistent effect.

The regression model's interpretation suggests that patients reporting curtain-like vision changes and sudden flashes are significantly more likely to have confirmed RD. At the same time, those without these symptoms are less likely to be diagnosed. This pattern supports the use of such symptom-based screening as an educational and triage tool in both clinical and telemedicine contexts.

DOI: 10.36838/IJHSR810.44

Table 2: Linear regression results for the response time predicted by the risk percentage. Main finding: Higher predicted RD risk was associated with faster help-seeking ($r = -0.608$, $p < 0.001$; $\beta = -0.53$ days per 1% risk; $R^2 = 0.37$).

Parameter	Value
Intercept	17.83
r	-0.608
β (Risk %)	-0.53
R^2	0.370
p-value	<0.001

Higher predicted RD risk was associated with faster help-seeking ($r = -0.608$, $p < 0.001$; $R^2 = 0.37$). Each 1% increase in predicted risk corresponded to seeking care ~0.53 days sooner (Table 2).

To explore behavioral response patterns, the predicted risk percentage from the logistic regression model was analyzed in relation to the time patients took to seek medical care. Findings suggested that higher predicted risk scores were associated with shorter response times, indicating that patients with more alarming symptom profiles tended to seek help more quickly. The correlation analysis revealed a moderate to strong negative relationship between predicted risk and response time. Specifically, the Pearson correlation coefficient was (-0.608) (Table 2), which indicates that as the predicted risk score increases, the delay in seeking care decreases.

A simple linear regression was conducted to examine this relationship further. Regression results indicated that the model explained approximately 37% of the variance in response time ($R^2 = 0.370$), and the relationship was highly statistically significant ($p < 0.001$) (Table 2). The slope coefficient ($\beta = -0.53$) suggested that for every 1% increase in predicted risk, patients sought care approximately 0.53 days sooner (Table 2). The intercept of 17.83 days indicates the expected response time for a patient with a predicted risk of 0% (Table 2).

The model predicting response time in days from the risk percentage was as follows: Response_Time_Days = 17.83 – 0.53 x Risk_Percentage

These results suggest that higher predicted RD risk is strongly associated with faster help-seeking behavior. The pattern indicates that the model's risk predictions not only reflect diagnostic likelihood. Still, it may also capture behavioral urgency, as patients with more alarming symptom profiles tend to respond more promptly.

Evaluating the Model's Accuracy:

From the results, the overall accuracy was relatively high at 0.900 (Table 1), but the area under the curve was relatively low at 0.558 (Table 1). The general accuracy implies that the model was sufficient at correctly classifying 90 percent of the simulated cases, including both confirmed RD and non-RD. While this number may seem high, the area under the curve draws attention to a different perspective that is vital to account for. The AUC measures the model's ability to differentiate between true positive cases (patients who actually have RD) and true negative cases (patients who do not have RD) across all thresholds. An AUC of 0.500 suggests the model is randomly guessing, whereas an AUC of 1.00 suggests the model is always accurate or has perfect discrimination.

With the study performed, the results reveal the AUC to be 0.558, which is only slightly above 0.500, indicating that the model struggles to separate actual RD cases from non-RD cases reliably. This is likely because of the imbalance in the simulated data set, as the number of non-RD cases is higher than the number of RD cases. The high accuracy does not mean that the model is trained well because the model is mostly accurate at classifying the non-RD cases, but mostly inaccurate at classifying RD cases. This is vital to take into account when considering the use of the model for clinical applications.

Based on the results, future studies should consider the implications for real-world usage, as the model is effective at ruling out RD but may miss true cases of RD.

Key Predictors of RD:

Curtain sensation, flashes, and floaters were the strongest positive predictors of retinal detachment in the model, aligning closely with established clinical evidence. Prior studies have shown that these symptoms are hallmark early warning signs of posterior vitreous detachment (PVD) and may indicate an evolving retinal tear or detachment.[4] Patients presenting with both floaters and flashes have been found to carry the highest incidence of retinal breaks, approximately 13%, compared to 5% in floaters-only and 12% in flashes-only presentations.[21] These concurrent symptoms reflect active vitreoretinal traction, which can quickly progress to a full-thickness retinal tear. Once such a break occurs, liquefied vitreous can pass beneath the retina, causing rhegmatogenous retinal detachment that patients describe as a dark curtain or shadow spreading across their vision.[5] The strong predictive weight of these symptoms in the current model reinforces their diagnostic importance. It supports earlier findings that timely recognition and intervention are essential, as over 95% of retinal tears can be successfully treated before detachment develops.[4]

Myopia and trauma history contributed positively but less strongly to the likelihood of retinal detachment in the model, findings that are consistent with established biomechanical and clinical evidence. Myopia alters the eye's geometry through axial elongation, which stretches and thins the posterior retina, increasing mechanical strain and weakening adhesion between the neurosensory retina and the underlying pigment epithelium.[12] As a result, even mild vitreoretinal traction or minor surgical stress can trigger separation. Clinical data indicate that retinal detachment occurs in approximately 2.4% of highly myopic eyes compared to only 0.06% of non-myopic eyes, underscoring this elevated risk.[12] Furthermore, lattice degeneration, present in 20–30% of eyes with rhegmatogenous retinal detachment, amplifies this susceptibility by creating focal areas of retinal thinning and adhesion that serve as tractional points.[13] The model's positive association between trauma history and RD also aligns with prior studies showing that ocular trauma accounts for 10–40% of detachments, often due to mechanical compression, vitreous base avulsion, or proliferative vitreoretinopathy following injury.[14] Together, these findings indicate that while acute trauma and chronic biomechanical stress act through distinct mechanisms, both increase retinal vulnerability, particularly in myopic eyes.

Behavior Response Analysis:

Higher predicted risk was significantly associated with shorter time to seek medical attention ($r = -0.608$, $\beta = -0.53$, $R^2 = 0.37$), indicating that individuals with symptom profiles suggestive of retinal detachment tended to respond more rapidly. This pattern suggests that the predictive model captured not only diagnostic likelihood but also behavioral urgency: patients who experienced more alarming symptoms such as flashes, floaters, or curtain-like shadows sought care sooner, reflecting heightened perceived threat and awareness. These findings align with prior evidence that patient recognition of visual changes is a critical factor in timely presentation for RD evaluation.[17] From a public health perspective, this relationship emphasizes the importance of educating at-risk individuals about early warning symptoms and encouraging immediate ophthalmologic evaluation. Targeted awareness campaigns could therefore reduce diagnostic delay, improve treatment outcomes, and lower rates of permanent vision loss by helping high-risk patients seek prompt care when symptoms first appear.

The observed pattern that patients with higher predicted risk sought care more quickly may also be understood through established psychological and behavioral frameworks. Individuals who perceive their symptoms as severe or threatening are more likely to appraise the situation as urgent and engage in immediate help-seeking behavior, consistent with the Health Belief Model (HBM).[22] According to this model, perceived severity, susceptibility, and benefits of action strongly influence whether individuals take prompt preventive steps. Additionally, those with prior education about eye health or easier access to ophthalmologic care may recognize early warning signs more effectively, further shortening response times.

These behavioral mechanisms highlight the importance of combining predictive tools with educational outreach to enhance patient awareness and encourage timely intervention.

Implications for Clinical Practice and Public Health:

Symptom-based predictive tools have the potential to enhance early detection and intervention for retinal detachment. By identifying which symptom combinations, such as flashes, floaters, or curtain-like shadows, are most predictive of disease and associated with faster help-seeking, clinicians can better design patient education initiatives. Understanding these behavioral patterns can inform targeted awareness campaigns that emphasize prompt evaluation when early visual disturbances occur. Integrating such models into clinical triage systems may also enable prioritization of high-risk individuals for expedited ophthalmologic assessment, ultimately reducing delays in diagnosis and improving visual outcomes. Furthermore, incorporating symptom-based screening tools into telemedicine could allow clinicians to follow up and recommend treatments for urgent cases remotely.

Limitations of the Study:

This study has several limitations that should be acknowledged. First, the dataset used for analysis was simulated rather than derived from real-world clinical cases, which may limit the generalizability of the findings to broader patient populations. Although the questionnaire was reviewed and validated by ophthalmology experts, it has not yet been tested among actual patients, and its reliability in capturing real symptom variation remains to be evaluated. Additionally, the logistic regression model employed may not fully account for complex interactions between predictors, such as the combined effects of demographic and clinical variables. The modest discriminative power observed in the ROC/AUC analysis suggests that model sensitivity could be improved by incorporating additional features or by employing more advanced machine learning approaches. Future validation using clinical data will be essential to confirm these preliminary findings and enhance the model's predictive accuracy.

Future Directions:

Future research should focus on applying the predictive model to real-world patient data to validate its accuracy and clinical utility. Testing the model on larger, diverse populations would help confirm whether the observed relationships between symptoms, risk factors, and behavioral response hold across different clinical settings. Also, collecting data from real-world patients could help refine variable weighting and validate predictive reliability. Additionally, exploring machine learning or nonlinear modeling approaches may improve sensitivity and capture more complex interactions among variables. Expanding the model to include additional behavioral and demographic factors, such as awareness, anxiety, or access to care, could further clarify what influences patient response times and enhance its effectiveness as a public health screening and educational tool.

■ Conclusion

This study demonstrated the potential of data-driven models to identify key symptoms and behavioral patterns associated with retinal detachment. Using a simulated dataset of patient-reported symptoms and medical histories, the model achieved high overall accuracy but limited discriminative ability, highlighting the influence of uneven class distribution. Curtain-like shadows, flashes, and floaters were identified as the strongest predictors of retinal detachment, consistent with established clinical findings, while myopia and trauma contributed less strongly. Behavioral analysis revealed that patients with higher predicted risk sought care more quickly, suggesting that symptom severity influences help-seeking behavior. Together, these findings emphasize the value of integrating patient-reported data into predictive tools for early detection and public health education. Although further validation with real-world clinical data is needed, this study provides a foundational step toward developing symptom-based screening systems that could improve timely diagnosis and reduce preventable vision loss.

■ Acknowledgments

I would like to express my deepest gratitude to Dr. Bahae Samhan for mentoring me throughout this invaluable research opportunity, providing guidance and feedback throughout.

DOI: 10.36838/IJHSR810.44

References

1. Cleveland Clinic. (2023). *Retinal Detachment: Symptoms and Causes*. https://my.clevelandclinic.org/health/diseases/10705-retinal-detachment
2. Serhan, H. A., Ashraf, S., Shaukat, A., Singh, A., Abdelrhem, H., Irfan, H., ... & Ahmed, A. (2025). Incidence and risk factors of rhegmatogenous retinal detachment following paediatric cataract surgery: A systematic review and meta-analysis. *Acta Ophthalmologica*.
3. Lin, J. B., Narayanan, R., Philippakis, E., Yonekawa, Y., & Apte, R. S. (2024). Retinal detachment. Nature Reviews Disease Primers, 10(1), 18.
4. Hollands, H.; Johnson, D.; Brox, A. C.; Almeida, D.; Simel, D. L.; Sharma, S. Acute-Onset Floaters and Flashes: Is This Patient at Risk for Retinal Detachment? *JAMA* 2009, *302* (20), 2243–2249. https://doi.org/10.1001/jama.2009.1714.
5. Gariano, R. F.; Kim, C.-H. Evaluation and Management of Suspected Retinal Detachment. *American Family Physician* 2004, *69* (7), 1691–1699.
6. Smt, C.; Santhamma, K. Subhadra Jalali MS. *Community Eye Health* 2003, *16* (46).
7. Ferrara, M.; Al-Zubaidy, M.; Song, A.; Avery, P.; Laidlaw, D. A.; Williamson, T. H.; Yorston, D.; Steel, D. H. W.; Babar, A.; Balaggan, K. S.; Casswell, A. G.; Chandra, A.; Charles, S.; Cochrane, T.; Crama, N.; Di Simplicio Cherubini, S.; Ellabban, A. A.; Ellis, J.; van Etten, P.; Figueroa, M. S. The Effect of Age on Phenotype of Primary Rhegmatogenous Retinal Detachment. *Eye* 2022, *37* (6), 1114–1122. https://doi.org/10.1038/s41433-022-02061-y.
8. Hayashi, K.; Sato, T.; Manabe, S.; Hirata, A. Sex-Related Differences in the Progression of Posterior Vitreous Detachment with Age. *Ophthalmology Retina* 2019, *3* (3), 237–243. https://doi.org/10.1016/j.oret.2018.10.017.
9. Enders, P.; Schick, T.; Schaub, F.; Kemper, C.; Fauser, S. RISK of MULTIPLE RECURRING RETINAL DETACHMENT after PRIMARY RHEGMATOGENOUS RETINAL DETACHMENT REPAIR. *Retina* 2017, *37* (5), 930–935. https://doi.org/10.1097/iae.0000000000001302.
10. Bita Momenaei; Wakabayashi, T.; Kazan, A. S.; Oh, G. J.; Kozarsky, S.; Vander, J. F.; Gupta, O. P.; Yoshihiro Yonekawa; Hsu, J. Incidence and Outcomes of Recurrent Retinal Detachment after Cataract Surgery in Eyes with Prior Retinal Detachment Repair. *Ophthalmology Retina* 2024, *8* (5), 447–455. https://doi.org/10.1016/j.oret.2023.11.005.
11. Ober, R. R.; Wilkinson, C. P.; Fiore, J. V.; Maggiano, J. M. Rhegmatogenous Retinal Detachment after Neodymium-YAG Laser Capsulotomy in Phakic and Pseudophakic Eyes. *American Journal of Ophthalmology* 1986, *101* (1), 81–89. https://doi.org/10.1016/0002-9394(86)90468-x.
12. Lakawicz, J. M.; Bottega, W. J.; Fine, H. F.; Prenner, J. L. On the Mechanics of Myopia and Its Influence on Retinal Detachment. *Biomechanics and modeling in mechanobiology* 2019, *19* (2), 603–620. https://doi.org/10.1007/s10237-019-01234-1.
13. Burton, T. C. The Influence of Refractive Error and Lattice Degeneration on the Incidence of Retinal Detachment. *Transactions of the American Ophthalmological Society* 2025, *87*, 143.
14. Nowomiejska, K.; Choragiewicz, T.; Borowicz, D.; Brzozowska, A.; Moneta-Wielgos, J.; Maciejewski, R.; Jünemann, A. G.; Rejdak, R. Surgical Management of Traumatic Retinal Detachment with Primary Vitrectomy in Adult Patients. *Journal of Ophthalmology* 2017, *2017*, 1–4. https://doi.org/10.1155/2017/5084319.
15. Amro Alhazimi; Khalaf, A.; Alharbi, M.; Ghada Alshehri; Aljefri, S.; Faisal Albalawi; Alqarawi, L.; Saeed Alshahrani; Sadique Zameer. The Prevalence of Tractional Retinal Detachment in Diabetic Retinopathy at King Fahad Medical City in Riyadh, Saudi Arabia. *Journal of the Egyptian Ophthalmological Society* 2025, *118* (2), 190–196. https://doi.org/10.4103/ejos.ejos_63_24.
16. Go, S. L. Genetic Risk of Rhegmatogenous Retinal Detachment. *Archives of Ophthalmology* 2005, *123* (9), 1237. https://doi.org/10.1001/archopht.123.9.1237.
17. Goezinne, F., van der Valk, R., & Hoyng, C. (2009). Patient ignorance is the main reason for treatment delay in retinal detachment. Eye, 23(2), 372–377.
18. Ge, J. Y., Teo, A. W. J., Andrew, S., Tsai, H., Tan, G. S. W., Lee, S. Y., ... & Chou, H. D. (2025).
Macular Buckle, Vitrectomy or combined approach for the management of Macular Hole Retinal Detachment: A Systematic Review and Network Meta-Analysis. Ophthalmology Retina.
19. Xiang, J., Fan, J., & Wang, J. (2023). Risk factors for proliferative vitreoretinopathy after retinal detachment surgery: a systematic review and meta-analysis. PLoS One, 18(10), e0292698.
20. Al-Dwairi, R., Saleh, O., Mohidat, H., Al Beiruti, S., Alshami, A., El Taani, L., ... & Aleshawi, A. (2025). Characteristics, risks, and prevention of rhegmatogenous retinal detachment in the contralateral eye. Journal of Clinical Medicine, 14(1), 222.
21. Hikichi, T.; Trempe, C. L. Relationship between Floaters, Light Flashes, or Both, and Complications of Posterior Vitreous Detachment. *American Journal of Ophthalmology* 1994, *117* (5), 593–598. https://doi.org/10.1016/s0002-9394(14)70065-0.
22. Rosenstock, I. M. (1974). The health belief model and preventive health behavior. Health Education Monographs, 2(4), 354–386

Author

Mahi Kumar has a deep passion for STEM, especially in the fields of Artificial Intelligence applied to Medical Sciences. She aims to pursue a future in AI, focusing on solving medical and world problems through innovative technologies.

IJHSR
ijhighschoolresearch.org
RESEARCH ARTICLE

Epidemiological Study on the Evaluation of Adolescent Height Development and Its Multidimensional Influencing Factors

Qiran Zhou[1], Jianfeng Long[2]

1) Department of International, Changsha No.1 High School, Changsha, Hunan, 410005, China; hhqq090103@gmail.com
2) Department of Nutrition, the Second Xiangya Hospital of Central South University, Changsha, Hunan, 410011, China

ABSTRACT: To examine height development traits and influencing factors in 15-18-year-olds, and provide empirical evidence for adolescent growth strategies. A cross-sectional study collected data on demographics, sleep, diet, exercise, and anxiety of 520 adolescents via Wenjuanxing. A multivariate linear regression model identified height-influencing factors. The results of this study suggest that participants' average height was 167.2 ± 6.8 cm, with males (172.6 ± 5.8 cm) significantly taller than females (161.8 ± 5.3 cm) (t=19.74, P < 0.001). Mean anxiety score was 35.6 ± 12.3, with 128 cases (24.6 %) scoring ≥ 40 (moderate-severe anxiety). Age, gender, daily sleep ≥ 8 h, weekly exercise ≥ 3 times, balanced diet, and anxiety score < 40 were independent height predictors (adjusted R^2=0.42, P < 0.001). Each extra year added 3.2 cm to average height (95%CI: 2.8-3.6); males were 10.8 cm taller than females (95%CI: 9.6-12.0); those with anxiety < 40 were 2.3 cm taller than those with anxiety≥ 40 (95%CI: 1.5-3.1). The result of this study indicates that adolescent height is affected by multiple factors. Better sleep, more exercise, improved diet, and reduced anxiety may promote height growth.

KEYWORDS: Biomedical and Health Sciences, Nutrition and Natural Products, Influencing Factors, Epidemiological Survey, Adolescent Height.

Introduction

Adolescence is a critical juncture in the context of height development. Growth throughout this period not only serves as an indicator of an individual's health but also has a significant bearing on the susceptibility to chronic diseases in adulthood and their social adaptability capabilities.[1] On a global perspective, adolescent height has demonstrated a persistent upward trajectory over time. Nevertheless, distinct regional disparities continue to be evident.

In China, the differential in height between urban and rural adolescents decreased from 3.2 cm in 2010 to 1.8 cm in 2020. Despite this, substantial individual variability in growth persists.[2]

Historically, research has often centered on the effects of individual factors, such as nutrition or exercise, on height. There has been a dearth of comprehensive investigations into the multidimensional interactions, encompassing the possible influence of mental health factors like anxiety.[3] Anxiety is a common mental health issue among adolescents. By exerting an effect on the hypothalamic-pituitary-adrenal axis, it can interfere with the secretion of growth hormone, potentially impeding the process of height development.[4] However, relatively few studies have integrated anxiety into the complex set of factors that impact adolescent height.

This study, by utilizing data sourced from 520 adolescents aged between 15 and 18 years, combines epidemiological methods with multi-factor statistical modeling techniques. It systematically delves into the independent and interactive effects of factors, including age, gender, sleep, diet, exercise, and anxiety, on height development. The research provides a scientific foundation for implementing targeted interventions that promote growth.

The key innovative features are as follows: (1) the inclusion of a combined "bedtime-sleep duration" measure to more precisely evaluate the influence of sleep on growth hormone secretion; (2) the establishment of a "diet pattern-exercise intensity" interaction term to analyze the synergistic relationships between behaviors; (3) the addition of an anxiety assessment to explore the connection between mental health and height; and (4) the reference to the "Standards for the Growth and Development of Chinese Children and Adolescents (2023 Edition)" to ensure the use of contemporary evaluation standards.[5]

Subjects and Methods

2.1. Study Subjects:

A multi-center survey was conducted through the Wenjuanxing platform from September to December 2023. Inclusion criteria include: (1) Aged 15-18 years; (2) No severe endocrine diseases, bone diseases, or chronic disease history; (3) Voluntarily participating and completing valid questionnaires. Exclusion criteria include: (1) The missing rate of questionnaire filling > 20%; (2) Abnormal height data (outside ± 3SD); (3) Incomplete anxiety assessment data.

Finally, 520 valid samples were included, including 327 males (62.9 %) and 193 females (37.1 %); 359 from urban areas (69.0 %) and 161 from rural areas (31.0 %).

Age distribution of the samples includes: 17 cases (3.3 %) aged 15, 23 cases (4.4 %) aged 16, 55 cases (10.6 %) aged 17, and 423 cases (81.3 %) aged 18. This study was approved by the Ethics Committee (Ethics No.: EC-2023-042), and all participants signed informed consent forms.

DOI: 10.36838/IJHSR810.50

2.2. Study Methods:

2.2.1. Questionnaire Design and Variable Definition:

Referring to the "Chinese Adolescent Health Behavior Monitoring Questionnaire" and international adolescent growth survey standards, a structured questionnaire was designed, including:

1. Demographic characteristics: Gender (male/female), age (years), region (urban/rural), parental height (cm);

2. Sleep indicators: Daily sleep duration (< 7 h/7-8 h/≥ 8 h), bedtime (< 23:00/≥ 23:00);

3. Dietary factors: Daily water intake (< 2000 ml/> 2000 ml), type of cooking oil (animal oil/vegetable oil/mixed), weekly frequency of milk/egg/fruit intake. The "balanced diet pattern" factor was extracted through principal component analysis (eigenvalue > 1.0, including the intake of whole grains, high-quality protein, vegetables, and fruits).

4. Exercise indicators: Weekly exercise frequency (almost no exercise/1-2 times/3-5 times/> 5 times), single exercise duration (< 30 min/30-60 min/> 60 min), main exercise type (brisk walking/jogging/swimming/ball games/stair climbing/ dance/ rope skipping/aerobics/strength training/tai chi/ others;

(5) Anxiety indicators: Adopting the Self-Rating Anxiety Scale (SAS), including 20 items (e.g., "I feel more nervous or anxious than usual", "I feel scared for no reason"). Each item is scored on a 4-point scale (1=rarely, 2=sometimes, 3=often, 4=almost always), with the total score ranging from 20 to 80. A total score of≥40 is defined as moderate to severe anxiety.

2.2.2. Height Measurement and Evaluation:

Height data were self-reported by participants and verified by comparing with parental height-based prediction (using the formula: male height = (father's height + mother's height + 13)/2 ± 5 cm; female height = (father's height + mother's height - 13)/2 ± 5 cm). Data outside the predicted range ±3 cm were reconfirmed with participants, and those still abnormal were excluded. Height was expressed as mean ± standard deviation (x±s).

2.2.3. Quality Control:

1. Questionnaire design: Before launching the formal survey, we ran a pre-survey with 30 adolescents to test the questionnaire's usability. We went through their feedback carefully—any items that were confusing or questions that lacked clarity were revised. This step made sure every part of the survey was easy to understand, so respondents wouldn't misinterpret questions when filling it out later.

2. Data collection: The survey was distributed online, and we marked core items (like age, height, and anxiety scores) as required. This meant respondents couldn't skip these key fields, which helped cut down on missing data. By doing this, we made sure we had complete information for the variables that mattered most to our analysis.

3. Data entry: We used Epidata 3.1 software for double data entry. Two researchers worked independently to input the same set of survey data. After both entries were done, we checked for consistency—if there were differences between the two versions (like a typo in a height value), we fixed them by cross-referencing with the original survey forms. This process kept the entered data accurate.

(4) 3SD (three standard deviations) method. Every outlier we found was checked against the original questionnaires. This lets us tell apart real data mistakes (like a wrong number entered) from valid extreme values. Erroneous data was either corrected or left out, depending on what the original records showed.

2.2.4. Statistical Analysis:

Data were analyzed using SPSS 26.0 software. Measurement data were expressed as x±s, and comparison between groups was conducted using a t-test or ANOVA; counting data were expressed as frequency (constituent ratio, %), and comparison between groups was conducted using a chi-square test. A Multivariate linear regression model was used to analyze the independent influencing factors of height, with height as the dependent variable and factors with P < 0.1 in univariate analysis as independent variables.

The test level was α=0.05, and all statistical tests were two-sided.

■ Results and Discussion

3.1. Results:

3.1.1. Basic Characteristics of Subjects:

A total of 520 adolescents aged 15-18 years were included, with 327 males (62.9 %) and 193 females (37.1 %); 359 from urban areas (69.0 %) and 161 from rural areas (31.0 %). In terms of age, 17 cases (3.3 %) were 15 years old, 23 cases (4.4 %) were 16 years old, 55 cases (10.6 %) were 17 years old, and 423 cases (81.3 %) were 18 years old (Table 1).

Table 1: Distribution of age, gender, and region of the subjects (n=520). Among the 520 participants, males and 18-year-olds were the most represented groups; additionally, the majority resided in urban regions.

Item	Group	n	Constituent ratio (%)
Gender	Male	327	62.9 %
	Female	193	37.1 %
Age	15 years old	17	3.3 %
	16 years old	23	4.4 %
	17 years old	55	10.6 %
	18 years old	423	81.3 %
Region	Urban	359	69.0 %
	Rural	161	31.0%

3.1.2. Distribution of Sleep, Diet, Exercise, and Anxiety:

1. Among the 520 subjects, 278 cases (53.5 %) had daily sleep duration ≥ 8 h, 165 cases (31.7 %) had 7-8 h, and 77 cases (14.8 %) had < 7 h; 58 cases (11.2 %) went to bed before 23:00, and 462 cases (88.8 %) went to bed at or after 23:00 (Table 2).

2. 34 cases (6.5 %) had daily water intake > 2000 ml; 114 cases (21.9 %) had a balanced diet pattern, and 406 cases (78.1 %) had an unbalanced diet pattern (Table 2).

(3) 145 cases (27.9 %) exercised ≥ 3 times a week (82 cases for 3-5 times and 63 cases for > 5 times); 246 cases (47.3 %) had a single exercise duration ≥ 30 min (157 cases for 30-60 min and 89 cases for > 60 min). The main exercise types were brisk walking (215 cases, 41.3 %), jogging (233 cases, 44.8 %), and stair climbing (187 cases, 36.0 %) (Table 2).

(4) The average anxiety score of the subjects was 35.6 ± 12.3. Specifically, 245 cases (47.1 %) had an anxiety score < 30

(mild anxiety), 147 cases (28.3 %) had a score of 30-39 (mild to moderate anxiety), and 128 cases (24.6 %) had a score ≥ 40 (moderate to severe anxiety) (Table 3).

Table 2: Distribution of sleep, diet, and exercise of the subjects (n=520). Most participants reported ≥8 hours of daily sleep, and a bedtime tended to be late; meanwhile, most participants had insufficient daily water intake and exercise duration, and jogging and brisk walking were the most common exercise types.

Indicator	Category	n	Constituent ratio (%)
Daily sleep duration	< 7 h	77	14.8 %
	7-8 h	165	31.7 %
	≥ 8 h	278	53.5 %
Bedtime	< 23:00	58	11.2 %
	≥ 23:00	462	88.8 %
Daily water intake	< 2000 ml	486	93.5 %
	> 2000 ml	34	6.5 %
Weekly exercise frequency	Almost no exercise	99	19.0 %
	1-2 times	272	52.3 %
	3-5 times	82	15.8 %
	> 5 times	63	12.1 %
Single exercise duration	< 30 min	428	82.3 %
	30-60 min	157	30.2 %
	> 60 min	89	17.1 %
Main exercise type	Brisk walking	215	41.3 %
	Jogging	233	44.8 %
	Swimming	18	3.5 %
	Ball games	152	29.2 %
	Stair climbing	187	36.0 %
	Dance	24	4.6 %
	Rope skipping	27	5.2 %
	Aerobics	65	12.5 %
	Strength training	106	20.4 %
	Tai chi	0	0.0%
	Others	197	37.9 %

Table 3: Distribution of anxiety score of the subjects (n=520). Among the 520 participants, nearly half reported mild anxiety, while over a quarter exhibited moderate to severe anxiety.

Anxiety score range	n	Constituent ratio (%)
< 30 (mild anxiety)	245	47.1 %
30-39 (mild to moderate anxiety)	147	28.3 %
≥ 40 (moderate to severe anxiety)	128	24.6 %

3.1.3. Univariate Analysis of Height Influencing Factors:

The average height of all subjects was 167.2 ± 6.8 cm. Univariate analysis showed significant differences in height among different genders, ages, daily sleep durations, weekly exercise frequencies, diet patterns, and anxiety score groups (all P < 0.001) (Table 4).

1. The average height of males (172.6 ± 5.8 cm) was significantly higher than that of females (161.8 ± 5.3 cm) (t=19.74, P < 0.001).

2. Height increased with age, with the average height of 18-year-olds (168.1 ± 6.9 cm) being higher than that of 15-year-olds (162.3 ± 6.1 cm) (F=12.87, P < 0.001).

3. Adolescents with daily sleep duration ≥ 8 h had an average height of 169.1 ± 6.3 cm, which was higher than those with 7-8 h (166.8 ± 6.5 cm) and < 7 h (164.2 ± 7.2 cm) (F=8.53, P < 0.001).

(4) Those who exercised ≥ 3 times a week had an average height of 169.8 ± 6.0 cm (combining 3-5 times and >5 times groups), higher than those who exercised 1-2 times (166.7 ± 6.8 cm) and almost no exercise (163.5 ± 7.5 cm) (F=10.21, P < 0.001).

(5) The average height of adolescents with a balanced diet (169.8 ± 6.2 cm) was higher than that of those with an unbalanced diet (165.7 ± 7.0 cm) (t=9.15, P < 0.001).

(6) Adolescents with anxiety score < 40 had an average height of 168.5 ± 6.5 cm, which was higher than those with score ≥ 40 (166.2 ± 7.1 cm) (t=6.38, P < 0.001).

Table 4: Height of subjects with different characteristics (cm, x±s). Males were significantly taller than females; height also increased with older age, longer daily sleep duration, more frequent exercise, lower anxiety scores, and balanced diet patterns.

Factor	Category	n	Height	t/F value	P value
Gender	Male	327	172.6 ± 5.8	19.74	< 0.001
	Female	193	161.8 ± 5.3		
Age	15 years old	17	162.3 ± 6.1	12.87	< 0.001
	16 years old	23	164.5 ± 5.8		
	17 years old	55	167.8 ± 6.2		
	18 years old	423	168.1 ± 6.9		
Daily sleep duration	< 7 h	77	164.2 ± 7.2	8.53	< 0.001
	7-8 h	165	166.8 ± 6.5		
	≥ 8 h	278	169.1 ± 6.3		
Weekly exercise frequency	Almost no exercise	99	163.5 ± 7.5	10.21	< 0.001
	1-2 times	272	166.7 ± 6.8		
	3-5 times	82	169.5 ± 6.1		
	> 5 times	63	170.2 ± 5.9		
Anxiety score	< 40	392	168.5 ± 6.5	6.38	< 0.001
	≥ 40	128	166.2 ± 7.1		
Diet pattern	Balanced	114	169.8 ± 6.2	9.15	< 0.001
	Unbalanced	406	165.7 ± 7.0		

3.1.4. Multivariate Linear Regression Analysis of Height Influencing Factors:

Taking height as the dependent variable and factors with P < 0.1 in univariate analysis as independent variables, multivariate linear regression analysis showed that age, gender, daily sleep duration ≥ 8 h, weekly exercise ≥ 3 times, balanced diet pattern, and anxiety score < 40 were independent influencing factors of adolescent height (adjusted R^2=0.42, P < 0.001) (Table 5).

(1) For each additional year of age, the average height increased by 3.2 cm (95% CI: 2.8-3.6, P < 0.001).

(2) Males were 10.8 cm taller than females on average (95% CI: 9.6-12.0, P < 0.001).

(3) Compared with adolescents with daily sleep duration <8 h, those with daily sleep duration of 8 h were 2.1 cm taller on average (95% CI: 1.2-3.0, P < 0.001).

(4) Compared with those who exercised < 3 times a week, those who exercised ≥3 times were 1.8 cm taller on average (95% CI: 0.78-2.82, P=0.001).

(5) Adolescents with a balanced diet were 2.5 cm taller than those with an unbalanced diet on average (95% CI: 1.5-3.5, P < 0.001).

(6) Compared with adolescents with an anxiety score ≥ 40, those with a score < 40 were 2.3 cm taller on average (95% CI: 1.5-3.1, P < 0.001).

Table 5: Multivariate linear regression analysis of influencing factors of adolescent height. Gender and age were the strongest positive predictors of height; longer sleep, more exercise, a balanced diet, and lower anxiety were also significantly associated with greater height, collectively explaining 42% of height variance.

Factor	β	SE	t value	P value	95%CI
Age	3.200	0.210	15.238	< 0.001	(2.800, 3.600)
Gender (Male=1, Female=0)	10.800	0.580	18.621	< 0.001	(9.600, 12.000)
Daily sleep duration (≥ 8 h=1, others=0)	2.100	0.450	4.667	< 0.001	(1.200, 3.000)
Weekly exercise frequency (≥ 3 times=1, others=0)	1.800	0.520	3.462	0.001	(0.780, 2.820)
Diet pattern (Balanced=1, Unbalanced=0)	2.500	0.510	4.902	< 0.001	(1.500, 3.500)
Anxiety score (< 40=1, ≥ 40=0)	2.300	0.390	5.897	< 0.001	(1.500, 3.100)
Adjusted R^2	0.42			< 0.001	

DOI: 10.36838/IJHSR810.50

3.2. Discussion:

This research comprehensively delved into the various influencing factors of height development among 520 adolescents aged 15-18 years. It was found that age, gender, sleep, exercise, diet, and anxiety independently shape adolescent height. This finding is in line with most previous studies and also enhances the understanding of the potential link between anxiety and height.

3.2.1. Effects of Demographic Factors on Height:

Gender and age are intrinsic, time-dependent factors affecting adolescent height. In this study, males were significantly taller than females, and height increased as age advanced, adhering to the principles of adolescent growth and development.[1] Females generally enter puberty earlier, around 10-12 years old, compared to males at 12-14 years old. As a result, females reach their growth peak earlier.

In contrast, males have a longer growth period and a higher growth rate during the peak, resulting in an eventual height advantage.[6] Cross-sectional data from national surveys further support this gender - related difference in growth timing and duration. These data indicate that over the past decade, the average height gap between 15-18-year-old males and females in China has remained relatively stable at approximately 10-12 cm.[7] The age distribution in this study reveals that 81.3 % of the subjects are 18 years old, and their height is still greater than that of younger age groups. This suggests that some adolescents may still have a certain amount of growth potential at 18 years old.

This is consistent with the "Standards for the Growth and Development of Chinese Children and Adolescents (2023 Edition)," which extends the growth-cessation age of adolescents to 18-19 years old.[8] It also corresponds to the findings of a 10-year follow-up study on Chinese adolescents, where 15 % of males and 8 % of females were reported to still experience a height increase of ≥ 2 cm after the age of 17.[9]

3.2.2. Effects of Lifestyle Factors on Height:

3.2.2.1. Sleep:

This study demonstrated that a daily sleep duration of at least 8 hours is conducive to height growth, in accordance with the growth hormone secretion mechanism. Growth hormone is mainly secreted during deep sleep at night, with the secretion peak emerging 1-2 hours after falling asleep.[10] Although 53.5 % of the subjects in this study have a sleep duration of ≥ 8 h, 88.8 % go to bed at 23:00 or later. A late bedtime might cause adolescents to miss the growth hormone secretion peak (22:00-2:00), leading to insufficient effective sleep time for growth.

This could explain why some adolescents with adequate total sleep duration still have relatively short heights. A study on Chinese urban adolescents aged 14-17 years further validated this: adolescents who went to bed before 23:00 and slept ≥ 8 h had an average height 2.4 cm higher than those who went to bed after 23:00 with the same sleep duration.[11] This highlights that "sleep quality," which includes bedtime and sleep continuity, is more important than "sleep duration" alone in promoting height, consistent with the view in previous studies that "bedtime-sleep duration" combined indicators should be used to evaluate sleep.[3] Additionally, sleep fragmentation, often associated with a delayed bedtime, can further reduce the deep-sleep duration, thereby inhibiting growth hormone secretion. This is a factor not measured in this study but worthy of consideration in future research.[12]

3.2.2.2. Exercise and Diet:

Exercising at least three times a week and maintaining a balanced diet are also protective factors for height. Exercise can stimulate bone growth plates, enhance bone metabolism and blood circulation, and further promote height growth.[13] A randomized controlled trial involving 300 adolescents showed that 6 months of regular medium-intensity exercise (3 times/week, 45 min/session) increased the average height of participants by 1.2 cm compared to the control group and also improved bone mineral density.[14] The main exercise types among the subjects are brisk walking, jogging, and stair climbing, which are low-to-medium intensity aerobic exercises. These exercises are easy to sustain and have a beneficial stimulating effect on bones, making them suitable for adolescents' daily exercise routine.

A balanced diet, composed of whole grains, high-quality protein, vegetables, and fruits, can supply sufficient nutrients such as protein, calcium, and vitamins for bone growth.[15] For instance, dietary protein intake is positively correlated with the synthesis of insulin-like growth factor-1 (IGF-1), a key hormone that promotes chondrocyte proliferation in growth plates.[16] However, only 6.5 % of the subjects have a daily water intake of over 2000 ml, and 78.1% have an unbalanced diet, indicating that adolescents still face issues such as insufficient water intake and an unbalanced diet structure. A national survey on Chinese adolescents' dietary behavior found that the insufficient intake rate of dairy products (a major source of calcium) and vegetables among 15-18-year-olds is 68.2% and 57.9 %, respectively. This situation requires improvement through school and family health education.[17] Moreover, the positive impact of a daily water intake of > 2000 ml may be related to the role of hydration in facilitating the excretion of metabolic waste and maintaining the stability of the cartilage matrix.[18] Adolescents with an exercise frequency of ≥ 3 times/week and a single-exercise duration of 30-60 minutes had the optimal height, consistent with the mechanism that moderate-intensity exercise stimulates periosteal stress and activates osteoblasts.[19] The advantages of ball games and jogging stem from their ability to longitudinally stretch bones, which can delay epiphyseal closure.[20] However, the height of the group with an exercise duration of > 60 minutes slightly decreased, suggesting that excessive exercise may inhibit growth hormone secretion through increased cortisol, emphasizing the importance of "moderate exercise".[21] The synergistic effect of "balanced diet × exercise frequency" indicates that nutrition is the basis for exercise to promote growth.

When protein intake is insufficient, exercise may lead to muscle breakdown rather than promoting bone growth.[22] This provides ideas for intervention: Urban adolescents can diver-

sify their exercise. In contrast, rural adolescents need to focus on increasing protein and dairy product intake to narrow the regional gap (currently 168.5 cm vs 164.3 cm).

3.2.3. Effect of Anxiety on Height:

A novel finding of this study is that anxiety is an independent influencing factor of adolescent height. Adolescents with an anxiety score of < 40 are 2.3 cm taller than those with a score of ≥ 40. The possible mechanism is that long-term anxiety activates the hypothalamic-pituitary-adrenal (HPA) axis, resulting in increased cortisol secretion. Excessive cortisol can inhibit the secretion of growth hormone-releasing hormone (GHRH) from the hypothalamus, reduce the secretion of growth hormone from the pituitary gland, and subsequently disrupt bone growth and development.[5] A study on prepubertal rats confirmed that chronic stress-induced high cortisol levels can reduce the number of chondrocytes in the epiphyseal growth plate and delay bone maturation.[23] In this study, 24.6% of adolescents have moderate to severe anxiety, which is higher than the 15%-20% anxiety incidence in Chinese adolescents reported in previous studies.[24] This may be associated with the increased academic pressure and social adaptation challenges that adolescents have faced in recent years.

A cross-sectional study involving 5000 Chinese high school students found that academic pressure ($\beta = 0.32$, $P < 0.001$) and parent-child conflict ($\beta = 0.28$, $P < 0.001$) are the main factors contributing to adolescent anxiety.[25] This implies that while paying attention to the physical growth of adolescents, we should also place more emphasis on their mental health and reduce the negative impact of anxiety on height.

3.2.4. Limitations of the Study:

This study has several limitations. Firstly, as a cross-sectional study, it can only confirm the association between factors and height, but cannot establish the causal relationship. A longitudinal study design, which follows adolescents over time, would be more appropriate for determining causality.[26] Secondly, the sample is drawn mainly from urban and rural areas in central China, and its representativeness may be limited. Because China's different regions differ significantly in many factors, such as economic development, dietary patterns, and lifestyles, which are closely related to adolescent growth and development.[27]

Since the sample primarily comes from the central region, this study may overestimate or underestimate the strength of the association between intervenable factors and height. This will affect its generalizability to high school student populations in other countries and also impact its reference value for formulating height intervention strategies for global high school students. Future research should expand the sample size, adopt stratified sampling methods, include participants from China's eastern, western, and northeastern regions, and balance urban and rural high schools to enhance regional representativeness.[28]

Third, anxiety assessment relies on self-rating scales, which in high school studies are prone to introducing subjective bias, recall bias, and social expectation bias.[29] This is because adolescents often struggle to accurately describe their emotional experiences, and the emotional fluctuations during survey completion may influence their responses. Such subjectivity can lead to misjudgment of anxiety levels, thereby diminishing the actual impact of anxiety on adolescent development. To reduce these biases in future research, anxiety assessment could be improved by combining self-rating scales with brief feedback from teachers or parents.[30]

Future studies should expand the sample to include eastern, western, and northeastern China to enhance regional representativeness. Finally, the study does not incorporate genetic factors (such as parental height) into the regression model. Although parental height is an important factor influencing children's height,[31] this study focuses on modifiable factors (sleep, exercise, diet, anxiety) to provide targeted intervention suggestions.

Thus, genetic factors are not included, which may lead to an underestimation of the genetic contribution.[32] Dietary data rely on self-reports, which are subject to recall bias. In the future, combining dietary diaries with biomarkers (such as serum 25-hydroxyvitamin D) can improve accuracy.[33]

■ Conclusion

A combination of multiple factors, including age, gender, sleep, exercise, diet, and anxiety, influences adolescent height development. Among these, age and gender are non-modifiable, while sleep, exercise, diet, and anxiety can be adjusted. To promote the healthy height growth of adolescents, the following targeted measures can be taken. Firstly, optimizing sleep habits is of great importance.

Since growth hormone is mainly secreted during the deep-sleep stage, especially from 22:00 to 2:00, adolescents should be guided to go to bed before 23:00 and ensure their daily sleep duration is at least 8 hours. This enables them to enter the deep-sleep stage during the growth hormone secretion peak, thereby improving sleep quality. Secondly, increasing exercise frequency can effectively stimulate bone growth. Adolescents are encouraged to engage in medium-intensity aerobic exercises like brisk walking or jogging at least 3 times a week, with each exercise lasting 30 minutes or more.

Such regular physical activities contribute to better bone development. In addition, improving the diet structure is also essential. A balanced diet should be promoted, including more whole grains, high-quality protein sources like milk and eggs, vegetables, and fruits. Moreover, ensuring that the daily water intake exceeds 2000 mL can supply sufficient nutrients for the growth and development of adolescents. Finally, alleviating anxiety symptoms is of significant importance.

Schools and families should strengthen mental health education and establish a favorable psychological support system for adolescents. For those with moderate to severe anxiety, psychological counseling services should be provided promptly. This measure can effectively reduce the negative impact of anxiety on height. Overall, by comprehensively and continuously implementing these measures, we can better promote the height development of adolescents and help them grow up healthy.

DOI: 10.36838/IJHSR810.50

In the future, longitudinal studies can be conducted further to confirm the causal relationship between modifiable factors and height, and expand the sample size and scope to improve the representativeness of the results, thus providing more scientific and comprehensive evidence for formulating national adolescent growth-promotion strategies.

Acknowledgments

The authors sincerely express their gratitude to all individuals and institutions that contributed to this study. Special thanks are given to our supervisor for the expert guidance throughout the research process. We also thank the 520 adolescents who participated, their parents and guardians, and the staff at all participating institutions for their support in data collection. The Ethics Committee granted ethical approval, and informed consent was obtained from all participants. Finally, we appreciate the unwavering support from our families and friends.

References

1. Ji CY, Li Y. The necessity for strengthening adolescent health practice: a point of view from the secular growth changes of Chinese adolescents[J]. Chin J Reprod Health, 2003, 14(5):271-275.
2. National Health Commission of the People's Republic of China. Report on Chinese Children and Adolescents' Growth and Development Status (2023) [M]. Beijing: People's Medical Publishing House, 2023.
3. Wen B, Dong YH, Yang ZG, Wang C, *et al.* Association between sleeping time and age at spermarche among Chinese boys aged 11-18 years[J]. Chin J Sch Health, 2018, 39(8):1140-1143.
4. Miller KK, Downey LS, Amory JK, Amrhein JA, *et al.* Stress-induced cortisol elevation and growth hormone secretion in prepubertal children[J]. J Clin Endocrinol Metab, 2007, 92(10):3868-3873.
5. National Health Commission of the People's Republic of China. Standards for the Growth and Development of Chinese Children and Adolescents (2023 Edition) [S]. Beijing: Standards Press of China, 2023.
6. Zhang C, Tang YY, Yan YM, Ma Z. Pubertal development status of 4030 adolescents in Shandong Province[J]. Chin J Sch Doct, 2013, 27(5):335-337.
7. Wang Y, Zhang J, Liu J, Zhu D, *et al.* Secular trends in height and weight of Chinese adolescents aged 15-18 years, 2010-2020[J]. Chin J Epidemiol, 2022, 43(7):1123-1129.
8. Chinese Center for Disease Control and Prevention. Chinese Adolescent Health Behavior Monitoring Questionnaire (2022 Version) [Z]. Beijing: Chinese Center for Disease Control and Prevention, 2022.
9. Li M, Chen J, Zheng H, Wang S, *et al.* Longitudinal study on height growth of Chinese adolescents aged 15-19 years[J]. Chin J Child Health Care, 2021, 29(5):521-524.
10. Carlsson LMS, Rosberg S, Vitangcol RV, Albertsson-Wikland K, *et al.* Analysis of 24-hour plasma profiles of growth hormone (GH)-binding protein, GH/GH-binding protein-complex, and GH in healthy children[J]. J Clin Endocrinol Metab, 1993, 77(2):356-361.
11. Zhao L, Wang X, Li J, Chen Y, *et al.* Association between bedtime, sleep duration and height among urban adolescents aged 14-17 years in China[J]. Sleep Med, 2020, 76:158-163.
12. Jiang Y, Zhang H, Yang Y, Li X, *et al.* Sleep fragmentation and growth hormone secretion in adolescents: a cross-sectional study[J]. J Sleep Res, 2019, 28(3):e12815.
13. Xi HJ, Li WH, Wen YF, Zhang XC, *et al.* Analysis of environmental factors influencing on growth and development of plateau children and adolescents in China[J]. AAS, 2018, 49(6):770-781.
14. Chen L, Liu Y, Zhang M, Wang J, *et al.* Effect of regular moderate-intensity exercise on height and bone mineral density in adolescents: a randomized controlled trial[J]. J Sports Med Phys Fitness, 2023, 63(4):289-295.
15. Cheng G, Buyken AE, Shi L, Karaolis-Danckert N, *et al.* Beyond overweight: nutrition as an important lifestyle factor influencing timing of puberty[J]. Nutr Rev, 2012, 70(3):133-152.
16. Zhu H, Wang L, Sun X, Wu Y, *et al.* Dietary protein intake and insulin-like growth factor-1 levels in Chinese adolescents[J]. Nutrients, 2022, 14(12):2489.
17. Chinese Nutrition Society. Report on Chinese Adolescent Dietary Guidelines Compliance Status (2022) [M]. Beijing: Science Press, 2022.
18. Armstrong LE, Johnson EC. Hydration and physical performance[J]. Current Sports Medicine Reports, 2021, 20(6): 301-306.
19. Robling AG, Turner CH. Mechanical signaling for bone modeling and remodeling[J]. Critical Reviews in Eukaryotic Gene Expression, 2020, 30(1): 33-45.
20. Cheng S, Zhang X, Ma J. Effects of different types of exercise on bone mineral density in adolescents: a systematic review and meta-analysis[J]. Journal of Bone and Mineral Metabolism, 2022, 40(2): 209-220.
21. O'Connor DP, Marsland AL, Dimsdale JE. Exercise and the neurobiology of stress[J]. Current Diabetes Reports, 2023, 23(2): 89-98.
22. Meyer T, Puhlmann M, Bosy-Westphal A. Interaction of nutrition and physical activity on body composition in adolescents[J]. Current Diabetes Reports, 2022, 22(5): 327-336.
23. Wang Z, Li Y, Zhang Q, Chen J, *et al.* Chronic stress-induced cortisol elevation impairs epiphyseal growth plate development in prepubertal rats[J]. Horm Metab Res, 2020, 52(10):721-728.
24. Liu X, Zhang Y, Wang Y, Feng Z, *et al.* Prevalence of anxiety and depression among Chinese adolescents: a meta-analysis[J]. BMC Psychiatry, 2020, 20(1):1-11.
25. Huang X, Zhao J, Li D, Wang J, *et al.* Factors associated with anxiety among Chinese high school students: a cross-sectional study of 5000 participants[J]. BMC Public Health, 2021, 21(1):1-9.
26. WHO. Guidelines on Conducting Longitudinal Studies for Adolescent Health (2020) [R]. Geneva: World Health Organization, 2020.
27. Wang Y, Zhang L, Li M, *et al.* Regional disparities in economic development, dietary patterns, and lifestyles and their impact on adolescent growth in China[J]. Chinese Journal of School Health, 2020, 41(5): 645-649.
28. Liu X, Chen J, Wang Q, *et al.* Sampling representativeness and its influence on the association between intervenable factors and height in Chinese adolescents[J]. Journal of Adolescent Health, 2019, 65(3): 345-351.
29. Brown R, Smith J, Johnson L. Subjective and recall biases in self-rating anxiety scales among high school students[J]. Journal of Youth and Adolescence, 2022, 51(4): 789-805.
30. Taylor S, Anderson B, Thomas J. Combining self-rating scales with teacher and parent feedback for accurate anxiety assessment in adolescents[J]. School Psychology Quarterly, 2019, 34(1): 45-58.
31. Zhang C, Li Q, Hu MY, Wang H, *et al.* The effects of parent hereditary factors on the stature of children[J]. China Foreign Med Treat, 2010, 29(18):20-21.
32. Yang J, Loos RJ, Visscher PM. Genetic architecture of human height[J]. Current Diabetes Reports, 2020, 20(1): 1-9.

33. Cashman KD, Kiely M, Seamans KM. Vitamin D and bone health in children and adolescents: an update[J]. Current Osteoporosis Reports, 2021, 19(2): 121-132.

Authors

Zhou Qiran: A 12th-grader at Changsha No.1 Middle School. Passionate about biology, public health, and also enjoys music, basketball, and reading. Conducted research at the University of Pennsylvania and Second Xiangya Hospital. “National Bronze” in 2025 USA-China BioOlympiad; “National Finalist” in HOSA 2024. Desire to study biomedicine or public health.

DOI: 10.36838/IJHSR810.50

IJHSR
ijhighschoolresearch.org
REVIEW ARTICLE

Finger Injuries among Adolescent Climbers: Causes, Prevention, and Rehabilitation

Rohan Tare

St. Mark's School of Texas, 10600 Preston Road, Dallas, Texas, 75230, USA; rohantare126@gmail.com
Mentor: Ioannis Delis

ABSTRACT: Rock climbing's increase in popularity brings more intense training methods, leading to more instances of finger injuries. Adolescents in particular are prone to finger injuries, as physiological changes during puberty cause the fingers to be less resistant to the biomechanics involved in climbing. To ensure a balanced risk-reward ratio, understanding and assessing the cause, prevention, and rehabilitation of any kind of injury is of the utmost importance. This review paper covers adolescent hand anatomy to determine what makes it more susceptible to certain injuries. Finger Flexor Pulley Injuries (FFPIs) and Epiphyseal Growth Plate Injuries (EPGIs) are common among adolescents, and a proper recovery plan is necessary to prevent an acute injury from developing into a chronic condition, such as osteoarthritis. It is proposed that adolescents are more prone to injuries because of the body's priority on growth rather than reinforcement. After an injury, the initial diagnosis is the most important part of the recovery process.

KEYWORDS: Biomedical and Health Sciences, Pathophysiology, Pulley, Injury, Growth Plate, Fracture, Osteoarthritis.

Introduction

Rock climbing as a sport is increasing in popularity, and along with it comes more intense training methods. As a result, injuries are appearing more often as the competitive setting sees more serious climbers. In a 2000 study, a total of 126 injuries were examined: 63% were located in the hand, and 37% were located elsewhere in the upper body.[1] These injuries are typically a result of the intense forces applied to the fingers, most notably in the "half crimp" and "full crimp" hand positions. This technique forces the proximal interphalangeal joint (PIP) to be flexed at 90 degrees and hyperextends the distal interphalangeal joint (DIP). These practices can cause gradual strain, breaks, or ruptures to parts of the hand, such as the epiphyseal growth plate or pulley system.[2]

The issue persists when considering the population of youth climbers as well. Many teenage climbers undergo the same intensive training as professionals, and the injuries they sustain as a result can cause lifelong issues.[3] A handful of climbers experience early chronic developments in their career with conditions such as osteoarthritis making themselves present, and others go a long time in their career without experiencing any physiological change.[4] This presents us with the question of what variables are in play that allow an otherwise acute injury to an adolescent to become chronic. It is hard to know for certain if a permanent pathological change is a result of the injury itself or failure to nurse the injury back to health efficiently.[5] In the case of the latter, it is vital that both athletes and doctors are aware of what the proper steps should be in recovery to maintain a long-lasting climbing career.

In this paper, I will examine the physiology of an adolescent rock climber's hand as it experiences growth to determine what factors a) make it more susceptible to injury, and b) contribute to an injury becoming chronic vs staying acute. I will analyze what rehabilitation processes have been proven to be most effective in ensuring full and stable recovery.

Review Methodology

The articles included in this review article were sourced from PubMed by searching keywords listed above. Articles with relevance to growth plate injuries, pulley injuries, and osteoarthritis were closely examined. If the author decided an article was especially useful, more articles from the same author or authors were prioritized. The date of publication was examined on all articles for the author to compare how research in adolescent hand injuries has evolved and what questions remain unanswered.

Hand Anatomy

Included in the human hand is a finger flexor pulley system (FFPS), which consists of synovial and retinacular tissue, known as pulleys. The combination of both these tissues allows for fluid movement and flexion of the fingers within the tendon sheath, as well as securing tendons in place. Within each finger (excluding the thumb), there are 5 annular pulleys labeled A1-A5 and 3 cruciate pulleys labeled C1-C3. Together, the pulley system forms a lubricated tunnel that contains the flexor digitorum profundus (FDP) and flexor digitorum superficialis (FDS), keeping them close to the bone. (See Figure 1) The A2 and A4 pulleys attach directly to bone, while the A1, A3, and A5 pulleys attach to the volar plate.[2] The volar plate, which is found on the palmar side of the hand, works to prevent hyperextension and connects the proximal phalanx to the middle phalanx.

In addition to the FFPS, epiphyseal growth plates are located at the bases of interphalangeal joints. These growth plates

DOI: 10.36838/IJHSR810.57

are made up of chondrocytes, cells that secrete proteins that collectively form the extracellular matrix. Specifically, chondrocytes in fingers' growth plates make up hyaline cartilage, a type of cartilage that ossifies when fully mature, producing new bone. These cells will undergo apoptosis, making room for new chondrocytes to continue bone growth.[3] Within both males and females, the hormone estradiol also contributes to slowing down bone growth and allowing the growth plates to fuse. During periods of rapid growth, estradiol levels are low, which allows for stimulation of bone growth. Once estradiol levels pick up, bone growth is inhibited, and the growth plates begin to close and eventually fuse.[6] Considering females have more estrogen, their growth plates finish growing and fuse earlier than those of males. This may lead to male climbers experiencing a higher rate of injury during adolescence in comparison to females.

A study done on the German Junior National Team and additional recreational climbers revealed that the hands of climbers undergo cortical hypertrophy over time.[5] To bear the intense forces experienced during climbing, many climbers' fingers experience thickening of the cortical bone, which makes up the outer layer of phalanges. This change is not rapid; hypertrophy occurs slowly over the course of a climber's career, as proven in a study of male elite climbers after a 10-year follow-up.[7] Although this study had a primary focus on adults, it was observed that adolescents experience the same cortical hypertrophy but at a slower rate. These changes to the fingers are adaptive rather than pathologic.

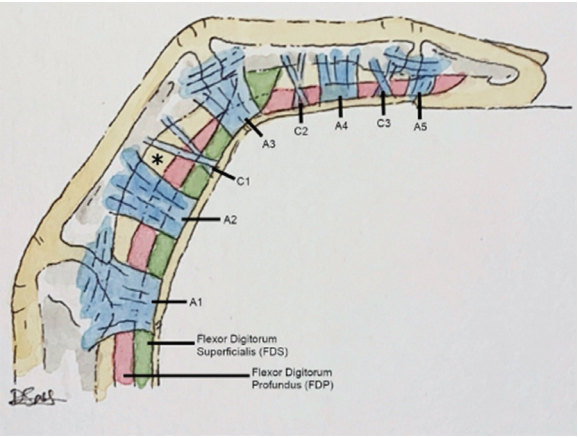

Figure 1: The Finger Flexor Pulley System is made up of five annular pulleys labeled as A1-A5 and three cruciate pulleys labeled as C1-C3. The FDS and FDP flexor tendons are contained within the lubricated tendon sheath.[2]

Pathological Changes

Injuries vary from being acquired from an acute onset event or over a period of time in which repetitive microtrauma has occurred. The most common site of acute injuries is the FFPS. They are the most common injuries in rock climbing, as proved by studies done in the periods 2017-2018, 2009-2012, and 1998-2001. In each study, the percentages of pulley injuries among the climbers studied were 31.1%, 29.5%, and 49.4%, respectively, among the full group.[8] As mentioned above, "crimping" is a hand position that climbers commonly use to pull themselves from small ledges. To assist the FDP and FDS tendons in generating the force possible to make this movement possible, the FFPS works to keep these tendons close to the bone to generate torque in a similar way as drawing a bowstring would work.[9] When too much force is applied for the pulleys to handle (e.g, the climber "pulls too hard"), this can cause a partial tear, full tear, or full rupture of the pulley.

These acute events can be identified by a pop or snapping sound in any of the fingers, along with a tearing sensation after attempting to bear a load with it. As a result, the FDP and FDS tendons are contained to the bone by one less anchor point, a condition known as "bowstringing". (See Figure 2) Although inconclusive, an accepted tendon-to-bone distance is around 2 mm, with anything greater showing the possibility of pulley injury.[2] Of the 5 annular pulleys, the A2 is the thickest and strongest, with an average length of 16.3mm. It attaches directly to the bone at the proximal phalanx and bears the most load, but this consequently means it also has the greatest possibility for injury when bearing load.[10]

A grading system proposed by Volker Schoffl et al. exists that classifies the injury with a grade from 1-4: a Grade 1 injury is a simple strain with a tendon-bone length of <2 mm without any real bowstringing; a Grade 2 injury is either a full rupture of the A4 or a partial rupture of the A2 or A3; a Grade 3 is a full rupture of the A2 or A3; and a Grade 4 consists of many ruptures throughout the entire FFPS. Both MRI and Ultrasound are viable radiographs in accurately detecting the injury.[2]

Comparing adolescent climbers to adult climbers, FFPS injuries don't present many differences. In both age ranges, they occur as a result of intense, acute events, and the degree to which the injury presents itself is more correlated with the intensity of the activity in which the pulley was injured rather than the physiological anatomy of the aging hand.

Although acute FFPS injuries are the most common type of injury in the rock-climbing community as a whole, epiphyseal growth plate injuries (EPGIs) are incredibly common among adolescent athletes.[6]

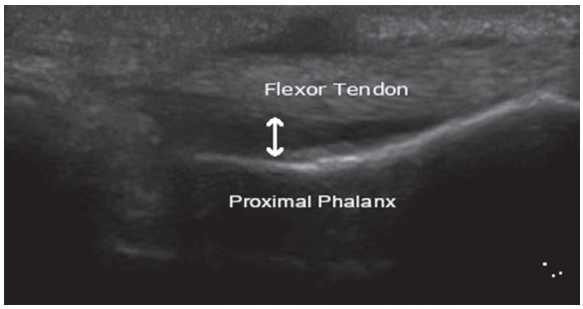

Figure 2: Bowstringing is depicted by the flexor tendon being unnaturally far from the bone. A greater distance between the flexor tendon and the proximal phalanx results in a loss of mechanical torque.[2]

Unlike FFPS injuries, EGPIs are typically a result of repetitive use rather than an acute event. As noted above, epiphyseal growth plates are made up of chondrocytes that secrete cartilage matrix. This phase of bone formation is highly important to hand development in adolescents. The problem arises when adolescents experience repetitive mechanical stress as a result of intense training. Repetitive mechanical stress is thought to

disrupt blood supply to the physis of the hand, and therefore hypertrophied chondrocytes struggle to mineralize cartilage.[3] Based on these findings, it is proposed that growth plates become more fragile and prone to fracture, explaining why adolescents are more prone to these kinds of injuries.

Growth plate fractures can be classified using the Salter-Harris classification system. A Salter-Harris fracture refers to a fracture in the growth plate that can be classified as one of 5 types, with types 1 and 3 being the most common among rock climbers.[6-11] A type 1 is when the break occurs straight through the growth plate at the proximal phalanx, and a type 3 is when the break extends through the growth plate to the end of the bone. (See Figure 3) Both these injuries can cause a great amount of stiffness, swelling, restricted range of motion, and pain in the target area.[11]

Furthermore, a diagnostic study done with 57 male climbers and 38 female climbers presented 137 injuries across the body. Of the entire catalog, 45.3% of the injuries were growth plate injuries, with males making up the majority. Although the diagnosis was done with more male than female climbers, evidence supports that males are even more prone to EPGIs than females, especially when considering that they have open growth plates for a longer period of time than females, as mentioned above.[12]

Chronic Developments

As mentioned above, it has been observed that over the course of a person's climbing career, their cortical bones tend to broaden at the joint base of their fingers to adapt to the intense rigor of the sport.[5] Evidence of cortical hypertrophy supports the notion that climbers' hands undergo adaptive changes, but it is unclear whether changes can be pathologic beyond injury. The most common example is the development of the condition osteoarthritis, a disease process that causes a breakdown of cartilage that can result in pain, swelling, decreased range of motion, difficulty gripping, or a decrease in pinch strength.[13] Across a vast amount of research, there appears to be an uncertainty in the risk of adolescent climbers developing osteoarthritis.

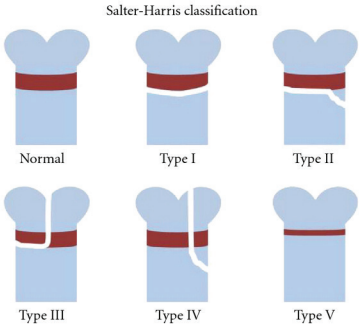

Figure 3: Salter-Harris breaks the visualized diagram. The red band indicates the growth plate. Type 1 is a fracture that goes through the growth plate, separating the end of the bone from the growth plate. Type 2 is a fracture that goes through the growth plate and extends into the metaphysis (below the red band). Type 3 is a fracture that goes through the growth plate and extends into the epiphysis (above the red band). Type 4 is a fracture that extends through the growth plate, metaphysis, and epiphysis. Type 5 is a fracture that compresses or crushes the growth plate.[19]

In one case, climbers as young as 20 years old have been radiographed and shown signs of osteoarthritis, while a group of tested Swiss climbers in the age range of 10-17 years showed no signs of the condition despite a climbing career of up to 7 years.[4] A reasonable hypothesis is that the adolescent climbers have not had a long enough climbing career for these pathological changes to occur. Of course, as mentioned above, cortical hypertrophy is still present, but these changes are adaptive rather than pathologic.

In another study, this hypothesis that adolescent climbers have not climbed long enough for pathological changes to occur is supported regarding investigating the development of osteophytes, bony outgrowths at the base of bone, most commonly found at the DIP.[7] It was suggested that base osteophytes start forming in the first 15 years of a rock climber's career. After reexamining the patients 10 years later, it was observed that the already present osteophytes progressed to such a point that they can be considered symptoms of osteoarthritis.[7] This data suggests that, along with adaptive cortical hypertrophy, base osteophytes develop over the course of a climber's career. However, whereas cortical hypertrophy occurs as an adaptive measure, base osteophytes slowly progress during the first 15 years of a climber's career in an insignificant way. After this time period, osteophytes manifest themselves as radiographic signs of osteoarthritis.

To summarize, an adolescent climber may go a long way in their career without experiencing any of the injuries mentioned above, such as an EPGI or FFPI, but along with adaptive changes their hands and fingers undergo, pathological changes may develop along with them. This does not mean that adolescents develop osteoarthritis during this age, but rather it should not be surprising for the condition to manifest itself more prolifically later in a climber's career. Time is always a factor, but there is still the question of the minority group that contracts osteoarthritis at such a young age.

In addition to slow-rate osteoarthritis developing with base osteophytes over a long period of time, EGPIs contracted under intense training measures, such as campus boarding, are another way for osteoarthritis to occur. As mentioned above, radiographic evidence is the most common and most efficient way to diagnose a case of osteoarthritis. Doctors use the Kellgren-Lawrence Classification system to assign the subject bone a grade from 0-4, with a grade 0 signifying no evidence of osteoarthritis and a grade 4 signifying severe osteoarthritis. Doctors make this conclusion by searching for the presence of osteophytes, joint space narrowing, and any bone deformity.[15]

In the study done on the German Junior National Team mentioned above, there was only one case of osteoarthritis, and it so happens that the climber experienced an epiphyseal growth plate fracture. In addition, the climber was also reported to have engaged in intense campus board training. This presents the hypothesis that EGPIs may be a cause for early-onset osteoarthritis, and the EPGI itself may be a result of intense training. Moreover, if osteoarthritis does not present itself immediately after the injury, it has been observed in some cases that it still presents itself up to 10 years later.[5-10]

DOI: 10.36838/IJHSR810.57

Another study over the course of a 4-year period examining EGPIs of adolescent climbers reported that almost half of the athletes trained on campus boards. The question of whether or not campus boarding in particular is the root cause of EPGIs and, therefore, some cases of osteoarthritis is now present. Above, I mentioned that EPGIs are typically the result of repetitive overuse injuries, and this remains the case with campus boarding. However, campus boarding is a special type of training most commonly used to build raw finger strength and, therefore, adds to the already intense load being placed on the fingers during normal climbing sessions. In summary, intense training that puts the growth plates at risk of injury, such as campus boarding or heavy reliance on crimping, can lead to EPGIs. These, in turn, have a high likelihood of manifesting into osteoarthritis via the Kellgren-Lawrence scale.[6]

Diagnosis and Rehabilitation

Like any other sport, athletes who have experienced any sort of finger injury should prioritize proper rehabilitation and healing before returning to climbing. To indicate a fully healed finger, an athlete must be pain-free, have a full/close-to-full range of motion, have minimal swelling, and have qualitative radiographic data that proves complete internal healing.[6] Before designing a proper recovery program for climbers, it is vital for doctors to properly identify the kind of injury as well as the severity.

For the FFPS, grade 1-3 injuries can be approached non-surgically with taping methods and specified weeks of rest. Taping with methods such as H-tape helps reduce bowstringing in the A2 by up to 50%.[8] Grade 1-2 injuries can heal in 6 weeks, and taping for an additional 3 months is recommended after the athlete begins climbing again. For a Grade 3, immobilization of the finger with a splint or ring is recommended for up to 2 weeks before carrying out the same process as a Grade 1-2. As for Grade 4 injuries, surgery is the best course of action. Grafting tissue is an efficient way of repairing a ruptured pulley or tendon, and the return-to-climb protocol remains the same in ensuring complete healing.[16]

For EPGIs, X-ray should be the priority, but it is important to note that fractures may take a few months to show up on an X-ray.[17] In this study, with 28 climbers, many came into the clinic with finger pain but did not actually have a visible fracture present. The pain without a visible break can be concluded as early-stage EPGI, in which the bone starts to atrophy and becomes brittle as a result of intense training. In this case, it is recommended for doctors to follow up with their patients for 2-3 months until the patient has no pain. In this way, we prevent the development of an actual stress fracture.[18]

In the case of a visible fracture, CT scans are the most effective radiographs in assessing damage. Although both MRIs and CT scans are promising diagnostic techniques, MRIs are not well-suited to depict the full severity of the injury. CT scans present a much more accurate image of the injury, but both scans are costly in the medical industry. To compensate, it is suggested that CT scans are only ordered if doctors are unable to determine if the bone is healing with only X-rays.[17]

Salter-Harris fractures can be treated conservatively in a non-surgical manner as long as a correct diagnosis is made at an early enough point. Splinting the finger into one position to allow the bone to heal is the most common method of rehabilitation for around 3 months. In one case, a patient went many months without consulting a doctor about finger pain, and the result was severe osteoarthritis.[17] This leads me to conclude that, in addition to the climber following through with immobilizing the finger to ensure proper healing, a correct diagnosis from a doctor early on is vital in preventing any long-term effects, such as osteoarthritis.

Outlook

Rock climbing is a high-risk sport that constantly puts athletes at risk of injury, especially with its growing population of both adult climbers and youth climbers.[1-3] The purpose of this paper was to dive into the specifics of finger injuries, with a focus on their presence in adolescent climbers.

Injuries to the finger flexor pulley system are common in climbers of all ages, and injuries to epiphyseal growth plates are exclusive to adolescents.[2,3] Both injuries are caused by excessive load placed on the fingers as a result of the intense biomechanics needed to generate force.[2] FFPS injuries happen in a single acute event in which the intense load causes a pulley to sprain, tear, or rupture. This decreases the amount of support holding the flexor tendon to the bone, causing the finger to lack stability and strength while climbing.[2]

After a critical review of literature regarding the body's development phase during the adolescent stage of life, I concluded that the body prioritizes growth rather than reinforcement, causing the fingers to be more brittle as the bone develops. EPGIs happen as a result of repetitive stress to the fingers that eventually fractures the growth plate while it is fragile.[3] It is normalized for adolescent climbers to engage in rigorous training methods such as hangboarding, but such training methods put a great deal of stress on the fingers.[5]

This paper also explored the conditions under which climbers end up developing more serious pathological chronic issues, such as osteoarthritis. Climbers' fingers undergo a great deal of cortical hypertrophy as an adaptive measure to bear with the intense load they experience, but bony outgrowths along the base of the bone, called osteophytes, also start developing along the first 15 years of a climber's career.[5] These osteophytes can grow to the point of causing symptoms of osteoarthritis without the climber ever experiencing any injury.[13] In the case of an EPGI, osteoarthritis may manifest itself sooner in a climber's career.[5]

To effectively treat these injuries, a proper diagnosis and recovery plan are essential. For FFPS injuries, anything under a grade 4 injury can be approached conservatively with time and taping to help heal.[8] Grade 4 injuries with multiple pulley ruptures need to be approached surgically.[16] For EPGIs, it is important to diagnose first with x-ray imaging and then treat the injury with adequate rest time till the climber is pain-free. If there is no visible fracture on an X-ray but the climber still feels pain, a CT scan can give a clearer picture to visualize the break.[17] The climbers should avoid putting any stress on the

finger until they are completely pain-free, and treatment is typically conservative, involving splinting the finger into one position.

In both adolescent and mature rock-climbing athletes, thickening of the cortical bone occurs as an adaptive measure to the intense load placed on the fingers. However, because of the adolescent body's priority on growing and developing, they are more prone to growth plate injuries. In addition, younger athletes should be cautious of rigorous training methods such as campus boarding, for it can increase the chances of getting injured. To ensure an injury has the highest likelihood of successful healing without developing into a pathologic chronic condition such as osteoarthritis, a correct diagnosis of the injury and a proper recovery plan are essential. The top priority is ensuring the climber has no pain, and climbing should be fully put on hold or severely limited in time and intensity till pain subsides. Many finger injuries can be treated conservatively with either taping or splinting, and surgical repair should be considered in cases of severe ruptures or breaks. Altogether, youth climbers should be consistent in warming up properly to minimize the risk of injury, and any injuries should be approached carefully to ensure a long-lasting climbing career.

References

1. Rohrbough, Joel T.; Mudge, M. Kenneth; Schilling, Robert C. Overuse injuries in the elite rock climber. Medicine & Science in Sports & Exercise 32(8): pp. 1369-1372, August 2000.https://journals.lww.com/acsm-msse/fulltext/2000/08000/overuse_injuries_in_the_elite_rock_climber.2.aspx.
2. Miro, Paulo H.; Eric vanSonnenberg; Dylan M. Sabb; and Volker Schöffl. "Finger Flexor Pulley Injuries in Rock Climbers." Wilderness and Environmental Medicine 32, no. 2 (May 6, 2021): 247–58. https://doi.org/10.1016/j.wem.2021.01.011.
3. Jones, Gareth; Rowena Johnson; Volker Schöffl; Isabelle Schöffl; Chris Lutter; Mark I Johnson; and Tim Halsey. "Primary Peripheyseal Stress Injuries of the Fingers in Adolescent Climbers: A Critical Review." Current Sports Medicine Reports 21, no. 12 (December 1, 2022): 436–42. https://doi.org/10.1249/jsr.0000000000001016.
4. Schlegel, Christian, Ueli Büchler, and Susi Kriemler. "Finger injuries of young elite rock climbers." Institute of Sports Science, Federal Office for Sports, Magglingen, Switzerland. 2002. https://sems.ch/fileadmin/user_upload/Zeitschrift/50-2002-1/3-2002-1.pdf.
5. Schöffl, Volker; Thomas Hochholzer; and Andreas Imhoff. "Radiographic Changes in the Hands and Fingers of Young, High-Level Climbers." The American Journal of Sports Medicine 32, no. 7 (October 2004): 1688–94. https://doi.org/10.1177/0363546503262805.
6. Schöffl V, Schöffl I, Flohé S, El-Sheikh Y, Lutter C. Evaluation of a Diagnostic-Therapeutic Algorithm for Finger Epiphyseal Growth Plate Stress Injuries in Adolescent Climbers. Am J Sports Med. 2022 Jan;50(1):229-237. Doi: 10.1177/03635465211056956. Epub 2021 Nov 24. PMID: 34817275. https://pubmed.ncbi.nlm.nih.gov/34817275/
7. Pastor T, Fröhlich S, Pastor T, Spörri J, Schweizer A. Cortical Bone Thickness, Base Osteophyte Occurrence and Radiological Signs of Osteoarthritis in the Fingers of Male Elite Sport Climbers: A Cross-Sectional 10-Year Follow-Up Study. Front Physiol. 2022 Jun 2;13:893369. Doi: 10.3389/fphys.2022.893369. PMID: 35721555; PMCID: PMC9203125. https://pmc.ncbi.nlm.nih.gov/articles/PMC9203125/
8. V. Schöffl, I. Schöffl, L. Frank, T. Küpper, M. Simon, C. Lutter. "Tendon Injuries in the Hands in Rock Climbers: Epidemiology, Anatomy, Biomechanics and Treatment - An Update". https://www.researchgate.net/profile/Thomas-Kuepper/publication/342208111_Tendon_Injuries_in_the_Hands_in_Rock_ClimbersEpidemiology_Anatomy_Biomechanics_and_Treatment_An_Update/links/5ee8da40458515814a62dae9/Tendon-Injuries-in-the-Hands-in-Rock-ClimbersEpidemiology-Anatomy-Biomechanics-and-Treatment-An-Update.pdf
9. Roloff, Isabelle, Volker Rainer Schöffl, Laurent Vigouroux, and Franck Quaine. "Biomechanical Model for the Determination of the Forces Acting on the Finger Pulley System." Journal of Biomechanics 39, no. 5 (January 2006): 915–23. https://doi.org/10.1016/j.jbiomech.2005.01.028.
10. Berrigan W, White W, Cipriano K, Wickstrom J, Smith J, Hager N. Diagnostic Imaging of A2 Pulley Injuries: A Review of the Literature. J Ultrasound Med. 2022 May;41(5):1047-1059. doi: 10.1002/jum.15796. Epub 2021 Aug 2. PMID: 34342037; PMCID: PMC9292555. https://pmc.ncbi.nlm.nih.gov/articles/PMC9292555/
11. Levine RH, Thomas A, Nezwek TA, Waseem M. Salter-Harris Fracture. 2023 Aug 10. In: StatPearls [Internet]. Treasure Island (FL): StatPearls Publishing; 2025 Jan–. PMID: 28613461. https://www.ncbi.nlm.nih.gov/books/NBK430688/
12. Schöffl VR, Schöffl I, Jones G, Klinder A, Küpper T, Gunselmann L, Simon M, Moser O, Bayer T, Lutter C. Prospective analysis of injury demographics, distribution, severity and risk factors in adolescent climbers. BMJ Open Sport Exerc Med. 2025 Feb 22;11(1):e002212. doi: 10.1136/bmjsem-2024-002212. PMID: 39995613; PMCID: PMC11848689. https://pmc.ncbi.nlm.nih.gov/articles/PMC11848689/pdf/bmjsem-11-1.pdf
13. Estes JP, Bochenek C, Fassler P. Osteoarthritis of the fingers. J Hand Ther. 2000 Apr-Jun;13(2):108-23. doi: 10.1016/s0894-1130(00)80035-6. Erratum in: J Hand Ther 2001 Jan-Mar;14(1):42. Fassler P [corrected to Fassler P]. PMID: 10855746. https://pubmed.ncbi.nlm.nih.gov/10855746/
14. Kohn MD, Sassoon AA, Fernando ND. Classifications in Brief: Kellgren-Lawrence Classification of Osteoarthritis. Clin Orthop Relat Res. 2016 Aug;474(8):1886-93. Doi: 10.1007/s11999-016-4732-4. Epub 2016 Feb 12. PMID: 26872913; PMCID: PMC4925407.https://pmc.ncbi.nlm.nih.gov/articles/PMC4925407/pdf/11999_2016_Article_4732.pdf
15. Crowley TP. The flexor tendon pulley system and rock climbing. J Hand Microsurg. 2012 Jun;4(1):25-9. doi: 10.1007/s12593-012-0061-3. Epub 2012 Jan 18. PMID: 23730085; PMCID: PMC3371120. https://pmc.ncbi.nlm.nih.gov/articles/PMC3371120/pdf/12593_2012_Article_61.pdf
16. Bärtschi N, Scheibler A, Schweizer A. Symptomatic epiphyseal sprains and stress fractures of the finger phalanges in adolescent sport climbers. Hand Surg Rehabil. 2019 Sep;38(4):251-256. doi: 10.1016/j.hansur.2019.05.003. Epub 2019 May 16. PMID: 31103479. https://www.sciencedirect.com/science/article/pii/S2468122919300726?via%3Dihub
17. Meyers, Rachel N. BA; Schöffl, Volker R. MD; Mei-Dan, Omer MD; Provance, Aaron J. MD. Returning to Climb after Epiphyseal Finger Stress Fracture. Current Sports Medicine Reports 19(11) p 457-462, November 2020. | DOI: 10.1249/JSR.0000000000000770 https://journals.lww.com/acsm-csmr/fulltext/2020/11000/returning_to_climb_after_epiphyseal_finger_stress.7.aspx
18. Chung R, Foster BK, Xian CJ. Preclinical studies on mesenchymal stem cell-based therapy for growth plate cartilage injury repair. Stem Cells Int. 2011;2011:570125. doi: 10.4061/2011/570125. Epub 2011 Jul 26. PMID: 21808649; PMCID: PMC3144692.

DOI: 10.36838/IJHSR810.57

https://pmc.ncbi.nlm.nih.gov/articles/PMC3144692/pdf/SCI2011-570125.pdf

Author

Rohan Tare is a junior at St. Mark's School of Texas. He wishes to study at Brown and pursue a pre-med track. He plans on majoring in biology or chemistry.

IJHSR
ijhighschoolresearch.org
RESEARCH ARTICLE

Adolescent Substance Use and Peer Influence

Chloe Lee

Gilbert High School, 312 Gretten St, Gilbert, Iowa, 50105; sunshine25chloe@gmail.com

ABSTRACT: This study examines the role of peer influence in adolescent substance use, focusing on two key dimensions: peer substance use exposure and peer cohesion. Research presents contrasting views on the effects of peer cohesion. Identity-related theories suggest a positive association, arguing that strong peer cohesion amplifies the perceived rewards of substance use. In contrast, social isolation studies propose a negative relationship, suggesting that peer cohesion alleviates stress, thereby reducing substance use risk. Using a nationally representative U.S. sample of adolescents (N = 6,051), this study investigates factors influencing substance use in young adulthood. The findings indicate that peer substance use exposure significantly increases adolescent substance use, consistent with behavioral and identity-based theories. However, the effect of peer cohesion varies by substance type. It is positively associated with "soft drug" use, which is more socially accepted, but negatively associated with "hard drug" use, which carries greater stigma. These results suggest that the seemingly conflicting predictions of peer influence and social isolation theories can be reconciled by accounting for the social acceptability of different substances.

KEYWORDS: Biomedical and Health Sciences, Other, Adolescent Substance Use, Peer Influence, Peer Cohesion.

Introduction

An alarming 6,694 adolescents in the United States lost their lives to substance misuse in 2022.[1] Notably, between 2019 and 2020, the rate of substance overdose deaths among adolescents surged by 94%, compared to a 30% increase across the general population.[2] Due to the incomplete maturation of the adolescent brain, individuals in this developmental stage are more prone to risk-taking behaviors and heightened sensitivity to peer influence, thereby increasing their susceptibility to substance use.[3-6] Despite the stark increase in adolescent substance overdose deaths, current research has yet to uncover the underlying causes contributing to this rise fully. This gap underscores the urgent need for further research to develop more effective prevention strategies for this vulnerable population.

Peer Influence on Substance Use:

The widespread prevalence of substance use among adolescents can be attributed to factors such as peer pressure, amplified by the pervasive influence of social media.[7] Although peer influence (also referred to as peer socialization or peer contagion effects)[8] can affect all demographics, it has a particularly strong impact on adolescents, as it coincides with critical developmental periods.[7,9]

Most existing theories of peer influence draw upon both behavioral and identity-related frameworks.[7] From a behavioral perspective, peer influence is grounded in social learning theory, which posits that individuals are likely to replicate behaviors observed in their peers, particularly when those behaviors are socially rewarded.[10] This modeling behavior plays a crucial role in socialization, fostering friendships with individuals who actively shape behaviors and attitudes. The concept of social learning, or behavioral contagion, is especially pertinent during adolescence, as peers often serve as key reference groups, more influential than adults. This dynamic is highly relevant in contexts such as substance use. For instance, adolescents are more likely to mirror their peers' substance use, such as consuming alcohol or cigarettes, particularly when such actions are perceived as socially rewarding and associated with popularity within their peer groups.[11]

From an identity-focused perspective, theories propose that conforming to peer influence plays a significant role in enhancing self-esteem and fostering a positive self-concept.[7] During adolescence, the approval, feedback, and sense of belonging provided by peers are pivotal in shaping self-esteem and identity development.[9] Adopting the behaviors and attitudes of valued peers can yield intrinsic rewards, as it reinforces a favorable self-image and strengthens feelings of social inclusion.[9,12-15] In the context of substance use, adolescents whose close peers engage in such behaviors may perceive activities like drinking alcohol or smoking cigarettes as a way to strengthen their bonds with admired peers and enhance their self-image. This notion is further substantiated by developmental neuroscience research.[16]

In addition to mirroring peer substance use, peer cohesion represents another critical dimension of peer influence. Defined as the sense of support and connectedness individuals experience within their peer group or social network,[17] peer cohesion may influence adolescent substance use in two ways: either as a facilitator or as a protective buffer. Identity-related theories suggest that peer cohesion may promote substance use among adolescents when behaviors like smoking or drinking are associated with favorable attributes, such as projecting a "cool" or "mature" image.[18] In such cases, strong peer cohesion may amplify intrinsic rewards and enhance adolescents' self-perception through substance use. This dynamic fosters an environment where adolescents engage in substance use to strengthen their social identity and affirm their status within the peer group.

DOI: 10.36838/IJHSR810.63

Consequently, identity-related theories predict a positive association between peer cohesion and substance use.

Conversely, research on social isolation suggests that elevated levels of peer cohesion can act as a protective buffer against stress, thereby reducing the likelihood of engaging in substance use.[17] These studies have demonstrated that adolescents experiencing social isolation are at a heightened risk of substance use, including behaviors such as cocaine self-administration and amphetamine or nicotine-induced locomotor activity.[19] This connection is largely attributed to the stress triggered by social isolation, which can drive adolescents to use substances as a coping mechanism. Stress is not only a risk factor for the initiation of substance use but also contributes to its maintenance and escalation over time.[20] Therefore, social isolation theories predict a negative association between peer cohesion and substance use.

Gaps in the Literature:

Research on peer influence and social isolation reveals two contrasting perspectives regarding the relationship between peer cohesion and adolescent substance use. Identity-related theories and studies on social isolation have independently explored the roles of peer influence in shaping substance use behaviors. However, few studies have addressed the contradictory implications of these perspectives. On the one hand, identity-related theories suggest a positive relationship between peer cohesion and substance use. Strong peer cohesion may amplify intrinsic rewards for behaviors such as smoking and drinking, as these activities are often viewed favorably within adolescent peer groups. On the other hand, research on social isolation proposes a negative relationship, arguing that greater peer cohesion reduces social isolation, which in turn may lower the likelihood of substance use. Given the rising prevalence of substance use among adolescents, it is crucial to explore the nuanced correlations between peer cohesion and substance use. This approach could offer a deeper understanding of the social contexts contributing to substance misuse among this high-risk group.

Furthermore, much of the existing research has narrowly focused on a single substance, overlooking the broader spectrum of substances adolescents may use.[21,22] Examining the impact of peer cohesion across a variety of substances is essential, as different substances vary in their popularity and social acceptability among adolescents. For instance, smoking and drinking might be perceived as socially acceptable or even "cool" behaviors, whereas using substances like cocaine may be stigmatized. This study seeks to examine the impact of peer cohesion on a diverse range of substances to reconcile the seemingly conflicting predictions from these two streams of research.

Hypothesis:

Drawing on prior research, I have developed the following research questions and hypotheses.

First, I will examine whether peer cohesion of adolescents is associated with substance use. Based on the literature on behavioral and identity-related theories and social isolation theory, I formulate a null hypothesis that reflects two competing theoretical perspectives.

H1: Peer cohesion is not associated with substance use in adolescents.

Second, I will examine whether peer substance use exposure is associated with adolescent substance use.

H2: Peer substance use exposure is positively associated with the substance use of adolescents.

Methods

The Add Health study includes approximately 20,000 nationally representative young adults and examines the influence of health behaviors from adolescence to early adulthood. The Institutional Review Board (IRB) at the University of North Carolina-Chapel Hill reviewed and approved the study, with written consent secured for each phase of data collection. Participants were initially surveyed while in grades 7 to 12 in 1995 and have been followed through four additional waves of data collection, concluding in 2018. This study focused on the first wave of the Add Health dataset in 1995 out of the five available waves, as it includes information on adolescents' substance use, peer cohesion, and their peers' substance use. The publicly available dataset for Wave I includes data from 6,504 respondents, representing about one-third of the full sample. At the time of data collection, the respondents in Wave I were between 12 and 21 years old. To focus specifically on adolescent substance use, I restricted the sample to individuals aged 12 to 18, thereby excluding 453 respondents aged 19 to 21. As a result, the final analytical sample consists of 6,051 respondents.

Substance use (cigarettes, alcohol, cocaine, inhalants). Adolescent substance use, defined as the tendency for adolescents to use substances such as alcohol, was measured through responses to four types of questions, each addressing a different substance: cigarettes, alcohol, cocaine, and inhalants. Participants were asked if they had ever tried cigarette smoking, whether they had consumed alcohol more than two or three times in their life, and the age at which they first tried cocaine or inhalants, with an option to indicate if they had never used these substances. The first two questions capture adolescents' substance use related to cigarettes and alcohol, represented as binary indicator variables. For the last two questions, which measure substance use involving cocaine and inhalants, age responses are converted into binary indicators.

Peer cohesion. Peer cohesion refers to the sense of support and care individuals perceive from their peers. In Wave I of the Add Health study, this was assessed through adolescents' responses to the question about how much they felt their peers cared about them. This question showcases peer cohesion by asking how cared-for individuals feel within their social group, reflecting their perceived support and belonging as measured on a 5-point Likert scale. In addition to peer cohesion, this study also incorporates adult care, which represents the support and care adolescents perceive from adults, such as parents and teachers. This variable is recognized as a critical protective factor against adolescent substance use. In the Add Health study, adult care was assessed through responses to a question

about how much they felt adults cared about them. Including this variable allows us to account for broader social and relational protective factors beyond peer cohesion.

Peer substance use exposure. Peer substance use exposure refers to the influence and relationships that peers may have on an individual's substance use behaviors. In Wave I of the Add Health study, peer substance use exposure was assessed through adolescents' responses to questions regarding their three closest peers: how many smoked at least one cigarette per day and how many consumed alcohol at least once a month. These questions effectively capture peer substance use exposure by focusing on the behaviors of the adolescents' close peers. This information provides a foundation for exploring potential links to peer influence.

Results and Discussion

The mean, standard deviation, minimum, and maximum values for the participants' scores are provided in Table 1, which also reports the percentages of substance use among adolescents. Smoking cigarettes and drinking alcohol are often classified as soft drugs because those substances are generally perceived to have a lower potential for addiction, abuse, and harmful physical or mental effects compared to hard drugs. In contrast, cocaine and inhalants are typically categorized as hard drugs. While inhalants are readily available and may be legal for their intended purposes, their substantial health dangers and high likelihood of addiction often place them in the hard drug category. Descriptive statistics in Table 1 support these classifications, showing that 55.1% of adolescents reported smoking and 54.3% reported drinking, whereas only 4.6% reported using cocaine, and 7.3% reported using inhalants. These results highlight the higher prevalence of soft drug use among adolescents compared to the lower prevalence of hard drug use. The mean age of participants is approximately 16 years, with ages ranging from 12 to 18. In terms of race, the majority of respondents are Caucasian, comprising 66.4% of the sample, while African American respondents make up 24.9%. The sample also includes 3,139 females (51.9%) and 2,912 males.

Table 1: Descriptive statistics.This table reports the descriptive statistics for substance use, peer cohesion, peer substance use exposure, and demographic variables.

Variable	Obs	Mean	Std. Dev.	Min	Max
Smoking	6,010	0.551	0.497	0	1
Drinking	6,004	0.543	0.498	0	1
Cocaine	6,051	0.046	0.210	0	1
Inhalants	6,051	0.073	0.259	0	1
Peer_Cohesion	6,035	4.252	0.792	1	6
Peer_Smoking	5,937	0.800	1.057	0	3
Peer_Drinking	5,920	1.075	1.164	0	3
Adult_Care	6,036	4.391	0.819	1	6
Age	6,051	15.804	1.604	12	18
Caucasian	6,038	0.664	0.472	0	1
African American	6,038	0.249	0.433	0	1
Female	6,051	0.519	0.500	0	1

The correlations between the primary variables of interest (dependent variables and main independent variables, excluding control variables) are presented in Table 2. The use of substances such as smoking, drinking, cocaine, and inhalants exhibits positive associations. Among these, smoking and drinking exhibit stronger correlations with each other, while cocaine and inhalants are also closely associated. The univariate analysis of substance use and peer cohesion reveals noteworthy findings. While peer cohesion shows a positive but nonsignificant association with soft drugs, such as smoking and drinking, it exhibits a negative and significant association with hard drugs, including cocaine and inhalants. Peer substance use exposure, specifically smoking and drinking, is positively and significantly correlated with smoking and drinking behaviors. Although the Wave I survey did not collect data on peer use of cocaine and inhalants, peer smoking and drinking are positively and significantly associated with the use of these hard drugs.

Table 2: Correlations among the interest variables. This table reports the correlations among substance use, peer cohesion, and peer substance use exposure. The correlation coefficient is displayed in bold if its significance level is at or below 10 percent.

	Smoking	*Drinking*	*Cocaine*	*Inhalants*	*Peer_ Cohesion*	*Peer_ Smoking*	*Peer_ Drinking*
Smoking	**1**						
Drinking	**0.4755**	**1**					
Cocaine	**0.1322**	**0.1224**	**1**				
Inhalants	**0.1588**	**0.1458**	**0.3267**	**1**			
Peer_Cohesion	0.0057	-0.0002	**-0.0507**	**-0.0473**	**1**		
Peer_Smoking	**0.3735**	**0.3208**	**0.2121**	**0.1501**	**-0.0351**	**1**	
Peer_Drinking	**0.3643**	**0.4921**	**0.1689**	**0.1541**	-0.0165	**0.5044**	**1**

Table 3: Regression analysis of peer influence on adolescent substance use. This table reports the regression results of peer influence and adolescent substance use. Peer cohesion is positively associated with soft drug use but negatively associated with hard drug use. Z-statistics are presented in parentheses. Standardized Betas are presented in the third row. *** p<0.01, ** p<0.05, * p<0.1.

Panel A. Model 1: Control variables

	(1)	(2)	(3)	(4)
VARIABLES	Smoking	Drinking	Cocaine	Inhalants
Adult_Care	-0.2454***	-0.2256***	-0.4921***	-0.4263***
	(-7.19)	(-6.54)	(-7.90)	(-8.14)
	-0.4030	-0.3691	-1.9610	-1.3601
Age	0.2331***	0.3344***	0.1583***	-0.0448
	(13.64)	(18.99)	(3.76)	(-1.40)
	0.7517	1.0752	1.2354	-0.2797
Caucasian	0.3677***	0.1377	-0.3468**	0.1079
	(4.34)	(1.59)	(-1.96)	(0.68)
	0.3476	0.1301	-0.7969	0.1985
African American	-0.2850***	-0.3911***	-0.8294***	-0.3522*
	(-3.08)	(-4.14)	(-3.76)	(-1.91)
	-0.2462	-0.3377	-1.7456	-0.5934
Female	0.0620	-0.0552	-0.3468***	-0.2640***
	(1.14)	(-1.01)	(-2.70)	(-2.59)
	0.0622	-0.0554	-0.8434	-0.5140
Constant	-2.6008***	-4.0695***	-2.9734***	0.0747
	(-7.97)	(-12.22)	(-3.98)	(0.13)
Observations	5,911	5,898	6,021	6,021
Pseudo R^2	0.0453	0.0641	0.0479	0.0277

DOI: 10.36838/IJHSR810.63

Panel B. Model 2: Main interest variables

	(1)	(2)	(3)	(4)
VARIABLES	Smoking	Drinking	Cocaine	Inhalants
Peer_Cohesion	**0.0887****	**0.0740***	**-0.2024*****	**-0.1529****
	(2.26)	**(1.79)**	**(-2.60)**	**(-2.39)**
	0.1403	**0.1167**	**-0.7802**	**-0.4716**
Peer_Substance	**0.7969*****	**0.9831*****		
	(23.69)	**(30.27)**		
	1.6915	**2.2969**		
Adult_Care	-0.1904***	-0.1691***	-0.4378***	-0.3873***
	(-5.04)	(-4.27)	(-6.60)	(-7.02)
	-0.3128	-0.2766	-1.7446	-1.2357
Age	0.1632***	0.1738***	0.1611***	-0.0432
	(8.98)	(8.76)	(3.83)	(-1.35)
	0.5263	0.5588	1.2574	-0.2697
Caucasian	0.2155**	0.0141	-0.2913	0.1464
	(2.40)	(0.15)	(-1.63)	(0.91)
	0.2037	0.0133	-0.6696	0.2694
African American	-0.2025**	-0.3310***	-0.8312***	-0.3551*
	(-2.08)	(-3.16)	(-3.76)	(-1.92)
	-0.1749	-0.2858	-1.7495	-0.5984
Female	0.0446	-0.0798	-0.3030**	-0.2294**
	(0.77)	(-1.29)	(-2.33)	(-2.23)
	0.0448	-0.0801	-0.7366	-0.4466
Constant	-2.5779***	-2.9456***	-2.4652***	0.4794
	(-7.14)	(-7.61)	(-3.20)	(0.79)
Observations	5,911	5,898	6,021	6,021
Pseudo R^2	0.132	0.212	0.0509	0.0295

Table 3 reports the results of the hierarchical logistic regression analyses, which build on the univariate evidence presented in Table 2. Rather than estimating a single logistic model, Table 3 presents a stepwise hierarchical specification to illustrate how explanatory power evolves as key variables are introduced. Panel A reports Model 1, which includes only control variables, while Panel B reports Model 2, which adds the main variables of interest alongside the controls. Across all four outcomes, the inclusion of the main explanatory variables leads to substantial increases in model fit, as reflected in the pseudo R^2 values, highlighting the importance of peer influence in shaping adolescent substance use. In particular, the pseudo R^2 for the smoking regression in column (1) increases from 0.0453 to 0.132, while the pseudo R^2 for the drinking regression in column (2) rises from 0.0641 to 0.212. The pseudo R^2 values for the cocaine and inhalant regressions in columns (3) and (4) also increase, although to a lesser extent.

Overall, the multivariate regression results reveal that peer cohesion has a positive influence on the use of soft drugs, such as smoking and drinking, among adolescents. Conversely, peer cohesion has a negative influence on the use of hard drugs, including cocaine and inhalants, highlighting its complex role in substance use behaviors. The estimated average marginal effect of peer cohesion on smoking is 0.018 ($p = 0.023$), indicating that higher peer cohesion increases the likelihood of smoking by approximately 1.8 percentage points. The corresponding marginal effect for drinking is 0.014 ($p = 0.073$). In contrast, peer cohesion is associated with lower probabilities of hard drug use, with marginal effects of −0.008 for cocaine use ($p = 0.010$) and −0.010 for inhalant use ($p = 0.017$). In comparison, peer substance use exhibits substantially larger effects, with the average marginal effect of peer smoking equal to 0.164 ($p < 0.001$) and that of peer drinking equal to 0.180 ($p < 0.001$).

To further examine the protective effects of different social relationships, we include adult care as a control variable, allowing for a comparison of the influence of peer cohesion and peer cohesion with that of adult care in mitigating adolescent substance use. Unlike peer cohesion, adult care exhibits a consistently negative impact on all forms of substance use, suggesting that greater adult care effectively reduces substance use among adolescents. These findings emphasize the distinct and contrasting influences of peer and adult relationships on adolescent substance use.

Peer substance use exposure is positively associated with substance use among adolescents, which is consistent with the univariate correlation results. I do not include peer substance use for cocaine and inhalants because the Wave I survey did not collect data on peer use of cocaine and inhalants. Age-related findings reveal that as adolescents grow older, they become more likely to engage in smoking, drinking, and cocaine use, whereas inhalant use decreases with age. Challenging perceived stereotypes, Caucasian adolescents appear more susceptible to substance use (except for inhalants), whereas African American adolescents report lower rates of substance use across all categories. Female adolescents are less likely than their male counterparts to use hard drugs, but there is no significant difference between genders in the use of soft drugs.

Table 4: Regression analysis of the interaction between peer influence and race and gender. This table reports regression results examining interaction effects between peer influence and race and gender. None of the interaction terms is statistically significant. Z-statistics are presented in parentheses. Standardized Betas are presented in the third row. *** p<0.01, ** p<0.05, * p<0.1.

	(1)	(2)	(3)	(4)
VARIABLES	Smoking	Drinking	Cocaine	Inhalants
Peer_Cohesion	0.2244**	0.2307**	-0.0734	-0.0860
	(2.15)	(2.07)	(-0.43)	(-0.54)
Peer_Substance	0.7962***	0.9830***		
	(23.67)	(30.25)		
Adult_Care	-0.1942***	-0.1712***	-0.4442***	-0.3891***
	(-5.12)	(-4.31)	(-6.68)	(-7.03)
Age	0.1624***	0.1731***	0.1591***	-0.0446
	(8.93)	(8.72)	(3.78)	(-1.39)
Peer_Cohesion	-0.1386	-0.1627	-0.0892	0.0119
× Caucasian	(-1.30)	(-1.43)	(-0.49)	(0.07)
Caucasian	0.7932*	0.6905	0.0419	0.0866
	(1.74)	(1.43)	(0.06)	(0.13)
Peer_Cohesion	-0.1494	-0.1152	-0.3054	-0.1653
× African American	(-1.31)	(-0.95)	(-1.39)	(-0.87)
African American	0.4164	0.1412	0.3248	0.2823
	(0.86)	(0.27)	(0.38)	(0.37)
Peer_Cohesion	-0.0192	-0.0557	-0.0247	-0.0798
× Female	(-0.26)	(-0.71)	(-0.17)	(-0.66)
Female	0.1246	0.1569	-0.2093	0.0939
	(0.39)	(0.46)	(-0.35)	(0.19)
Constant	-3.1110***	-3.5698***	-2.8996***	0.2493
	(-5.91)	(-6.33)	(-3.05)	(0.31)
Observations	5,911	5,898	6,021	6,021
Pseudo R^2	0.132	0.212	0.0519	0.0301

Given the significant main effects of race and gender, I examine whether the effect of peer cohesion varies across these characteristics by introducing interaction terms in Table 4. Building on the baseline specification in Table 3, I include in-

teractions between peer cohesion and indicators for Caucasian, African American, and Female. Across all four regressions, none of the interaction terms is statistically significant. These results suggest that although peer cohesion and race or gender independently influence adolescent substance use, the effect of peer cohesion does not differ systematically by race or gender.

Table 5: Regression analysis of peer influence on adult substance use. This table reports the regression results of peer influence and adult substance use. Peer cohesion is not associated with substance use in adults. Z-statistics are presented in parentheses. Standardized Betas are presented in the third row. *** p<0.01, ** p<0.05, * p<0.1.

	(1)	(2)	(3)
VARIABLES	Smoking	Drinking	Cocaine
Peer_Cohesion	**0.1571**	**0.0353**	**-0.0154**
	(1.45)	**(0.49)**	**(-0.07)**
	0.2925	**0.0416**	**-0.0551**
Teen_Substance	0.6706***	0.5068***	1.0761***
	(5.17)	(6.60)	(2.89)
	1.1892	0.5704	1.3964
Age	-0.0165	-0.0706***	-0.0546
	(-0.47)	(-3.26)	(-0.86)
	-0.1036	-0.2812	-0.6604
Caucasian	0.4744**	0.0908	-0.8791***
	(2.19)	(0.76)	(-3.11)
	0.7717	0.0936	-2.7532
African American	0.7952***	0.0955	-0.7848**
	(3.47)	(0.71)	(-2.20)
	1.1615	0.0885	-2.2058
Female	-1.8104***	-0.3973***	-0.8034***
	(-12.79)	(-5.18)	(-3.48)
	-3.1865	-0.4431	-2.7178
Constant	-2.0844	3.5278***	-0.6791
	(-1.55)	(4.24)	(-0.28)
Observations	3,766	3,774	3,800

We demonstrate significant peer influence on adolescent substance use above. We further investigate peer influence as these respondents transition into adulthood, using longitudinal data from Wave V, administered between 2016 and 2018, when they were between 34 and 41 years old. Table 4 presents the results of a multiple hierarchical logistic regression analysis examining peer influence on adult substance use. While peer influence is significant during adolescence, peer cohesion is not significantly associated with substance use in adulthood. However, the results indicate that Teen_Substance (adolescent substance use) is positively associated with adult substance use. This finding suggests that adolescents who engage in substance use are more likely to continue using substances into adulthood.

Conclusion

Between 2019 and 2020, adolescent substance use deaths rose by a staggering 94%, bringing attention to the roles of peer cohesion and peer substance use exposure as significant contributing factors. According to social learning theory, adolescents are likely to replicate behaviors exhibited by their peers, particularly when those behaviors are socially rewarded. It is expected that adolescents are more likely to mimic their peers' substance use when they have close friends who engage in such behaviors. The results confirm this expectation, showing a positive association between peer substance use exposure and adolescents' substance use.

Regarding the relationship between peer cohesion and substance use, existing research offers competing predictions. Identity-related theories suggest a positive relationship, positing that peer cohesion amplifies the intrinsic rewards of engaging in socially accepted substance use. In contrast, studies on social isolation propose a negative relationship, arguing that stronger peer cohesion reduces social isolation, thereby decreasing the likelihood of substance use. Analysis of the data does not exclusively support one perspective, but it demonstrates that both perspectives are valid, depending on the specific substance being examined. Peer cohesion is positively associated with the use of "soft drugs," which are more socially accepted among adolescents. Conversely, it is negatively related to the use of "hard drugs," which carry a stronger stigma. These findings suggest that the seemingly conflicting expectations from the two research streams can be reconciled by considering the differing social acceptability of various substances. Peer cohesion influences adolescent drug use in contrasting ways. For example, it encourages the consumption of soft drugs due to their social acceptance within peer groups, while simultaneously discouraging the use of hard drugs because of their stigmatized status among adolescents. This dichotomy reflects the complex interplay between peer influence and drug perception in youth social dynamics. Additionally, the findings challenge prevailing stereotypes, showing that African American adolescents exhibit lower rates of substance use compared to their Caucasian counterparts.

This study has several limitations. First, it relied solely on cross-sectional data and only included data from the first wave, in which participants were adolescents. Additionally, contextual factors, such as neighborhood characteristics or socioeconomic status (SES), were neither measured nor controlled for in the analysis. Furthermore, parental substance use was not assessed, which may have either positively or negatively influenced adolescent substance use outcomes.

Acknowledgments

I would like to express my sincere gratitude to Dr. Sunghan Lee at Iowa State University for his invaluable support and guidance in the development and construction of this paper. His assistance was instrumental in helping me comprehend the essential steps involved in creating a research paper and in drawing connections between various studies to my own research. Without his mentorship throughout this process, I would not have gained a comprehensive understanding of how to engage with and contribute to research literature effectively. I would also like to extend my thanks to Dr. Jeong Eun Lee at Iowa State University for her dedicated supervision throughout this process. Her guidance ensured that I remained on the right track and contributed significantly to the successful completion of this paper. Without her support, I would not have been able to fully navigate the complexities of this research endeavor and achieve the desired outcomes.

DOI: 10.36838/IJHSR810.63

References

1. Centers for Disease Control and Prevention (CDC). Mortality trends and patterns: United States, 2022. National Center for Health Statistics, Data Brief No. 522. 2024. https://www.cdc.gov/nchs/products/databriefs/db522.htm.
2. Centers for Disease Control and Prevention (CDC). Notes from the field: Increase in pediatric emergency department visits related to mental health conditions during the COVID-19 pandemic—United States, 2020–2021. MMWR. Morbidity and Mortality Weekly Report 2022;71(50):1654-1656.
3. Burke AR, McCormick CM, Pellis SM, Lukkes JL. Impact of adolescent social experiences on behavior and neural circuits implicated in mental illnesses. Neuroscience & Biobehavioral Reviews 2017; 76:280-300.
4. Destinations. Why teens are more susceptible to drug addiction? Destinations Blog 2024; Sep 2. https://www.destinationsforteens.com/destinations-blog/why-teens-are-more-susceptible-to-drug-addiction.
5. Larsen B, Luna B. Adolescence as a neurobiological critical period for the development of higher-order cognition. Neuroscience & Biobehavioral Reviews 2018; 94:179-195.
6. Lisdahl KM, *et al.* Adolescent Brain Cognitive Development (ABCD) study: Overview of substance use assessment methods. Developmental Cognitive Neuroscience 2018; 32:80-96.
7. Giletta M, Choukas-Bradley S, Maes M, Linthicum KP, Card NA, Prinstein MJ. A meta-analysis of longitudinal peer influence effects in childhood and adolescence. Psychological Bulletin 2021;147(7):719-747.
8. Dishion TJ, Tipsord JM. Peer contagion in child and adolescent social and emotional development. Annual Review of Psychology 2011; 62:189-214.
9. Brechwald WA, Prinstein MJ. Beyond homophily: A decade of advances in understanding peer influence processes. Journal of Research on Adolescence 2011;21(1):166-179.
10. Helms SW, Choukas-Bradley S, Widman L, Giletta M, Cohen GL, Prinstein MJ. Adolescents misperceive and are influenced by high-status peers' health risk, deviant, and adaptive behavior. Developmental Psychology 2014; 50(12):2697-2714.
11. Dishion TJ, Spracklen KM, Andrews DW, Patterson GR. Deviancy training in male adolescent friendships. Behavior Therapy 1996;27(3):373-390.
12. Berger S, Christandl F, Bitterlin D, Wyss AM. The social insectivore: Peer and expert influence affect consumer evaluations of insects as food. Appetite 2019; 141:104338.
13. Blanton H, Köblitz A, McCaul KD. Misperceptions about norm misperceptions: Descriptive, injunctive, and affective "social norming" efforts to change health behaviors. Social and Personality Psychology Compass 2008;2(3):1379-1399.
14. Gibbons FX, Helweg-Larsen M, Gerrard M. Prevalence estimates and adolescent risk behavior: Cross-cultural differences in social influence. Journal of Applied Psychology 1995;80(1):107-121.
15. Prentice DA, Miller DT. Pluralistic ignorance and alcohol use on campus: Some consequences of misperceiving the social norm. Journal of Personality and Social Psychology 1993;64(2):243-256.
16. Sherman LE, Payton AA, Hernandez LM, Greenfield PM, Dapretto M. The power of the like in adolescence: Effects of peer influence on neural and behavioral responses to social media. Psychological Science 2016;27(7):1027-1035.
17. Copeland M, Kamis C. Who does cohesion benefit? Race, gender, and peer networks associated with adolescent depressive symptoms. Journal of Youth and Adolescence 2022;51(9):1787-1797.
18. Watson NA, Clarkson JP, Donovan RJ, Giles-Corti B. Filthy or fashionable? Young people's perceptions of smoking in the media. Health Education Research 2003;18(5):554-567.
19. Noschang C, Lampert C, Krolow R, De Almeida RMM. Social isolation at adolescence: A systematic review on behavior related to cocaine, amphetamine, and nicotine use in rats and mice. Psychopharmacology 2021;238(4):927-947.
20. Aguilar MA, García-Pardo MP, Montagud-Romero S, Miñarro J, Do Couto BR. Impact of social stress in addiction to psychostimulants: What we know from animal models. Current Pharmaceutical Design 2013;19(40):7009-7025.
21. Leung RK, Toumbourou JW, Hemphill SA. The effect of peer influence and selection processes on adolescent alcohol use: A systematic review of longitudinal studies. Health Psychology Review 2014;8(4):426-457.
22. Liu J, Zhao S, Chen X, Falk E, Albarracín D. The influence of peer behavior as a function of social and cultural closeness: A meta-analysis of normative influence on adolescent smoking initiation and continuation. Psychological Bulletin 2017;143(10):1082-1115.

Author

Chloe Lee is a junior at Gilbert High School in Ames, Iowa. She became interested in the connection between social interactions and substance use after observing how peer environments shape teen decision-making. Her research compares two leading theories on social behavior and substance abuse, highlighting the importance of prevention and early intervention. Beyond her academic interests, Chloe is passionate about contributing to her community through volunteer work.

IJHSR
ijhighschoolresearch.org
RESEARCH ARTICLE

Investigating the Quality of Biodiesel Synthesized from Used Cooking Oils

Navaj Nune

Hanford High School, 450 Hanford St, Richland, WA, 99354, USA; navaj.nune@gmail.com

ABSTRACT: Biodiesel, an alternative to fossil-derived diesel, offers numerous advantages and is produced from used oils through a transesterification reaction. In a transesterification reaction, the triglyceride molecules of oil break down into glycerin and three fatty acid esters (biodiesel). This process for generating biodiesel is relatively simple and cost-effective. Biodiesel contains oxygenated species (esters) and variable unsaturation; hence, the cetane numbers technique is commonly used but cannot directly quantify biodiesel quality. In this project, I used a transesterification reaction to produce seven different biodiesels from used oils. My goal in this project was to investigate various characterization analytical tools to analyze biodiesel quality and identify suitable feedstock for producing high-quality biofuel. I used proton NMR measurements to determine the quality of biodiesel. The ratio of ester protons to unsaturation protons was used to estimate the number of double bonds of freshly prepared and air-treated biodiesels. NMR results revealed that the biodiesel derived from restaurant frying oil is stable to oxidation and ranked the best in quality. The kinematic viscosity of biodiesels is between 4.7 and 6.5 at 20 °C. Biodiesels derived from restaurant-used frying oil are rated the best of all biodiesels produced.

KEYWORDS: Energy, Chemical, Alternative Fuels, Biodiesel, Transesterification.

Introduction

Diesel was invented approximately 150 years ago, and modern society relies heavily on it. It is impossible to imagine a day without diesel.[1,2] Do you know there are about 86 million diesel-engine vehicles in the US? According to the US Energy Information Administration (EIA), in 2021, the transportation sector in the US consumed about 47 billion gallons (1.11 billion barrels) of diesel, an average of about 128 million gallons per day, and diesel is commonly used in large vehicles because diesel engines produce more torque than gasoline engines. Diesel has greater compression resistance and stability.[3,4] Therefore, diesel engines are at least 33% more fuel efficient than comparably sized gasoline engines.

In today's world, diesel drives the economy, and we use diesel for everything. Most daily materials must be shipped and moved from place to place in diesel-operated vehicles. Due to international politics, diesel prices have been unpredictable, and regular diesel prices have increased drastically over the last few years. The most significant disadvantage of using traditional diesel is that it leads to environmental issues, including global warming.

To address this issue, researchers have attempted to develop an eco-friendly fuel equivalent to diesel, biodiesel, which is a form of diesel fuel derived from plants, food, or animals.[1,2] Biodiesel produced from various cooking oils can be seen in Figure 1. Something that needs to be understood is that biodiesel does not directly reduce carbon emissions, but can slow overall emissions into the environment, positively influencing climate change. Biodiesel and diesel both will expel carbon-based products into the atmosphere. Still, the key difference is where the carbon source is coming from.[3,4] When diesel burns, carbon that was once trapped underground is released into the atmosphere. On the other hand, when burning biofuels, we are simply recycling carbon through our atmospheric system. Plants absorb the carbon as they grow and then return it to the air when we burn fuel from those plants. Burning biofuels, therefore, does not increase the overall amount of CO_2 in the atmosphere and has the potential to help slow climate change. Biodiesel is superior to diesel because of its renewable nature, and biodiesel has esters; in contrast, fossil-derived diesel has no oxygens (Figure 2). Oxygen in biodiesel enhances ignition properties and ensures total, proper combustion of the hydrocarbons.

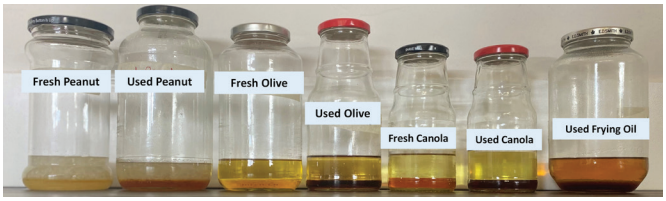

Figure 1: Biodiesels are produced from used cooking oils. The feedstock used to create each biodiesel is specified on labels on the jars. The top visible layer is the biodiesel, and the bottom visible layer is the glycerin.

Although biodiesel came into existence about 30 years ago, due to the diverse nature of the feedstocks (raw materials) and cost, the quantification of biodiesel is still not mature enough, and more work needs to be done.[5] To address this issue, in this project, I investigated the transesterification method for producing and characterizing biodiesel from used cooking oils, an inexpensive feedstock.[6,7] I also studied the factors that influence the quality of biodiesel by using various analytical methods, including Nuclear Magnetic Resonance (NMR).[8] The quality of biodiesel obtained from various cooking oils was qualitatively compared with conventional diesel and identified by the best feedstock for producing the best biodiesel.[3,4,9] I started this

DOI: 10.36838/IJHSR810.69

project with the hypothesis that the biodiesel made from olive oil would be better than that produced from other feedstocks (frying oil, peanut oil, and canola oil) because it has more saturated hydrocarbon linkages. The structure resembles a regular diesel but contains an additional ester moiety vital to improving combustion.

Fuel	Renewable	Structural Difference	Origin	Limited/ Unlimited	Density/ Viscosity	Freezing Point	Energy Density (MJ/Kg)
Diesel	No	No Ester Hydrocarbon	Fossil	Limited	Relatively Low	Relatively Low	~43*
Bio-Diesel	Yes	Hydrocarbon With Ester	Renewable (Plant Matter)	Unlimited	Relatively High	Relatively High	~39*

* Data based on literature.

Figure 2: Key differences and similarities between diesel and biodiesel. This chart specifies different properties of diesel and biodiesel that are important to compare. The advantages of biodiesel are clear due to its renewability and limitless supply.

In this project, biodiesel was produced using a transesterification approach. Used vegetable oils comprise triglyceride molecules, a combination of fatty acids attached to a glycerol backbone. In the transesterification reaction of used oil, a triglyceride reacts with an alcohol in the presence of a catalyst (sodium hydroxide) to produce a biodiesel mixture and glycerol. I used four different oils that differ in unsaturated fatty acid content to produce different biodiesels that differ in unsaturation. Proton nuclear magnetic resonance (NMR) and density techniques have been used to evaluate the biodiesel quality.

Methods

All cooking oil materials used in this project were purchased from local grocery stores. Methanol and sodium hydroxide were from Sigma Aldrich.

For the creation of biodiesel, the following materials were used: canola oil (150 mL), used canola oil (150 mL), oil from a restaurant [highly used frying oil blend] (150 mL), peanut oil (150 mL), used peanut oil (150 mL), fresh olive oil (150 mL), used olive oil (150 mL), methanol, sodium hydroxide (NaOH), glass jars.

Transesterification:

In this project, I used a transesterification reaction (Figures 3, 4) in which methanol and the catalyst sodium hydroxide were used to perform transesterification on used and fresh cooking oils.[10,11] Oils contain triglyceride molecules, which are esters of three fatty acids linked to glycerol. When alcohol, such as methanol, is introduced and reacts with triglyceride in the presence of a base such as sodium hydroxide (catalyst), the fatty acids (saturated, unsaturated, and polyunsaturated) break away from the glycerin as methyl esters and become the biodiesel (Figures 4, 5).[12] The glycerol, NaOH, and other waste products solidify at the bottom, making the biodiesel easily accessible at the top. The key difference in the feedstocks used is the amount of oil saturation. Saturated fats and oils contain only single bonds, and upon transesterification, they yield biodiesels resembling diesel.[11] On the other hand, some of the oils used contain monounsaturated fatty acids that contain one double bond and polyunsaturated fatty acids that contain more double bonds between carbon atoms, which are not present in diesel.

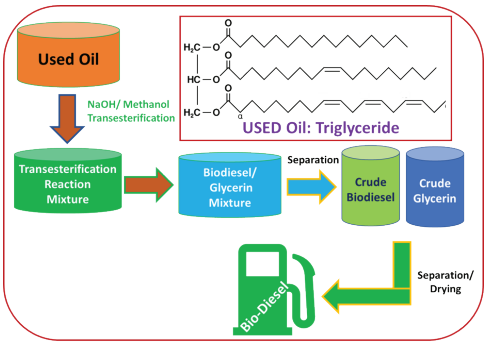

Figure 3: Experimental setup for producing biodiesel. The method of producing usable biodiesel from the feedstock of used oil is outlined. A chemical diagram of a molecule of crude oil is also shown. The black is the glycerol part, while the blue chains become the biodiesel.

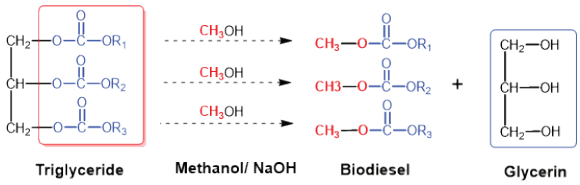

Figure 4: Illustration of the transesterification reaction. *R1, R2,* and *R3* are representatives of 3 different carbon chains. These figures illustrate the reaction that creates the biodiesel and glycerin molecules.

Procedure for Producing Biodiesel:

To the contaminant-free fresh or used cooking oil (150 mL) in a glass jar was added a freshly prepared clear solution comprising 33 mL of methanol and 1.05 g of NaOH. A clear solution of methanol and NaOH was obtained by continuous stirring using a magnetic stir bar. After the addition, the final mixture was vigorously shaken for 5 min to initiate the transesterification process. The resulting two-phase solution was allowed to sit for about 48 hours (2 days) to complete the transesterification reaction. The biodiesel (methyl esters) formed are on the top layer, and glycerin, a transesterification by-product, is at the bottom of the jar. This process was repeated the same way for all seven different feedstock cooking oils, ensuring biodiesel production from each.

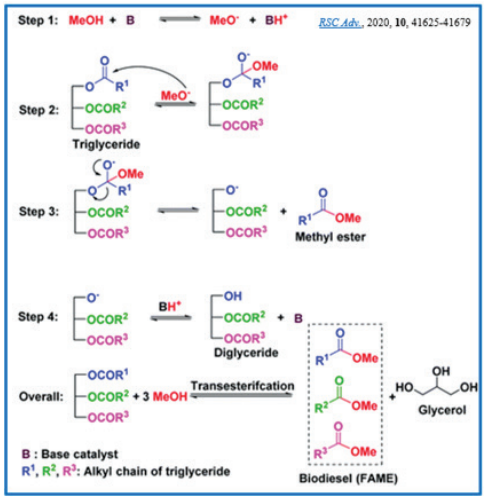

Figure 5: Detailed outline of the chemical reaction for obtaining biodiesel. This figure portrays the steps taken to convert the triglycerides from the oil into biodiesel.

Procedure for Conducting Flash Point and Carbon Residue Tests:

The open cup method determined the flash point and carbon residue test. For each Biofuel, one measurement of the flash point was made. In the case of biodiesel-derived canola oil, two measurements were made to validate the measurements. Biodiesel samples of known weight were placed in an evaporating crucible on a hot plate with a heating ramp rate of 10 ˚C/ min. The flame source was placed above the evaporating crucible; when the biodiesel reached the flash point, a flash occurred, called the flash temperature. The biodiesel was allowed to burn until it was entirely consumed. The weights of the evaporating crucible were compared before and after to determine the carbon residue.

Procedure for Oxidation Stability Tests:

Oxidation stability tests of biodiesels were conducted to test the stability of the biodiesels to air at room temperature and high temperature. The biodiesels were kept in the air for three days for room temperature oxidation stability tests. NMR analyzed the samples to compare ester protons to unsaturated protons to determine the number of double bonds that ultimately define the oxidation stability of biodiesels. For high-temperature oxidation stability tests, the biodiesels were heated at 75 ˚C for 2 hours, and samples were allowed to cool to room temperature. The methanol contaminant was also removed by heating the biodiesel. The samples were analyzed by NMR (Nuclear Magnetic Resonance) to compare ester protons to unsaturated protons.

Procedure for Conducting Copper Corrosion Test:

For the corrosion test, a specific number of strips of copper metal were placed in biodiesels and allowed to be in contact with them for seven days. The weight of the metal before and after it was put in the biodiesel was checked to see if there was any corrosion after seven days. If there is corrosion, metal oxide will form on the copper's surface, and the metal's weight will increase after corrosion.

Procedure for Conducting Viscosity Tests:

A Lovis 2000 ME Viscometer was used to measure the viscosity tests. The density of the biodiesel is used to measure kinematic viscosity. Kinematic viscosity is a measure of the resistance to flow of a fluid under the influence of gravity.

Procedure for Conducting NMR Test:

An Anasazi Instruments EFT-90 MHz NMR spectrometer was used to measure the NMR of all biodiesels. About 400 microliters of CDCl3 with TMS standard and 400 microliters of biodiesel were added to the NMR, and NMR measurements were obtained.

■ Results and Discussion

Risk and Safety:

For my experiments, I worked with various fresh and used oils. I also used methanol and sodium hydroxide as catalysts for the transesterification reaction. Proper protective equipment, like gloves, lab coats, and goggles, was used while experimenting. Many precautions were taken to prevent spills or mistakes by doing the reactions in a safe, secure space where spills can be cleaned up rapidly and not disturbed when stored. In the process, the mixing of the two solutions was done in a glass jar. One last potential hazard is the flammability of the substances being made and tested. The biodiesel flash point is high, and it was stored in safe locations to ensure that it would never reach a point of combustion when not desired. Carbon residue and flash point tests were conducted in a laboratory hood at Columbia Basin College (CBC), WA. All waste (used oil, biodiesel, glycerol, sodium hydroxide, and methanol) was disposed of appropriately.

Data Analysis:

The following feedstock (oil) parameters influence the overall quality of the biodiesel derived after transesterification. The parameters are:

1. Carbon chain length in fatty acids (8 to 22 carbons long)
2. Amount of unsaturation or the number of double bonds in fatty acids (saturated, monounsaturated, polyunsaturated)
3. Location of unsaturation in fatty acids
4. Simple triglycerides (made up of the same three fatty acids) vs. mixed triglycerides (made up of different fatty acids).

Because of these variations, the biodiesel derived from these diverse feedstocks can be very different from the actual structure of diesel. Some of these properties favor ignition characteristics, but some do not. Therefore, quantifying the combustive properties of these biodiesels remains a huge issue today.

Cetane numbers are currently considered the gold standard for quantifying the quality of fossil diesel (Figure 6).[13] The cetane number is measured using a scale that reflects auto-ignition properties. The cetane number scale is based on the auto-ignition characteristics of two reference fuels.[14-16] Hexadecane ($C_{16}H_{36}$) with spontaneous autoignition property is assigned a cetane rating of 100. Heptamethylnonane ($C_{16}H_{34}$) has a much lower autoignition property and is rated 15.

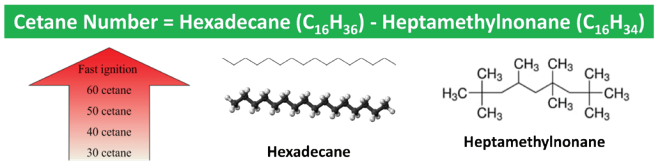

Figure 6: Illustration of Cetane number. The figure displays what the cetane number is and how it can be calculated. The higher the cetane number, the faster the ignition.

However, determining cetane numbers is an intense, challenging, and expensive process involving high-end equipment in highly controlled environments. More importantly, the cetane number heavily relies on the property of hexadecane, which is one of the ingredients in biodiesel. Because the amount and nature of fatty acids differ in different oils, the structural and functional properties of biodiesels derived from these feedstocks differ significantly from oil to oil or between batches (Figure 7).[17] Therefore, determining the cetane numbers may not be sufficient to quantify the quality of the

DOI: 10.36838/IJHSR810.69

biodiesels derived from different feedstocks. Due to the vast structural and functional variation that occurs due to the nature of fatty acid characteristics of the feedstocks, it is hard to narrow down the quality based on one technique alone, such as the cetane number.

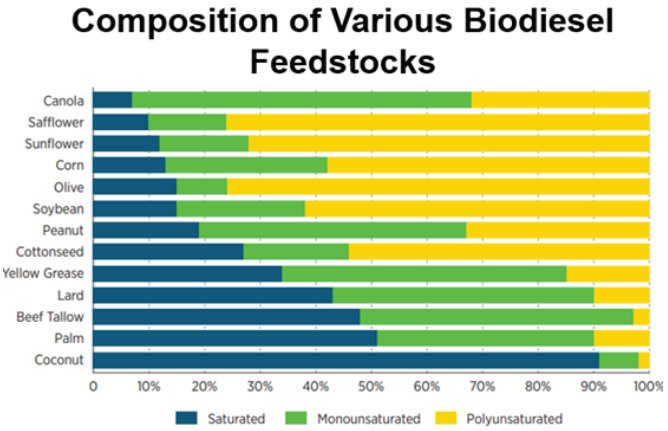

➢ **Biodiesel feedstock has significant differences in saturation to unsaturation.**

Figure 7: Composition of various biodiesel feedstocks. The figure outlines the different levels of saturation present in different feedstocks. The different proportions will affect the quality of the biodiesels.

In this science fair project, I attempted to utilize commonly available characterization methods and analytical tools to assess the quality of biodiesel qualitatively.[18] These methods and tools include Infrared Spectroscopy (IR), Nuclear Magnetic Resonance spectroscopy (NMR), density, freezing point, flash point, carbon residue, corrosion test, oxidation stability, and viscosity measurements (Figure 8).[17,18]

DOE Requirements for 100% Biodiesel (B100)

Property	ASTM Limits	Units
Flash Point	130	°C
Methanol	0.2	% Mass
Water	0.05	% Volume
Sulfur	0.02	% Mass
Cetane	47	
Carbon Residue	0.05	mg/g
Acids	0.8	% Mass
Glycerin	0.24	% Mass
Phosphorus	0.001	% Mass
Distillation Temperature	360	°C

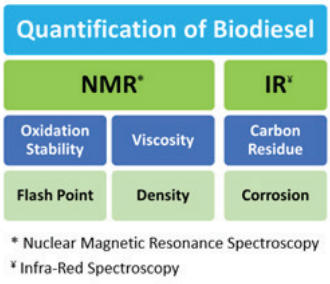

Figure 8: The requirements set by the US Department of Energy (DOE) for commercially usable Biodiesel. The table on the right specifies the exact tests that I ran.

NMR is an analytical chemistry technique used primarily in quality control and research to determine a sample's content and molecular structure. I utilized the NMR characterization to verify the spectral variations in the unsaturated and esters region of different synthesized biodiesels.[8,19] The NMR spectra have offered excellent information and guidance on the presence of saturation and unsaturation in biodiesel (Figure 9).[20] I also utilized Infrared Spectroscopy (IR) to understand the presence of unsaturation in biodiesels. The C- H and C=C stretching peaks in the IR of different biodiesels offered insights into unsaturation in biodiesel. On the other hand, regular diesel is entirely composed of saturated carbons, meaning the molecule has only single bonds (C-C) and no double bonds.

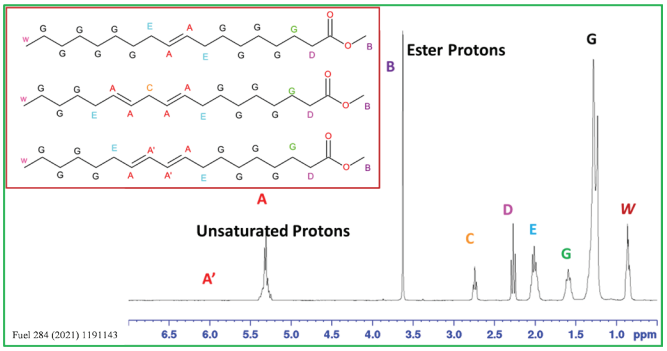

Figure 9: Sample proton NMR of sample biodiesel. These figures demonstrate how I analyzed the NMR of the biodiesels to determine their quality.

To compare the properties of biodiesels with regular diesel, I also performed density experiments that provided some insights into the flow properties. The effect of freezing temperatures on different biodiesels was also tested by keeping the samples outside overnight. The viscosity of cold biodiesel was tested to see if it could withstand the cold temperatures as much as diesel. Interestingly, the biodiesel derived from three different feedstocks has different freezing points and viscosity properties. However, regular diesel has a very low freezing point; it does not freeze under the same conditions.

I also investigated many other physical attributes, including the carbon residue of the biodiesel, to verify the safety qualifications and ensure the synthesized biodiesel meets the Department of Energy's (DOE's) specifications requirements for biodiesel. I conducted flash point testing to determine at what temperature the different biodiesels are ignitable in a controlled environment under expert supervision. This is important because flash points of biodiesel below room temperature will be more hazardous. I also conducted oxidation stability experiments on biodiesels because their double bonds oxidize due to their high reactivity with oxygen in the atmosphere. Additionally, I conducted viscosity measurements of seven biodiesels at room temperature and performed viscosity measurements of the best biodiesel at high temperatures. Viscosity measurements are critical because highly viscous fuels often produce large spray droplets on injection during combustion, resulting in poor performance. I also conducted corrosion resistance experiments on copper to determine the impact of biodiesel on metals. All the above-discussed tests have been performed to investigate whether biodiesel synthesized from used oils meets the requirements set by the DOE.

Findings and Analysis:

Proton NMR analysis was used to quantify the ratio of unsaturated protons to ester protons. Figure 9 illustrates the sample NMR of biodiesel, which provides insight into NMR analysis to understand what peaks represent different protons and carbons to analyze structural properties such as double bonds (unsaturation) and esters.

The amount of unsaturation from the proton NMR spectra can be used to evaluate the quality of different biodiesels (Figures 10, 11).[18] It is reported that biodiesels with mono-unsaturated fatty acids (MUFAs) and an ester in a 1:1 ratio generally offer higher cetane numbers.[21] This means only one double bond for every hydrocarbon chain with one ester. Since every triglyceride produces three separate hydrocarbon chains after the transesterification process, each with an ester (3 Protons), I used this information in my NMR analysis. I compared the ratio of ester to unsaturated protons to rank the biodiesel by quality.[21] Biodiesels with higher unsaturation tend to have better cold flow properties and faster ignition rates, which result in better engine performance.[8]

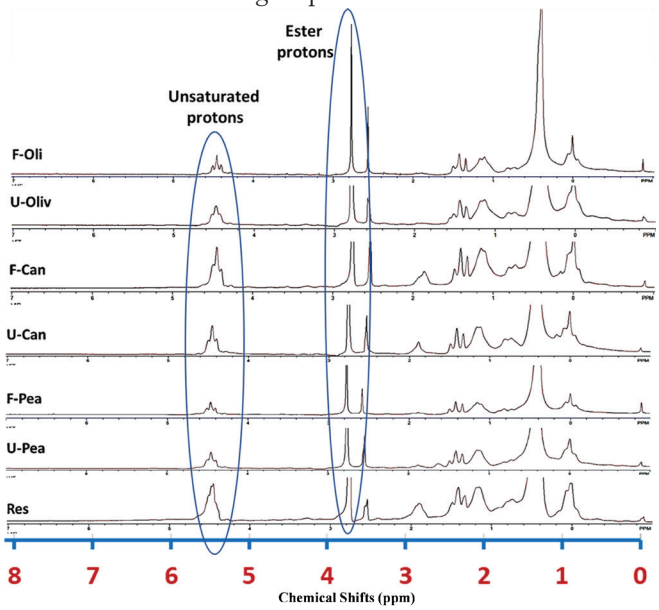

Figure 10: Stacked proton NMR of all freshly synthesized biodiesel samples. It provides a relative number of electrons with similar frequencies, which can be used to calculate the # of esters to the # of unsaturated protons ratio.

Biodiesel	Unsaturation Proton's	Ester Proton's	Ester/ Unsaturation	# of Unsaturated Protons*	# of Double Bonds*	Ranking of Bio-Diesel Quality
BD-F Canola	0.17	0.12	0.71	12.75	6.38	3
BD- U Canola	0.18	0.13	0.72	12.46	6.23	2
BD-F Olive	0.22	0.09	0.41	22.00	11.00	6
BD-U Olive	0.18	0.07	0.39	23.14	11.57	7
BD-F Peanut	9.32	4.92	0.53	17.05	8.52	5
BD- U Peanut	0.19	0.1	0.53	15.55	7.77	4
BD-U Restaurant	0.2	0.17	0.85	10.59	5.29	1

* In every 3 fatty acids, esters (biodiesel molecules) derived from a Triglyceride

Figure 11: Analysis of proton NMR of biodiesel samples. The table shows the calculations for understanding the saturation level of all the biodiesels tested. Biodiesel from used restaurant oil performed the best.

Oxidation stability tests were performed by exposing the samples to air for three days (Figures 12-14). I further tested the oxidation stability by heating the biodiesel at 75 ˚C for 2 hours.[22-24] NMR analysis was performed on all the samples to compare the ester proton to unsaturation proton ratio in the three conditions (fresh, air, heated). Biodiesel derived from highly used restaurant oil has the highest oxidation stability, showing the least change in all three conditions tested. The biodiesels derived from fresh and used olive oils have the least oxidation stability.

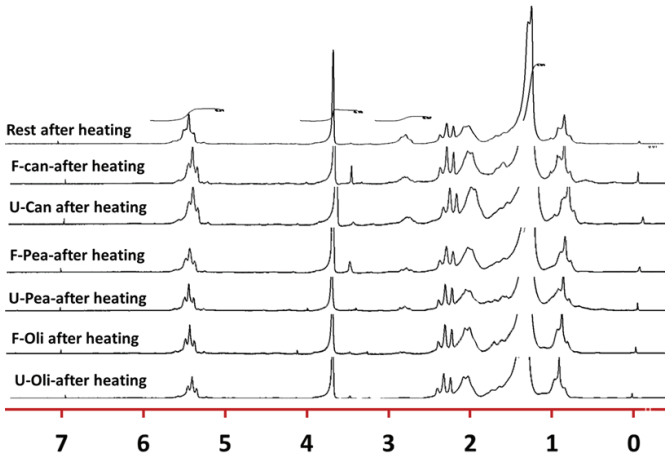

Figure 12: NMR spectra of all heat-treated biodiesel samples (oxidation stability). This can be used to determine which biodiesel is the most stable by comparing it with the NMRs of raw samples.

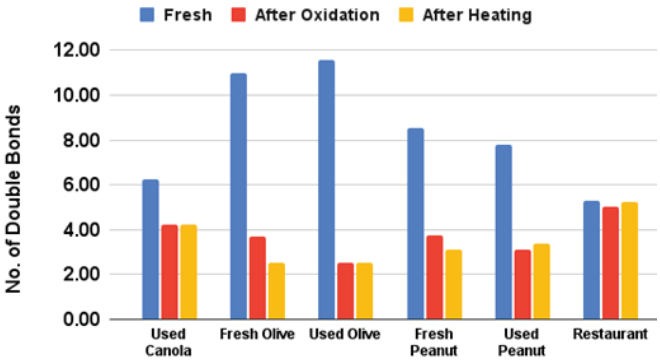

Figure 13: Oxidation stability of biodiesels. This graph proves that biodiesel from used restaurant oil is the most stable due to the least change from fresh to after oxidation and heating.

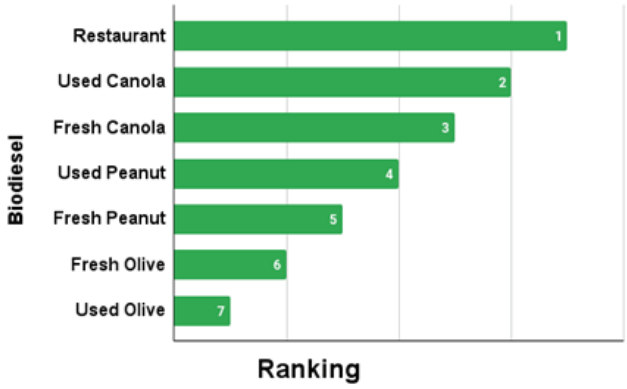

Figure 14: Ranking of produced biodiesels based on Oxidation stability.

The DOE recommended range for kinematic viscosity is 4-6 at 40 ˚C. Biodiesels synthesized in this project have DOE-specified kinematic viscosity between 4-6.[25, 26] Temperature affects viscosity. As the temperature increased, overall viscosity decreased. The viscosity difference between biodiesel and fossil diesel becomes much smaller at high temperatures. At 60 ˚C, the kinematic viscosity is 2.8 (Figures 15-17).

DOI: 10.36838/IJHSR810.69

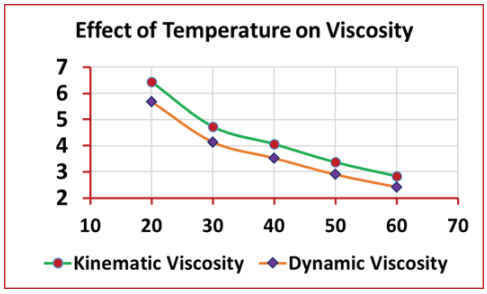

Figure 15: Temperature effect on biodiesel viscosity. This graph shows how the viscosity of biodiesels, on average, reduces as temperature increases.

Figure 16: Image of a viscometer, an instrument used to measure viscosity.

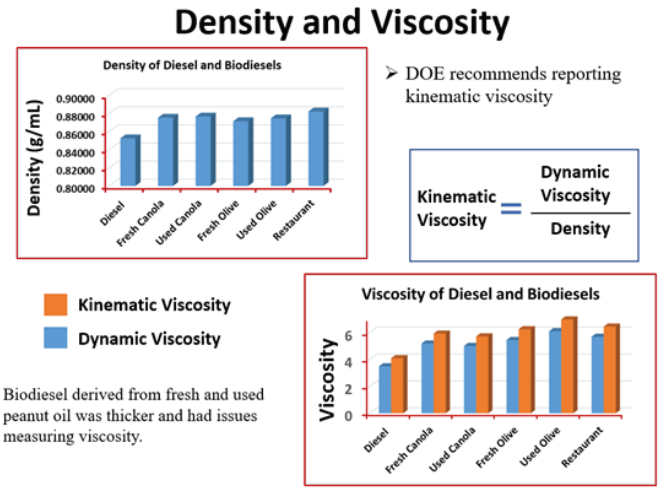

Figure 17: Density and viscosity measurements for the biodiesel samples compared to diesel.

The flash point is the lowest temperature at which the vapors of biodiesel will ignite. The flash point of biofuels is important for understanding safety-related fuel processing, transportation, and storage properties. Biodiesel derived from fresh olive oil has the lowest flash point. Biodiesel derived from highly used oil from restaurants has the highest flash point. The higher the flash point, the less flammable the liquid. The flash point of biodiesel derived from highly used restaurant oil is the highest (199.5 °C), and that of fresh olive oil is the lowest (133.2 °C) (Figure 18). Using an open cup method, the amount of carbon residue obtained for biodiesels aligns with what is expected for diesel (Figure 19).

Property	ASTM Limits	Units	Diesel	BD-F-Canola	BD-U-Canola	BD-F-Peanut	BD-U-Peanut	BD-F-Olive	BD-U-Olive	BD-R-Rest
Flash Point	130	°C	85	148.7	180.3	149.6	161.5	133.2	146.7	199.5

Figure 18: Flash point testing experimental setup and results. This shows the stability of the biodiesel and whether it meets the ASTM limit.

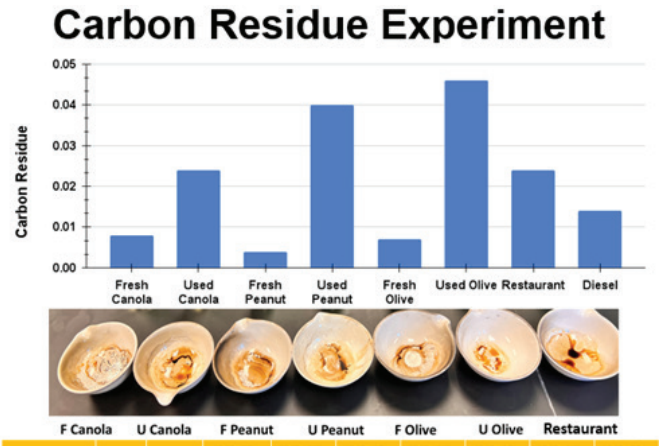

Property	Units	Diesel	BD-F-Canola	BD-U-Canola	BD-F-Peanut	BD-U-Peanut	BD-F-Olive	BD-U-Olive	BD-R-Rest
Carbon Residue	g	0.014	0.008	0.024	0.004	0.04	0.007	0.046	0.024

Figure 19: Carbon residue test results. This shows the visible results and the mass of the carbon residue after testing. This test is done to determine safety and waste consumption.

Conclusion

I used a transesterification reaction to produce seven different biodiesels from several fresh and used oils in this project. Feedstock oils are diverse and contain different amounts of unsaturation and hydrocarbon chain length. Due to this, the biodiesel derived from these various oils is different from the actual structure of diesel. Although some of these characteristics favor ignition properties, some do not, making it very challenging to quantify the combustion properties of biodiesels. Biodiesel contains oxygenated species (esters) and unsaturation, so the cetane number, currently considered the gold standard for quantifying the quality of fossil-derived diesel, cannot be directly used to quantify biodiesel quality. I used non-destructive methods such as Infrared Spectroscopy (IR), Nuclear Magnetic Resonance spectroscopy (NMR), density, and freezing measurements to assess the quality of biodiesel. From NMR data, I compared the ratios of ester protons (fixed at 9 per chain) to unsaturated protons (varying per chain) to determine the amount of unsaturation. Out of seven biodiesels produced in this project, biodiesel derived from highly used frying oil is closest to a monounsaturated fatty acid ester with a 1:1 ester to double bond ratio. Biodiesels with about one double bond (unsaturation) per chain tend to have better cold flow

properties and faster ignition rates, which results in better engine performance.

Biodiesel derived from highly used restaurant oil has the highest oxidation stability, as it showed the least change in all three conditions tested (freshly synthesized, oxidized by air, and heated in air). Biodiesels synthesized in this project have a kinematic viscosity in the range of 4–6 as specified by US-DOE. As the temperature increased, overall viscosity decreased, and the viscosity difference between biodiesel and fossil diesel became much smaller at high temperatures (at 60 °C). The flash point of biodiesel derived from highly used restaurant oil is the highest (199.5 °C), and fresh olive oil has the lowest (133.2°C). The amount of carbon residue obtained for biodiesels using an open cup method is in line with that of diesel.

My experimental data and analysis revealed that used frying oil from restaurants yielded the highest quality biodiesel. This is likely because restaurant frying oil has already undergone many cycles of heating, which can reduce the polyunsaturated bonds and increase the proportion of more stable monounsaturated fatty acids. As a result, the resulting biodiesel contains a better ester-to-unsaturation ratio, giving it higher oxidation stability, improved ignition properties, and overall making it have superior fuel quality. These results proved that my hypothesis that olive oil would be the best feedstock was wrong. NMR analysis offered insights into carbon structure and oxidation stability by using the number of double bonds per ester to quantify biodiesel quality. With further optimization, these tests and analysis methods can produce biodiesel that meets industry quality standards. My results show that using biodiesel derived from restaurant oil could be a viable alternative to diesel. This can have many environmental and economic benefits. Reducing the use of diesel is beneficial to the environment, and using waste cooking oils prevents waste build-up and expensive disposal processes. The conversion to biodiesel is much cheaper. Doing this can have a positive impact on the world.

Acknowledgments

I would like to take this opportunity to thank my chemistry teacher, Mr. Samuel Koch at Hanford High School, for his support with the experiments. I would also like to thank Colin Bradley at Columbia Basin College for his help accessing NMR instruments and David J. Bazak for his help with viscosity measurements.

References

1. Hoekman, S. K.; Broch, A.; Robbins, C.; Ceniceros, E.; Natarajan, M. Review of biodiesel composition, properties, and specifications. *Renew Sust Energ Rev* **2012**, *16* (1), 143-169. DOI: 10.1016/j.rser.2011.07.143.
2. Sajjadi, B.; Raman, A. A. A.; Arandiyan, H. A comprehensive review on properties of edible and non-edible vegetable oil-based biodiesel: Composition, specifications, and prediction models. *Renew Sust Energ Rev* **2016**, *63*, 62-92. DOI: 10.1016/j.rser.2016.05.035.
3. Hassan, T.; Rahman, M. M.; Rahman, M. A.; Nabi, M. N. Opportunities and challenges for the application of biodiesel as automotive fuel in the 21st century. *Biofuel Bioprod Bior* **2022**, *16* (5), 1353-1387. DOI: 10.1002/bbb.2375.
4. Lin, L.; Zhou, C. S.; Vittayapadung, S.; Shen, X. Q.; Dong, M. D. Opportunities and challenges for biodiesel fuel. *Appl Energ* **2011**, *88* (4), 1020-1031. DOI: 10.1016/j.apenergy.2010.09.029.
5. Singh, D.; Sharma, D.; Soni, S. L.; Sharma, S.; Sharma, P. K.; Jhalani, A. A review on feedstocks, production processes, and yield for different generations of biodiesel. *Fuel* **2020**, *262*. DOI: ARTN 11655310.1016/j.fuel.2019.116553.
6. Mendow, G.; Veizaga, N. S.; Sánchez, B. S.; Querini, C. A. Biodiesel production by two-stage transesterification with ethanol by washing with neutral water and water saturated with carbon dioxide. *Bioresource Technol* **2012**, *118*, 598-602. DOI: 10.1016/j.biortech.2012.05.026.
7. Fukuda, H.; Kondo, A.; Noda, H. Biodiesel fuel production by transesterification of oils. *J Biosci Bioeng* **2001**, *92* (5), 405-416. DOI: DOI 10.1263/jbb.92.405.
8. Doudin, K. I. Quantitative and qualitative analysis of biodiesel by NMR spectroscopic methods. *Fuel* **2021**, *284*. DOI: ARTN 11911410.1016/j.fuel.2020.119114.
9. Silitonga, A. S.; Masjuki, H. H.; Mahlia, T. M. I.; Ong, H. C.; Chong, W. T.; Boosroh, M. H. Overview properties of biodiesel diesel blends from edible and non-edible feedstock. *Renew Sust Energ Rev* **2013**, *22*, 346-360. DOI: 10.1016/j.rser.2013.01.055.
10. Meher, L. C.; Sagar, D. V.; Naik, S. N. Technical aspects of biodiesel production by transesterification - a review. *Renew Sust Energ Rev* **2006**, *10* (3), 248-268. DOI: 10.1016/j.rser.2004.09.002.
11. Salaheldeen, M.; Mariod, A. A.; Aroua, M. K.; Rahman, S. M. A.; Soudagar, M. E. M.; Fattah, I. M. R. Current State and Perspectives on Transesterification of Triglycerides for Biodiesel Production. *Catalysts* **2021**, *11* (9). DOI: ARTN 1121 10.3390/catal11091121.
12. Changmai, B.; Vanlalveni, C.; Ingle, A. P.; Bhagat, R.; Rokhum, L. Widely used catalysts in biodiesel production: a review. *Rsc Adv* **2020**, *10* (68), 41625-41679. DOI: 10.1039/d0ra07931f.
13. García-Martín, J. F.; Alés-Alvarez, F. J.; López-Barrera, M. D. C.; Martín-Domínguez, I.; Alvarez-Mateos, P. Cetane number prediction of waste cooking oil-derived biodiesel prior to transesterification reaction using near infrared spectroscopy. *Fuel* **2019**, *240*, 10-15. DOI: 10.1016/j.fuel.2018.11.142.
14. Ardabili, S. F.; Najafi, B.; Shamshirband, S. Fuzzy logic method for the prediction of cetane number using carbon number, double bounds, iodic, and saponification values of biodiesel fuels. *Environ Prog Sustain* **2019**, *38* (2), 584-599. DOI: 10.1002/ep.12960.
15. Giakoumis, E. G.; Sarakatsanis, C. K. Estimation of biodiesel cetane number, density, kinematic viscosity and heating values from its fatty acid weight composition. *Fuel* **2018**, *222*, 574-585. DOI: 10.1016/j.fuel.2018.02.187.
16. Giakoumis, E. G.; Sarakatsanis, C. K. A Comparative Assessment of Biodiesel Cetane Number Predictive Correlations Based on Fatty Acid Composition. *Energies* **2019**, *12* (3). DOI: ARTN 42210.3390/en12030422.
17. Alleman, T L.; McCormick, R.; Christensen, E. D.; Fioroni, G.; Moriarty, K.; Yanowitz, J. Biodiesel Handling and Use Guide (Fifth Edition), **2016**, US. Department of Energy.
18. Knothe, G. Analytical methods used in the production and fuel quality assessment of biodiesel. *T Asae* **2001**, *44* (2), 193-200.
19. Nagy, M.; Alleman, T. L.; Dyer, T.; Ragauskas, A. J. Quantitative NMR Analysis of Partially Substituted Biodiesel Glycerols. *J Biobased Mater Bio* **2009**, *3* (1), 108-111. DOI: 10.1166/jbmb.2009.1004.
20. Doudin, K. I. Quantitative and qualitative analysis of biodiesel by NMR spectroscopic methods. *Fuel* **2021**, *284*. DOI: ARTN119114, 10.1016/j.fuel.2020.119114.
21. Cao, Y. J.; Liu, W.; Xu, X.; Zhang, H. B.; Wang, J. M.; Xian, M. Production of free monounsaturated fatty acids by metabolically

DOI: 10.36838/IJHSR810.69

engineered. *Biotechnol Biofuels* **2014**, *7*. DOI: Artn 5910.1186/1754-6834-7-59.
22. Camur, H.; Al-Ani, A. M. R. Prediction of Oxidation Stability of Biodiesel Derived from Waste and Refined Vegetable Oils by Statistical Approaches. *Energies* **2022**, *15* (2). DOI: ARTN 40710.3390/en15020407.
23. Isah, A. G.; Faruk, A. A.; Musa, U.; Garba, U. M.; Alhassan, M.; Abdullahi, U. B.; Damian, A. T. Oxidation stability and cold flow properties of biodiesel synthesized from castor oil: Influence of alkaline catalyst type and purification techniques. *Mater Today-Proc* **2022**, *57*, 748-752. DOI: 10.1016/j.matpr.2022.02.220.
24. Rajamohan, S.; Gopal, A. H.; Muralidharan, K. R.; Huang, Z. H.; Paramasivam, B.; Ayyasamy, T.; Nguyen, X. P.; Le, A. T.; Hoang, A. T. Evaluation of oxidation stability and engine behaviors operated by biodiesel/diesel fuel blends with presence of synthetic antioxidant. *Sustain Energy Techn* **2022**, *52*. DOI: ARTN 10208610.1016/j.seta.2022.102086.
25. Huang, Y. D.; Li, F. S.; Bao, G. R.; Wang, W. C.; Wang, H. Estimation of Kinematic Viscosity of Biodiesel Fuels from Fatty Acid Methyl Ester Composition and Temperature. *J Chem Eng Data* **2020**, *65* (5), 2476-2485. DOI: 10.1021/acs.jced.9b01127.
26. Kassem, Y.; Gökçekus, H.; Çamur, H. Prediction of Kinematic Viscosity and Density of Biodiesel Produced from Waste Sunflower and Canola Oils Using ANN and RSM: Comparative Study. *Adv Intell Syst* **2020**, *1095*, 880-887. DOI: 10.1007/978-3-030-35249-3_117.

Author

Navaj Nune is a talented, highly motivated junior at Hanford High School, Richland, WA. He is an aspiring Orthopedic surgeon. Navaj plans on studying pre-med-related courses at university to pursue his passion for medicine. Navaj enjoys scientific research and actively engages in its pursuit with high dedication.

IJHSR
ijhighschoolresearch.org
RESEARCH ARTICLE

Thermoelectric Performance of n-Type Argyrodite Ag_8GeTe_6 with Ultralow Lattice Thermal Conductivity and High Mobility Near Room Temperature

Juyoung Chang[1], Runyu Che[2], Beomjun Kim[3], Chaemin Lee[4], Abhijit Debnath[5], Woo Rin Lee*

1. Seoul Foreign School, Seoul, South Korea 03723
2. Gyeonggi Suwon International School, Gyeonggi-Do, South Korea 16706
3. Seoul International School, Gyeonggi-do, South Korea 13113
4. Phillips Exeter Academy, Exeter, NH 03833-2460 USA
5. IEM, Newtown, University of Engineering and Management, Kolkata, India, 700160.
*gosyber1@gmail.com

ABSTRACT: Polycrystalline Ag_8GeTe_6 was synthesized by solid-state melting and spark plasma sintering, and its thermoelectric properties were investigated from 2 to 380 K. X-ray diffraction confirmed a cubic argyrodite structure with high phase purity, while diffuse reflectance spectra indicated a band gap of ~0.45 eV. Transport measurements revealed a semiconducting-to-metallic transition near 244 K. Hall data showed n-type conduction with carrier concentrations ~1017 cm-3 and exceptionally high room-temperature mobility (~3090 cm2 V-1 s-1). The Seebeck coefficient remained negative, reaching −140 μV/K at 380 K, with a power factor of 74 μWm-1K-2. The thermal conductivity was ultralow (0.13–0.33 $W \cdot m^{-1} \cdot K^{-1}$), dominated by a nearly temperature-independent lattice term arising from disordered Ag cations, consistent with phonon liquid–electron crystal behavior. Heat-capacity analysis confirmed low-energy Einstein modes consistent with localized vibrations. Compared with previous reports, the n-type Ag_8GeTe_6 synthesized in this work exhibits enhanced thermoelectric performance, achieving a maximum ZT of 0.10 at 380 K—approximately twice the previously reported value—due to the synergistic combination of ultralow lattice thermal conductivity, exceptionally high carrier mobility, and reduced electrical resistivity.

KEYWORDS: Materials Science, Thermoelectric Materials, Argyrodite Ag_8GeTe_6, Ultralow Lattice Thermal Conductivity, High Carrier Mobility.

Introduction

The study of thermoelectric (TE) materials has advanced quickly due to the global call for sustainable and environmentally friendly energy sources. TE materials can directly convert thermal gradients into electricity and vice versa, without moving parts or harmful emissions.[1] The efficacy of TE materials is commonly expressed by the dimensionless figure of merit, $ZT = (S^2/\rho\kappa)T$, where S is the Seebeck coefficient, ρ is the electrical resistivity, κ is the total thermal conductivity (which includes both electronic, κ_e, and lattice, κ_l, contributions), and T is the absolute temperature.[2] These parameters are strongly attached to the carrier concentration (n). A high S, low ρ, and low κ are required to achieve a high ZT.[3,4] Therefore, strategies that decouple these parameters are essential for further improvement.

Over the past two decades, several new classes of promising TE materials have been developed, such as skutterudites,[5,6] half-Heuslers,[7,8] and clathrates.[9,10] Approaches to increase the power factor (S^2/ρ) include band structure engineering (band convergence[11,12] and band nesting[13,14]) and the introduction of resonant states.[15,16] Methods to reduce κ involve introducing point defects,[17] and nano-inclusions[18] atomic rattlers,[19] complex crystal structures,[20] and soft phonon modes.[21]

Recently, superionic conductors have emerged as attractive TE materials for medium- to high-temperature applications.[22] Among them, Ag- and Cu-based chalcogenides such as Cu_2Se,[23] Cu_2S,[24] Ag_2Se,[25,26] and CuAgSe[27] have been widely investigated. Their low lattice thermal conductivity (κ_l) is the main factor contributing to high ZT, since κ_l is largely independent of other transport parameters. Superionic conductors typically have two distinct structural sublattices: a rigid anion framework and a disordered cation sublattice.[28,29] This exclusive structure allows partial decoupling of charge and phonon transport. The rigid anion network supports high electronic mobility (electron-crystal behavior), while the disordered cations exhibit liquid-like dynamics that strongly scatter phonons, leading to ultralow κ_l.[30,31] Building on the phonon glass–electron crystal perception, this behavior has been described as a phonon liquid–electron crystal feature in disordered superionic conductors.

Ag_8GeTe_6 fits the argyrodite family, with the common formula $A^{m+}{}_{(12-n)/m}B^{n+}X^{2-}{}_6$ (A = Li, Ag, Cu; B = Si, Ge, Sn, and X = S, Se, Te; where m and n are the valence states of A and B).[32] Argyrodites typically adopt orthorhombic, hexagonal, or cubic structures at room temperature, and change to a high-symmetry cubic superionic phase at elevated temperatures.[33] In this phase, A-site cations are mobile and only weakly bonded to the rigid B–X sublattice. Their disordered distribution generates soft phonon modes and intense phonon scattering, resulting in ultralow κ_l.[34] While several groups have studied Se-based

DOI: 10.36838/IJHSR810.77

argyrodites for TE applications, Te-based systems have been much less explored.[28,30,35,36]

Here, we report n-type Ag_8GeTe_6. This compound crystallizes in a cubic phase with the space group $F\bar{4}3m$ above 244 K, and retains the *Fm3m* space group below this temperature.[37] Earlier reports described n-type Ag_8GeTe_6 with high ρ and poor *ZT*, largely due to poor sample density.[38] Subsequent studies by Charoenphakdee *et al.* and Zhu *et al.* demonstrated improved TE properties in p-type Ag_8GeTe_6 at elevated temperatures.[39,40] In the present work, n-type Ag_8GeTe_6 shows improved *ZT* near room temperature because of its ultralow κ_l, reduced ρ, and very high carrier mobility, μ. These results suggest that Ag_8GeTe_6 is a promising argyrodite TE material at room temperature, supported by its characteristic PLEC behavior.

Methods

Polycrystalline Ag_8GeTe_6 was synthesized by the melting method followed by annealing. High-purity elements Ag (shots, 99.99%), Ge (shots, 99.99%), and Te (shots, 99.99%) were weighed according to stoichiometric ratios and sealed in a vacuum quartz tube (~10^{-5} mbar). The sealed ampoule was heated to 1323 K over 12 h, held for 24 h, and then cooled to 873 K, where it was annealed for 72 h. The annealing stage was essential to suppress the creation of binary secondary phases. The obtained ingot was cleaned with sandpaper, ground into powder with an agate mortar and pestle, and then loaded into 10 mm graphite dies for spark plasma sintering (SPS211-LX, Dr. Sinter Lab). Sintering was carried out under ~10^{-3} mbar vacuum at 693 K for 5 min under a pressure of 45 MPa, yielding dense cylindrical pellets. The theoretical density of Ag_8GeTe_6 (7.02 g·cm^{-3}) was calculated from the refined lattice parameter (a = 11.5604 Å) and the crystallographic formula units per unit cell. The measured density (6.70 g·cm^{-3}, Archimedes method) corresponds to ~95.4% of the theoretical density. The density (*d*) of the sintered samples was determined using Archimedes' method. Polished specimens were cut for electrical and thermal transport measurements.

Phase purity and crystal structure were studied by X-ray diffraction (XRD, Rigaku Smartlab) in Bragg–Brentano geometry with Cu Kα radiation (λ = 1.5406 Å). Microstructure and chemical composition were characterized by field emission scanning electron microscopy with energy-dispersive spectroscopy (FESEM, Nova Nano SEM-450, JFEI, USA). Optical diffuse reflectance spectra were collected using a Cary 5000 UV–Vis–NIR spectrophotometer in the range 600–2400 nm at a scan rate of 600 nm min^{-1} at room temperature. The optical band gap was estimated using the Kubelka–Munk function, $F(R) = \alpha = (1-R)2/2R$, where α and R are the extinction and reflectance coefficients, respectively. Seebeck coefficient (S) and thermal conductivity (κ) were measured simultaneously from 2 to 380 K using the Quantum Design Physical Property Measurement System (PPMS) under helium atmosphere at ~10^{-5} Torr. Measurements were performed in continuous slow-warming mode using the steady-state heat flow method. Electrical contacts were completed with gold-coated copper leads attached by silver epoxy to samples of typical dimensions ~10 × 2 × 2 mm^3. Electrical resistivity (ρ), Hall coefficient (R), and heat capacity were also measured in the PPMS. Heat capacity was determined by the relaxation method using the two-τ model. The Hall carrier concentration (n) and mobility (μ) were calculated from $n = 1/eR$ and $\mu = R/\rho$, where e is the elementary charge.

Results and Discussion

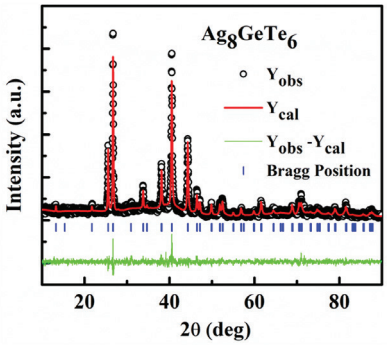

Figure 1: Room-temperature powder X-ray diffraction pattern of Ag_8GeTe_6 with Rietveld refinement. All reflections correspond to a cubic argyrodite structure (space group F$\bar{4}$3m) with no secondary phases detected, confirming high phase purity. The refined lattice parameter (a = 11.5604 Å) agrees with literature values, demonstrating successful synthesis of single-phase n-type Ag_8GeTe_6.

Figure 1 displays the XRD pattern of Ag_8GeTe_6 with a cubic structure (space group F$\bar{4}$3m). All reflections match ICDD card #04-006-4970. The nonappearance of minor peaks is confirmed by Rietveld refinement, and the refined lattice parameter a = 11.5604 Å agrees with previous reports, which indicates high sample purity.[37] The crystal structure of Ag_8GeTe_6 has been studied extensively. It undergoes a first-order, temperature-dependent phase transition near 244 K.[41] The room-temperature phase is cubic, similar to argyrodite compounds such as Cu_8GeSe_6 and Ag_8SiSe_6. The structure can be described as a Te^{2-} framework in which four tetrahedral $[GeTe_4]^{4-}$ units and four Te^{2-} ions fill tetrahedral voids, while Ag^+ cations partially occupy the remaining interstitial sites. Three crystallographically distinct Ag sites are present: 48*h* (0.422, 0.422, 0.223), 48*h* (0.473, 0.473, 0.218), and 96*i* (0.153, 0.445, 0.205), with occupancies of 1.00, 0.504, and 0.113, respectively. This disordered cation arrangement is typical of superionic semiconductors, where Ag ions can drift among partially occupied sites.

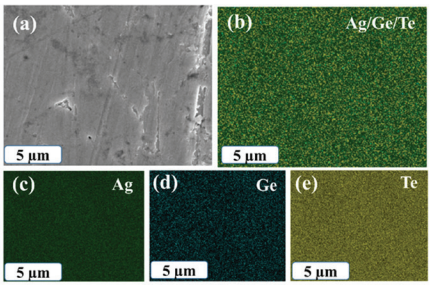

Figure 2: (a) SEM image of the prepared Ag_8GeTe_6 sample. EDS elemental mapping showing (b) combined distribution of all elements, and individual maps of (c) Ag, (d) Ge, and (e) Te. Uniform distribution of Ag, Ge, and Te is evident, and no impurity phases or agglomerations are observed. These results confirm compositional homogeneity and high-quality sample preparation essential for reliable transport measurements.

Figure 2 shows FESEM images and EDX elemental maps (Ag, Ge, Te) of Ag8GeTe6. The polished topmost surface of the bulk pellet appears clean, and the maps indicate uniform distributions of Ag, Ge, and Te with no visible secondary-phase agglomerates. EDX quantification yields an average composition of $Ag_{7.93}(\pm0.04)Ge_{1.00}(\pm0.02)Te_{6.05}(\pm0.06)$, indicating slight Ag deficiency and marginal Te enrichment within experimental uncertainty. This deviation from nominal stoichiometry is consistent with the observed n-type conduction, as Ag vacancies can contribute electron-donor–like behavior and modify carrier density in argyrodite chalcogenides.

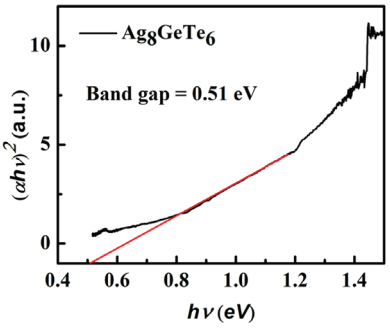

Figure 3: Tauc plot of $(\alpha h\nu)^2$ versus photon energy $h\nu$ for Ag_8GeTe_6 powder at room temperature. The optical band gap is obtained by linear extrapolation of the high-energy region (red line) using the Kubelka–Munk method. The extrapolated band gap of ~0.45 eV agrees with reported values, indicating semiconducting behavior with a narrow gap favorable for thermoelectric performance.

The optical band gap was estimated from the room-temperature diffuse reflectance spectrum (Figure 3). An analysis using $((\alpha h\nu)^2$ vs phonon energy $h\nu$ plot Eg ~0.45E_g eV, which is consistent with Bendorius *et al.*, who reported Eg ~0.43E_geV.[42]

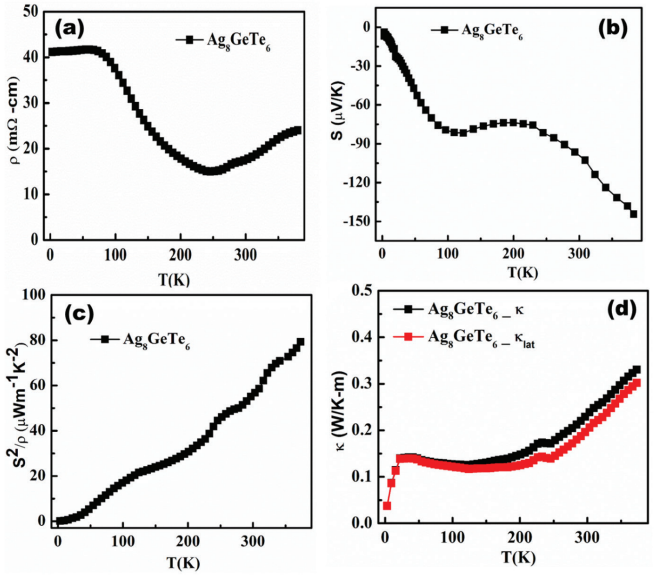

Figure 4: Temperature dependence of (a) electrical resistivity (ρ), (b) Seebeck coefficient (S), (c) power factor (S2/ρ), and (d) total thermal conductivity (κ, black symbols) and lattice contribution (κ_l, red symbols). Ag_8GeTe_6 exhibits a semiconducting-to-metallic transition near 244 K, n-type conduction throughout, and ultralow κ_l of 0.13–0.33 $W{\cdot}m^{-1}{\cdot}K^{-1}$. Together, these properties yield an enhanced power factor and confirm the phonon liquid–electron crystal behavior of the material.

To examine the transport behavior of Ag_8GeTe_6, the temperature dependences of ρ(T), S(T), and κ(T) are shown in Figure 4. The resistivity exhibits semiconducting behavior between 80 and 240 K, with ρ decreasing as T increases. In comparison, a metallic-like trend appears below 80 K. A first-order structural transition at ~240 K produces marked changes in all transport coefficients. As seen in Figure 4(a), ρ(T) shows a metallic-like temperature dependence above 240 K, which we attribute to a reduction in mobility (discussed below). The room-temperature resistivity, $\rho_{300}\sim10^{-2}$ Ω·cm, is higher than that of many state-of-the-art thermoelectrics. Yet, it is about two orders of magnitude less than earlier reports on p-type Ag_8GeTe_6, likely due to differences in stoichiometry and synthesis.

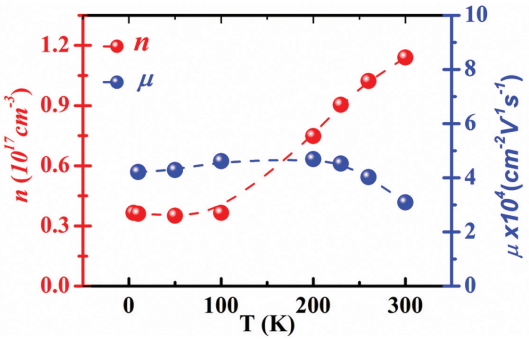

Figure 5: Temperature dependence of Hall mobility (μ) and carrier concentration (*n*) of Ag_8GeTe_6. Negative Hall coefficients confirm n-type conduction, while an exceptionally high room-temperature mobility (~3090 $cm^2{\cdot}V^{-1}{\cdot}s^{-1}$) and low carrier concentration (~10^{17} cm^{-3}) demonstrate decoupled charge and phonon transport. This combination explains the material's low resistivity and high thermoelectric potential.

An activation analysis using the Arrhenius relation between $ln\rho$ and 1/T below the transition (around 100 K) gives an intrinsic gap of approximately 0.023 eV. Hall measurements (Figure 5) show a negative Hall coefficient, indicating electrons as the majority carriers. The carrier concentration increases across the transition and reaches 1.14×10^{17} cm^{-3}, about one order of magnitude lower than previous reports.[40] In contrast, the Hall mobility is exceptionally high; the room-temperature value is μ ~3090 cm^2 V^{-1} s^{-1}, which is among the highest for known thermoelectric materials. This behavior is consistent with an "electron-crystal" response and aligns with room-temperature superionic chalcogenides such as Ag_8SiSe_6 and Ag_9GaSe_6. In the superionic state, the decrease of μ(T) points to enhanced carrier scattering from cation disorder.

The negative Seebeck coefficient S(T) over the whole temperature range designates that electrons are the main carriers, consistent with the Hall data. The n-type behavior of Ag_8GeTe_6 likely arises from a slight Ag deficiency, as suggested by the EDX results. As shown in Figure 4 (b), S(T) increases nearly linearly with temperature up to 120 K and reaches −82 μV/K, which is consistent with extrinsic transport inferred from ρ(T) at low temperature. In the semiconducting regime, S(T) becomes less negative and approaches ~−74 μV/K, which we attribute to a bipolar contribution associated with the small band gap. The onset of this effect is supported by the rise in carrier concentration to $n \sim 0.75\times10^{17}$ cm^{-3} at

DOI: 10.36838/IJHSR810.77

200 K (Figure 5). Above the superionic transition, the magnitude of S(T) increases and reaches −140 μV/K at 380 K. The inset of Figure 4 (c) shows the power factor S^2/ρ, which grows with temperature due to the increasing |S|. At 380 K, the power factor is 74 $\mu Wm^{-1}K^{-2}$, advanced than previous reports at a similar temperature.[39,40]

The total thermal conductivity κ(T) of Ag_8GeTe_6 lies between 0.13 and 0.33 $Wm^{-1}K^{-1}$ over 100 –380 K (Figure 4 (d)). The room-temperature value, κ_{300} = 0.24 $Wm^{-1}K^{-1}$, is markedly lower than that of many state-of-the-art thermoelectrics and most superionic TE chalcogenides. The lattice contribution, κ_l, was obtained by subtracting the electronic term, κ_e, from the total κ using the Wiedemann–Franz relation $\kappa_e = LT/\rho$, where the Lorenz number L was evaluated from the measured Seebeck coefficient using a standard SPB-based expression,[43]

$$L = 1.5 + \exp\left[-\frac{|S|}{116}\right] \quad \text{(Eq. 1)}.$$

At room temperature, κ_l ~0.20 $Wm^{-1}K^{-1}$ after the phase transition, which is lower than values reported for comparable superionic thermoelectrics.[23,44,45] With increasing temperature, κ_l (T) shows a slight rise across the transition and then remains nearly temperature independent up to 380 K. This contrasts with the conventional 1/T trend observed in crystalline solids at high temperature owing to Umklapp phonon scattering. The weak temperature dependence here is consistent with strong cation disorder and liquid-like motion of Ag^+ within a rigid anion framework, a hallmark of superionic systems.[28,30]

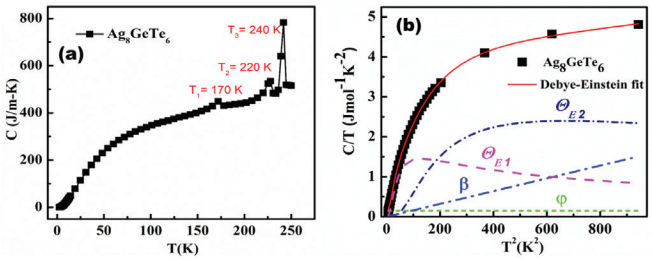

Figure 6: (a) Temperature dependence of heat capacity C(T)) for Ag_8GeTe_6. (b) Plot of C/T versus T^2 in the range 2–30 K. The red solid line shows the Debye–Einstein fit. Separate contributions from the electronic term (ϕ), the Debye term (β), and two Einstein modes (Θ_{E1}, Θ_{E2}) are also shown. The fit reveals two low-energy Einstein modes corresponding to localized Ag vibrations, consistent with a "phonon glass" state. These modes explain the suppressed lattice thermal conductivity and confirm the liquid-like dynamics of Ag^+ cations.

To investigate the source of the glass-like thermal conductivity at low temperature, we measured the heat capacity C(T) from 2 to 250 K (Figure 6 (a)). The C–T curve shows anomalies near ~170, ~220, and ~244 K. The higher-temperature features (~220 and ~244 K) are associated with symmetry changes reported for Ag_8GeTe_6. The weaker anomaly near ~170 K is discussed here as a likely precursor event involving partial ordering or local rearrangement of Ag^+ ions among partially occupied sites, indicating that cation dynamics evolve progressively with temperature. While this lowtemperature feature may subtly influence transport at cryogenic temperatures, the dominant thermoelectric behavior near room temperature is governed by the superionic disorder above the main transition.[41] The transitions ~220–240 K are associated with changes in crystal symmetry. We first fitted the low-temperature data using $C/T = \gamma + \beta T^2$, where γ is the electronic (Sommerfeld) coefficient, and β is the lattice term. The fit yielded a negative γ, which is unphysical. Given the presence of two sublattices, a rigid Ge–Te framework and liquid-like Ag cations, the data are better described by a combined Debye–Einstein model (Figure 6(b)).[46]

$$\frac{C}{T(x)} = \phi + \beta x + A\Theta_{E1}^2 x^{-\left(\frac{3}{2}\right)} \frac{e^{\frac{\Theta_{E1}}{\sqrt{x}}}}{\left(e^{\frac{\Theta_{E1}}{\sqrt{x}}} - 1\right)^2} + B\Theta_{E2}^2 x^{-\left(\frac{3}{2}\right)} \frac{e^{\frac{\Theta_{E2}}{\sqrt{x}}}}{\left(e^{\frac{\Theta_{E2}}{\sqrt{x}}} - 1\right)^2} \quad \text{(Eq. 2)}$$

Here x denotes T^2. The parameter ϕ represents the electronic contribution to the heat capacity, and β is the Debye term arising from acoustic phonons. Θ_{E1} and Θ_{E2} are Einstein temperatures that describe two local vibrational modes, and A and B are their weighting factors. Skutterudite thermoelectrics provide a well-known example of Debye–Einstein specific heat, where filler "rattler" atoms act as Einstein oscillators.[47] Using one Debye and two Einstein terms, the fitted temperature-dependent heatcapacity parameters are summarized in Table S3. The Debye temperature of Ag_8GeTe_6 is estimated as $\theta_D = \left(\frac{12\pi^4 NR}{5\beta}\right)^{1/3}$, where N=15 is the number of atoms per formula unit, and R=8.314 J $mol^{-1}K^{-1}$ is the gas constant. For Ag_8GeTe_6, we obtain θ_D=236 K. The Einstein temperatures are Θ_{E1}=29.24 K (≈2.52 meV) and Θ_{E2}=66.62 K (≈5.74 meV). Similar low-energy modes, often associated with weak chemical bonds, have been reported in skutterudites and other materials with liquid-like cation dynamics.[44] These modes enhance phonon scattering of the acoustic heat carriers and thereby suppress lattice thermal conductivity.

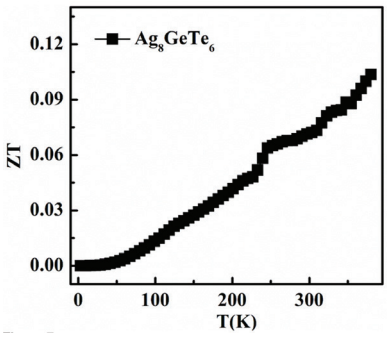

Figure 7: Temperature dependence of thermoelectric figure of merit (ZT) for Ag_8GeTe_6. A maximum ZT value of 0.10 is achieved at 380 K, nearly double previous reports for undoped Ag_8GeTe_6. This improvement arises from the synergy of high carrier mobility and ultralow lattice thermal conductivity, validating the design strategy for enhanced thermoelectric efficiency.

Using the measured ρ(T), S(T), and κ(T), we calculated the thermoelectric figure of merit ZT for Ag_8GeTe_6 (Figure 7). The maximum value is ZT_{max} =0.10 at 380 K, which is about twice the previously reported value for undoped Ag_8GeTe_6. The enhanced room-temperature ZT arises from the higher power factor S^2/ρ together with the very low thermal conductivity.

At room temperature, n-type Ag_8GeTe_6 from this work exhibits S = −101 μV/K, ρ = 0.018 Ω·cm, a power factor S^2/ρ = 56.84 $\mu Wm^{-1}K^{-2}$, κ = 0.24 $Wm^{-1}K^{-1}$, and a Hall mobility μ = 3090 $cm^2\ V^{-1}\ s^{-1}$, yielding ZT=0.074. Prior n-type Ag_8GeTe_6 reported by Fujikane *et al.* shows S = −123 μV/K and ρ = 0.19 Ω·cm, corresponding to a lower power factor of 7.96 $\mu Wm^{-1}K^{-2}$; at 770 K, that study lists κ=0.30 $Wm^{-1}K^{-1}$ and ZT=0.0014.[38] For p-type compositions, Charoenphakdee *et al.* reports S = 519 μV/K, ρ = 1.0 Ω·cm, S^2/ρ = 26.93 $\mu Wm^{-1}K^{-2}$, κ = 0.25 $Wm^{-1}K^{-1}$, and ZT = 0.035[39] while Zhu *et al.* demonstrates S = 580 μV/K, ρ = 1.0 Ω·cm, S^2/ρ = 33.64 $\mu Wm^{-1}K^{-2}$, κ = 0.27 $Wm^{-1}K^{-1}$, μ = 0.028 $cm^2\ V^{-1}\ s^{-1}$, and ZT = 0.037.[40] Compared with these literature values, the present n-type sample combines a much lower resistivity with an ultralow thermal conductivity and very high mobility, which results in the highest room-temperature power factor among the entries and a correspondingly improved ZT.

Conclusion

The structural, optical, and transport studies of Ag_8GeTe_6 demonstrate that this argyrodite compound combines ultralow lattice thermal conductivity with high carrier mobility. The observed phonon liquid–electron crystal characteristics arise from a rigid anion framework and disordered Ag cations, which generate strong phonon scattering and liquid-like dynamics. Compared with earlier reports, the present n-type samples show significantly reduced resistivity, higher power factor, and improved *ZT*, reaching 0.10 at 380 K. Although this *ZT* remains modest compared with state-of-the-art thermoelectrics, the results confirm the potential of Ag_8GeTe_6 as a model system for exploiting cation disorder and low-energy vibrational modes in argyrodite-type thermoelectrics. Future studies should focus on precise control of carrier concentration, Ag-site disorder (cation sublattice tuning), and defect engineering to further enhance the power factor and maximize ZT in Ag_8GeTe_6-based thermoelectric devices operating near room temperature.

Acknowledgments

We want to thank Prof. Woo Rin Lee for supporting this project.

References

1. T. Tritt, *Advances in Thermoelectric Materials I*, Elsevier Science, **2000**.
2. D. M. Rowe, *CRC Handbook of Thermoelectrics*, CRC Press, **1995**.
3. G. J. Snyder and E. S. Toberer, *Nat Mater,* **2008**, *7*, 105-114.
4. A. J. Minnich, M. S. Dresselhaus, Z. F. Ren and G. Chen, *Energy & Environmental Science*, **2009**, *2*, 466-479.
5. X. Shi, J. Yang, J. R. Salvador, M. Chi, J. Y. Cho, H. Wang, S. Bai, J. Yang, W. Zhang and L. Chen, *Journal of the American Chemical Society*, **2011**, *133*, 7837-7846.
6. R. Carlini, A. U. Khan, R. Ricciardi, T. Mori and G. Zanicchi, *Journal of Alloys and Compounds*, **2016**, *655*, 321-326.
7. H. Zhu, R. He, J. Mao, Q. Zhu, C. Li, J. Sun, W. Ren, Y. Wang, Z. Liu, Z. Tang, A. Sotnikov, Z. Wang, D. Broido, D. J. Singh, G. Chen, K. Nielsch and Z. Ren, *Nature Communications*, **2018**, *9*, 2497.
8. H. Zhu, J. Mao, Z. Feng, J. Sun, Q. Zhu, Z. Liu, D. J. Singh, Y. Wang and Z. Ren, *Science Advances*, **2019**, *5*, eaav5813.
9. G. S. Nolas, J. L. Cohn, G. A. Slack and S. B. Schujman, *Applied Physics Letters*, **1998**, *73*, 178-180.
10. X. Shi, J. Yang, S. Bai, J. Yang, H. Wang, M. Chi, J. R. Salvador, W. Zhang, L. Chen and W. Wong-Ng, *Advanced Functional Materials*, **2010**, *20*, 755-763.
11. Y. Pei, X. Shi, A. LaLonde, H. Wang, L. Chen and G. J. Snyder, *Nature*, **2011**, *473*, 66-69.
12. R. Chen, Y. Wang, L. Jiang, R. Min, H. Kang, Z. Chen, E. Guo, X. Yang, X. Jiang and T. Wang, *Materials Today Physics*, **2023**, *30*, 100957.
13. Y. Pei, H. Wang and G. J. Snyder, *Advanced Materials*, **2012**, *24*, 6125-6135.
14. J. Xin, Y. Tang, Y. Liu, X. Zhao, H. Pan and T. Zhu, *npj Quantum Materials*, **2018**, *3*, 9.
15. J. P. Heremans, B. Wiendlocha and A. M. Chamoire, *Energy & Environmental Science*, **2012**, *5*, 5510-5530.
16. L. Wu, X. Li, S. Wang, T. Zhang, J. Yang, W. Zhang, L. Chen and J. Yang, *NPG Asia Mater*, **2017**, *9*, e343.
17. Z. Du, J. He, X. Chen, M. Yan, J. Zhu and Y. Liu, *Intermetallics*, **2019**, *112*, 106528.
18. J. Hwang, J. H. Yun, K. Y. Lee, J.-S. Rhyee, J. Kim, S. Acharya, J. Kim, W. Kim, S. Kim and S.-J. Kim, *Materials Today Physics*, **2023**, *33*, 101053.
19. M. K. Jana, K. Pal, A. Warankar, P. Mandal, U. V. Waghmare and K. Biswas, *Journal of the American Chemical Society*, **2017**, *139*, 4350-4353.
20. A. F. May, E. S. Toberer, A. Saramat and G. J. Snyder, *Physical Review B*, **2009**, *80*, 125205-125201 - 125205-125212
21. S. Acharya, J. Pandey and A. Soni, *Applied Physics Letters*, **2016**, *109*, 133904.
22. S. Acharya, J. Pandey and A. Soni, *ACS Applied Energy Materials*, **2019**, *2*, 654-660.
23. H. Liu, X. Shi, F. Xu, L. Zhang, W. Zhang, L. Chen, Q. Li, C. Uher, T. Day and G. J. Snyder, *Nat Mater*, **2012**, *11*, 422-425.
24. M.-J. Guan, P.-F. Qiu, Q.-F. Song, J. Yang, D.-D. Ren, X. Shi and L.-D. Chen, *Rare Metals*, **2018**, DOI: 10.1007/s12598-018-1007-0.
25. T. Day, F. Drymiotis, T. Zhang, D. Rhodes, X. Shi, L. Chen and G. J. Snyder, *Journal of Materials Chemistry C*, **2013**, *1*, 7568-7573.
26. W. Mi, P. Qiu, T. Zhang, Y. Lv, X. Shi and L. Chen, *Applied Physics Letters*, **2014**, *104*, 133903.
27. X. Wang, P. Qiu, T. Zhang, D. Ren, L. Wu, X. Shi, J. Yang and L. Chen, *Journal of Materials Chemistry A*, **2015**, *3*, 13662-13670.
28. K. S. Weldert, W. G. Zeier, T. W. Day, M. Panthöfer, G. J. Snyder and W. Tremel, *Journal of the American Chemical Society*, **2014**, *136*, 12035-12040.
29. S. Bhattacharya, R. Basu, R. Bhatt, S. Pitale, A. Singh, D. K. Aswal, S. K. Gupta, M. Navaneethan and Y. Hayakawa, *Journal of Materials Chemistry A*, **2013**, *1*, 11289-11294.
30. B. K. Heep, K. S. Weldert, Y. Krysiak, T. W. Day, W. G. Zeier, U. Kolb, G. J. Snyder and W. Tremel, *Chemistry of Materials*, **2017**, *29*, 4833-4839.
31. B. Jiang, P. Qiu, H. Chen, Q. Zhang, K. Zhao, D. Ren, X. Shi and L. Chen, *Chemical Communications*, **2017**, *53*, 11658-11661.
32. W. F. Kuhs, R. Nitsche and K. Scheunemann, *Materials Research Bulletin*, **1979**, *14*, 241-248.
33. B. Jiang, P. Qiu, E. Eikeland, H. Chen, Q. Song, D. Ren, T. Zhang, J. Yang, B. B. Iversen, X. Shi and L. Chen, *Journal of Materials Chemistry C*, **2017**, *5*, 943-952.
34. S. Lin, W. Li, S. Li, X. Zhang, Z. Chen, Y. Xu, Y. Chen and Y. Pei, *Joule*, **2017**, *1*, 816-830.

DOI: 10.36838/IJHSR810.77

35. L. Wen, L. Siqi, G. Binghui, Y. Jiong, Z. Wenqing and P. Yanzhong, *Advanced Science*, **2016**, *3*, 1600196.
36. B. Jiang, P. Qiu, H. Chen, J. Huang, T. Mao, Y. Wang, Q. Song, D. Ren, X. Shi and L. Chen, *Materials Today Physics*, **2018**, *5*, 20-28.
37. F. Boucher, M. Evain and R. Brec, *Journal of Solid State Chemistry*, **1993**, *107*, 332-346.
38. M. Fujikane, K. Kurosaki, H. Muta and S. Yamanaka, *Journal of Alloys and Compounds*, **2005**, *396*, 280-282.
39. A. Charoenphakdee, K. Kurosaki, H. Muta, M. Uno and S. Yamanaka, *physica status solidi (RRL) – Rapid Research Letters*, **2008**, *2*, 65-67.
40. T. J. Zhu, S. N. Zhang, S. H. Yang and X. B. Zhao, *physica status solidi (RRL) – Rapid Research Letters*, **2010**, *4*, 317-319.
41. H. Kawaji and T. Atake, *Solid State Ionics*, **1994**, *70-71*, 518-521.
42. R. Bendorius, A. Iržikevičius, A. Kindurys and E. V. Tsvetkova, *Physica Status Solidi (a)*, **1975**, *28*, K125-K127.
43. H.-S. Kim, Z. M. Gibbs, Y. Tang, H. Wang and G. J. Snyder, *APL Materials*, **2015**, *3*, 041506-041501 - 041506-041505.
44. H. Liu, J. Yang, X. Shi, S. A. Danilkin, D. Yu, C. Wang, W. Zhang and L. Chen, *Journal of Materiomics*, **2016**, *2*, 187-195.
45. L. Li, Y. Liu, J. Dai, A. Hong, M. Zeng, Z. Yan, J. Xu, D. Zhang, D. Shan, S. Liu, Z. Ren and J.-M. Liu, *Journal of Materials Chemistry C*, **2016**, *4*, 5806-5813.
46. I. K. Dimitrov, M. E. Manley, S. M. Shapiro, J. Yang, W. Zhang, L. D. Chen, Q. Jie, G. Ehlers, A. Podlesnyak, J. Camacho and Q. Li, *Physical Review B*, **2010**, *82*, 174301-174301 - 174301-174308.
47. R. P. Hermann, R. Jin, W. Schweika, F. Grandjean, D. Mandrus, B. C. Sales and G. J. Long, *Physical Review Letters*, **2003**, *90*, 135505.

Authors

Juyoung Chang is a student at Seoul Foreign School. His research focuses on materials chemistry and solid-state physics, with a particular interest in the design and synthesis of high-performance thermoelectric compounds for sustainable energy applications.

Runyu Che is a high school researcher from Gyeonggi Suwon International School. He contributed to the structural and optical characterization of argyrodite compounds, with research interests in crystallography and renewable energy materials.

Beomjun Kim studies at Seoul International School. His research focuses on electronic transport and semiconductor materials, with a particular emphasis on mobility optimization in thermoelectric systems.

Chaemin Lee is a student at Phillips Exeter Academy. He participated in the analysis of temperature-dependent transport phenomena and is interested in applying physics and materials science to energy-efficient technologies.

IJHSR
ijhighschoolresearch.org
REVIEW ARTICLE

Migration-Driven Adaptations in Avian Species

Arshi Aggarwal

International School of Beaverton, 7770 SW Blanton St, Beaverton, OR 97078, USA; arshiraleigh@gmail.com

ABSTRACT: Avian migratory flight is one of the most extreme endurance feats in the animal kingdom, requiring highly optimized physiological and cellular systems. This review synthesizes current research to evaluate how migratory pressures have driven adaptations in cellular, musculoskeletal, cardiovascular, and digestive systems in avian species. Details of these adaptations are discussed and compared with those of non-migratory birds to highlight the tradeoffs of traits selected for migration. The role of geographical and migratory constraints in shaping convergent or divergent evolution in avian species is also discussed. Finally, by linking structure, function, and performance, this work proposes a distinct migratory phenotype shaped by ecological pressures and offers insight into avian evolution.

KEYWORDS: Ecology, Avian Biology, Evolution, Migration, Migratory Phenotype.

Introduction

"Bird" (class Aves) is an umbrella term that encompasses more than 10,000 species of warm-blooded vertebrates, distinguishable by their unique feather-covered bodies and lightweight, aerodynamic physiques.[1,2] Their fused skeletal structure and high metabolic rates have enabled them to evolve the most sophisticated flight capabilities in the animal kingdom, supporting an extraordinary ecological and evolutionary diversification of the species.[1,2] Historically, this diversity was even greater, including species now extinct due to natural and anthropogenic causes.[3,4]

Migration is a behavior observed across animal taxa, involving a periodic, large-scale relocation in response to predictable environmental variation.[5] In birds, however, migration represents more than movement alone; it constitutes a coordinated syndrome of behaviors, physiological, and morphological traits that together enable survival under extreme energetic and ecological demands.[6] Migratory movements are often categorized as short-distance when occurring within a continent and long-distance when spanning continents. However, avian migration is best understood as a continuum of migratory distances rather than discrete categories. Along this continuum, short-distance migration likely evolved from local foraging expansions. In contrast, long-distance migration arose across evolutionary timescales through strong selection on genetic, physiological, and behavioral mechanisms that support endurance flight.[7,8]

Zugunruhe (derived from the German words *Zug*, meaning "migration" or "movement," and *Unruhe*, meaning "restlessness") describes a seasonally timed increase in nocturnal activity and agitation that occurs even in captive birds.[9,10] Research on *Zugunruhe* has provided key insights into the endogenous control of migration and established that migratory behavior is partially hardwired and regulated by internal circannual and circadian clocks.[9,10] While the precise migratory triggers are not fully understood, migration is thought to be initiated through the interaction of photoperiod, weather patterns, food availability, and endogenous hormonal signaling.[8,11]

Migratory flight imposes extreme physiological challenges that exert strong selective pressure across multiple biological systems. Sustained flapping requires continuous aerobic ATP production, lipid-based metabolism, and optimized oxygen delivery.[12-15] Birds must accumulate and efficiently mobilize large fat reserves, remodel digestive organs for rapid nutrient assimilation, and maintain muscle performance while minimizing oxidative damage.[14,16,17] Simultaneously, migratory species face tradeoffs between weight reduction and fuel storage, and the need for precise navigation and timing to exploit favorable atmospheric conditions.[18,19] Migratory distances can be extreme, exemplified by the Arctic tern (*Sterna paradisaea*), whose lifetime flight distance has been estimated as equivalent to three round-trips to the moon. Such feats are possible only through highly specialized and finely tuned biological systems that function in concert.[20] Migratory pressures distinguish migration from other forms of movement and necessitate integrated, whole-organism adaptations.

While there is extensive literature focused on individual traits associated with migration, there are relatively few reports examining how these traits are integrated across skeletal, muscular, cellular, cardiovascular, and digestive systems to form a unified migratory phenotype.[14,15] This review builds on earlier foundational work by synthesizing literature across levels of biological organization to frame migration as a distinct phenotype rather than the optimization of isolated traits.

Discussion

Skeletal Adaptations:

Axial Fusion:

Birds have a specialized axial skeleton characterized by extensive vertebral fusion that enhances rigidity and stability during flight, thereby limiting axial deformation and mechanical energy loss during wingbeats.[21,22] While vertebral fusion is a general feature of avian flight anatomy, this trait may be more

DOI: 10.36838/IJHSR810.83

pronounced in species adapted for sustained aerial activity, including many long-distance migrants.[21-24] Fusing multiple vertebrae into a single structure reduces both bone count and the amount of soft tissue and muscle needed to move individual segments.[21,25,26] This structural adaptation likely contributes to reduced body weight and the energy required per wingbeat.[27] In contrast, many non-migratory birds retain greater axial flexibility, which enhances terrestrial maneuverability and perching agility.[23,24,28]

A central component of axial fusion in birds is the synsacrum, a rigid structure formed from the fusion of the thoracic, lumbar, and sacral vertebrae.[29] The synsacrum plays a critical role in stabilizing the trunk and pelvis and in resisting mechanical stress generated from continuous flapping.[30] In addition to stabilizing posture, the synsacrum contributes to a rigid axial framework that indirectly anchors the pectoral girdle, supporting the pectoralis and supracoracoideus muscles.[31,32] In birds adapted for sustained aerial activity, the synsacrum is often elongated and tightly ossified, increasing axial stiffness and reducing the need for continual postural adjustments to maintain stable flight alignment over long distances.[26,29] Together, these features illustrate how skeletal fusion in migratory birds integrates structural stability and muscular support, enabling efficient long-distance flights.

Pneumatized Bones:

All birds have hollow, pneumatized bones, which are lined with spongy, lightweight trabeculae that reinforce the internal walls.[23] Some migratory taxa show increased or strategically redistributed pneumatization in related bones, such as the humerus (upper wing bone), sternum (breastbone), and vertebrae; these bones are also under the most strain during sustained flight.[23,24] A study by Machado *et al.* on avian bone mass distribution confirmed that pneumatization in bones is strategically concentrated in areas to reduce wing loading and optimize energy efficiency, supporting migratory endurance.[27] Another study by Louis *et al.* comparing the skeletons of resident and migratory subspecies of Dark-eyed juncos (*Junco hyemalis*) observed that the humeri of the migratory subspecies were thinner and wider, with a higher geometric stiffness. This feature helps support increased weight during migration. Furthermore, the femora (thigh bone) of the migratory birds were shorter and thinner, with lower geometric stiffness than those of resident juncos, reducing skeletal leg mass.[24] Stiffer wing bones support increased weight associated with migratory fattening and also key flight muscles.[24] Lighter and weaker thigh bones in migratory birds demonstrate an adaptive compromise, reflecting the importance of optimizing essential migratory components.[23,24]

Both the body and cranium of migratory birds show specialized adaptations that enhance flight efficiency, including centralized mass distribution and lightweight skeletal structures.[23,24] This centralization reduces rotational inertia, increasing aerodynamic control during prolonged flights.[24] Furthermore, mass centralization of the avian skull in migratory species demonstrates evolutionary specialization for flight. Migratory birds possess cranial morphologies that differ significantly from those of non-migratory species, with migration being an important predictor of skull shape across a broad comparative sample of birds. In addition, migratory lineages show faster rates of skull shape evolution than non-migratory birds, consistent with directional selection on cranial anatomy associated with long-distance movement.[33] Comparative morphometric work on specific passerines further supports this pattern. Migratory Yellow-breasted bunting (*Emberiza aureola*), resident House sparrow (*Passer domesticus*), and Eurasian tree sparrow (*Passer montanus*) differ in skull and cranial indices, with resident species exhibiting larger cranial indices than the migratory bunting, indicating distinct structural adaptations tied to migratory versus resident lifestyle.[23] In contrast, non-migratory species are more likely to maintain their robust cranial structures due to less evolutionary pressure to adapt to long-distance flight energy efficiency.[23]

While pneumatization decreases bone marrow space and calcium storage capacity, migratory birds compensate for these limitations through increased dietary calcium absorption during breeding or from medullary bone formation in females.[12] Such adaptations reflect an evolutionary tradeoff in which migratory performance is prioritized over skeletal mineral storage, highlighting the skeletal system's role as a flight-specialized structure.

Appendicular Modifications:

The appendicular skeleton of migratory birds (legs and wings) has undergone evolutionary refinement to ensure endurance and efficiency.[24,34-37] Wing morphology is an excellent example of this evolution. A comparative study of Eurasian barn swallows (*Hirundo rustica*) revealed that populations with the longest migrations had longer and more pointed wings than resident or short-distance counterparts in Israel and Spain.[36] These adaptations reduce drag and enhance the lift-to-drag ratio, allowing for greater energy conservation over long flights. This study also found that wingtip concavity, a measure related to aspect ratio (the ratio of wing length to wing width), did not differ significantly between short-distance and long-distance migrants.[36] This suggests that migratory adaptations target traits with the greatest payoff for endurance while other features remain stable, possibly due to biomechanical constraints or the need to preserve maneuverability.

More broadly, migratory birds typically have a higher wing aspect ratio (wingspan^2/wing area) in comparison to resident birds.[34] A higher aspect ratio signifies longer and narrower wings, enhancing endurance and energy efficiency while reducing drag.[34] This contrasts with the shorter and rounder wings of resident birds, which allow for quick takeoffs and maneuverability desirable for more frequent and shorter flights. Additionally, migratory birds typically have lower wing loading (weight/wing area) than resident or short-distance migratory birds.[36] A lower wing loading results in a lighter body relative to wing area, contributing to a greater lift and more efficient flight.[36] Feather structure, too, reflects migratory stress: primary feathers of long-distance migratory birds often have a thicker dorsoventral rachis and shorter barbs. These features improve feather durability during long flights.[37]

Beyond wings, avian leg morphology reflects trade-offs among flight performance, habitat use, and terrestrial locomotion rather than migration alone. Comparative analyses across birds demonstrate that relative leg length, commonly measured as tarsus length, is strongly associated with ecological function. Species that rely heavily on terrestrial locomotion or ground-based foraging tend to have longer leg elements, whereas species adapted for more efficient flights often exhibit relatively shorter tarsi.[24,38,39]

In this context, some migratory birds, particularly aerial specialists such as long-distance passerine migrants, may exhibit reduced hindlimb length compared with highly terrestrial species. This pattern is consistent with a shift in locomotor emphasis toward sustained flight rather than ground movement.[40,41] However, this trend is not universal across migratory taxa. Many long-distance migrants, including shorebirds and cranes, retain elongated legs that are functionally important for wading or terrestrial foraging.[38,39] Collectively, these findings suggest that there appears to be a trend toward relatively reduced leg length in some migratory lineages with limited terrestrial locomotion, but leg morphology in migratory birds remains highly variable and shaped primarily by ecological niche rather than migration distance alone.

Muscular Adaptations:

Seasonal Hypertrophy of Flight Muscles:

In preparation for migration, the pectoralis major (the primary downstroke muscle) and the supracoracoideus (the upstroke muscle) undergo seasonal hypertrophy, which is increased muscle growth through muscle fiber enlargement.[42] Studies show that these muscles can increase by 20-30% in mass in just a few weeks.[43-46] The pectoralis major and supracoracoideus muscles are specialized for prolonged aerobic metabolism, enabling birds to sustain flight for hours or even days without fatigue.[1,31] In small migratory songbirds, these muscles are predominantly composed of fast oxidative glycolytic (Type IIa) fibers, rather than Type I fibers found in larger waterfowl such as ducks and geese.[47-49] Type IIa fibers provide a balance of high contractile power and aerobic endurance, supporting both sustained light and daily movement requirements.[49] Seasonal modulation of fiber-type composition, coupled with increases in oxidative enzyme activities, enhances the oxidative capacity of these muscles during migration.[48,49] In addition, the fibers are densely packed with mitochondria and supported by a rich capillary network, allowing efficient oxygen delivery and near-exclusive reliance on fat metabolism during long-distance flights.[50]

Hypertrophy is not simply passive weight gain. It is an actively regulated process, shaped by hormones and physiology. Hormonal and molecular signals play a key role in triggering these changes. Research has shown that Insulin-like Growth Factor 1 (IGF1) mRNA expression significantly increases during pre-migratory weight gain, promoting protein synthesis and muscle fiber growth.[44] Simultaneously, myostatin mRNA (a negative regulator of muscle development) is suppressed.[44] This dual mechanism removes molecular constraints on growth, priming the muscles for the extreme workload of migration. Beyond molecular regulation, environmental and behavioral factors also influence hypertrophy. Photoperiod changes, food availability, and fat deposition all act as signals that coordinate muscle growth for migration readiness.[8,12,51] Even exercise outside the migratory window can partially activate these pathways, suggesting that flight muscles retain a year-round ability for remodeling, though migration amplifies the effect.[43,52]

Seasonal hypertrophy of migratory birds is distinct from that of non-migratory birds. Resident species exposed to similar photoperiods and environmental cues show little to no increase in flight muscle mass or fiber-type remodeling.[48] For example, comparative studies in White-crowned sparrows (*Zonotrichia leucophrys*) show significantly higher pre-migratory pectoralis mass and oxidative enzyme activity in migratory individuals relative to resident conspecifics.[48] This reinforces that this plasticity is a migratory adaptation rather than a general response to seasonal changes. However, not all migrants follow the same muscular hypertrophy pattern. Comparative studies on sparrow species suggest that long-distance migrants may exhibit greater seasonal shifts in muscle mass and fiber type composition than short-distance migrants or resident species.[48] However, these patterns are not universal. In some species, including short- and medium-distance migrants, the pectoralis muscle transverse area may decrease during the migratory season while fiber density increases, as shown in Yellow-rumped warblers (*Setophaga coronata*).[53] This change may improve oxygen and nutrient delivery to individual fibers rather than increasing absolute force production.[53] Migration timing and ecological context further influence these traits, with individuals departing earlier or facing more demanding routes often showing higher proportions of oxidative fibers and elevated aerobic enzyme activity.[49]

Once migration begins, hypertrophied muscles enter a delicate balancing act. They must sustain continuous wingbeats without fatigue while minimizing excess weight that could hinder flight.[1] After prolonged flights, post-migratory atrophy occurs as a controlled, adaptive response.[13] Studies show that after long-distance flights, the cross-sectional area of flight muscles such as the pectoralis can decrease, with altered contractile properties that reflect strategic remodeling rather than damage.[44] This reduction is part of a broader muscle adaptation that includes the breakdown of muscle proteins, providing amino acids for energy and metabolic water, which are crucial during hydration-stressed flights.[7] Experimental work on species like Yellow-rumped warblers further supports this, showing that flight-induced pectoralis atrophy occurs at a rate of about 4 mg dry mass per hour with minimal immediate loss in force production or aerobic capacity.[52] This indicates a balance between reducing tissue mass and maintaining function. Similarly, research on Black-necked grebes (*Podiceps nigricollis*) reveals that during migration, flight muscles can lose up to 50% of their mass, yet the mitochondrial density remains relatively high, suggesting that muscle reduction is a controlled adaptation.[54] At the same time, the lighter musculature reduces overall body mass, balancing the trade-off between force production and metabolic efficiency until the bird can replenish

DOI: 10.36838/IJHSR810.83

energy stores.[55] This cycle of muscle growth and reduction reflects an extraordinary flexibility in avian physiology, allowing birds to optimize their flight performance while adapting to the demands of migration.

Fiber Composition and Enzymatic Function:

The flight muscles of migratory birds rely primarily on fast oxidative-glycolytic (FOG) fibers, which combine high fatigue resistance with the contractile speed necessary for sustained flapping flight.[53] These fibers are characterized by high mitochondrial density, elevated myoglobin content, and extensive capillarization, supporting efficient oxygen delivery and high rates of aerobic metabolism.[53,56] Comparative studies of migratory and resident sparrows demonstrate that while FOG fibers dominate the pectoralis muscle in both groups, migratory species exhibit substantially greater seasonal plasticity in muscle phenotype than resident species.[48,57]

Rather than undergoing major shifts in fiber type, migratory birds enhance the oxidative capacity of existing FOG fibers during migration through coordinated biochemical and metabolic changes. Activities of key aerobic enzymes, including citrate synthase (CS), a marker of mitochondrial abundance, and β-hydroxyacyl-CoA dehydrogenase (HOAD), a central enzyme in fatty-acid β-oxidation, rise significantly during migratory periods.[16,48] These enzymatic changes are accompanied by the seasonal upregulation of fatty acid transporters in flight muscle, which enhances lipid uptake and supports sustained reliance on fat as a primary fuel source for long-distance flight.[58] Similar seasonal increases in CS activity have been documented in Yellow-rumped warblers, indicating elevated mitochondrial oxidative capacity relative to non-migratory states.[50,59] In contrast, resident sparrows show little to no seasonal variation in muscle fiber morphology, enzyme activity, or lipid transport capacity, maintaining relatively stable metabolic profiles year-round.[48]

This suggests that migratory birds undergo a reversible, migration-triggered metabolic reprogramming that optimizes endurance capacity when needed. Early-departing individuals often display larger mitochondrial densities and greater oxidative capacity, suggesting that intra-species variation is tuned to individual migratory schedules.[60,61] This muscle-level plasticity aligns with broader seasonal modulation across the oxygen transport cascade, including coordinated changes in oxygen delivery, diffusion, and utilization documented in migratory songbirds.[53]

Cellular Specialization:

One particularly striking adaptation is how flight muscles handle water balance during long flights. When Blackpoll warblers (*Setophaga striata*) fly thousands of kilometers over the Atlantic, muscle catabolism during extreme dehydration appears to create metabolic water: a critical survival mechanism under low-humidity conditions.[52,55] This dual use of muscle tissue, as both a power source and an emergency water reservoir, illustrates the versatility of migratory physiology.

Migratory birds also show structural adaptations at the myofibrillar and extracellular matrix (ECM) level. High-endurance species have tightly packed sarcomeres, increased elasticity, and optimized cytoskeleton anchoring, which together enhance contractile efficiency.[56] These specializations allow muscles to sustain repeated contractions with minimal energy loss. The ECM further contributes to mechanical stability by transmitting force laterally, supporting the integration of individual fibers, resisting fatigue, and reducing the risk of micro-tears during repetitive wingbeats.[1,56,62] Collagen composition, cross-linking, and alignment with the ECM are critical for minimizing mechanical stress and preserving structural integrity in vertebrate skeletal muscles, including those of birds.[62] Together, these structural adaptations provide stiffness and help distribute force efficiently across the muscle.

Mitochondrial Adaptations:

Increased Aerobic Energy Production:

Migratory birds have much higher mitochondrial density in their flight muscles than resident species, as indicated by enhanced mitochondrial enzyme activity and respiratory performance in migratory individuals.[50] This is crucial to fueling the intense, energetic demands of long-distance flight. In the pectoralis muscles of White-crowned sparrow subspecies, migratory Gambel (*Zonotrichia leucophrys gambelii*) showed greater markers of mitochondrial remodeling and enhanced capacity for mitochondrial oxidative metabolism compared with non-migratory Nuttall (*Zonotrichia leucophrys nuttalli*), supporting the link between mitochondrial adaptations and migration energetics.[63] This spatial arrangement minimizes diffusion distance for both oxygen and fatty acids, ensuring efficient delivery of fuel and oxygen directly into the oxidative machinery of the cell.[13,59]

In Yellow-rumped warblers, flight mitochondria have about 60% higher citrate synthase activity than non-migratory phenotypes, reflecting a stronger capacity for sustained aerobic metabolism.[50] Additionally, State 3 respiration rates, indicative of phosphorylating respiration, are approximately 70% higher in migratory birds when oxidizing palmitoylcarnitine.[50] Palmitoylcarnitine is an intermediate in mitochondrial fatty acid oxidation, a process that generates significant amounts of ATP required for high-powered flight.[64]

Interestingly, ROS (reactive oxygen species) emission rates are similar between migratory and non-migratory phenotypes, despite the higher metabolic rates in migrants.[13,50,65] Normally, elevated oxidative metabolism increases ROS production because oxygen partially reduces to superoxide at complexes I and III of the electron transport chain.[66] The maintenance of low ROS levels in migratory birds indicates adaptations that allow enhanced oxidative capacity without incurring oxidative damage.[67] These adaptations include the upregulation of redox-sensitive signaling pathways and redox-balancing proteins such as SIRT1, SOD1, and NF-κB.[67] Evidence for this comes from migratory Redheaded buntings (*Emberiza bruniceps*), which display tissue-specific control of oxidative stress during long-distance flights.[67]

Furthermore, in migratory species, flight muscles show mitochondrial adaptations that enhance ATP production, including changes in mitochondrial morphology and electron transport

chain activity that optimize oxidative phosphorylation.[68] Such structural and functional optimization reduces metabolic bottlenecks and supports the extreme endurance required during migration.[7,13,68]

Seasonal Remodeling and Phenotypic Flexibility:

Mitochondrial adaptations in migratory birds are highly plastic. Seasonal cues, such as photoperiod, trigger the proliferation of mitochondria and increase oxidative enzyme activity in preparation for migration.[50,61,63] After migration, seasonal mitochondrial remodeling regresses, conserving energy during non-migratory flights.[57] This plasticity entails fine-tuned adjustments based on migratory distance and environmental conditions. For example, White-crowned sparrows and many boreal-breeding bird species have higher respiratory capacity and CS activity during migratory periods than at other times of year, indicating flexible mitochondrial performance across seasons.[57,69] This suggests that even subtle differences in ecological demands can shape cellular bioenergetics.[50,70] Such remodeling emphasizes the cost-benefit tradeoff inherent in maintaining high-performance mitochondria. While sustaining them year-round would be energetically expensive, repeatedly rebuilding mitochondrial machinery before and after migration also carries an energetic cost. This suggests that birds balance the benefits of high oxidative capacity during migration with the energetic demands of seasonal remodeling.

Fuel Utilization and Metabolic Efficiency:

Migratory birds predominantly fuel long-distance flight with fatty acids, as fats contain substantially more energy per gram than carbohydrates and are the dominant substrate for aerobic metabolism.[7,71] In flight muscles, mitochondria are closely associated with intramyocellular lipid droplets, allowing immediate access to fat stores without the delay of mobilizing distant reserves.[13,45,46] Fatty acids derived from stored triacylglycerides are transported to flight muscles, where they undergo β-oxidation and oxidative phosphorylation to meet high ATP demands.[1] Seasonal increases in fatty acid transporters and catabolic enzymes such as carnitine palmitoyltransferase (CPT) and HOAD support enhanced lipid uptake and oxidation in flight muscles during migration.[13,45,46,62] The upregulation of these enzymes and transport proteins ensures that the oxidative machinery can continuously process large amounts of lipid fuel during hours of intense aerobic flight.[62] Migratory birds also exhibit tighter coupling in oxidative phosphorylation, minimizing proton leak and maximizing ATP yield per unit oxygen consumed.[44] This combination of high-energy-density fats, enzyme specialization, and increased mitochondrial oxidative capacity enables migratory birds to maintain prolonged flights while meeting their energetic demands.[44,59]

Cardiovascular Adaptations:

Compared to resident species, migratory birds typically exhibit larger hearts relative to body size, a pattern that reflects evolutionary adaptation for the higher circulatory demands of endurance flight.[2,72,73] Migratory taxa such as Arctic terns and Blackpoll warblers show consistently greater relative heart mass than short-distance or resident species, suggesting selection for enhanced cardiovascular capacity.[12,20,72,73] Increased heart mass enhances stroke volume, particularly through left ventricular hypertrophy, elevates systemic cardiac output without disproportionately raising pulmonary circuit pressures.[1,74,75] Seasonal phenotypic flexibility also contributes to this process. In migratory passerines such as Yellow-rumped warblers and Warbling vireos (*Vireo gilvus*), heart mass is higher in spring before migration and declines after the migratory period.[73] This demonstrates reversible cardiac remodeling in preparation for and recovery from long flights. The cardiovascular system is tightly linked to muscle and mitochondrial performance. Hypertrophied flight muscles demand a higher oxygen influx, which drives selection for larger hearts and increased capillarization.[44,46] In turn, efficient mitochondrial networks utilize this oxygen effectively, converting it into ATP to sustain continuous wingbeats.[13,59]

Oxygen delivery is further facilitated by higher capillary density in the flight muscles of migratory birds, which reduces diffusion distances and supports robust oxygen supply to active fibers during flight.[1,53] While the capillary-to-fiber ratio may not change uniformly across all seasons or species, seasonal modulation in multiple components of the oxygen cascade has been documented in migratory songbirds.[53] This improves oxygen uptake and transport under migratory conditions.[53] Hemoglobin concentration and oxygen-binding properties also vary across migratory states, though the specific mechanism remains an area of active research.[53] Anatomical features such as specialized pneumatic bones and extensive air sac systems complement these cardiovascular traits. They increase respiratory efficiency and oxygen availability for sustained aerobic metabolism during long flights.[1] Together, these cardiovascular adaptations illustrate how migratory birds fine-tune heart morphology and function, both evolutionarily and seasonally, to meet the circulatory requirements for long-distance flight.

Digestive System Adaptations:

Migratory birds exhibit remarkable plasticity in their digestive system, allowing them to adjust gut structure and function in response to changing energetic demands. In waders (*Charadrii*), Kovtun *et al.* demonstrated that pre-migratory individuals significantly increase their intestinal length, mass, and absorptive surface area relative to non-migratory periods.[76] Supporting this, Western sandpipers (*Calidris mauri*) show increases of up to 25% in small intestine mass before migration, a change that coincides with peak fat deposition and maximized energy storage.[76,77] Comparable digestive flexibility has also been documented in migratory songbirds. Studies of passerines such as Garden warblers (*Sylvia borin*) and other long-distance migrants reveal reversible enlargement of digestive organs during fueling phases at stopover sites, facilitating the processing of energy-rich foods encountered during frequent migratory stops.[11,78]

In addition to structural remodeling, liver mass and digestive enzyme activity increase prior to migration, enhancing lipid processing and carbohydrate assimilation during periods

DOI: 10.36838/IJHSR810.83

of hyperphagia.[14,77] These changes are reversible: post-migratory birds exhibit regression of gut size and reduced digestive enzyme activity, minimizing maintenance costs once maximal digestive performance is no longer required.[11,17,46,76] Digestive plasticity is not exclusive to migratory species. Experimental studies in White-throated sparrows demonstrate that increased seasonal demands, such as cold exposure, can induce reversible enlargement of intestinal and hepatic tissues.[79] This suggests that gut flexibility is a generalized adaptive response to fluctuating energetic constraints rather than migration alone.[11,17]

Pre-migratory fattening is crucial to migratory success. Across multiple passerine and wader species, fat stores can reach 30-50% of body mass before departure, providing the primary fuel for sustained flight.[13,46,80] This fat accumulation is driven by pronounced hyperphagia and selective feeding, with birds preferentially consuming lipid and carbohydrate rich foods.[14,76] Experimental studies in migratory buntings and sparrows show that caloric intake can increase up to 60% above baseline during fueling periods, with the majority of assimilated energy directed towards subcutaneous and visceral fat stores.[13,14,80]

Hormonal regulation plays a central coordinating role in these digestive and metabolic changes. Cornelius *et al.* showed that pre-migratory corticosterone peaks coincide with elevated foraging activity, gut growth, and food intake, while rising thyroid hormone levels enhance metabolic rate and lipid mobilization.[8] Together, these endocrine shifts synchronize behavior, digestive organ remodeling, and nutrient assimilation, ensuring that energy acquisition and storage are optimally aligned with the timing and energetic demands of migration.[8,13]

The digestive system also undergoes molecular adaptations that facilitate rapid and efficient energy transfer from dietary intake to aerobic power output. In Western sandpipers, Guglielmo *et al.* found that fatty acid binding proteins (FABPs) are upregulated in both intestinal tissue and flight muscle during pre-migratory fattening, enhancing intracellular transport of absorbed fatty acids toward sites of oxidation.[45] By accelerating fatty acid trafficking from the gut to mitochondria, elevated FABP expression supports sustained lipid oxidation during flight and reduces dependence on carbohydrate metabolism.[13,14] This ensures that the high-energy demand of sustained wingbeats is met without delay, conserving limited muscle glycogen reserves.[13,14]

Seasonal shifts in digestive enzyme activity further reinforce this fuel-delivery system. Kovtun *et al.* reported pre-migratory increases in intestinal lipase and amylase activity in waders, reflecting enhanced capacity to process both lipid-rich and carbohydrate-rich diets during periods of rapid mass gain.[76] Comparable patterns of enzyme modulation and digestive upscaling have also been documented in migratory passerines.[11,46] This indicates that the biochemical flexibility of the gut is a general feature of migratory preparation rather than a shorebird-specific phenomenon. Together, these molecular and enzymatic adjustments tightly synchronize energy storage and utilization across organ systems during migration.

Convergent and Divergent Migratory Adaptations:

While the preceding sections emphasize shared physiological solutions to migration, not all migratory adaptations evolve uniformly. The interaction between geography, ecology, and phylogenetic history can result in both convergent and divergent evolution (Figure 1). On one hand, distantly related species often converge on similar morphological, physiological, and behavioral traits when exposed to the shared demands of long-distance flights. On the other hand, closely related lineages may diverge when ecological, geographical, and genetic variations impose distinct selective pressures. Together, these patterns highlight migration as both a unifying force shaping shared solutions and a diversifying driver promoting lineage-specific adaptations.[18]

On a generalized level, unrelated species frequently converge on similar migratory strategies when constrained by geography and atmospheric conditions. For example, many Western Hemisphere migrants undertaking trans-Gulf flights adopt looped or seasonally asymmetrical routes that exploit prevailing wind systems to reduce energetic costs.[81,82] In Central America and Northern South America, the narrowing of land corridors and the orientation of major mountain ranges channel migrants into partially overlapping pathways, promoting convergence in route selection across phylogenetically diverse lineages.[19] However, migration in the Americas does not follow a single uniform pathway. North American birds move through multiple north-south flyways that may diverge, merge, or shift seasonally depending on destination, weather, and ecological context.[83] This complexity highlights that convergence is strongest where geographic and atmospheric constraints are most restrictive, whereas divergence dominates in regions that offer multiple viable migratory options.

Behavioral strategies illustrate divergence under different ecological contexts. Within the wide-ranging songbird Northern wheatear (*Oenanthe oenanthe*), contrasting stopover and departure tactics have been documented between populations facing different onward migration distances.[84] Scandinavian wheatears (*Oenanthe oenanthe oenanthe*), crossing relatively short distances of up to 500 kilometers, typically depart stopover sites quickly regardless of immediate weather conditions. In contrast, Greenlandic and Icelandic conspecifics undertaking flights of up to 25,000 kilometers often prolong stopovers and time departures in relation to favorable conditions such as tailwinds and clear skies.[84] This intraspecific divergence in behavior underscores how ecological context can lead to distinct stopover and departure strategies within a single species. Moreover, divergent migratory strategies are linked to physiological performance at stopover in other songbirds as well. Long-distance migrating Gray catbirds (*Dumetella carolinesis*) exhibit a higher increase in plasma triglyceride concentration per unit increase in body mass compared to short-distance migrants during spring refueling.[85] This indicates variation in refueling performance tied to migratory distance within a species.

At the cellular level, high-performance mitochondrial traits have repeatedly evolved across distant species. Long-distance shorebirds, passerines, and high-altitude sparrows

independently show increased mitochondrial density, elevated oxidative enzyme activity, and optimized cristae organization to increase ATP production efficiency.[44,86] This convergence highlights the intense selective pressures imposed by migration and demonstrates that natural selection can generate similar cellular "solutions" in unrelated lineages.[13,59] Convergent traits extend beyond energy output. For instance, species performing overwater migrations show reduced ROS emission even under high mitochondrial flux, suggesting that selection favors not only endurance but also cellular resilience to oxidative stress.[13,55,63] It is important to note that most of these studies are taxonomically concentrated toward passerines, shorebirds, and a few model species such as white-crowned sparrows and blackpoll warblers, with a strong emphasis on extreme long-distance migrants. Intermediate strategies, such as those employed by partial or short-distance migrants, remain poorly characterized, leaving gaps in understanding the spectrum of mitochondrial adaptations across the avian phylogeny. Expanding research to include diverse migratory behaviors and lineages could clarify the evolutionary and functional limitations of these cellular adaptations.

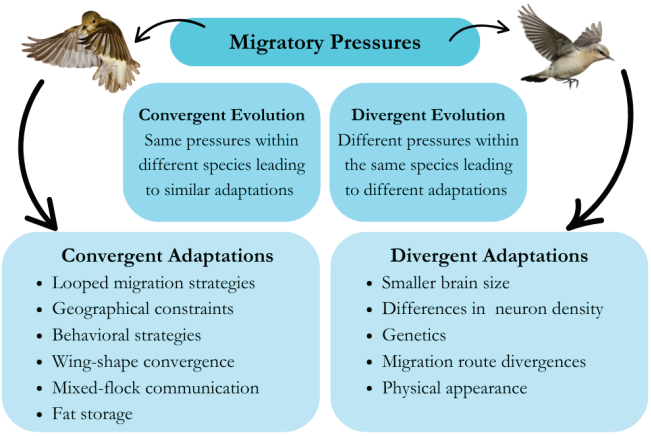

Figure 1: Schematic showing convergent and divergent evolution in migratory birds. Same migratory pressures promote similar traits across different species, while different migratory pressures can result in different traits in the same species.

At the genetic level, Common yellowthroats (*Geothlypis trichas*) with both migratory and resident populations illustrate how convergence and divergence can occur simultaneously within a single species. Eastern and western clades are genetically distinct, each carrying unique sets of single-nucleotide polymorphisms (SNPs) that reflect lineage-specific divergence.[87] Yet despite these differences, 27 out of 42 candidate genes overlap across populations, and these loci are associated with migratory timing, morphology, and metabolism.[87] Functionally, both migratory lineages have converged to have a similar adaptive response through different genetic routes. Moreover, resident populations in both clades show strong selection signals, suggesting that residency has independently evolved as a convergent response to year-round ecological pressures.[87] The Common yellowthroats therefore demonstrate that migration can drive both divergence in genetic pathways and produce convergence in phenotypic features.

Divergence is also evident in neurological evolution. Migratory Dark-eyed juncos have significantly higher hippocampal neuron density and superior spatial memory compared to their resident conspecifics, supporting advanced navigation during long-distance migration.[88] Similarly, adult sparrows show elevated hippocampal neurogenesis associated with migratory behavior, whereas juveniles do not, suggesting that neural plasticity is linked to both experience and the demands of migration.[89] Across passerines, migratory species may have smaller overall brain sizes compared to resident birds, which may reflect an energetic tradeoff in favor of specialized navigation and reduced developmental costs.[90] Hippocampal volume is also influenced by seasonal experience. Studies in warblers demonstrate that individuals exposed to migratory challenges exhibit larger hippocampi, highlighting the combined effects of environmental demands and age-related plasticity.[91] These findings illustrate how divergence and convergence in neurological structures enable migratory birds to balance spatial memory, cognitive demands, and energetic efficiency relative to resident species.

Morphological convergence further demonstrates the interplay of convergent and divergent evolution. Ficedula flycatchers show predictable scaling of wing pointedness and body size with migratory distance, within intermediate forms among short-distance migrants.[28,92] Long-distance migratory *Ficedula* species from different breeding and wintering grounds also display similar morphologies that have evolved independently.[28] These patterns highlight the sliding scale of migratory pressures that sculpt wing morphology in proportion to distance. Comparisons in shorebirds further reinforce this trend: among *Charadriidae* and *Scolopacidae*, long-distance migrants consistently evolve more pointed wings with reduced roundness and enhanced fat stores.[92] Quantitative analyses indicate that migration distance alone can explain up to 53% of the variation in wing shape.[92] These findings confirm a predictable, convergent relationship between wing pointedness and migration strategy, while interfamily differences emphasize lineage-specific divergence in achieving flight efficiency.

Convergence extends beyond morphology and physiology to communication and flight behaviors. Among North American wood warblers, migration has also shaped vocal behavior. Gayk *et al.*'s study on 36 species of wood warblers (*Parulidae*) found that birds with overlapping migratory ranges, breeding latitude, or migration distances had more acoustic similarities in their flight calls. In contrast, species with distinct migratory routes exhibited divergent calls. This suggests that acoustic convergence can be shaped by migratory pressures for communication within mixed flocks, increasing migratory success with a mixed variety of predator detectability and navigational knowledge.[93]

Together, migratory adaptations reveal the multi-layered strategies birds employ, linking molecular, cellular, and systemic changes into a unified migratory phenotype.

DOI: 10.36838/IJHSR810.83

Conclusion

Migration has shaped more than isolated traits; it has forged a specialized, whole-organism phenotype finely tuned to the extreme demands of long-distance flight. This migratory phenotype represents a tightly integrated unit of anatomical, physiological, and molecular traits honed by natural selection to optimize endurance and efficiency. It is the coordination of skeletal, muscular, mitochondrial, cardiovascular, and digestive systems, and neural systems that underpins migratory success. The components of these adaptations that create the migratory phenotype are summarized in Figure 2.

At the core of the migratory phenotype is precise cross-system coupling. Lightweight, fused skeletal structures reduce mechanical stress and enhance flight stability. But this is only advantageous when paired with hypertrophied, oxidative-rich flight muscles capable of sustaining continuous wingbeats. These muscles rely on high mitochondrial density, optimized enzyme activity, and perfected oxygen delivery systems to maintain aerobic demands. Cardiac remodeling, including seasonal left ventricular hypertrophy, adjusts circulatory capacity to muscular workload, while digestive organs showcase pronounced phenotypic flexibility to maximize nutrient absorption during pre-migratory fattening. Even at the cellular scale, mitochondrial positioning ensures synchronized delivery of oxygen and lipid fuel, and endocrine signals trigger coordinated remodeling across muscle, heart, and gut. Collectively, these systems operate as an integrated network in which performance emerges from alignment rather than the sum of isolated traits.

Understanding the migratory phenotype has critical implications for conservation. Migratory success depends on tight cross-system coordination, and disruptions at any single stage can cascade across the migratory phenotype. Climate change has already been shown to alter photoperiod-temperature relations, leading to mistimed *Zugunruhe*, premature fattening, or departures that no longer align with peak food availability. This increases starvation risk and reduces reproductive success. Habitat loss at key stopover sites limits opportunities for refueling and digestive remodeling, resulting in incomplete migratory preparation and failed breeding attempts. Artificial light pollution further disrupts circadian and circannual cues, interfering with endocrine regulation of migration and increasing mortality through distortion and collision. These examples demonstrate that protecting migratory species requires conserving not only breeding and wintering grounds, but also the ecological corridors and environmental signals that allow the migratory phenotype to function as an integrated whole. Migration, therefore, stands as a powerful illustration of how evolution coordinates multi-level biological systems for extraordinary endurance and how vulnerable such calibrated adaptations are to anthropogenic change.

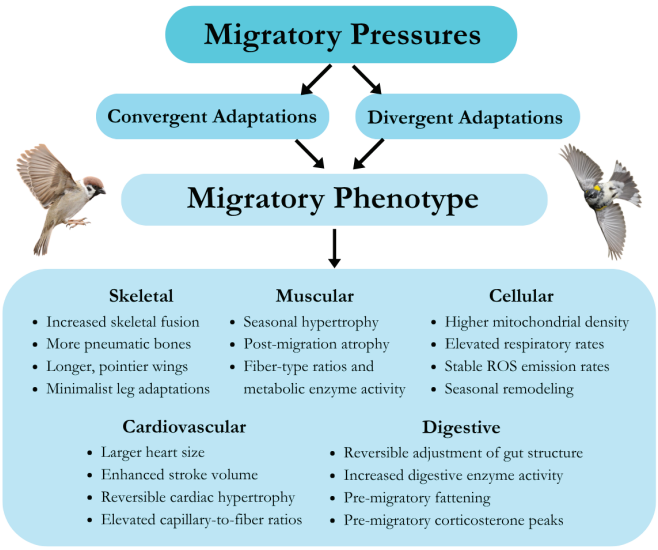

Figure 2: Schematic summarizing avian adaptations across skeletal, muscular, cellular, cardiovascular, and digestive systems in response to migratory pressures. These adaptations define the migratory phenotype, which is crucial for migratory success.

References

1. Butler, P. J. (2016). The physiological basis of bird flight. *Philosophical Transactions of the Royal Society B: Biological Sciences, 371*(1704), 20150384.
2. OBrien, S. J., Haussler, D., & Ryder, O. (2014). The birds of Genome10K. *GigaScience, 3*(1), 2047-217X.
3. Cooke, R., Sayol, F., Andermann, T., Blackburn, T. M., Steinbauer, M. J., Antonelli, A., & Faurby, S. (2023). Undiscovered bird extinctions obscure the true magnitude of human-driven extinction waves. *Nature Communications, 14*(1), 8116.
4. Matthews, T. J., Triantis, K. A., Wayman, J. P., Martin, T. E., Hume, J. P., Cardoso, P., ... & Sayol, F. (2024). The global loss of avian functional and phylogenetic diversity from anthropogenic extinctions. *Science, 386*(6717), 55-60.
5. Lennox, R. J., Chapman, J. M., Souliere, C. M., Tudorache, C., Wikelski, M., Metcalfe, J. D., & Cooke, S. J. (2016). Conservation physiology of animal migration. *Conservation Physiology, 4*(1), cov072.
6. Piersma, T., PÉREZ-TRIS, J. A. V. I. E. R., Mouritsen, H., Bauchinger, U. L. F., & Bairlein, F. (2005). Is there a "migratory syndrome" common to all migrant birds?. *Annals of the New York Academy of Sciences, 1046*(1), 282-293.
7. Jenni, L., & Jenni-Eiermann, S. (1998). Fuel supply and metabolic constraints in migrating birds. *Journal of Avian Biology*, 521-528.
8. Cornelius, J. M., Boswell, T., Jenni-Eiermann, S., Breuner, C. W., & Ramenofsky, M. (2013). Contributions of endocrinology to the migration life history of birds. *General and Comparative Endocrinology, 190*, 47-60.
9. Helm, B., & Gwinner, E. (2006). Migratory restlessness in an equatorial nonmigratory bird. *PLoS biology, 4*(4), e110.
10. Pickett, S. M. (2021). *Zugunruhe (migratory restlessness)*. University of Kansas.
11. McWilliams, S. R., & Karasov, W. H. (2001). Phenotypic flexibility in digestive system structure and function in migratory birds and its ecological significance. *Comparative Biochemistry and Physiology Part A: Molecular & Integrative Physiology, 128*(3), 577-591.

12. Mandal, S., Sant, S., Ahirwar, M. K., & Kumar, A. (2021). Migratory birds' physiology: A review. *Journal of Pharmaceutical Innovation*, *10*, 35-40.
13. Guglielmo, C. G. (2018). Obese super athletes: fat-fueled migration in birds and bats. *Journal of Experimental Biology, 221*(Suppl_1), jeb165753.
14. McWilliams, S. R., Guglielmo, C., Pierce, B., & Klaassen, M. (2004). Flying, fasting, and feeding in birds during migration: a nutritional and physiological ecology perspective. *Journal of Avian Biology, 35*(5), 377-393.
15. Piersma, T., & Van Gils, J. A. (2010). *The flexible phenotype: a body-centred integration of ecology, physiology, and behaviour*. OUP Oxford.
16. Marasco, V., Sebastiano, M., Costantini, D., Pola, G., & Fusani, L. (2021). Controlled expression of the migratory phenotype affects oxidative status in birds. *Journal of Experimental Biology, 224*(6), jeb233486.
17. Piersma, T. (2002). Energetic bottlenecks and other design constraints in avian annual cycles. *Integrative and comparative biology, 42*(1), 51-67.
18. Alerstam, T., Hedenström, A., & Åkesson, S. (2003). Long-distance migration: evolution and determinants. *Oikos, 103*(2), 247-260.
19. La Sorte, F. A., Fink, D., Hochachka, W. M., DeLong, J. P., & Kelling, S. (2014). Spring phenology of ecological productivity contributes to the use of looped migration strategies by birds. *Proceedings of the Royal Society B: Biological Sciences, 281*(1793), 20140984.
20. Egevang, C., Stenhouse, I. J., Phillips, R. A., Petersen, A., Fox, J. W., & Silk, J. R. (2010). Tracking of Arctic terns Sterna paradisaea reveals longest animal migration. *Proceedings of the National Academy of Sciences, 107*(5), 2078-2081.
21. James, H. F. (2009). Repeated evolution of fused thoracic vertebrae in songbirds. *The Auk, 126*(4), 862-872.
22. Aires, A. S., Reichert, L. M., Müller, R. T., & Andrade, M. B. (2022). Review of morphology, development, and evolution of the notarium in birds. *The Anatomical Record, 305*(9), 2079-2098.
23. Singh, N. S., Bamon, I., Dixit, A. S., & Sougrakpam, R. (2015). Structural variations and their adaptive significances in the bones of some migratory and resident birds. *The Journal of Basic & Applied Zoology, 70*, 33-40.
24. Louis, L. D., Bowie, R. C., & Dudley, R. (2022). Wing and leg bone microstructure reflects migratory demands in resident and migrant populations of the Dark-eyed Junco (Junco hyemalis). *Ibis, 164*(1), 132-150.
25. Schwarz, D., Kundrát, M., Tischlinger, H., Dyke, G., & Carney, R. M. (2019). Ultraviolet light illuminates the avian nature of the Berlin Archaeopteryx skeleton. *Scientific reports, 9*(1), 6518.
26. Skawiński, T., Kuziak, P., Kloskowski, J., & Borczyk, B. (2022). Phylogenetic Diversity of Ossification Patterns in the Avian Vertebral Column: A Review and New Data from the Domestic Pigeon and Two Species of Grebes. *Biology, 11*(2), 180.
27. Machado, J. P., Johnson, W. E., Gilbert, M. T. P., Zhang, G., Jarvis, E. D., O'Brien, S. J., & Antunes, A. (2016). Bone-associated gene evolution and the origin of flight in birds. *BMC genomics, 17*(1), 1-15.
28. Outlaw, D. C., & Nijman, V. (2011). Morphological evolution of some migratory Ficedula flycatchers. *Contributions to Zoology, 80*(4), 279-284.
29. Bui, H. N. N., & Larsson, H. C. (2021). Development and evolution of regionalization within the avian axial column. *Zoological Journal of the Linnean Society, 191*(1), 302-321.
30. Heers, A. M. (2023). Unexpected performance in developing birds. *Integrative and comparative biology, 63*(3), 772-784.
31. Biewener, A. A. (2011). Muscle function in avian flight: achieving power and control. *Philosophical Transactions of the Royal Society B: Biological Sciences, 366*(1570), 1496-1506.
32. Sullivan, S. P., McGechie, F. R., Middleton, K. M., & Holliday, C. M. (2019). 3D muscle architecture of the pectoral muscles of European Starling (Sturnus vulgaris). *Integrative Organismal Biology, 1*(1), oby010.
33. Hunt, E. S., Felice, R. N., Tobias, J. A., & Goswami, A. (2023). Ecological and life-history drivers of avian skull evolution. *Evolution, 77*(7), 1720-1729.
34. Norberg, U. M. (1995). Wing design and migratory flight. *Israel Journal of Ecology and Evolution, 41*(3), 297-305.
35. Vágási, C. I., Pap, P. L., Vincze, O., Osváth, G., Erritzøe, J., & Møller, A. P. (2016). Morphological adaptations to migration in birds. *Evolutionary Biology, 43*(1), 48-59.
36. Matyjasiak, P., López-Calderón, C., Ambrosini, R., Balbontín, J., Costanzo, A., Kiat, Y., ... & Rubolini, D. (2023). Wing morphology covaries with migration distance in a highly aerial insectivorous songbird. *Current Zoology, 69*(3), 255-263.
37. de la Hera, I., Hernández-Téllez, I., Pérez-Rigueiro, J., Pérez-Tris, J., Rojo, F. J., & Tellería, J. L. (2020). Mechanical and structural adaptations to migration in the flight feathers of a Palaearctic passerine. *Journal of Evolutionary Biology, 33*(7), 979-989.
38. Xu, Y., Price, M., Que, P., Zhang, K., Sheng, S., He, X., ... & Wang, B. (2023). Ecological predictors of interspecific variation in bird bill and leg lengths on a global scale. *Proceedings of the Royal Society B, 290*(2003), 20231387.
39. Zeffer, A., Johansson, L. C., & Marmebro, Å. (2003). Functional correlation between habitat use and leg morphology in birds (Aves). *Biological Journal of the Linnean Society, 79*(3), 461-484.
40. Kotnour, J., McPeek, S. J., Wedig, H., Dominguez, J., & Wright, N. A. (2022). Relative forelimb–hindlimb investment is associated with flight style, foraging strategy, and nestling period, but not nest type. *Ornithology, 139*(2), ukab084.
41. Heers, A. M., & Dial, K. P. (2015). Wings versus legs in the avian bauplan: development and evolution of alternative locomotor strategies. *Evolution, 69*(2), 305-320.
42. Evans, P. R., Davidson, N. C., Uttley, J. D., & Evans, R. D. (1992). Premigratory hypertrophy of flight muscles: an ultrastructural study. *Ornis Scandinavica*, 238-243.
43. Bauchinger, U. L. F., & Biebach, H. (2005). Phenotypic flexibility of skeletal muscles during long-distance migration of garden warblers: muscle changes are differentially related to body mass. *Annals of the New York Academy of Sciences, 1046*(1), 271-281.
44. Price, E. R., Bauchinger, U., Zajac, D. M., Cerasale, D. J., McFarlan, J. T., Gerson, A. R., ... & Guglielmo, C. G. (2011). Migration-and exercise-induced changes to flight muscle size in migratory birds and association with IGF1 and myostatin mRNA expression. *Journal of Experimental Biology, 214*(17), 2823-2831.
45. Guglielmo, C. G., Haunerland, N. H., & Williams, T. D. (1998). Fatty acid binding protein, a major protein in the flight muscle of migrating western sandpipers. *Comparative Biochemistry and Physiology Part B: Biochemistry and Molecular Biology, 119*(3), 549-555.
46. Biebach, H. (1996). Energetics of winter and migratory fattening. In *Avian energetics and nutritional ecology* (pp. 280-323). Boston, MA: Springer US.
47. Chang, R. M., Guglielmo, C. G., & Ivy, C. M. (2024). Seasonal modulation of pectoralis muscle fiber type composition in migratory songbirds. *Journal of Ornithology, 165*(4), 889-895.
48. Lewicki, L. M., Zhang, M., Staples, J. F., Guglielmo, C. G., & Ivy, C. M. (2025). A comparison of seasonal flexibility in pec-

DOI: 10.36838/IJHSR810.83

toralis muscle fiber type and enzyme activity in migratory and resident sparrow species. *Journal of Experimental Biology, 228*(3), JEB249392.
49. Zhang, S., DuBay, S., Cheng, Y., Dong, Z., Liu, Z., & Wu, Y. (2025). Inter-and intraspecific variation in flight muscle fibers is associated with migratory timing. *Avian Research, 16*(1), 100223.
50. Coulson, S. Z., Guglielmo, C. G., & Staples, J. F. (2024). Migration increases mitochondrial oxidative capacity without increasing reactive oxygen species emission in a songbird. *Journal of Experimental Biology, 227*(9), jeb246849.
51. Dawson, W. R., Marsh, R. L., & Yacoe, M. E. (1983). Metabolic adjustments of small passerine birds for migration and cold. American Journal of Physiology-Regulatory, Integrative and Comparative Physiology, 245(6), R755-R767.
52. Groom, D. J., Black, B., Deakin, J. E., DeSimone, J. G., Lauzau, M. C., Pedro, B. P., ... & Gerson, A. R. (2023). Flight muscle size reductions and functional changes following long-distance flight under variable humidity conditions in a migratory warbler. *Physiological Reports, 11*(20), e15842.
53. Ivy, C. M., & Guglielmo, C. G. (2023). Migratory songbirds exhibit seasonal modulation of the oxygen cascade. *Journal of Experimental Biology, 226*(17), jeb245975.
54. Gaunt, A. S., Hikida, R. S., Jehl, J. R., & Fenbert, L. (1990). Rapid atrophy and hypertrophy of an avian flight muscle. *The Auk, 107*(4), 649-659.
55. Weber, J. M. (2009). The physiology of long-distance migration: extending the limits of endurance metabolism. *Journal of Experimental Biology, 212*(5), 593-597.
56. Cao, T., & Jin, J. P. (2020). Evolution of flight muscle contractility and energetic efficiency. *Frontiers in Physiology, 11*, 1038.
57. Rhodes, E. M., Yap, K. N., Mesquita, P. H., Parry, H. A., Kavazis, A. N., Krause, J. S., ... & Hood, W. R. (2024). Flexibility underlies differences in mitochondrial respiratory performance between migratory and non-migratory White-crowned Sparrows (Zonotrichia leucophrys). *Scientific Reports, 14*(1), 9456.
58. McFarlan, J. T., Bonen, A., & Guglielmo, C. G. (2009). Seasonal upregulation of fatty acid transporters in flight muscles of migratory white-throated sparrows (Zonotrichia albicollis). *Journal of Experimental Biology, 212*(18), 2934-2940.
59. Coulson, S. Z. (2024). *Effects of evolved migration strategy, seasonal flexibility, and endurance flight on songbird mitochondrial bioenergetics* (Doctoral dissertation, The University of Western Ontario (Canada)).
60. Toews, D. P., Mandic, M., Richards, J. G., & Irwin, D. E. (2014). Migration, mitochondria, and the yellow-rumped warbler. *Evolution, 68*(1), 241-255.
61. Trivedi, A. K., Malik, S., Rani, S., & Kumar, V. (2015). Adaptation of oxidative phosphorylation to photoperiod-induced seasonal metabolic states in migratory songbirds. *Comparative Biochemistry and Physiology Part A: Molecular & Integrative Physiology, 184*, 34-40.
62. Gillies, A. R., & Lieber, R. L. (2011). Structure and function of the skeletal muscle extracellular matrix. *Muscle & nerve, 44*(3), 318-331.
63. Mesquita, P. H., Rhodes, E. M., Yap, K. N., Mueller, B. J., Hill, G. E., Hood, W. R., & Kavazis, A. N. (2024). Mitochondrial remodelling supports migration in white-crowned sparrows (Zonotrichia leucophrys). *Proceedings B, 291*(2036), 20242409.
64. Jenni-Eiermann, S., Liechti, F., Briedis, M., Rime, Y., & Jenni, L. (2024). Energy supply during nocturnal endurance flight of migrant birds: effect of energy stores and flight behaviour. *Movement Ecology, 12*(1), 41.
65. Bhardwaj, N., Kumar, A., & Gupta, N. J. (2023). Altered dynamics of mitochondria and reactive oxygen species in the erythrocytes of migrating red-headed buntings. *Frontiers in Physiology, 14*, 1111490.
66. Napolitano, G., Fasciolo, G., & Venditti, P. (2021). Mitochondrial management of reactive oxygen species. *Antioxidants, 10*(11), 1824.
67. Kumar, A., Bhardwaj, N., Rajaura, S., Afzal, M., & Gupta, N. J. (2024). Inter-organ differences in redox imbalance and apoptosis depict metabolic resilience in migratory redheaded buntings. *Scientific Reports, 14*(1), 20184.
68. Hood, W. R. (2024). Mechanisms that Alter Capacity for Adenosine Triphosphate Production and Oxidative Phosphorylation: Insights from Avian Migration. *Integrative and Comparative Biology, 64*(6), 1811-1825.
69. Pegan, T. M., Berv, J. S., Gulson-Castillo, E. R., Kimmitt, A. A., & Winger, B. M. (2024). The pace of mitochondrial molecular evolution varies with seasonal migration distance. *Evolution, 78*(1), 160-173.
70. Rhodes, E. M., Yap, K. N., Hill, G. E., & Hood, W. R. (2024). A comparison of the mitochondrial performance between migratory and sedentary mimid thrushes. *Integrative and Comparative Biology, 64*(6), 1859-1870.
71. Cornelius, J. M., Hahn, T. P., Robart, A. R., Vernasco, B. J., Zahor, D. L., Glynn, K. J., ... & Watts, H. E. (2021). Seasonal patterns of fat deposits in relation to migratory strategy in facultative migrants. *Frontiers in Ecology and Evolution, 9*, 691808.
72. Soriano-Redondo, A., Gutiérrez, J. S., Hodgson, D., & Bearhop, S. (2020). Migrant birds and mammals live faster than residents. *Nature Communications, 11*(1), 5719.
73. King, M. O., Zhang, Y., Carter, T., Johnson, J., Harmon, E., & Swanson, D. L. (2015). Phenotypic flexibility of skeletal muscle and heart masses and expression of myostatin and tolloid-like proteinases in migrating passerine birds. *Journal of Comparative Physiology B, 185*(3), 333-342.
74. Hahn, S., Emmenegger, T., Riello, S., Serra, L., Spina, F., Buttemer, W. A., & Bauer, S. (2022). Short-and long-distance avian migrants differ in exercise endurance but not aerobic capacity. *BMC zoology, 7*(1), 29.
75. Ramenofsky, M., Campion, A. W., Hwee, D. T., Wood, S. K., Krause, J. S., Németh, Z., ... & Bodine, S. (2024). Comparison of the phenotypic flexibility of muscle and body condition of migrant and resident white-crowned sparrows. *Ecological and evolutionary physiology, 97*(1), 11-28.
76. Kovtun, M. F., Lykova, I. O., & Kharchenko, L. P. (2018). The plasticity and morphofunctional organization of the digestive system of waders (charadrii) as migrants.
77. Stein, R. W., Place, A. R., Lacourse, T., Guglielmo, C. G., & Williams, T. D. (2005). Digestive organ sizes and enzyme activities of refueling western sandpipers (Calidris mauri): contrasting effects of season and age. *Physiological and Biochemical Zoology, 78*(3), 434-446.
78. Biebach, H. (1998). Phenotypic organ flexibility in Garden Warblers Sylvia borin during long-distance migration. *Journal of Avian Biology*, 529-535.
79. McWilliams, S. R., & Karasov, W. H. (2014). Spare capacity and phenotypic flexibility in the digestive system of a migratory bird: defining the limits of animal design. *Proceedings of the Royal Society B: Biological Sciences, 281*(1783), 20140308.
80. Biebach, H., Friedrich, W., & Heine, G. (1986). Interaction of bodymass, fat, foraging and stopover period in trans-Sahara migrating passerine birds. *Oecologia, 69*(3), 370-379.
81. Alerstam, T. (1979). Wind as selective agent in bird migration. *Ornis Scandinavica*, 76-93.

82. Buler, J. J., & Moore, F. R. (2011). Migrant–habitat relationships during stopover along an ecological barrier: extrinsic constraints and conservation implications. *Journal of Ornithology, 152*(Suppl 1), 101-112.
83. La Sorte, F. A., Fink, D., Hochachka, W. M., & Kelling, S. (2016). Convergence of broad-scale migration strategies in terrestrial birds. *Proceedings of the Royal Society B: Biological Sciences, 283*(1823), 20152588.
84. Dierschke, V., & Delingat, J. (2001). Stopover behaviour and departure decision of northern wheatears, Oenanthe oenanthe, facing different onward non-stop flight distances. *Behavioral Ecology and Sociobiology, 50*(6), 535-545.
85. Griego, M., Ramirez, M. G., & Gerson, A. R. (2025). Divergent migratory strategies lead to variable refueling performance amongst Gray Catbirds (Dumetella carolinensis) during spring stopover in the Gulf of Mexico. *Movement Ecology, 13*(1), 1-12.
86. Burskaia, V., Artyushin, I., Potapova, N. A., Konovalov, K., & Bazykin, G. A. (2021). Convergent adaptation in mitochondria of phylogenetically distant birds: does it exist?. *Genome Biology and Evolution, 13*(7), evab113.
87. Zamudio-Beltrán, L. E., Bossu, C. M., Bueno-Hernández, A. A., Dunn, P. O., Sly, N. D., Rayne, C., ... & Ruegg, K. C. (2025). Parallel and convergent evolution in genes underlying seasonal migration. *Evolution Letters, 9*(2), 189-208.
88. Cristol, D. A., Reynolds, E. B., Leclerc, J. E., Donner, A. H., Farabaugh, C. S., & Ziegenfus, C. W. (2003). Migratory dark-eyed juncos, Junco hyemalis, have better spatial memory and denser hippocampal neurons than nonmigratory conspecifics. *Animal behaviour, 66*(2), 317-328.
89. LaDage, L. D., Roth, T. C., & Pravosudov, V. V. (2011). Hippocampal neurogenesis is associated with migratory behaviour in adult but not juvenile sparrows (Zonotrichia leucophrys ssp.). *Proceedings of the Royal Society B: Biological Sciences, 278*(1702), 138-143.
90. Sol, D., Garcia, N., Iwaniuk, A., Davis, K., Meade, A., Boyle, W. A., & Szekely, T. (2010). Evolutionary divergence in brain size between migratory and resident birds. *PLoS One, 5*(3), e9617.
91. Healy, S. D., Gwinner, E., & Krebs, J. R. (1996). Hippocampal volume in migratory and non-migratory warblers: effects of age and experience. *Behavioural Brain Research, 81*(1-2), 61-68.
92. Minias, P., Meissner, W., Włodarczyk, R., Ożarowska, A., Piasecka, A., Kaczmarek, K., & Janiszewski, T. (2015). Wing shape and migration in shorebirds: a comparative study. *Ibis, 157*(3), 528-535.
93. Gayk, Z. G., Simpson, R. K., & Mennill, D. J. (2021). The evolution of wood warbler flight calls: Species with similar migrations produce acoustically similar calls. *Evolution, 75*(3), 719-730.

Author

Arshi Aggarwal is a senior at the International School of Beaverton in Oregon. She has been fascinated by birds and other animals since childhood. In college, she wants to pursue an understanding of human-animal interactions through an anthropology and ecology lens.

DOI: 10.36838/IJHSR810.83

IJHSR
ijhighschoolresearch.org
RESEARCH ARTICLE

The Role of Epigenetics in Gene Regulation: A Study of Histone Modifications

Vinayak Ramakrishnan

Clarkstown High School North, 7 York Ct., New City, NY, 10956, USA; vikrmkrshnn@gmail.com

ABSTRACT: Epigenetics, the study of genetic changes to chromatin that can impact gene expression, has emerged as a significant component of understanding cellular behavior and disease development. This work delves into the relationship between histone modifications and gene expression to explore the impact of epigenetic changes on gene behavior. Modification of Histone proteins in chromatin modifies the binding of histones to DNA. This influences gene accessibility to proteins such as RNA polymerase, thereby regulating gene expression levels. Histone modifications influence cellular behavior and play a critical role in biological processes, such as memory formation and cancer development. This paper explores the typical patterns of various histone modifications across genes, investigating how they interact and are related to gene expression. By examining these relationships, this study aims to understand the significant role of epigenetics in modulating gene behavior and its broader implications in biological systems. Epigenetics Research is crucial for developing drugs and understanding the inheritance of gene expression patterns in daughter cells and developmental biology. The latter deals with cellular differentiation and tissue-specific gene expression. This research examines the interplay between histone modifications and gene expression.

KEYWORDS: Animal Sciences, Genetics, Chromatin, DNA, Histone Modifications.

Introduction

Inheritance has long been related to the transmission of genetic information encoded within the DNA strands passed down from one generation of living organisms to the next. However, recent advancements in genetics have uncovered another layer of complexity in hereditary processes: epigenetics.[1] DNA sequence and the detailed assembly of DNA and proteins within the nucleus are crucial mediators of cellular behavior and inheritance. Recent studies have revealed that epigenetic modifications to chromatin also play a critical role in this regard.[2-4] These modifications, including changes to histone proteins, influence gene expression and affect basic yet important biological processes ranging from memory formation to developing diseases like cancer.

At the core of chromatin structure lies histone proteins, which are large biomolecules that DNA is wound around DNA forming nucleosomes. The modification of histones affects the accessibility of DNA, thus regulating gene expression levels. Histones can either promote or hinder the binding of regulatory proteins, such as the transcription factor TFIID, thereby regulating and modulating gene activity within the cell.

This research project focuses on the detailed interplay between histone modifications and gene expression, aiming to explain the underlying mechanisms of epigenetic regulation. By analyzing the positions and levels of histone modifications across genes and relating them to levels of transcription factors, RNA Polymerase, and nucleosome levels, this paper aims to explore the impact of histone modifications on transcription in active and inactive genes. In this work, typical patterns of various histone modifications across genes can be seen to unravel the complex and detailed web of epigenetics.[5] Central to this question is exploring how histone modifications correlate with gene expression profiles. By deciphering whether specific histone marks are associated with active or repressed genes, this paper aims to gain insights into the relevance of epigenetic modifications in shaping gene behavior and cellular processes. This study aims to reevaluate established research of transcriptional regulation by integrating ChIP-seq, MNase-seq, and NET-seq datasets within a unified metagene framework in yeast, *Saccharomyces cerevisiae*. The primary focus is to systematically examine how specific histone modifications like H3K4 methylation, H3 and H4 acetylation, and H2B ubiquitination relate to nucleosome positioning, transcription factor occupancy, and new RNA synthesis at and around the transcription start site (TSS). This work reexamines their interdependence by aligning and correlating transcription across thousands of genes. Through this approach, the study refines current understanding of how chromatin structure and chemical histone modifications such as methylations, acetylation, and ubiquitination dynamically interact to regulate transcription initiation and elongation.

The remainder of this paper is organized as follows. In this Section, the background and layout of the scope of our study are briefly described. Section 3 describes the methodology used to analyze the data sets and examine the role of histone modifications on gene expression. Section 4 describes the results obtained from our study, followed by a discussion of key findings in Section 5. Finally, the paper concludes with a summary of the study and areas and aspects that need further exploration.

Background:

Epigenetics refers to heritable changes in gene function that do not involve alterations to the underlying DNA sequence.

DOI: 10.36838/IJHSR810.94

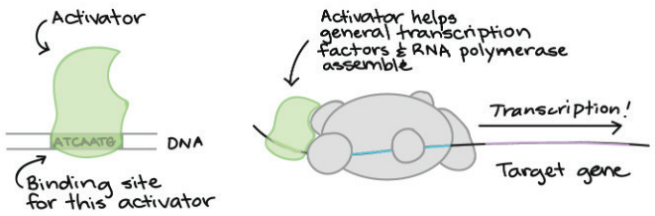

Figure 1: An activator, such as TFIID, a transcription factor that promotes transcriptional initiation, binds to a target DNA sequence. The subsequent binding of RNA polymerase and transcription factors to the activator initiates transcription. Transcription activators, as seen in Figure 1, are also impacted by histone modifications.

The N-terminus tails of histones undergo various chemical modifications, including methylation, acetylation, phosphorylation, and ubiquitination. These modifications alter the chromatin structure, influencing how tightly or loosely the DNA is packaged around histones. In turn, these histone modifications can regulate access to DNA by affecting the levels and/or types of transcription factors, repressors, and RNA polymerase present, subsequently changing levels of gene expression.

Various studies[1-3] have identified specific patterns of histone modifications that correlate with distinct gene activities in the context of transcriptional regulation for specific histone modifications. For example, histone acetylation is generally associated with open chromatin and active gene transcription. In contrast, histone methylation at certain lysine residues can mark either active or repressive chromatin states depending on the context.

The Transcription Start Site (TSS) in genes is where RNA polymerase binds to DNA to initiate transcription. Different histone modifications in the vicinity of the TSS affect chromatin structure, therefore regulating the accessibility of DNA to RNA polymerase. All histones show a common trend in affecting chromatin structure and regulating transcription. Histone modifications such as the promoter-associated H3K4me3 and the gene-body-enriched H3K36me3 show distinct positional patterns around the TSS that either promote or repress transcription.

Goal and Scope of the Present Study:

This study explores the role of histone modifications on gene expression using the yeast genome *Saccharomyces cerevisiae* as an example.[6] Though the study is limited to examining yeast, patterns of how histone modifications affect gene expression in this species represent how histones affect gene expression in other organisms as well. To limit the scope of the study and focus on understanding the fundamental role of histone modifications, the exploration is confined to certain histones and histone modification types. Histones considered in this study include H2, H3, H4, and H2B. Further, the exploration is limited to methylation, acetylation, and ubiquitination-based histone modifications.

■ Materials

This study draws on various datasets relating to the yeast genome *Saccharomyces cerevisiae*, which typically contains 6275 genes made available courtesy of the Cambridge Center of International Research. In this study, ChIP-seq data sets (Chromatin Immunoprecipitation Sequencing)* are used to identify regions of the genome enriched with specific histone modifications.[6] MNase-seq data (Micrococcal Nuclease Sequencing)* is used to assess nucleosome positioning and chromatin accessibility. By analyzing MNase digestion patterns, the influence of histone modifications on chromatin structure and DNA accessibility is explored, thereby impacting gene expression. MNase preferentially cuts exposed linker DNA but is blocked by tightly positioned nucleosomes. By analyzing MNase digestion patterns, we can determine where nucleosomes are positioned, how strongly they are packed, and how accessible the underlying DNA is. This is important because histone modifications often shift nucleosome positioning or stability, thereby altering chromatin accessibility and influencing whether transcription factors and RNA polymerase can access the DNA to initiate transcription.[7] This is repeated across the genome-wide dataset of histone modifications computationally. NET-seq data (Native Elongating Transcript Sequencing)* shows the level of RNA polymerase occupancy across genes, providing insights into active transcriptional activity.[8] This data is then analyzed in conjunction with histone modification profiles obtained from plotting histone levels across the gene body, and the correlation of specific modifications with transcription initiation, elongation, and termination processes is examined. This is carried out across the set of histone modifications considered.*

*Courtesy of the Cambridge Center of International Research (CCIR)

■ Methods

The analysis of the datasets and the analytical methods was completed as follows. First, a meta-gene data sequence of 5,331 functional genes in the S. cerevisiae yeast genome was created. Meta-genes embody a group of genes that refer to a collective gene expression analysis of histone-modification, MNase-seq, and NET-seq datasets, which was performed across a set of genes. They are used to summarize overall trends in transcriptional activity. The meta-genes data sequences were created by grouping genes exhibiting similar patterns of histone-modification enrichment profiles across genes and nucleosome levels.

Next, levels for each histone modification were plotted across the meta-gene. For each histone modification, 'average histone modification' refers to the mean ChIP-seq amount for that histone modification across all genes in the meta-gene. Gene bodies were divided into normalized bins relative to the TSS, and the signal in each bin was averaged across all genes of the same histone modification type to produce a quantitative meta-gene profile. For example, for the histone H3 lysine 4 methylation modification (H3K4me), three methylation states, monomethylation (H3K4me1), dimethylation (H3K4me2), and trimethylation (H3K4me3) were measured. The 'levels' of each modification refer to the ChIP-seq signal intensity associated with that modification at each genomic position. To generate an aggregate H3K4me profile across the meta-gene, the ChIP-seq signal intensities for H3K4me1,

H3K4me2, and H3K4me3 were averaged along the gene body. Histone modification levels were computed and plotted relative to the transcription start site (TSS) because the TSS marks the region where transcription is initiated. By analyzing the positional patterns of multiple histone modifications near the TSS, we can assess how activating and repressive marks correlate with transcriptional activity, including promoter accessibility and the recruitment of transcription factors and RNA Polymerase, which aid in the initiation of transcription. This approach allows us to specifically explore how different histone modifications influence gene expression at the promoter and early gene body regions.

MNase-seq (Micrococcal Nuclease Sequencing), ChIP-seq (Chromatin Immunoprecipitation Sequencing), and NET-seq (Native Elongating Transcript Sequencing) data were then analyzed across the meta-gene to assess nucleosome positioning, histone modification levels, and transcriptional activity, respectively. ChIP-seq datasets for the S. cerevisiae genome were used to obtain amounts of transcription factors across genes. MNase-seq data were used to assess nucleosome positioning and chromatin accessibility. By analyzing MNase digestion patterns, the influence of histone modifications on chromatin structure and DNA accessibility was explored, thereby affecting gene expression. MNase-seq uses micrococcal nuclease to preferentially digest exposed DNA between nucleosomes, while DNA wrapped around nucleosomes is protected. By closely observing MNase digestion patterns, nucleosome positions and occupancy can be mapped across the genome. Since histone modifications can alter nucleosome stability and positioning, these patterns reveal how specific modifications influence chromatin accessibility. Chromatin accessibility, in turn, affects the ability of transcription factors and the transcriptional machinery to engage DNA, thereby impacting gene expression. Thus, MNase digestion patterns provide a quantitative measure of how histone modifications modulate chromatin structure and regulate transcriptional activity. NET-seq data were used to measure nascent RNA associated with RNA polymerase II, providing maps of transcription across genes. This helps determine where transcription is actively initiating, how RNA polymerase progresses along the gene body, and where elongation may pause or terminate, thereby linking specific histone modification patterns to transcriptional activity. In addition to the meta-gene analyses, a genome-wide correlation plot was generated comparing H3K4me3 ChIP-seq signal to NET-seq nascent transcription levels. For this analysis, gene-body averaged H3K4me3 ChIP-seq values were computed for all genes and plotted against their corresponding NET-seq read densities. The resulting scatter plot provided a quantitative metric of the relationship between histone modification abundance and transcriptional output. This correlation analysis was used to validate whether positional enrichment patterns observed in the meta-gene profiles translated into genome-wide transcriptional behavior. The inclusion of this correlation plot in our analysis allowed us to directly test whether histone modification levels were predictive of transcriptional activity. By quantifying the association between H3K4me3 enrichment and RNA polymerase engagement, this method complemented the meta-gene-based approach and strengthened the overall interpretation that histone modifications actively contribute to transcriptional regulation. NET-seq data was also used to be analyzed in conjunction with histone modification profiles obtained in Step 1 to obtain a correlation of specific histone modifications with transcription initiation, elongation, and termination processes.

Correlation patterns between histone modification plots and MNase-seq, ChIP-seq, and NET-seq data plots were analyzed to find the relationship between transcription and histone modifications. In addition, the levels of various histone modifications across the genome were analyzed, which revealed the characteristic positional patterns of activating and repressive marks such as acetylation (e.g., H2AK5ac, H4AK8) and methylation (e.g., H3K4me1/2/3, H3K36me3) across gene promoters and gene bodies. These patterns reflect how specific chemical groups attached to histone tails are distributed along the genome and differ among the core histones (H2A, H2B, H3, and H4) that form the nucleosome. By examining these modification profiles, we identified how each histone mark varies relative to others and how their enrichment aligns with transcriptionally active or inactive chromatin regions.

Finally, correlations between patterns of histone modification levels and levels of transcription factors, RNA polymerase, and nucleosomes were established. These trends were compared against similar known trends reported in the literature that link gene expression to histone modifications.[4,20,25]

Results

In this section, the results of the analysis of histone modification data are presented, and their correlation to transcription is analyzed.

1. MNase-seq Data:

Figure 2 shows the nucleosome level across genes with high and low transcription in the constructed meta-gene of the *S. cerevisiae* genome. Genes with high transcription were used for metabolic processes, specifically in synthesizing enzymes that catabolize glucose, whereas inactive genes were used by the yeast far less often and are used only in rare, specific conditions. The plot shows active genes have a large deviation in nucleosome levels before the TSS, indicating the DNA is available for transcription. In contrast, more chromatin is present before the TSS in inactive genes, decreasing the likelihood that RNA polymerase can bind and initiate transcription.

DOI: 10.36838/IJHSR810.94

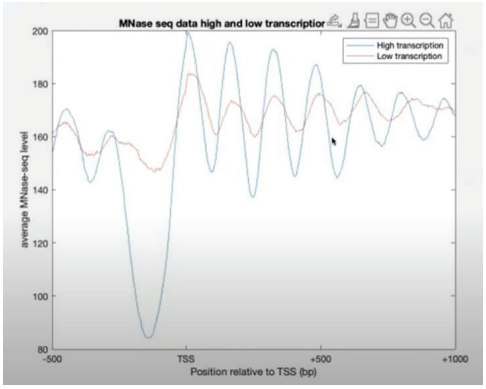

Figure 2: A plot of MNase-sequence data shows the nucleosome level across high-transcription and low-transcription genes. Active genes exhibit a sharp decline in nucleosome levels near the TSS, allowing RNA polymerase to bind and initiate transcription, whereas inactive genes have more nucleosomes before the TSS, which prevents transcription.

2. Net-Seq Data:

The Net-seq data plotted below shows the position at which RNA polymerase actively elongates and the density of RNA polymerase enzymes across the gene body (Figure 3). The position of RNA polymerase is primarily found at the TSS, where it initiates transcription, as indicated by the peak. RNA transcription then terminates at the end of the gene location, as evidenced by the significantly reduced density of RNA Polymerase near the gene index 1000 relative to the TSS, thus showing RNA Polymerase is not active in this position of the gene.

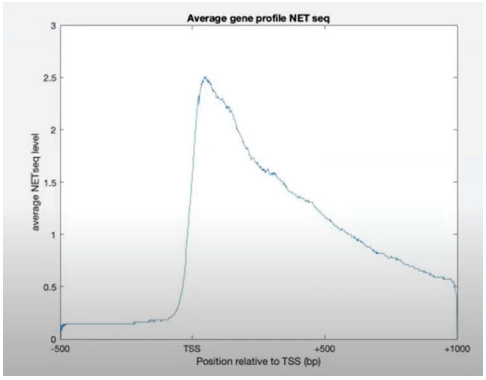

Figure 3: The Net-seq data show the locations of RNA polymerase enzymes across the gene body. Figure 3 shows that RNA polymerase levels peak at the TSS, where transcription begins, and decrease near the termination site, indicating the start and end of transcription.

3. ChIP-seq Data:

Figure 4 presents the ChIP-seq data analyzed for the S. cerevisiae genome, illustrating the distribution of transcription factors across gene bodies relative to the transcription start site (TSS). The figure reveals a pronounced enrichment of transcription factors near the TSS, indicating a high amount of transcription factors at this position. Histone modifications enriched at the TSS help recruit transcription factors, which, as seen in this figure, are found at the TSS, facilitating the initiation of transcription.

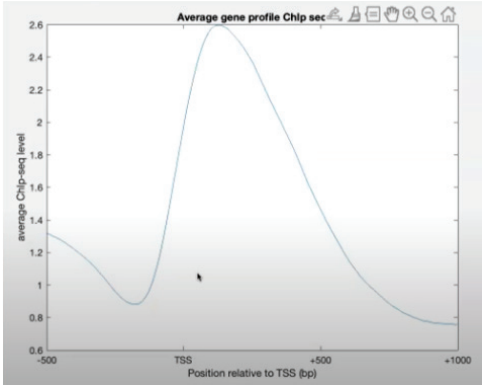

Figure 4: ChIP-seq data show transcription factors' locations across the gene body relative to the TSS. Transcription factors accumulate near the TSS, indicating their role in initiating transcription, as seen in Figure 4.

4. Average Level of H3K4 Methylation Across Genes:

This plot shows the level of H3K4 methylation across genes, including averaged levels across the H3K4me1, H3K4me2, and H3K4me3 modifications. H3K4 Methylation is associated with the transcription of genes and is therefore seen peaking at the TSS of actively transcribed genes. The dip observed just before the TSS corresponds to a H3K4 methylation-depleted region, where chromatin is open to allow transcriptional initiators and factors to access DNA, making it easier for RNA polymerase to bind to the DNA strand. In other words, the dip in H3K4 methylation indicates that fewer H3K4 methylation modifications are available, making chromatin less dense and signifying open chromatin. This histone modification also recruits transcription factors that aid in transcriptional initiation. H3K4 methylation peaks at the TSS, promoting transcription by facilitating open chromatin and recruiting transcription factors such as TFIID and CHD1, which bind to the methylated histone tail and help assemble the transcriptional initiation at the TSS.[19]

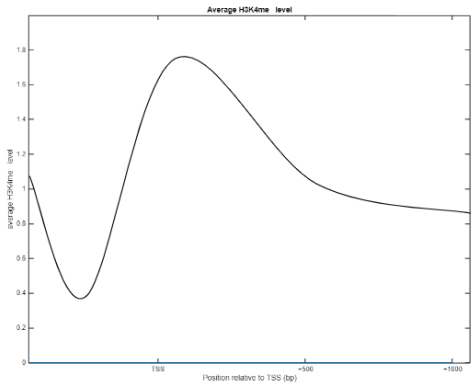

Figure 5: Average level of H3K4 methylation across the gene body relative to the TSS.

5. Average Level of H2AK5 Acetylation across genes:

Figure 6 displays the average levels of H2AK5 acetylation across genes, aligned relative to the transcription start site (TSS). The data show a clear peak of H2AK5 acetylation at the TSS, indicating that this modification is most abundant at the TSS of actively transcribed genes. This pattern suggests that H2AK5ac is associated with transcription initiation, consistent with its known role in loosening chromatin structure to facilitate access by the transcriptional factors and RNA polymerase,

as can be seen by the dip before the TSS. In the context of this study, the higher level of H2AK5ac near the TSS supports the broader finding that active histone modifications mark open chromatin regions, promoting gene expression.

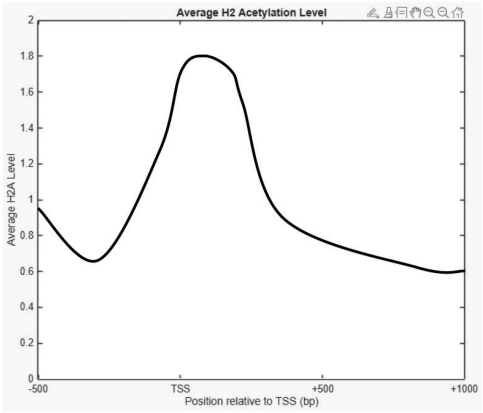

Figure 6: The level of H2AK5 acetylation across the gene body relative to TSS. H2AK5ac levels peak sharply at the TSS and decrease across the gene body.

6. Average Level of H3 Methylation Across Genes:

Figure 7 shows the level of other H3 methylations across genes. In this case, the levels do not peak at the TSS and are rather distributed across the gene body. H3 methylations promote transcription by stabilizing RNA polymerase II during elongation and by loosening nucleosomes, creating an open chromatin structure. This modification reduces nucleosome density and enhances chromatin accessibility, allowing RNA polymerase to move more efficiently along the DNA strand. Transcription is also facilitated by recruiting other transcription factors such as the FACT complex and Spt6, which interact with H3 methylation to reorganize nucleosomes and allow RNA polymerase II to move smoothly along the DNA strand.[20] that help make RNA polymerase move smoothly along the DNA strand. The plot shows the H3 methylation levels are distributed along the gene body, thereby promoting the recruitment of transcription factors that aid in the movement of RNA polymerase and facilitate transcription.

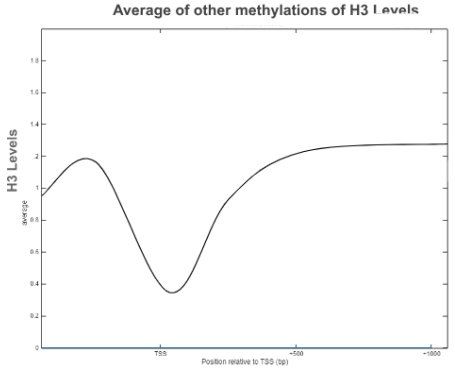

Figure 7: The average levels of H3 methylations across the gene body relative to the TSS. Histone 3 methylations are distributed along the gene body, which promotes transcription elongation by facilitating RNA polymerase movement.

7. Average Level of H3 Acetylation Across Genes:

Histone 3 acetylation peaks at the TSS of actively transcribed genes. A slight dip just upstream of the TSS corresponds to a histone-depleted region, where fewer histones are present, indicating a more open chromatin structure that allows transcription factors and RNA polymerase II to access the DNA. The high level of H3 acetylation at the TSS is consistent with its known role in reducing histone-DNA interactions, thereby loosening chromatin structure and facilitating transcription initiation by allowing RNA polymerase and transcription factors such as TFIID to easily initiate transcription and bind to the TSS region of the gene.

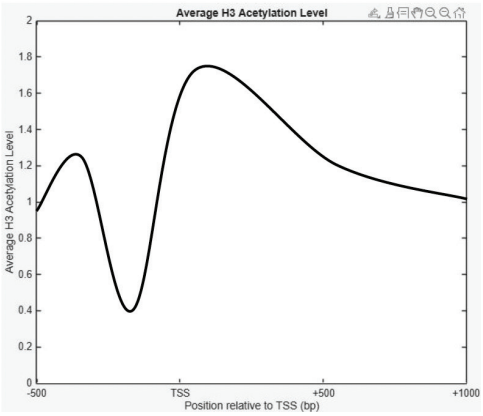

Figure 8: The Average histone 3 acetylations across the gene body relative to the TSS. Histone 3 acetylation peaks at the TSS, promoting transcription initiation by keeping an open chromatin structure, as seen in Figure 8.

8. Average Level of H4 Acetylation Across Genes:

Figure 9 depicts the level of H4 acetylation, which peaks at the TSS of actively transcribed genes. The dip before the TSS suggests an open chromatin structure, allowing RNA polymerase to bind easily to the DNA strand. H4 acetylation peaks at the TSS of actively transcribed genes, marking nucleosomes at the promoter. In addition, this modification recruits bromodomain-containing chromatin remodeling complexes, such as SWI/SNF, directly to the acetylated histone tails at the TSS and nearby nucleosomes.[21] These remodelers reposition nucleosomes downstream of the TSS, facilitating not only transcription initiation but also efficient elongation by RNA polymerase II along the gene body. Histone 4 acetylation peaks at the TSS, promoting transcription initiation by increasing DNA accessibility.

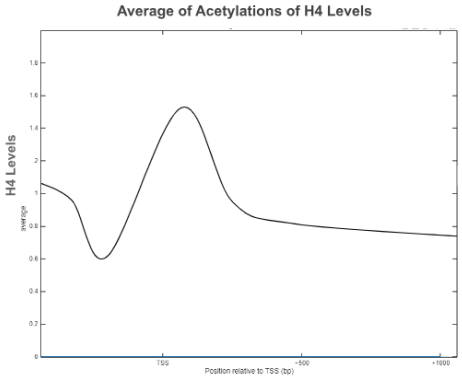

Figure 9: The Average level of H4 acetylation across the gene body relative to the TSS. Figure 9 shows H4 acetylation peaks at the TSS, promoting transcription initiation by increasing DNA accessibility.

9. Average Level of H2B123UB Across Genes:

The plot in Figure 10 shows the level of H2B123UB. It is seen to peak at the TSS, which is known to help with

DOI: 10.36838/IJHSR810.94

transcriptional elongation of RNA, thereby allowing RNA polymerase to move smoothly across the gene body. In addition, H2B123UB participates in histone crosstalk; in other words, the ubiquitination of H2B influences the methylation of adjacent histone tails (notably H3K4 and H3K79), thereby creating a chromatin environment more permissive for transcription. For example, ubiquitinated H2B has been shown to stimulate the activity of H3K4 methylation, which in turn creates binding sites for transcriptional regulators.[22,23] This histone modification also recruits transcriptional repressors in inactive genes.

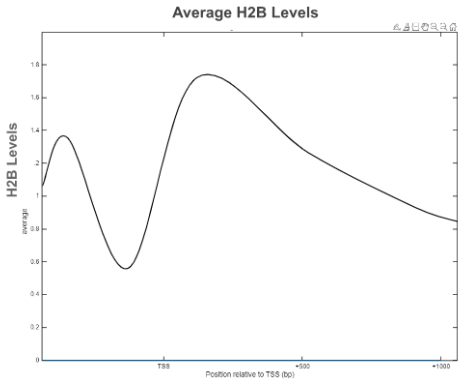

Figure 10: The level of histone H2B123Ub across the gene body relative to the TSS. H2B123Ub supports transcription elongation in active genes but also plays a role in gene repression when present in inactive genes, as seen in Figure 10.

10. Average Level of H3K9 and H3K27 Methylation Across Genes:

This plot shows the average amount of H3K9 and H3K27 methylation across genes relative to the TSS and transcription termination site (TTS). In actively transcribed genes, H3K9me and H3K27me levels are low at the TSS and gradually increase toward the TTS, reflecting their minor role in promoting the transcription of active genes. Instead, these modifications are associated with gene repression because they recruit chromatin-compacting proteins across the gene body that restrict access of RNA polymerase II and transcription factors to DNA.[2] In contrast, in inactive genes, H3K9me and H3K27me amounts are high upstream of the TSS, where their presence contributes to chromatin compaction and prevents transcription initiation, further repressing gene expression.[3]

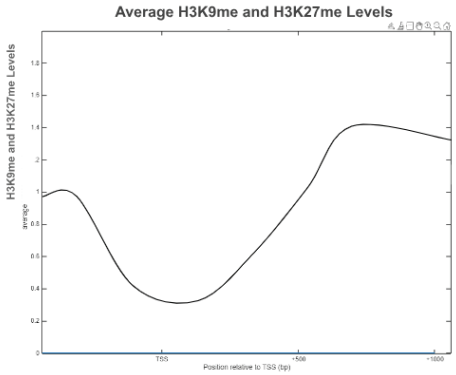

Figure 11: Average level of H3K9 and H3K27 methylations across the gene body. H3K9 and H3K27 methylations repress transcription by compacting chromatin and obstructing RNA polymerase binding.

11. ChIP-seq Data Across Active and Inactive Genes:

Figure 12 shows the enrichment of transcription factors across genes relative to the TSS in both high and low transcription genes. In active genes, general transcription factors such as TFIID, TBP (TATA-binding protein), and Spt6, along with elongation-associated factors like Spt16 (part of FACT) and Paf1, peak shortly downstream of the TSS. These factors facilitate transcription initiation and elongation by helping RNA polymerase II bind to promoters, stabilize its passage along nucleosomes, and coordinate chromatin remodeling. In contrast, in inactive genes, repressor proteins such as Ssn6-Tup1 or chromatin-bound histone readers may occupy similar regions, blocking RNA polymerase binding or impeding elongation. The varying binding of transcription factors in active versus inactive genes demonstrates how transcription factor recruitment regulates gene expression. In yeast, this ensures that only genes needed under specific conditions are expressed, while in higher eukaryotes, similar mechanisms allow precise control of gene transcription, contributing to cellular differentiation and response to environmental signals.

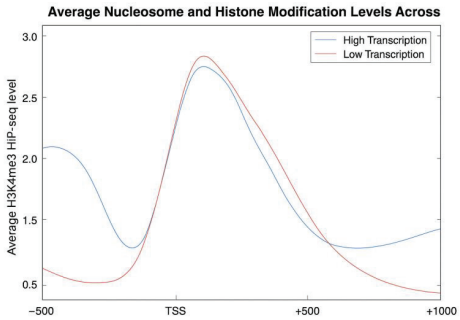

Figure 12: The ChIP-seq data show the locations of transcription factors across the gene body for genes with high and low transcription relative to the TSS. Transcription factors peak downstream of the TSS in highly transcribed genes, supporting RNA polymerase II elongation, while in lowly transcribed genes, factors are enriched near the promoter or upstream regions, consistent with repression of transcription initiation.

12. Histone Density Variation Across Genes:

In this study, the variation of levels of histone modifications was examined across the genome. Specifically, subsets of genes exhibiting high and low levels of histone were identified for each of the histone modifications. This was accomplished using two-way clustering of histone levels for each modification type using the K-median clustering algorithm.[31] A 1500 base-pair segment around the TSS was split into 30 equally-spaced intervals, and the mean histone level (density) was computed across these intervals. In the clustering scheme, the histone density over these 30 intervals was chosen to be the feature set, and the density vectors across the genes are the observations.

Figure 13 shows a high and low-histone level clustering for the H3K4me3 Histone modification, which is known to promote gene transcription. The plot shows more pronounced peaking of the histone level around the TSS for Cluster 1 (high-level) compared to Cluster 2 (low-level). This would in turn suggest a higher likelihood of the H3K4me3 Histone modification promoting gene transcription in the Cluster 1 genes compared to Cluster 2.

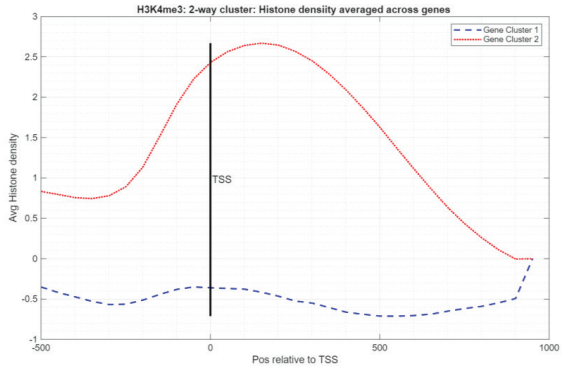

Figure 13: Average H3K4me3 density across gene bodies relative to the transcription start site (TSS), separated into two clusters. Cluster 1 (red) shows high enrichment downstream of the TSS, indicative of actively transcribed genes, while Cluster 2 (blue dashed) shows low enrichment, corresponding to lowly transcribed genes.

Figure 14 shows a high and low-histone level clustering for the H3K36me3 Histone modification, which is known to repress gene transcription in most cases. The plot shows more pronounced peaking of the histone level towards the end of the gene segment for Cluster 1 (high-level) compared to Cluster 2 (low-level). This finding suggests a higher likelihood of the H3K36me3 Histone modification in repressing gene transcription in the Cluster 1 genes compared to Cluster 2.

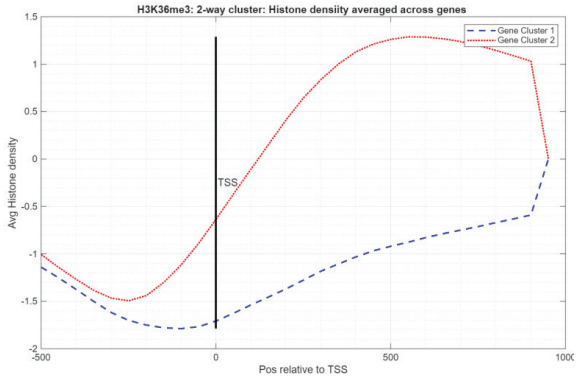

Figure 14: Average H3K36me3 density across gene bodies relative to the TSS, separated into two clusters. Cluster 2 (red) shows strong H3K36me3 accumulation toward the transcription termination site (TTS), consistent with genes undergoing elongation-coupled repression, while Cluster 1 (blue dashed) shows minimal enrichment across the gene body, characteristic of actively transcribed genes.

The bar plot in Figure 15 presents the variation of histone densities across genes, summarized for the entire histone set considered in this study. This plot shows the ratio of the number of genes exhibiting high histone levels relative to the number of genes exhibiting significantly lower levels of histone levels. The plot shows that different histone modifications are manifested to significantly varying degrees across genes.

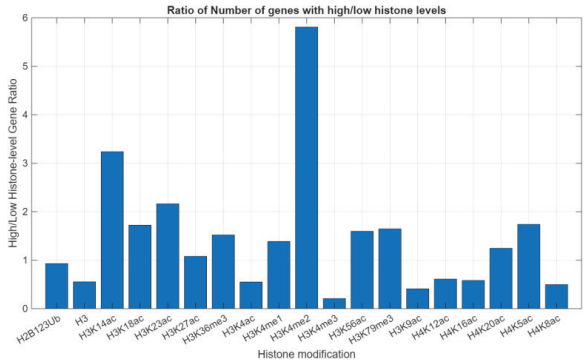

Figure 15: Ratio of the number of genes exhibiting a high level of histone modification relative to the gene subset with low histone levels. This data was obtained using a K-medioids-based two-way clustering scheme with signal over a fixed segment of base-pairs around the TSS as the features and genes as the observations.

13. Distribution of Histone Levels Relative to TSS:

In this section, we examine the distribution of histone levels over a gene segment in the vicinity of the TSS. Specifically, a gene segment ranging from 499 base-pairs on the leading side of the TSS and 1000 base-pairs to the trailing side of the TSS was considered. Histogramming of the histone level across this segment was then performed with the 5331-gene set treated as independent observations. This probabilistic analysis factors in the variation of histone levels across genes.

To assess the distribution of H3K4me3 across gene segments, we plotted the positions of minimum and maximum signal intensities relative to the TSS. The Max-signal histogram in Figure 14 shows a strong concentration of signal peaks near the TSS, consistent with H3K4me3's role in marking active promoters. The Min-signal histogram in Figure 15 shows a peak at the TTS and start of the gene, signifying its role as purely a transcription-promoting histone. The clustering of maximum signals around the TSS highlights its function in facilitating transcription initiation. These probabilistic profiles confirm that H3K4me3 is tightly localized to promoter regions and can reliably indicate transcriptional activity. These results reinforce the functional importance of H3K4me3's density across genes in transcriptional regulation and demonstrate that signal peak positions can be used to infer promoter activity and chromatin state across diverse gene sets.

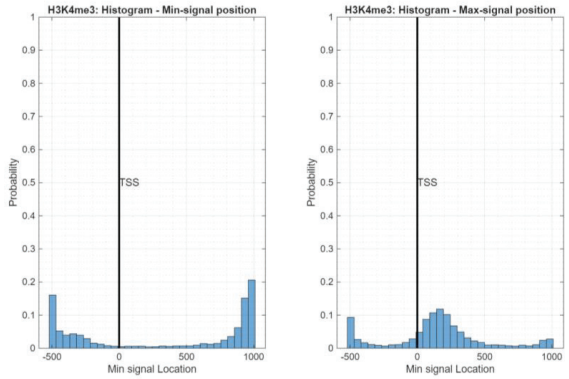

Figure 16: Histograms show the positions of minimum and maximum H3K4me3 signal intensities across genes relative to the TSS. Both distributions cluster sharply at the TSS, reflecting H3K4me3's localization to active promoters.

DOI: 10.36838/IJHSR810.94

To examine the signal distribution of H3K36me3, we plotted the probable positions of minimum and maximum signal intensities relative to the TSS. As shown in Figure 16, both histograms reveal that H3K36me3 signals are predominantly located towards the end of the gene, with maximum signal positions broadly distributed towards the TTS of the gene body, while the minimum-signal positions show the histones' reduced density at the start of the gene and the TSS showing its role as a transcriptional repressor. This pattern is consistent with H3K36me3's role as a repressive histone mark deposited during transcriptional elongation to suppress cryptic initiation and modulate gene output. These probabilistic plots highlight the gene-body localization of H3K36me3 and support its function in repressing transcriptional activity.

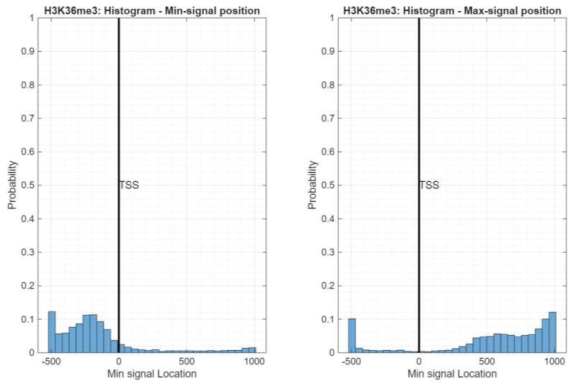

Figure 17: Histograms show the positions of minimum and maximum H3K36me3 signal intensities relative to the TSS. Maximum-signal positions are broadly distributed toward the TTS, reflecting H3K36me3 accumulation along the gene body, while minimum-signal positions cluster near the TSS. This distribution is consistent with H3K36me3's role as an elongation-linked repressive mark.

14. Correlation Between H3K4me3 Enrichment and Net-Seq Data:

To investigate the relationship between histone modifications and transcription, we compared gene-body H3K4me3 levels (measured by ChIP-seq) with nascent transcription (measured by NET-seq). Figure 17 shows a scatter plot of H3K4me3 ChIP-seq signal versus NET-seq signal across all analyzed genes. A positive correlation (r = 0.43) was observed, indicating that genes with higher H3K4me3 enrichment in their gene bodies tend to exhibit higher levels of transcription. This positive correlation is consistent with the known role of H3K4me3 as an activating histone mark, often enriched at promoters and early gene bodies of actively transcribed genes. The inclusion of this plot in our study provides quantitative evidence that H3K4me3 is functionally associated with transcriptional output in S. cerevisiae. By demonstrating this relationship, the figure supports our broader goal of linking specific histone modifications to transcriptional regulation. Specifically, it shows that H3K4me3 is not just present in genes, but its abundance quantitatively correlates with RNA polymerase engagement and transcriptional activity, validating its role as a marker of active gene expression in the context of our genome-wide analysis.

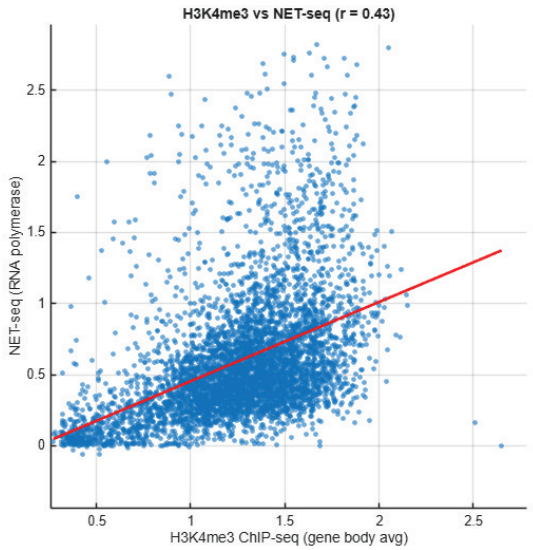

Figure 18: Scatter plot showing the relationship between gene-body H3K4me3 levels (ChIP-seq) and nascent transcription (NET-seq) across all analyzed genes in S. cerevisiae. A positive correlation (r = 0.43) indicates that higher H3K4me3 enrichment is associated with increased transcriptional activity because of increased amounts of RNA Polymerase at the TSS.

15. Histone Modification Summary Table:

Histone Modification:	Histone Role:	Observed Patterns:
1. H3K4 methylation	An activating histone modification that promotes transcription by recruiting transcription factors and RNA polymerase and opening chromatin at the TSS. H3K4me marks active promoters and stabilizes transcription initiation complexes.[18]	Strong peak immediately at the TSS in actively transcribed genes. A dip before this TSS reflects a histone-depleted region needed for RNA polymerase binding. High H3K4me3 correlates with increased NET-seq signal and transcription factor occupancy.
2. H2AK5 Acetylation	An activating acetylation mark that loosens chromatin, allowing transcription factors and RNA polymerase to access the promoter region. Associated with early transcription initiation.[20]	Sharp enrichment at the TSS with levels declining across the gene body. The dip before the TSS indicates open chromatin. Pattern reflects its role in promoter accessibility and transcription initiation.
3. H3 Methylation	Supports transcriptional elongation by stabilizing nucleosomes during RNA polymerase movement and recruiting elongation factors like FACT and Spt6.[10]	Distributed across the gene body rather than concentrated at the TSS. Levels increase towards the TTS of the gene body, reflecting a role in elongation rather than initiation.
4. H3 Acetylation	A strong transcription-activating modification associated with open chromatin, reduced nucleosome packing, and recruitment of TFIID and other initiation factors.[16]	High peak at the TSS in active genes with a small dip directly before the TSS (histone-depleted region). Enhances promoter accessibility and supports transcription initiation.
5. H4 Acetylation	Promotes transcription initiation by loosening chromatin at promoter regions and recruiting bromodomain-containing remodelers (e.g., SWI/SNF). Supports both initiation and early elongation.[29]	Strongly enriched at the TSS and decreases across the gene body. The dip before the TSS marks areas of open chromatin needed for RNA polymerase binding.
6. H2B	A ubiquitination mark that supports transcription elongation and activates methylation (H3K4 and H3K79) through histone crosstalk. Can also recruit repressive factors in inactive genes.[13,21,22]	Peaks at the TSS and early gene body. Supports RNA polymerase movement across genes but can also appear in inactive genes where it interacts with repressors.
7. H3K9, H3K27 and H3K36 Methylation	Repressive histone modifications that compact chromatin and prevent transcription initiation. - H3K9me and H3K27me: Promoter-proximal repression.[14] - H3K36me3: Deposited during elongation to suppress transcription and reduce gene output.[9]	In inactive genes there are high levels before the TSS, forming closed, compact chromatin(for H3K36me). In active genes there are low levels at the TSS but they increase toward the TTS.

■ Discussion

Histone Modification Enrichment in the Gene Body:

The results showed various patterns of histone modifications around genes and their effect on gene transcription.

Histone modifications, specifically H3K4me3, H3K4me1, and H3K4me2, exhibited enrichment near the TSS of the meta-gene, suggesting that they are likely to play a role in the transcription of active genes in S. cerevisiae. Results show a peak in amounts of H3K4me around the TSS. As shown by the Chip-seq data, the peak of transcription factors across the gene body also occurs at the TSS. This correlation is in line with H3K4me histone modifications recruiting transcription factors at the TSS for transcriptional initiation.[13] A similar peak around the TSS is also seen in the Net-seq data, showing RNA polymerase levels across the gene body. This relationship is further supported by the H3K4me3–NET-seq correlation (r = 0.43) seen in Figure 17, showing that higher levels of this activating mark correspond to increased nascent transcription. The high amount of H3K4me histones can recruit transcription factors.[11] Methylation contributes to an open chromatin structure, promoting transcriptional initiation.[9]

In contrast, other methylations, such as H3K36me3, were found to be more distributed over the gene body towards the TTS rather than concentrated at the TSS of the meta-gene. The meta-gene profiles show a clear separation of methylation states: H3K4 methylation concentrated at the TSS and H3K36 methylation increasing across the gene body. This pattern is not just correlative; it reflects the specialization of these methyl groups. H3K4me3 at the TSS functions as a landing for PHD-finger and Tudor-domain-containing proteins, which bind to the histones, allowing transcription factors to easily recruit transcription factors that stabilize the assembly of transcriptional initiation and early elongation factors, increasing transcriptional initiation at the TSS.[25] By contrast, H3K36 methylation deposited transcriptionally by elongation-coupled methyltransferases marks nucleosomes that have been traversed by RNA polymerase II and recruits chromatin regulators that act behind the polymerase.[10,26] In the data(Figure 18), the graded increase of H3K36me across gene bodies correlates quantitatively with NET-seq polymerase density, which is consistent with a role for H3K36me in coupling nucleosome state to polymerase processivity rather than simply reflecting past polymerase passage.[27-29]

H2AK5ac levels were found peaking at the TSS and steadily dropping towards the transcription termination site, suggesting a specific role in transcriptional initiation. The enrichment of H2AK5ac near the TSS likely facilitates transcription by promoting an open chromatin configuration, allowing easier access for RNA polymerase II and general transcription factors. This acetylation mark also serves as a recognition site for bromodomain-containing coactivators, which help recruit components of transcriptional initiation to the promoter.[24] The subsequent decline of H2AK5ac levels across the gene body suggests its primary involvement in the early stages of transcription, where the TSS accessibility and transcriptional initiation formation are most critical. Similarly, H4 acetylation is enriched at the TSS and decreased towards the transcription termination site. Among these modifications, methylation, ubiquitination, and acetylation are particularly significant. Each type of modification has distinct effects on histone function, leading to varying impacts on transcriptional activity. Methylation of histones generally occurs on lysine or arginine residues and can result in either transcriptional activation or repression, depending on the specific site. For example, H3K4me3 peaks at the TSS, consistent with previous reports that it recruits PHD- and Tudor-domain–containing proteins to facilitate pre-initiation complex assembly.[27]

Similarly, H2B123Ub and H3K36me show coordinated patterns along the gene body, supporting the concept of histone crosstalk in promoting transcriptional activity and also suppressing initiation.[24,26] Presenting this information here highlights how our findings corroborate and extend prior literature by mapping these modifications systematically across active and inactive gene regions in *S. cerevisiae*. The enzymes responsible for this modification are called methyltransferases. For instance, trimethylation of lysine 4 on histone H3 (H3K4me3) is enriched at the TSS of genes with high transcription. This modification is associated with gene activation and facilitates the recruitment of transcriptional machinery, enhancing transcription efficiency.[11] However, H3K27me3 is typically linked to gene repression.[12]

H3K4me3 is enriched at the TSS of genes with high transcription, promoting gene activation by serving as a binding platform for "reader" proteins containing PHD or Tudor domains, which recruit transcriptional activators, chromatin remodelers, and transcription factors such as TFIID. By stabilizing these factors at promoters, H3K4me3 increases accessibility of the DNA to RNA polymerase II, facilitating transcription initiation and early elongation.[5] Conversely, H3K27me3 results in repression by recruiting Polycomb repressive complexes (PRC1 and PRC2), which compact chromatin, limit nucleosome mobility, and prevent binding of transcription factors and RNA polymerase. In this way, H3K27me3 establishes a closed chromatin state that silences gene expression.[19] The level of H3K27 methylation is higher before the TSS, lower at the TSS, and higher at the transcription termination site, suggesting that it is a repressive histone.[11] High levels of H3K27me recruit Polycomb repressive complexes, which compact nucleosomes and reduce DNA accessibility, preventing RNA polymerase and transcription factors from binding.[29] Additionally, H3K27me interacts with other histone modifications, forming a coordinated network that reinforces gene-specific transcriptional states. Together, these observations indicate that H3K27 methylation actively enforces a stable, repressive chromatin environment in inactive genes.

Ubiquitination involves the attachment of ubiquitin molecules to specific lysine residues on histones, and this process is mediated by a group of enzymes known as ubiquitin ligases. Ubiquitination can have variable effects on transcriptional regulation. For example, H2B123Ub is associated with active transcription. However, this modification can recruit repressive factors that inhibit gene expression by promoting a closed chromatin conformation. H2B123Ub levels were higher near the transcription start sites of actively transcribed genes. This suggests a role in the initiation of transcription. H2B123Ub increases at the promoter of genes affecting gene expression by promoting transcription of certain genes while repressing others.[14] For example, transcription activators that

DOI: 10.36838/IJHSR810.94

are ubiquitinated are frequently degraded, thus repressing gene expression.[13]

Functionally, H3K36 methylation contributes to transcriptional repression by recruiting complexes (histone deacetylases and histone chaperones) that restore nucleosome structure and suppress spurious internal initiation. This explains why genes with strong amounts of H3K36me in our study show fewer signs of transcription when looking at NET-seq data: methylation helps re-establish a chromatin environment that prevents transcription within coding regions. Moreover, H2B123Ub and H3K4 methylation exhibit crosstalk. H2B123Ub enrichment at the TSS and early gene body coincides with downstream H3K4me and H3K79me levels, suggesting a cascade in which one influences the other. This interdependence implies that methylation patterns shape nucleosome dynamics not in isolation but as part of a coordinated modification network that helps transcriptional initiation and elongation. For example, acetylation of lysine residues on histones, including H4K8ac, neutralizes the positive charge of histones.[15] This reduces the closeness of histones to negatively charged DNA, loosening their grip on the DNA strand and making the chromatin structure more open and accessible.4 This open chromatin state allows transcription factors and RNA polymerase to access the DNA and initiate transcription. This is particularly relevant because peaks of H4 acetylation at the TSS correlate with regions of active transcription, indicating that this modification actively facilitates RNA polymerase and transcription factor binding in *S. cerevisiae*.[31] Therefore, H4K8ac and other H4 acetylation at promoters and enhancers increase gene expression. However, H3K9me and H3K27me are absent at the TSS of active genes because they are associated with gene repression.[6] These genes are not as crucial for yeast and are therefore repressed in most cases.[31]

Varying Histone Modifications and the Role of Histone Modification Patterns in Gene Expression:

Different histone modifications vary in location within genes. The methylation of histones can have repressive effects on transcription, but is also associated with transcription initiation, while the acetylation of histones is associated with transcriptionally active genes. Methylation can either repress or activate transcription depending on the specific residue and location within the gene; for example, H3K4me3 at promoters facilitates transcription initiation by recruiting transcription factors and coactivators, whereas H3K27me3 generally represses gene expression by promoting chromatin compaction.[13] Acetylation of histones, such as H3 and H4 lysine acetylation, is generally associated with transcriptionally active genes, particularly at the TSS, where it creates an open chromatin structure and increases DNA accessibility.[21]

However, the impact of acetylation can vary depending on the presence of other histone modifications and the local chromatin environment.[21]

In our study, observing peaks of H3 and H4 acetylation at the TSS supports their role in facilitating transcriptional initiation and aligns with the enrichment of RNA polymerase and transcription factors at these regions. Histone modifications can be enriched in specific gene regions, such as promoters, enhancers, or gene bodies.[15] At the same time, H3K4me histones were primarily found around the TSS.10 Certain histone modifications located in the gene body and towards the transcription termination site of genes also regulate gene expression. For example, H3K36me3 prevents premature transcriptional termination in the gene body, facilitates the movement of RNA polymerase along the gene body, and thus promotes gene expression.[16]

The ChIP-seq data show that peak levels of transcription factors across genes with low transcription and genes with high transcription are similar. Chip-seq data peaks after the TSS, showing there are many transcription factors and gene promoters at that position in the gene, and H3K4 histone modifications also peak after the TSS, showing that the level of H3K4 histone levels is high at this point. Analysis of the ChIP-seq data alongside the H3K4me data reveals a positive correlation at the TSS, where higher H3K4me levels coincide with increased binding of transcription factors.[19] This correlation is important because it provides evidence that H3K4me actively contributes to the recruitment of transcription factors that promote transcriptional initiation. This supports the interpretation that H3K4me acts as a functional recruiter for active transcription factors, linking histone modification to gene expression regulation in S. cerevisiae. MNase-seq data reveal differences in nucleosome occupancy between genes with high and low transcription. Genes with low transcription exhibit higher nucleosome levels immediately upstream of the TSS, creating a more compact chromatin structure that limits accessibility for RNA polymerase and transcription factors. In contrast, highly transcribed genes show a relative depletion of nucleosomes near the TSS, consistent with an open chromatin state that facilitates transcriptional initiation.[30] These patterns highlight the relationship between nucleosome positioning and gene activity, demonstrating how chromatin structure can directly influence transcriptional output.

An important difference seen in the MNase-seq data is that the level of nucleosomes for genes with low transcription was much higher than for genes before the TSS, which had high levels of transcription. In addition to this, the NET-seq analysis (Figure 18) revealed that genes with higher H3K4me3 levels also display higher nascent transcription, as shown by the positive correlation in our scatter plot. This indicates that H3K4me3 enrichment is not only associated with transcription factor binding but also quantitatively associated with RNA polymerase II occupancy along the gene body.

■ Future Directions

This study focused on the role of specific histone modifications and their nucleosome positioning on transcriptional activity. Future work is needed to determine the causal mechanisms underlying these relationships beyond what has already been reported in the literature. Targeted perturbations, such as mutating key histone residues or disrupting the enzymes responsible for their modifications, could clarify how individual histone modifications directly influence transcription initiation and elongation. Complementary approaches that include

ChIP-seq to assess factor binding, RNA-seq to measure transcript output, or high-resolution chromatin accessibility assays would provide a more detailed understanding of how histone modifications coordinate with transcriptional machinery. Additionally, exploring these dynamics under different environmental conditions or stress responses in *S. cerevisiae* could reveal how chromatin regulation adapts to changing cellular states. Overall, such studies would extend the insights gained from our meta-gene analyses and the larger body of work by other researchers in this area. In particular, this would help establish a mechanistic framework linking histone modifications to gene regulation.

Conclusion

In this study, the significant role of a select set of epigenetic histone modifications in S. cerevisiae was explored. The observed distributions of histone modification levels relative to the transcription start site and transcription termination site were found to be in agreement with these histone modifications being gene transcription promoters or repressors, as reported in prior studies. The research also depicts the varying levels of specific histone modifications across genes, highlighting their varying roles in different genes. The work also describes simple but powerful data-analytic methods to understand trans-gene trends of histone modifications. These methods can be improved and extended further in future studies to gain deeper insights into histone modification behaviors and their role in gene regulation.

Acknowledgments

Thank you to Professor Struan Murray of Cambridge University and Aiswarya Udayakumar for their help in this project. Their assistance made this project possible and ensured the understanding of all the material necessary.

References

1. Abdul, Q. A., Yu, B. P., Chung, H. Y., Jung, H. A., & Choi, J. S. (2017). Epigenetic modifications of gene expression by lifestyle and environment. *Archives of Pharmacal Research*, ***40***, 1219–1237. https://doi.org/10.1007/s12272-017-0973-3
2. Hu, G., & Zhao, K. (2014). Correlating histone modification patterns with gene expression data during hematopoiesis. In N. J. Clifton (Ed.), *Methods in Molecular Biology* (Vol. ***1150***, pp. 175–187). Humana Press. https://doi.org/10.1007/978-1-4939-0512-6_11
3. Chervona, Y., Arita, A., & Costa, M. (2012). Carcinogenic metals and the epigenome: Understanding the effect of nickel, arsenic, and chromium. *Metallomics*, ***4***(7), 619–627. https://doi.org/10.1039/c2mt20033c
4. Gibney, E. R., & Nolan, C. M. (2010). Epigenetics and gene expression. *Heredity*, ***105***, 4–13. https://doi.org/10.1038/hdy.2010.54
5. Dai, H., & Wang, Z. (2014). Histone modification patterns and their responses to environment. *Current Environmental Health Reports*, ***1***, 11–21. https://doi.org/10.1007/s40572-013-0008-2
6. Chereji, R. V., Ocampo, J., & Clark, D. J. (2017). MNase-sensitive complexes in yeast: Nucleosomes and non-histone barriers. *Molecular Cell*, ***65***(3), 565–577.e3. https://doi.org/10.1016/j.molcel.2016.12.009
7. Schaughency, P., Merran, J., & Corden, J. L. (2014). Genome-wide mapping of yeast RNA polymerase II termination. *PLoS Genetics*, ***10***(10), e1004632. https://doi.org/10.1371/journal.pgen.1004632
8. Tyler, A. L., Spruce, C., Kursawe, R., Haber, A., Ball, R. L., Pitman, W. A., … Carter, G. W. (2023). Variation in histone configurations correlates with gene expression across nine inbred strains of mice. *Genome Research*, ***33***(6), 857–871. https://doi.org/10.1101/gr.277467.122
9. Armfield, L. D. (2019). *The role of histone H3K36me3 in mammalian cell cycle regulation and genome stability* (Doctoral dissertation). University of Oxford.
10. Selth, L. A., Sigurdsson, S., & Svejstrup, J. Q. (2010). Transcript elongation by RNA polymerase II. *Annual Review of Biochemistry*, ***79***, 271–293.
11. Heinig, M., Colomé-Tatché, M., Taudt, A., Rintisch, C., Schäfer, S., Pravenec, M., … Johannes, F. (2015). histoneHMM: Differential analysis of histone modifications with broad genomic footprints. *BMC Bioinformatics*, ***16***, 60. https://doi.org/10.1186/s12859-015-0491-6
12. Dhar, G. A., Saha, S., Mitra, P., & Chaudhuri, R. N. (2021). DNA methylation and regulation of gene expression: Guardian of our health. *The Nucleus*, ***64***(3), 259–270. https://doi.org/10.1007/s13237-021-00367-y
13. Oss-Ronen, L., Sarusi, T., & Cohen, I. (2022). Histone mono-ubiquitination in transcriptional regulation and its mark on life: Emerging roles in tissue development and disease. *Cells*, ***11***(15), 2404. https://doi.org/10.3390/cells11152404
14. Mazzio, E. A., & Soliman, K. F. A. (2012). Basic concepts of epigenetics: Impact of environmental signals on gene expression. *Epigenetics*, ***7***(2), 119–130. https://doi.org/10.4161/epi.7.2.18764
15. Lelandais, G., Berretta, J., Mariotti, F. R., & Libri, D. (2016). ChIP-seq in yeast species. In *Methods in Molecular Biology* (pp. 185–202). Humana Press. https://doi.org/10.1007/978-1-4939-3079-1_11
16. Gelato, K. A., & Fischle, W. (2008). Role of histone modifications in defining chromatin structure and function. *Biological Chemistry*, ***389***(4), 353–363. https://doi.org/10.1515/BC.2008.048
17. Murray, S. C., Haenni, S., Howe, F. S., Fischl, H., Chocian, K., Nair, A., & Mellor, J. (2015). Sense and antisense transcription are associated with distinct chromatin architectures across genes. *Nucleic Acids Research*, ***43***(16), 7823–7837. https://doi.org/10.1093/nar/gkv666
18. Vermeulen, M., *et al.* (2007). Selective anchoring of TFIID to nucleosomes by trimethylation of histone H3 lysine 4. *Cell*, ***131***(1), 58–69.
19. Kizer, K. O., *et al.* (2003). A novel domain in Set2 mediates RNA polymerase II interaction and couples histone H3 K36 methylation with transcription. *Molecular Cell*, ***11***(3), 735–746.
20. Church, M. C., *et al.* (2017). A role for histone acetylation in regulating transcription via chromatin remodelling. *Biochimica et Biophysica Acta – Gene Regulatory Mechanisms*, ***1860***(1), 183–192.
21. Vlaming, H., *et al.* (2014). Flexibility in crosstalk between H2B ubiquitination and H3 methylation in vivo. *EMBO Reports*, ***15***(10), 1077–1084.
22. Kwon, M., *et al.* (2021). H2B ubiquitylation enhances H3K4 methylation activities of human KMT2 family complexes. *Nucleic Acids Research*, ***48***(10), 5442–5456.
23. Carrozza, M. J., *et al.* (2005). Histone H3 methylation by Set2 directs deacetylation of coding regions by Rpd3S to suppress spurious intragenic transcription. *Cell*, ***123***(4), 581–592.
24. Keogh, M.-C., *et al.* (2003). Set2 is required for histone H3 lysine 36 methylation and transcriptional elongation by RNA polymerase II. *Molecular Cell*, ***11***(4), 1085–1096.

DOI: 10.36838/IJHSR810.94

25. Krogan, N. J., *et al.* (2003). Set2 methylation of histone H3 lysine 36 links histone acetylation to transcriptional elongation. *Molecular Cell*, ***11***(3), 721–729.
26. Santos-Rosa, H., *et al.* (2002). Active genes are tri-methylated at K4 of histone H3. *Nature*, ***419***(6905), 407–411.
27. Wagner, E. J., & Carpenter, P. A. (2012). Understanding the language of histone modifications. *Nature Reviews Molecular Cell Biology*, ***13***(1), 36–49.
28. Eriksson, P. R., Ganguli, D., Nagarajavel, V., & Clark, D. J. (2012). Regulation of histone gene expression in budding yeast. *Genetics*, ***191***(1), 7–20. https://doi.org/10.1534/genetics.112.140145
29. Park, H. S. (2009). A simple and fast algorithm for K-medoids clustering. Expert Systems with Applications, ***36***(2), 3336-3341. https://doi.org/10.1016/j.eswa.2008.01.047

Author

Vinayak Ramakrishnan is a 15-year-old researcher from New York with a strong passion for computational biology. A Gold-level participant in the USA Computing Olympiad (USACO), Vinayak Ramakrishnan has combined expertise in computer science and biology to explore complex genetic mechanisms. They authored this paper on the role of histone modifications in gene expression in collaboration with the Cambridge Center for International Research. Currently, Vinayak Ramakrishnan is conducting cancer research, further deepening their understanding of molecular biology and bioinformatics. With a keen interest in scientific inquiry, they are dedicated to writing research papers and expanding their knowledge in the field of computational biology.

IJHSR
ijhighschoolresearch.org
REVIEW ARTICLE

Rebuilding Vision: Evaluating Biomaterials for Next-Generation Artificial Corneas

Ayaan Cheema

Glastonbury High School, 179 Penwood Xing, Glastonbury, Connecticut, 06033, USA; ayaanc2707@gmail.com

ABSTRACT: Corneal blindness is a health problem that affects around 10 million people worldwide, but only a fraction of patients receive a corneal transplant due to the lack of donor tissue. To combat this issue, artificial corneas are being developed and tested; however, their success depends heavily on the materials used. This literature review evaluates silk-based polymers, hydrogels, and decellularized corneal tissue for use in artificial corneas, focusing on optical transparency, structural integrity, and host tissue integration. Information was gathered from a wide range of sources, including peer-reviewed studies, clinical trials, and industry reports published since 2016. Findings show that decellularized tissues closely resemble natural corneal structure but face sourcing and immune risks. Hydrogels have good flexibility and transparency but often lack long-term strength. Nanomaterials allow for detailed control of surface and structural features but still require long-term safety assessments. Silk-based and hybrid materials show a balanced performance across the criteria considered, as they offer high strength and low immunogenicity. In the future, specific comparisons between each material and long-term clinical trials are recommended to find the most promising solutions for artificial corneas. These findings support hybrid biomaterial strategies as a practical path toward reducing global dependence on donor corneas.

KEYWORDS: Biomaterials, Nanomaterials, Artificial Corneas, Corneal Blindness, Bioengineered Solutions.

Introduction

Over 10 million people worldwide suffer from corneal blindness. The cornea is the transparent, outermost layer of the eye. It focuses light and protects the inner eye from dust, germs, and injury. The cornea consists of five distinct layers that collectively maintain its strength and transparency. Corneal blindness occurs when this layer becomes cloudy or damaged, which can then block incoming light and cause vision loss.[1]

Despite the effectiveness of corneal transplantation, most patients with corneal blindness never receive treatment due to the global shortage of donor corneas. Limited tissue availability, high costs, and surgical barriers further restrict access to transplantation, particularly in low-resource regions. These limitations underscore the need for artificial corneas as scalable alternatives to donor tissue.[2]

Several biomaterials are being studied for their application in artificial corneas, including silk-based polymers, hydrogels, and decellularized corneal tissues. To function successfully, each material must satisfy three key criteria: optical transparency, structural integrity, and host tissue integration.[2] It is found that Silk offers strength and a low immune response.[1,3] Hydrogels provide flexibility and transparency but break down over time.[4] Decellularized tissues closely match natural corneas but bring some immune concerns.[5,6]

This paper revolves around one question: Which biomaterials offer the most effective combination of transparency, strength, and biocompatibility for artificial corneas? The goal is to inform material selection for future designs and help reduce global reliance on human donor corneas.

Methodology

The objective of this study was to compare and evaluate three biomaterials that can be used for artificial corneas. The research compared each material in three categories: optical transparency, structural integrity, and biocompatibility/integration. The study aimed to collect information that would help show strengths and limitations regarding the materials for the different categories.

A literature review was conducted to compare and evaluate the three different biomaterials: silk-based polymers, hydrogels, and decellularized corneal tissues. The analysis of each of these materials focused on their optical transparency, structural integrity, and biocompatibility/integration with host tissue. A wide variety of sources, including peer-reviewed studies, systematic reviews, and clinical trials published between 2016 and 2025, were used in the research process. Sources were collected using databases like PubMed, ScienceDirect, Google Scholar, and other informational journal websites. Only articles and publications in the English language were considered for use. Search terms like “artificial cornea,” “corneal scaffold,” “silk fibroin,” “hydrogel cornea,” “decellularized corneal tissue,” and “nanomaterials for corneal regeneration” were used to find relevant information. All studies were synthesized using a qualitative comparative approach to identify relative strengths and limitations across the three biomaterials. Attention was given to emerging material modifications and composite strategies to provide context for current performance and future artificial cornea development. Studies evaluating corneal biomaterials for ophthalmic use were prioritized, and human clinical data trials were preferred over animal ones. Optical transparency was measured through light transmissibility and

DOI: 10.36838/IJHSR810.106

whether or not haze/fogginess occurred after placement of the implant. Structural integrity was assessed by comparing the tensile strength of the material to that of native human corneal tissue and whether or not elastic properties were comparable. Biocompatibility and integration were evaluated on the basis of immune responses, nerve regrowth, and long-term implant stability in the living body.

Across the reviewed literature, many strengths and weaknesses of the materials were highlighted. Silk showed good structural integrity but low immune responses. Hydrogels showed promising optical transparency, but lacked a bit in strength without modifications. Decellularized corneal tissues resemble the native cornea really well, but may take longer to facilitate nerve regrowth. A comparison of the advantages and disadvantages of silk-based polymers, hydrogels, and decellularized corneal tissues is presented in Table 1.

Silk-Based Polymers in Artificial Corneas

Silk fibroin, a protein taken from *Bombyx mori* silkworms and certain non-mulberry species, has become one of the most promising materials for artificial cornea design. This material exhibits favorable characteristics, including optical clarity, high tensile strength, adaptive mechanical properties, and low immunogenicity.[1,3] Silk can be processed into transparent films, membranes, or layered scaffolds that can closely resemble the precisely arranged layers of collagen fibrils that form the bulk of the cornea's middle layer. These arrangements are crucial for the cornea's primary function, which is transparency. Beyond its compositional properties, silk fibroin has been extensively evaluated as a corneal scaffold due to its ability to balance optical clarity with mechanical robustness, making it a strong candidate for artificial cornea applications.

Optical Transparency:

From an optical perspective, silk-based scaffolds perform favorably when compared to native corneal tissue under controlled fabrication conditions. When processed into ultra-thin films, silk fibroin can achieve light transmission comparable to that of a healthy human cornea. Silk fibroin films transmit a high percentage of visible light – e.g., a 30 μm film of *Antheraea mylitta* (non-mulberry) silk showed about 94.4% light transmittance (400–700 nm), comparable to the native cornea.[1] Such silk films have a refractive index (~1.38-1.44) similar to corneal tissue, enabling minimal optical distortion.[7] Notably, silk's transparency is maintained across various fabrication methods – films cast from different solvents and annealed under different conditions all retained >90% transmission in the visible range.[8] One challenge is that transparency can decrease as the scaffold thickness increases. Thicker silk constructs may scatter light due to β-sheet crystallites or micropores. Recent silk processing techniques (e.g., ethanol annealing or centrifugal casting) allow tuning of optical and mechanical properties without sacrificing clarity.[2] Although few transparency-related weaknesses have been noted, slight reductions in transmittance can occur under certain conditions. For instance, in hydrated hydrogels or hybrid films, the light transmission, while high, may drop to around 85% as seen in one silk/gelatin film study.[9] Unmodified silk hydrogels may lose some transparency over time, but blending with other polymers or applying chemical modifications can slow or prevent this change. Overall, silk-based polymers can meet the cornea's stringent transparency requirements when engineered at appropriate thickness and microstructure.

Structural Integrity

A reason silk is popular in corneal applications is because of its mechanical performance. Silk scaffolds can exceed the strength of most natural corneal substitutes. While native cornea tensile strength averages 3–4 MPa, silk scaffolds can equal or exceed these values. For example, multilayer silk film laminates have reported tensile strengths on the order of 10–30 MPa, far above native tissue.[1,2] Additionally, aligned 60:40 (silk: PCL) fibers showed significantly improved ultimate tensile strength and Young's modulus within the acceptable range for corneas.[10] In other words, by adding silk fibroin and aligning fibers, the scaffold's strength and stiffness became similar to native stromal tissue. Processing adjustments—such as glycerol annealing, crosslinking, or combining silk with poly (lactide-co-caprolactone)—allow tuning of stiffness and elasticity; some composites reach 9.3 MPa while maintaining flexibility.[2] One study showed that films cast in formic acid had higher ultimate tensile strength but also lower swelling (more rigidity) than aqueous-cast films, illustrating the trade-off between strength and flexibility that can be engineered.[8] While overly crystalline silk may become brittle, optimized formulations balance rigidity for surgical handling with sufficient elasticity to withstand physiological strain.[3,11] It is also important to note that thicker silk implants can diminish nutrient diffusion.[12] That said, it is essential to consider the trade-off between making silk scaffolds thin enough for transparency and strong enough for mechanical handling.

Biocompatibility and Integration:

Silk is generally regarded as a biocompatible and low-immunogenic material in ocular applications. Silk fibroin has a long history in sutures and is generally non-inflammatory.[13] *In vivo* implantation studies have shown excellent integration of silk corneal implants. No significant immune rejection or inflammation was observed when silk films were embedded in rabbit corneas.[1] Specifically, no neovascularization was reported in or around a silk fibroin film placed intrastromally for several weeks; the corneal surface remained smooth and clear.[1] Silk can also be chemically modified (e.g., with RGD peptides or methacrylation) to promote cell adhesion and integration further.[11] Silk from non-mulberry silkworms (which naturally contains RGD cell-binding sequences) promoted better cell adhesion than *Bombyx mori* silk: the non-mulberry silk films had significantly higher endothelial cell attachment and more robust focal adhesions, enabling an intact cell layer to form.[14] For corneal stromal cells, composite silk scaffolds have also performed well: a silk nanofibril/GelMA film supported vigorous stromal cell growth, with ~97% of the film area covered by cells after 5 days (versus only ~12% coverage on a pure silk-only film).[9] But there can be limitations to silk-based biomaterials when

it comes to corneal applications. A biological limitation of silk fibroin is its surface chemistry – SF lacks natural cell-binding motifs that many ECM proteins have. Corneal cells (epithelial, stromal, endothelial) can attach and grow on silk. Still, typically this requires the presence of serum or coating the silk with extracellular matrix proteins (like collagen, fibronectin, or vitronectin) to facilitate adhesion.[15] Additionally, native silk fibroin lacks the abundant cell-binding domains found in the extracellular matrix, so that unmodified silk can have lower cell affinity.[14] Overall, silk-based polymers demonstrate excellent biocompatibility, integrating with corneal tissue with minimal immune response. This makes silk a promising base material or component in artificial cornea composites. The main limitation is the need to maintain transparency in thicker formats. Overall, silk-based polymers demonstrate strong mechanical performance and high transparency, though maintaining clarity in thicker constructs remains a key design constraint.

Hydrogels

"Hydrogels" encompass a broad class of water-swollen polymer networks used for corneal implants. Many hydrogels have optical and biochemical similarity to the corneal extracellular matrix, which is ~78% water and composed of collagen and glycosaminoglycans.[16] Hydrogels are known for high transparency and permeability, but often face challenges in long-term mechanical stability. Advanced chemical crosslinking and composite strategies have improved their performance. In the context of artificial corneas, hydrogels are evaluated not only for their biomimetic composition but also for their long-term optical stability, mechanical durability, and capacity for tissue integration.

Optical Transparency:

Hydrogels can achieve optical clarity comparable to the native cornea, due to their high water content and homogeneous polymer network. A notable example is the bioengineered porcine collagen hydrogel implant (BPCDX, 280–440 μm), which demonstrated light transmission nearly identical to that of a healthy human cornea across the visible spectrum.[16] A 20-patient clinical study with the BPCDX hydrogel implant, all operated corneas maintained clear transparency (graded 4+ clarity) post-operatively.[16] Only a transient mild haze occurred in a few cases during early wound healing, which resolved by 1 week.[16] Another semi-synthetic hydrogel, *Kuragel*, composed of photocrosslinked gelatin and hyaluronic acid, displayed visible light transparency equivalent to a human cornea *in vitro* (above 94% transmission) while restoring corneal clarity in animal models (no scarring or vascularization noted).[17] Importantly, *in vivo* and clinical results affirm that transparent hydrogels can restore corneal clarity. In a rabbit model of corneal injury, a decellularized human-corneal ECM hydrogel prevented scar formation and opacification – treated corneas remained *indistinguishable from healthy corneas* on observation.[18] As for other clinical results, A cell-free recombinant collagen implant in 10 patients maintained full transparency in all implants over 4 years post-surgery.[19] However, earlier generation biosynthetic corneas (e.g., recombinant human collagen gels) sometimes experienced postoperative haze or thinning, but newer double-crosslinked hydrogels have largely overcome this.[16] Thus, optical performance is a major strength of hydrogels. The challenge is ensuring they remain clear over time (no degradation or cell overgrowth causing haze) and under physiological conditions.

Structural Integrity:

Despite their favorable biological properties, mechanical performance remains the primary limitation when hydrogels are assessed for corneal implantation. Historically, a drawback of hydrogels has been their lower mechanical strength relative to the native cornea, especially when highly hydrated. Many standard hydrogels (e.g., unmodified collagen or gelatin gels) have tensile strengths <0.5 MPa, well below the native cornea's tensile strength of ~3–4 MPa.[2] For instance, a low-solids collagen gel (≈0.8% w/v) exhibited an extremely low Young's modulus ~26–27 Pa.[20] Even at higher concentration (4% collagen), the modulus only reached ~243 Pa.[20] Recent reinforcement strategies have been highly effective in addressing this issue. One approach is chemical crosslinking of the polymer network. Collagen-based hydrogels can be crosslinked with agents like glutaraldehyde or genipin, UV-induced polymerization, or enzymatically (e.g., with transglutaminase), which increases network density and stiffness.[19] Another strategy is forming interpenetrating networks or composites. Incorporating a second polymer network (synthetic or biopolymer) can dramatically toughen the hydrogel. Embedding a thin electrospun polycaprolactone (PCL) mesh into a GelMA hydrogel increased tensile strength from ~0.1–0.5 MPa to ~3.5 MPa.[21] Similarly, blending collagen with synthetic polymers such as MPC doubled stiffness from 0.6 MPa to 2.1 MPa.[2] These modifications enable hydrogel scaffolds to withstand suturing and even minimally invasive implantation without tearing.[22]

Biocompatibility and Integration:

Hydrogels for corneal use are engineered to be biocompatible, supporting cell viability and integration with host tissue while minimizing immune rejection.[4] Zhao *et al.* observed over 95% viability of human corneal epithelial and stromal cells cultured on their HCSP scaffold, indicating no cytotoxic leachates. In a landmark Phase I clinical trial, a biosynthetic cornea made of crosslinked recombinant human collagen (RHCIII) was implanted in 10 patients with corneal blindness.[19] The outcomes demonstrated excellent biocompatibility: the cell-free collagen implants became stably integrated into the patients' own corneal stroma, with complete re-epithelialization over the implant and even nerve regeneration into the graft.[19] Another study introduced Kuragel, a gelatin/HA-based hydrogel, into rabbit corneal injuries affecting both epithelium and stroma. Kuragel was formulated for tissue adhesiveness and minimal swelling, allowing it to be applied as a sutureless filler in the defect. The *in vivo* results were notable: the hydrogel encouraged full re-epithelialization within 4 weeks, and within 3 months, the corneal stroma had regenerated with organized collagen and a restored sub-basal nerve plexus present.[17] Also, in a rabbit

DOI: 10.36838/IJHSR810.106

model of lamellar keratoplasty, the HCSP implants supported rapid re-epithelialization without sutures. They avoided the typical foreign-body complications – no significant haze, neovascularization, or graft rejection were observed.[4] However, long-term implant stability remains a consideration, and recent data are helping identify which designs perform best. For instance, a "LiQD" peptide–PEG hydrogel, designed as a fully synthetic corneal substitute, supported tissue regeneration in a pig study but developed some post-operative haze and neovascularization in all implanted eyes within 1 year. The transient haziness was attributed to the material's swelling and bioresorption profile, highlighting the need for balanced degradation rates. Nonetheless, even in those cases, there were no severe rejections – the immune response was manageable, and corneas achieved functional thickness and barrier function.[19] Overall, studies show that hydrogel corneal substitutes can biologically integrate with host tissue: they support epithelial coverage and nerve ingrowth, and remain stable long-term *in vivo*.[4,23] This favorable biocompatibility profile is critical, as it translates to improved healing, transparency maintenance, and implant longevity in artificial cornea applications. Collectively, hydrogels offer excellent optical clarity and biocompatibility, but long-term mechanical stability depends on reinforcement strategies.

■ Decellularized Corneal Tissue

Decellularized corneal tissue involves using a natural corneal extracellular matrix (ECM) – usually sourced from donated human corneas or animal corneas (e.g., porcine or bovine) – and removing all cellular components to mitigate immune rejection. A good approach aims to leverage the biomimicry of a real cornea's structure and chemistry, while eliminating donor cells that would cause rejection. When assessed as artificial corneal substitutes, decellularized tissues are primarily evaluated based on how effectively they preserve native corneal structure while minimizing immune rejection and supporting long-term integration.

Optical Transparency:

Decellularized corneal tissues can achieve high optical clarity, approaching that of the native cornea, provided swelling is controlled and tissue architecture is preserved. A 2024 study using high-hydrostatic pressure decellularization produced "transparent" acellular porcine corneas with ~86% light transmittance (380–770 nm average), comparable to fresh human corneas (~87%).[5] In rabbit implants, these grafts were essentially clear and indistinguishable from surrounding tissue within days post-surgery, indicating excellent restoration of transparency *in vivo*.[5] Similarly, a decellularized human corneal scaffold (deoxycholate/DNAse method with dextran) showed no significant loss in optical transmission versus native cornea.[24] But swelling and dehydration can affect performance in clarity. If osmotic measures are not used during decellularization, the corneal stroma tends to swell and become hazy. For example, decellularization without dextran led to a ~10–15% drop in transparency.[24] However, dehydration treatments can reverse this: simply incubating the decellularized tissue in glycerol or dextran solution rapidly restores transparency by collapsing excess fluid.[6,24] Overall, decellularized corneal tissue, being derived from a transparent tissue, can provide optical performance essentially on par with a donor cornea.

Structural Integrity:

Mechanical strength and elasticity of decellularized corneal scaffolds are critical for long-term durability. Research in the past six years indicates that while decellularization can alter corneal micro-architecture, proper processing (and optional crosslinking) yields scaffolds with robust mechanical properties comparable to donor tissue. To further improve strength and prevent any post-implant thinning or bulging, researchers have applied collagen crosslinking treatments to decellularized corneas. This can dramatically increase stiffness and resistance to deformation. A notable example is a proprietary 4-step processing of porcine corneal lenticules (including decellularization, enzymatic wash, tissue compression, and chemical crosslinking) developed for keratoconus treatment.[25] The result was a thin (~<90 μm) implant with a Young's modulus ~25 MPa – roughly 127% stiffer than the native cornea (unprocessed porcine stroma ~11 MPa).[25] Another study created a chemically cross-linked decellularized pig cornea (using EDC/NHS and γ-irradiation) and found its ultimate tensile strength and resistance to enzymatic digestion were significantly improved over native tissue.[26] Importantly, the transparency of these crosslinked grafts remained similar to that of untreated corneas.[26] Decellularized corneal scaffolds have also proven durable in both laboratory and surgical settings. For instance, acellular porcine grafts implanted in patients for more than 2 years showed no thinning; the grafts maintained their shape and thickness, similar to a normal cornea.[27] In a rabbit infection model, a cross-linked decellularized cornea withstood the proteolytic/inflammatory environment, preventing corneal perforation better than standard treatments.[26] Flexibility of the scaffold is also crucial for conformance to the ocular surface. High-pressure decellularized corneas, for example, had a refractive index of ~1.367 (vs 1.373 native) and normal hydration, indicating the stromal structure was intact enough to preserve biomechanical and optical function.[5] Surgeons in clinical trials noted that acellular grafts could be sutured similarly to donor tissue, facilitating standard keratoplasty techniques.[6] If anything, decellularized corneas are sometimes softer or easier to cut due to the absence of cells, but overall, handling characteristics are very close to a live cornea.

Biocompatibility and Integration:

Biological integration represents the defining advantage of decellularized corneal scaffolds, but it also introduces variability in healing outcomes. A decellularized corneal implant must integrate with the host tissue, supporting cell repopulation, normal wound healing, and nerve regeneration while avoiding immune rejection. Recent studies provide encouraging evidence that decellularized corneas are biocompatible and integrate well *in vivo*, though complete integration (especially neural) can be gradual. Clinical xenotransplantation trials in China implanted acellular porcine corneas in patients with

corneal ulcers and keratitis. After 2 years, 22 of 23 grafts remained clear and in place with no rejection episodes reported.[6] Only mild, transient postoperative inflammation was noted, manageable with standard steroids. Another cohort of 37 patients received decellularized porcine grafts for fungal keratitis and showed 100% retention at 3 years without immune rejection or significant complications.[6] Functional integration also requires that corneal nerves regrow into the graft to restore sensation and neurotrophic support, and this can be a long process. Clinical experience with human corneal transplants shows that stromal nerves begin to penetrate a graft by ~2–3 months post-op, but the superficial nerve plexus in the epithelium often takes 1–2 years to return fully, and normal corneal sensitivity may require ~3 years to recover. In decellularized porcine grafts, nerve trunks have been observed regrowing into the transplant during long-term follow-up (e.g., a 12-month dog study). The dog study also noted improved corneal nerve re-innervation in the decellularized scaffold that had been pre-populated with human cells, compared to a cell-free scaffold. This suggests that promoting a biologically active environment in the graft can influence nerve return. Furthermore, decellularized corneas generally induce a milder healing response than full-thickness grafts. Some studies note a delay in complete healing with decellularized grafts: for instance, initial corneal haze can persist for several months post-implant until remodeling resolves it. Over longer periods, however, remodeling tends to restore a more normal matrix structure. In clinical observations, patients with decellular cornea grafts experienced gradual clearing over a year or more.[27] In summary, decellularized corneal scaffolds closely replicate native tissue properties, though slower nerve regeneration and processing variability limit immediate clinical adoption.

Table 1: Advantages and Disadvantages of Artificial Corneal Biomaterials.

Material	Advantages	Disadvantages	References
Silk-based Polymers	• High optical clarity- 94.4% light transmittance (400–700 nm) • Tunable with various processing styles • High tensile strength depending on the formulation technique	• Optical clarity can decrease with thicker scaffolds • Risk of brittleness if overly crystalline. • Variable degradation rates *in vivo*.	Hazra *et al.* [1] Formisano *et al.* [2] Jameson *et al.* [11] Manoochehrabadi *et al.* [3]
Hydrogels	• High optical transparency (similar to native cornea) • Stable implants and improved vision were shown in clinical studies.	• Weaker tensile strengths (<0.5 MPa) • Long-term stability is currently dependent on reinforcement techniques.	Kong *et al.* [21] Rafat *et al.* [16] Zhao *et al.* [4]
Decellularized Corneal Tissue	• Mimics natural corneal transparency: ~86% light transmittance (380–770 nm average). • Crosslinking techniques can dramatically increase structural integrity	• Swelling and hazing can occur if not properly treated. • It can take a long time to heal and facilitate nerve regrowth	Hashimoto *et al.* [5] Polisetti *et al.* [24] Lin *et al.* [26] Fernández-Pérez *et al.* [27]

Table 1 highlights the strengths and limitations of the three biomaterials compared in this review. Silk-based polymers stand out for their high tensile strength and optical clarity, but they require levels of modification to facilitate their best performance. Hydrogels are excellent when it comes to optical clarity, but can lack in the category of strength, as they require chemical modifications and reinforcement strategies for the best long-term use. Decellularized Corneal tissue most clearly mimics the native cornea in terms of optical transparency and structural integrity. However, variable processing techniques and slower recovery times for these materials can be a limitation. Overall, these findings show that each material offers its own unique strengths, and it is important to recognize these strengths for future innovation in this field.

Discussion

Figure 1 illustrates the layered structure of the human cornea, highlighting the anatomical features that artificial cornea biomaterials aim to replicate in terms of transparency and mechanical support.

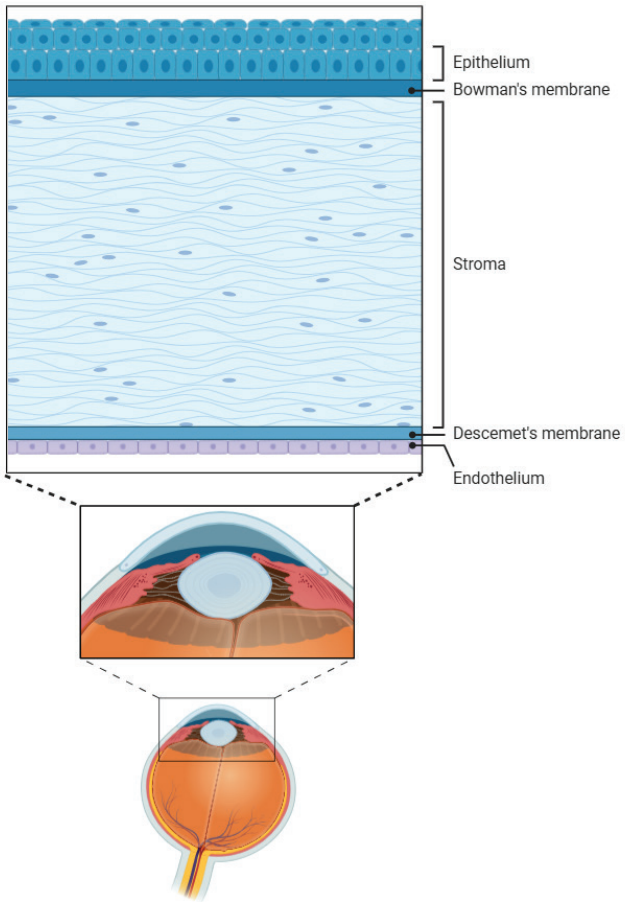

Figure 1: Layers of the Cornea. This figure shows the 5 main layers of the human cornea: the epithelium, Bowman's layer, stroma, Descemet's membrane, and the endothelium. These layers are essential for maintaining the cornea's strength and transparency, which are the same properties evaluated in this study to guide artificial cornea design. Created using BioRender.

The findings across the three biomaterials compared in this review highlight a promising future for the development of artificial corneas, yet challenges remain in the field. Each of the materials compared shows a strength in at least one of the categories used for assessment: optical transparency, structural integrity, and host tissue integration. But, no single method currently meets the capacity for a clinically functional substitute with exceptional performance in all three categories.

Optical transparency is the most consistently achieved property. Silk-based polymers and hydrogels regularly demonstrate light transmittance near that of the native cornea, while decellularized tissues preserve transparency when tissue architecture

DOI: 10.36838/IJHSR810.106

is maintained during processing. These findings, along with the analysis of each material in different contexts, demonstrate that transparency is very important for bioengineered corneas, but not a primary component for clinical success. The challenge lies in maintaining corneal clarity in long-term implantation trials, as postoperative haze and other scarring issues can occur in the process.

Structural integrity presents a wide variation of results across the three materials compared. For example, silk-based biomaterials continue to demonstrate tensile strength values that are comparable to those of the native cornea, and sometimes even exceed those values. Hydrogels, while flexible and compatible with outside tissue, can often degrade under physiological conditions. However, they can be reinforced and chemically modified with other polymers to increase robustness. Decellularized corneal tissues can maintain much of the natural strength of the natural cornea, especially when crosslinking techniques are applied. However, mechanical performance can still vary significantly depending on the donor source and other processing methods.

Biocompatibility and Integration represent another decisive factor for current and future clinical outcomes. Silk-based scaffolds are generally supportive of cell adhesion, though nerve regeneration with this biomaterial appears slower than with donor tissue. Hydrogels demonstrate strong compatibility, and clinical trials show minimal immune responses and rejection without the need for significant immunosuppression efforts. Decellularized tissues most closely replicate natural biology by supporting nerve regrowth processes, but they can carry risks of immune reaction responses if residual antigens are not fully removed. Long-term studies also show that decellularized corneal tissues may have initial haze or remodeling that can gradually recover over months to years.

Overall, these results signify that hybrid or compost strategies for corneal biomaterials are an effective path moving forward. Silk's mechanical strength, hydrogel's flexibility and optical clarity, and the biological similarity of decellularized corneal tissues provide promising characteristics for future studies. Combining each material's strength into multi-component scaffolds can help overcome challenges related to single-material composites.

Progress over the last decade points to a promising future for the potential of these materials to meet the urgent need for donor cornea alternatives. Yet, significant challenges continue to remain. Most studies are limited to animal trials or short-term human trials, with limited follow-up measures. Standard ways of testing optical, mechanical, and immunological trends are crucial for further comparison between the materials under examination. Additionally, expanding the duration of human clinical trials will be important for assessing safety and success in long-term applications.

Artificial corneas are an essential innovation to combat the global problem of corneal blindness. Further collaboration between material scientists and clinical ophthalmologists will be helpful to improve the biomaterials and their applications further.

■ Conclusion

Artificial corneas will continue to remain a critical area for research due to the fact that corneal blindness and other related issues will affect millions of people worldwide. This literature review compared silk-based polymers, hydrogels, and decellularized corneal tissue against three criteria: optical transparency, structural integrity, and biocompatibility. Each biomaterial proved successful in at least one category that was reviewed, but none showed complete excellence in all three fields. Silk showed strength and stability, hydrogels proved great transparency, and decellularized tissues most clearly exhibited natural corneal structure.

Evidence from studies points toward hybrid biomaterials being able to combine the strengths of multiple other biomaterials. For example, silk's strength, hydrogel's transparency, and decellularized tissues' biological resemblance could form composite scaffolds to address current restrictions.

Artificial corneas continue to become more clinically advanced as research on the topic progresses, but further refinements are still needed to achieve the safest and most functional solution. Continuing research on bioengineered solutions for artificial corneas will continue to be extremely impactful for the millions of people battling corneal blindness.

■ Acknowledgments

I would like to thank my research mentor, Professor Kristina Lilova, for her guidance and advice regarding this project. I also acknowledge the help and support of Professor Virgel Torremocha, who has given me amazing feedback in all aspects. Moreover, I extend my gratitude to everyone at the Gifted Gabber team for providing me with the resources necessary for my research journey. Finally, I would like to thank my family for their continuous support.

■ References

1. Hazra, S.; Nandi, S.; Naskar, D.; *et al.* Non-mulberry Silk Fibroin Biomaterial for Corneal Regeneration. *Sci. Rep.* **2016**, *6*, 21840. https://doi.org/10.1038/srep21840
2. Formisano, N.; van der Putten, C.; Grant, R.; Sahin, G.; Truckenmüller, R. K.; Bouten, C. V. C.; Kurniawan, N. A.; Giselbrecht, S. Mechanical Properties of Bioengineered Corneal Stroma. *Adv. Healthc. Mater.* **2021**, *10* (20), 2100972. https://doi.org/10.1002/adhm.202100972.
3. Manoochehrabadi, T.; Samadikuchaksaraei, A.; Solouki, A.; Daryabari, S. H.; Ghasemi, H.; Lotfi, E.; Mansourian, S.; Majidi, J.; Milan, P. B.; Gholipourmalekabadi, M. Substrate Engineering Using Naturally Biomimicking Corneal Cell Topography for Preserving Stemness of Corneal Limbal Epithelial-Stem Cells. *Iran. J. Basic Med. Sci.* **2025**, *28* (7), 916–928. https://doi.org/10.22038/ijbms.2025.86110.18601.
4. Zhao, L.; Shi, Z.; Zhang, X.; Wang, J.; Yang, S.; Wang, F.; Li, T.; Zhou, Q.; Wang, T.; Shi, W. Artificial Cornea Substitute Based on Hydrogel Skeletons with Natural Stromal Hierarchical Structure and Extracellular Matrix for Sutureless Transplantation. *Adv. Sci.* **2025**, *12* (19), 2411540. https://doi.org/10.1002/advs.202411540.
5. Hashimoto, Y.; Negishi, J.; Funamoto, S.; Kimura, T.; Kobayashi, H.; Oshika, T.; Kishida, A. Preparation, Physico-Biochemical Characterization, and Proteomic Analysis of Highly Transparent

Corneal Extracellular Matrices for Lamellar Keratoplasty and Tissue-Engineered Cornea Construction. *Mater. Today Bio* **2024**, *28*, 101241. https://doi.org/10.1016/j.mtbio.2024.101241.
6. Isidan, A.; Liu, S.; Chen, A. M.; Zhang, W.; Li, P.; Smith, L. J.; Hara, H.; Cooper, D. K. C.; Ekser, B. Comparison of Porcine Corneal Decellularization Methods and Importance of Preserving Corneal Limbus Through Decellularization. *PLoS One* **2021**, *16* (3), e0243682. https://doi.org/10.1371/journal.pone.0243682.
7. Wu, K. Y.; Belaiche, M.; Wen, Y.; Choulakian, M. Y.; Tran, S. D. Advancements in Polymer Biomaterials as Scaffolds for Corneal Endothelium Tissue Engineering. *Polymers* **2024**, *16* (20), 2882. https://doi.org/10.3390/polym16202882.
8. Beena, M.; Ameer, J. M.; Kasoju, N. Optically Clear Silk Fibroin Films with Tunable Properties for Potential Corneal Tissue Engineering Applications: A Process-Property-Function Relationship Study. *ACS Omega* **2022**, *7* (34), 29634–29646. https://doi.org/10.1021/acsomega.2c01579.
9. Farasatkia, A.; Kharaziha, M.; Ashrafizadeh, F.; Salehi, S. Transparent Silk/Gelatin Methacrylate (GelMA) Fibrillar Film for Corneal Regeneration. *Mater. Sci. Eng. C* **2021**, *120*, 111744. https://doi.org/10.1016/j.msec.2020.111744.
10. Salehi, O. M.; Nourbakhsh, M. S.; Rafienia, M.; Baradaran-Rafii, A.; Keshel, S. H. Corneal Stromal Regeneration by Hybrid Oriented Poly (ε-Caprolactone)/Lyophilized Silk Fibroin Electrospun Scaffold. *Int. J. Biol. Macromol.* **2020**, *161*, 377–388. https://doi.org/10.1016/j.ijbiomac.2020.06.045.
11. Jameson, J. F.; Pacheco, M. O.; Nguyen, H. H.; Phelps, E. A.; Stoppel, W. L. Recent Advances in Natural Materials for Corneal Tissue Engineering. *Bioengineering* **2021**, *8* (11), 161. https://doi.org/10.3390/bioengineering8110161.
12. Li, Y.; Wang, Z. Biomaterials for Corneal Regeneration. *Adv. Sci.* **2025**, *12* (6), 2408021. https://doi.org/10.1002/advs.202408021.
13. Luo, Y.; Kang, K. B.; Sartaj, R.; *et al.* Silk Films with Nanotopography and Extracellular Proteins Enhance Corneal Epithelial Wound Healing. *Sci. Rep.* **2021**, *11*, 8168. https://doi.org/10.1038/s41598-021-87658-1.
14. Ramachandran, C.; Gupta, P.; Hazra, S.; Mandal, B. B. *In Vitro* Culture of Human Corneal Endothelium on Non-Mulberry Silk Fibroin Films for Tissue Regeneration. *Transl. Vis. Sci. Technol.* **2020**, *9* (4), 12. https://doi.org/10.1167/tvst.9.4.12.
15. Nili, E.; Harkin, D. G.; Dawson, R. A.; Richardson, N. A.; Suzuki, S.; Chirila, T. V. Membranes Prepared from Recombinant RGD-Silk Fibroin as Substrates for Human Corneal Cells. *Molecules* **2021**, *26* (22), 6810. https://doi.org/10.3390/molecules26226810.
16. Rafat, M.; Jabbarvand, M.; Sharma, N.; *et al.* Bioengineered Corneal Tissue for Minimally Invasive Vision Restoration in Advanced Keratoconus in Two Clinical Cohorts. *Nat. Biotechnol.* **2023**, *41*, 70–81. https://doi.org/10.1038/s41587-022-01408-w.
17. Agrawal, P.; Tiwari, A.; Chowdhury, S. K.; *et al.* Kuragel: A Biomimetic Hydrogel Scaffold Designed to Promote Corneal Regeneration. *iScience* **2024**, *27* (5), 109641. https://doi.org/10.1016/j.isci.2024.109641.
18. Chameettachal, S.; Venuganti, A.; Parekh, Y.; *et al.* Human Cornea-Derived Extracellular Matrix Hydrogel for Prevention of Post-Traumatic Corneal Scarring: A Translational Approach. *Acta Biomater.* **2023**, *171*, 289–307. https://doi.org/10.1016/j.actbio.2023.09.002.
19. Holland, G.; Pandit, A.; Haiek, A.; Loinaz, I.; Dupin, D.; Gonzalez, M.; Larra, E.; Bidaguren, A.; Lagali, N.; Moloney, E. B.; Ritter, T. Artificial Cornea: Past, Current, and Future Directions. *Front. Med.* **2021**, *8*, 770780. https://doi.org/10.3389/fmed.2021.770780.
20. Gao, Q.; Yu, K.; Shang, Y.; Lin, Z.; Zhu, M.; Lu, L.; Jiang, T.; Zhang, P. Effect of 3D Printing Parameters on the Transparency of Medical Hydrogels for Corneal Stroma Fabrication. *Gels* **2025**, *11* (7), 528. https://doi.org/10.3390/gels11070528.
21. Kong, B.; Chen, Y.; Liu, R.; *et al.* Fiber Reinforced GelMA Hydrogel to Induce the Regeneration of Corneal Stroma. *Nat. Commun.* **2020**, *11*, 1435. https://doi.org/10.1038/s41467-020-14887-9.
22. Chaudhary, R.; Tan, J.; Lee, C.; Chang, K.; Lin, Y.; Wu, P.; Su, H.; Huang, J. 3D-Printed Artificial Cornea Featuring Aligned Fibrous Structure and Enhanced Mechanical Strength. *Int. J. Bioprint.* **2024**, *10*, 4687. https://doi.org/10.36922/ijb.4687.
23. Xeroudaki, M.; Thangavelu, M.; Lennikov, A.; *et al.* A Porous Collagen-Based Hydrogel and Implantation Method for Corneal Stromal Regeneration and Sustained Local Drug Delivery. *Sci. Rep.* **2020**, *10*, 16936. https://doi.org/10.1038/s41598-020-73730-9.
24. Polisetti, N.; Schmid, A.; Schlötzer-Schrehardt, U.; *et al.* A Decellularized Human Corneal Scaffold for Anterior Corneal Surface Reconstruction. *Sci. Rep.* **2021**, *11*, 2992. https://doi.org/10.1038/s41598-021-82678-3.
25. Wilson, A.; Jones, J.; Marshall, J. Biomechanical Evaluation of Decellularized and Crosslinked Corneal Implants Manufactured from Porcine Corneas as a Treatment Option for Advanced Keratoconus. *Front. Bioeng. Biotechnol.* **2022**, *10*, 862969. https://doi.org/10.3389/fbioe.2022.862969.
26. Lin, Y.; Zheng, Q.; Hua, S.; *et al.* Cross-Linked Decellularized Porcine Corneal Graft for Treating Fungal Keratitis. *Sci. Rep.* **2017**, *7*, 9955. https://doi.org/10.1038/s41598-017-08207-3.
27. Fernández-Pérez, J.; Madden, P. W.; Brady, R. T.; Nowlan, P. F.; Ahearne, M. The Effect of Prior Long-Term Recellularization with Keratocytes of Decellularized Porcine Corneas Implanted in a Rabbit Anterior Lamellar Keratoplasty Model. *PLoS One* **2021**, *16* (6), e0245406. https://doi.org/10.1371/journal.pone.0245406.

Author

Ayaan Cheema, a senior at Glastonbury High School, explores artificial corneas in his biomedical research. Passionate about innovation at the intersection of engineering and medicine, he aspires to study biomedical engineering and medicine, seeking to merge research and clinical practice to develop groundbreaking solutions for restoring vision and improving lives.

DOI: 10.36838/IJHSR810.106

IJHSR International Journal of High School Research

is a publication of

terra science and education

N.Y. based 501.c.3 non-profit organization
dedicated for improving K-16 education